Development, characterization and evaluation of switchable façade elements

Thibault Pflug

UNIVERSITÉ DE STRASBOURG

ÉCOLE DOCTORALE MSII

Laboratoire ICube, département mécanique

THÈSE présentée par :

Thibault PFLUG

Soutenance prévue le : **06 Juillet 2016**

Pour obtenir le grade de : **Docteur de l'université de Strasbourg**
Discipline/ Spécialité : ÉNERGÉTIQUE

Développement, Caractérisation et Évaluation d'Éléments de Façades Commutables

-

Development, Characterization and Evaluation of switchable façade elements

THÈSE dirigée par :

SIROUX Monica	Professeur, Laboratoire ICUBE, INSA Strasbourg

RAPPORTEURS :

SALAGNAC Patrick	Professeur, Laboratoire LASIE, Université la Rochelle
LASSUE Stéphane	Professeur, Laboratoire LGCGE, Université d'Artois

---

AUTRES MEMBRES DU JURY :

KUHN Tilmann	Docteur, Institut Fraunhofer ISE, Freiburg
MAURER Christoph	Docteur, Institut Fraunhofer ISE, Freiburg
MARCHIO Dominique	Professeur, CES, Mines ParisTech

Table of contents

Acknowledgements

Thanks to Christoph Maurer, for his constant backing, availability and numerous advises!

Thanks to Julie. Your love and trust brings me forward. Thanks also to my parents, parents in law, brother and sisters for their constant support.

Thanks to Bruno Bueno, for the freedom you gave me.

Thanks to Cosima Braesch, for your motivation and commitment to the task!

Thanks to Professor Monica Siroux for being a comprehensive tutor, and helping me pushing this thesis to an end.

Thanks to Tilmann Kuhn, for your efforts to allow me to do this thesis in good conditions.

Thanks to Christoph Cappel. One cannot think of a better office buddy !

Thanks to Johannes Hanek for his creative mind!

Thanks to the whole Sofa team from the Fraunhofer Institut for Solar Energy Systems (ISE), working with you was a great experience.

The author wants to thank Mr. Sergej Kvasnin for his great ideas and enthusiasm !

Part of this work was funded by the BMWi (Germany ministry of economic affairs) under the auspices of grant 03ET1032B (Integriertes Wärmemanagement-Fassadenelement (WaMaFat)) which is part of the EnOB (Forschung für Energieoptimiertes Bauen) initiative.

The author wants to thank Nikolas Nestle for being an impressive and honest project leader. Thanks to all the team of the Wamafat project for the great work and the productive project meetings.

The work presented in this thesis was partially done in cooperation with the company of Mr. Sergej Kvasnin, the I[n]solation UG (haftungsbeschränkte Unternehmergesellschaft, Waldecker Strasse 5B, 33647 Bielefeld, Germany). This cooperation has been financed by the foundation Rud. Otto Meyer-Umwelt-Stiftung.

Part of the research leading to these results has received funding from the European Community's Seventh Framework Program (FP7/2007-2013) under grant agreement n°314461.

Abstract

English version

The new building energy regulations in Europe imply always better insulated building facades. The increase of the building insulation level reduces significantly the heating energy demand of buildings. However, it can also increase prevent the building to cool down during the cooling period, when the external conditions are favorable, which can create additional cooling loads and overheating in summer. In this thesis, the concept of façade elements with switchable thermal properties, or switchable insulation, is developed. Switchable insulations are insulation systems that can be deactivated whenever it is of advantage considering the external conditions. The overall heat transfer coefficient of the façade, the U-value, can then be switched from a low, insulating value, to a high, heat conducting value: during the cooling period, this can be used to cool down the building's mass during the night or colder periods. During the heating period, the switchable insulation can be used to whenever it is warm outside and solar gains can be used. In this thesis the potential of switchable insulation for an European continental climate and for office buildings is investigated. Also, two new concepts of switchable insulation are introduced and developed. The new façade elements are characterized experimentally, with numerous U-value and optical properties measurements. For the first technology, a detailed thermal nodal model has been introduced, validated and used to assess the impact of relevant parameters on the performance of the new façade element. The second new façade element has been investigated from individual forms of heat transfer on the level of an air cavity to the level of a whole façade element. A prototype has been tested experimentally. The potential of switchable insulation in general and the two new elements in particular is investigated on a building level, using building energy simulation. Several control strategies have been developed, introduced and compared. The influence of thermal mass on the reduction of heating and cooling demand was also investigated, as well as the influence of the orientation or the elements' frame. It was shown that the heating and cooling demand can be reduced by up to 30 % by using switchable insulations.

Keywords: switchable insulation, heat transfer, façade elements, building heating and cooling energy demand, experimental investigation, U-value, physical model, thermal model, optical model, potential analysis, thermal mass, comfort.

French version

Les nouvelles réglementations énergétiques en Europe impliquent des façades de bâtiments mieux isolées. L'augmentation du niveau d'isolation des bâtiments permet de réduire considérablement les besoins de chauffage. Cependant, ces résistances thermiques importantes des parois peuvent aussi diminuer le refroidissement du bâtiment en été,

quand les conditions extérieures sont favorables. Ceci peut créer des charges de refroidissement supplémentaires et cause des surchauffes en été. Dans cette thèse, le concept d'éléments de façade à propriétés thermiques commutables, ou isolations commutable, est développé. Les isolations commutables sont des systèmes d'isolation qui peuvent être désactivés à chaque fois qu'il est possible de profiter des conditions extérieures pour diminuer les besoins de refroidissement ou de chauffage du bâtiment. Le coefficient de transmission thermique de la façade U peut alors être commuté d'une faible valeur (état isolant) à valeur élevée (état conducteur): pendant les périodes de refroidissement, cela peut être utilisé pour refroidir la masse du bâtiment pendant la nuit ou quand il fait plus froid à l'extérieur qu'à l'intérieur. Pendant les périodes de chauffage, ce concept peut être utilisé à chaque fois qu'il que les températures extérieures sont assez chaudes ou que les gains solaires peuvent être utilisés. Dans cette thèse, le potentiel des isolations commutables pour un climat continental européen est étudié. En outre, deux nouveaux concepts d'isolations commutables sont introduits et développés. Les nouveaux éléments de façade sont caractérisés expérimentalement, avec de nombreuses mesures de la valeur de U ainsi que des mesures des propriétés optiques. Pour la première technologie présentée, un modèle nodal détaillé a été mis en place, validé et utilisé pour évaluer l'impact des paramètres les plus pertinents sur la performance énergétique du nouvel élément de façade. Le second nouvel élément de façade a été étudiée en allant des transferts de chaleurs dans une cavité d'air jusqu'à l'élément de façade dans son ensemble. Un prototype a été testé expérimentalement. Le potentiel des isolations commutables en général et des deux nouveaux éléments en particulier a été étudié au niveau en utilisant la simulation énergétique dynamique du bâtiment. Plusieurs stratégies de contrôle ont été mises au point, introduites et comparées. L'influence de la masse thermique sur les réductions des besoins de chauffage et refroidissement a également été étudiée, ainsi que l'influence de l'orientation ou du cadre des éléments. Il a été montré que les besoins de chauffage et de refroidissement être réduits jusqu'à 30 % grâce aux isolations commutables.

Mots-clés: isolation commutable, transfert de chaleur, éléments de façade, réduction des besoins de chauffage et refroidissement, étude expérimentale, coefficient de transmission thermique U, modèle thermique et optique, analyse de potentiel, influence de l'inertie thermique, confort.

German version

Die neuen Gebäuderegelungen in Europa führen zu immer besser isolierten Gebäudehüllen. Die Erhöhung der Gebäudedämmung reduziert deutlich den Heizenergiebedarf während der Heizperiode deutlich. Durch die erhöhte Isolierung der Gebäudehülle kann aber auch die nächtliche Abkühlung des Gebäudes während der Kühlperiode vermindert werden wenn die äußeren Bedingungen günstig sind, was zusätzliche Kühllasten verursachen kann sowie eventuelle Überhitzungszeiten im Sommer. In dieser Arbeit wird das Konzept von

Fassadenelementen mit schaltbaren thermischen Eigenschaften -oder schaltbare Isolierung- entwickelt. Schaltbare Isolierungen sind Dämmsysteme, die deaktiviert werden können wenn es von Vorteil ist. Der Wärmedurchgangskoeffizient der Fassade (U-Wert) schaltet dabei von einem niedrigen zu einem hohen Wert (wärmeleitender Zustand): in der Kühlperiode kann dann die Gebäudemasse zum Beispiel in der Nacht durch die Außentemperatur gekühlt werden. In der Heizperiode kann die Isolierung deaktiviert werden um zu Beispiel solaren Gewinne zu sammeln. In dieser Arbeit wird das Potential von zwei innovativen schaltbaren Isolierungen für ein europäisches Kontinentalklima und für Bürogebäude untersucht. Die beiden Ideen werden vorgestellt und verschiedene Varianten werden entwickelt. Diese neuen Fassadenelemente werden experimentell charakterisiert mit zahlreichen U-Wert Messungen sowie Messungen der optischen Eigenschaften. Für die erste Technologie wird ein detailliertes thermisches Knotenmodell entwickelt, validiert und verwendet um den Einfluss der Gestaltungsparameter auf die Leistung des neuen Fassadenelements zu quantifizieren. Die zweite Technologie wird von der Ebene der Wärmetransporte in einer einzelne Kavität bis zur Untersuchung der Leistung von den gesamten Fassadenelementen analysiert. Das Potential von schaltbarer Isolierung im Allgemeinen und von den beiden neuen Elementen insbesondere wird auf Gebäudeebene untersucht anhand von Gebäudeenergiesimulation. Mehrere Steuerungsstrategien wurden entwickelt, eingeführt und verglichen. Der Einfluss der thermischen Masse auf die Einsparung wurde auch untersucht, sowie den Einfluss der Fassadenausrichtung oder des Rahmens der Elemente. Dabei konnte gezeigt werden, dass sich der Heiz- und Kühlbedarf durch jede Technologie um bis zu 30 % reduzieren lässt.

Stichwörter: schaltbare Isolierung, Wärmeübertragung, Fassadenelemente, Heiz- und Kühlbedarf, Nachtkühlung, Messung, physikalisches Modell, physikalisches Modell, optisches Modell, Potenzialanalyse, thermische Masse, Komfort.

Nomenclature

Thermal and airflow properties and variables:

α	[m^2*s^{-1}] the thermal diffusivity of a fluid.
A_r	[-] the aspect ratio of a duct.
β	[K^{-1}] the thermal expansion coefficient of a fluid.
C_p	[$J*kg^{-1}*K^{-1}$] the specific heat of a fluid.
D_h	[m] the hydraulic diameter.
ΔP	[Pa] a pressure drop.
ΔT	[K] a temperature difference.
ε	[-] the longwave emissivity of a surface.
ζ	[-] a drag coefficient.
g	[-] the center-of-glazing solar heat gain coefficient.
h	[$W*m^{-2}*K^{-1}$] a heat transfer coefficient.
H	[m] a height.
I	[$W*m^{-2}$] the solar irradiance incoming at the façade.
J	[$W*m^{-2}$] the longwave radiosity.
λ	[$W*m^{-1}*K^{-1}$] the thermal conductivity of a fluid or solid.
L	[m] the length of a duct or air gap in the direction of the airflow.
$\dot{m}$	[$kg*s^{-1}$] the mass flow rate in a duct.
ν	[m^2*s^{-1}] the kinematic viscosity.
q_{int}	[$W*m^{-2}$] the heat flux from the façade's internal surface to the interior through convection, conduction and longwave radiation.
ρ	[$kg*m^{-3}$] the mass density of a fluid.
σ	[$W*m^{-2}*K^{-4}$] the Stefan-Boltzmann constant.

T_x [K] a surface (x=surf), exterior (x=ext), interior (x=int or room) or gas (x=gas) temperature.

U or U_g [W*m^{-2}*K^{-1}] the center-of-glazing U-value or overall heat transfer coefficient of a façade system.

U_f [W*m^{-2}*K^{-1}] the U-value of the frame of a façade system.

v [m*s^{-1}] a velocity.

Optical properties and variables:

α_x [-] the absorptance of a material or layer in the visible (x=vis) or solar (x=sol) spectral range.

ρ_x [-] the reflectance of a material, layer or system in the visible (x=vis) or solar (x=sol) spectral range. The reflectance can be normal-hemispherical (x=n-h), direct-hemispherical (x=dir-h=d-h) or hemispherical-hemispherical (x=h-h).

τ_x [-] the transmittance of a material, layer or system in the visible (x=vis) or solar (x=sol) spectral range. The transmittance can be normal-hemispherical (x=n-h), direct-hemispherical (x=dir-h=d-h) or hemispherical-hemispherical (x=h-h).

Dimensionless numbers:

Gr [-] the Grashof number.

Nu [-] the Nusselt number.

Pr [-] the Prandtl number.

Ra [-] the Rayleigh number.

Re [-] the Reynolds number.

Abbreviations:

IR Infrared

dir, dif Respectively direct and diffuse radiation

n., hem Respectively normal and hemispherical radiation

1 Introduction

1.1 Context

In 2010, the European Union defined its 2020 goals on the energy performance of buildings in the recast European Energy Performance in Buildings Directive (EPBD) (European Parliament 2010), since the building sector accounted for 40 % of the total energy consumption in the Union: in order to decrease energy dependency and reduce greenhouse effects, the European Union gave ambitious goals for 2020, one of them being that all new buildings have to be nearly zero energy buildings by 31 December 2020 (public buildings by 31 December 2018). Also, on the national levels, new and more restrictive building energy performance regulations appeared in the last decade, such as the Energieeinsparverordnung (EnEV 2009) in Germany (actualized in 2014) or the Réglementation Thermique 2012 (RT2012) in France. More challenging labels for the energy performance of buildings exists, such as the PassivHaus (Passivhaus Institut 2015) or Minergie (Verein MINERGIE 2014) labels. This regulations and labels have always more constraining targets for the building energy demand, with for example the Réglementation Thermique 2012 requiring for example a maximum of 50 $kWh*m^{-2}*yr^{-1}$ of primary energy demand for heating, cooling, artificial lighting, warm water, pumps and fan (slightly variable depending on location, etc.). The PassivHaus regulation implies that the total annual primary energy consumption (heating, cooling hot water and electricity) must not exceed 120 $kWh*m^{-2}$, and an annual heating demand limit of 15 $kWh*m^{-2}$ in heating and cooling energy, or a maximum heat load of 10 $W*m^{-2}$ (PassivHaus Institute 2015). Often, this regulation also give an upper limit for the U-value of insulated opaque walls, such as 0.15 $W*m^{-2}*K^{-1}$ for the PassivHaus label (PassivHaus Institute 2015). The Italian legislative decree No. 311/2006 also aims at maximum reduction in wintertime heat losses and consequently important thermal insulation (Stazi et al. 2009).

The traditional and obvious way to decrease the building heating energy demand is to insulate the surfaces in contact with the exterior. The decrease of this maximum building energy demand allowed by regulations as well as the increasing price of energy implied an increase of the overall insulation thickness and the development of insulation materials. The goal is to minimize conduction, convection and longwave radiation within the material, illustrated by Figure 1 (Kuhn 2015):

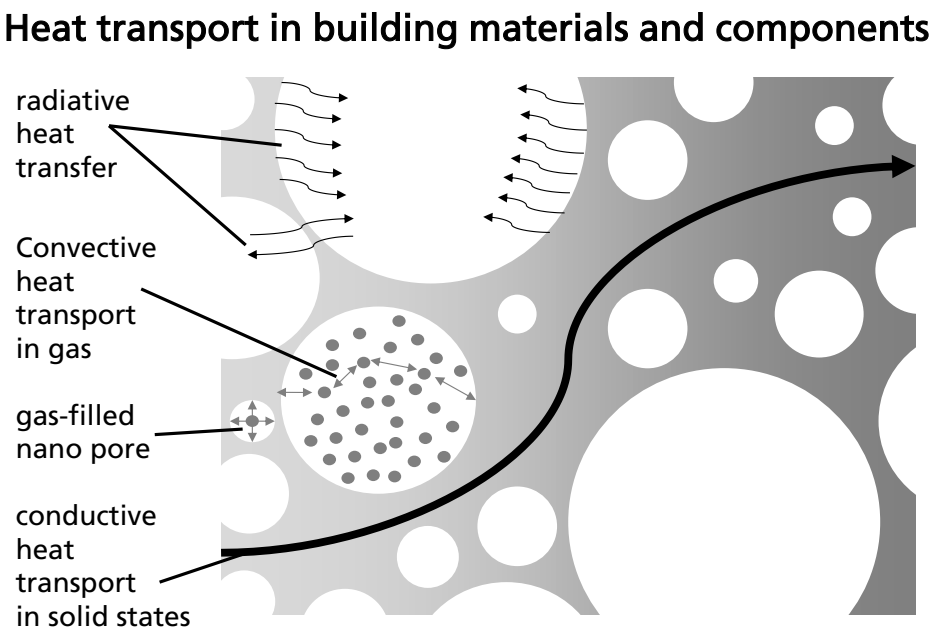

Figure 1 – The different ways of heat transport in building materials: Convection within the gas gaps, thermal conduction via the solid skeleton/solid pore walls (bold black arrow) or the filling gases (small arrows) and thermal radiation heat transfer between the pore walls and through the pore walls in case of IR-transparent materials (curved arrows). These heat transport phenomena are detailed more in section 3.2.2.1.1. Source: (Kuhn 2015).

Traditional insulation materials such as expanded polystyrene (EPS) and extruded polystyrene (XPS) are closed-cell material that use trapped air as the insulating medium, avoiding convection due to the small sizes of the cells. The thermal conductivity of such material is typically between 0.031 $W*m^{-1}*K^{-1}$ and 0.040 $W*m^{-1}*K^{-1}$. Neopor® (BASF 2016) is a further development of XPS where longwave radiation exchange has been minimized by the use of graphite, reducing the longwave transmittance of the cells' walls and thus reaching a thermal conductivity of about 0.031 $W*m^{-1}*K^{-1}$. By using gases with a lower thermal conductivity than air, Polyurethane (PUR) has values typically ranging from 0.020 to 0.030 $W*m^{-1}*K^{-1}$ (Jelle et al. 2010). Innovative products have been developed recently, a good review of them having been done in (Jelle et al. 2010) and (Jelle 2011): vacuum insulation reaches for example conductivities around 0.004 $W*m^{-1}*K^{-1}$ in fresh condition, but could increase to 0.008 $W*m^{-1}*K^{-1}$ after 25 years of use, due to water vapor and air diffusion through the VIP envelope and into the VIP core material which has an open pore structure (Baetens et al. 2010; Jelle 2011). Also, VIP cannot be adjusted by cutting at the building site nor perforated. Gas filled panels (for example with Argon) don't need to be maintained at such a low pressure, but the thermal conductivity is similar to conventional

insulation. Aerogel technologies are also very promising, with commercially available aerogels reaching conductivities down to 0.013 $W*m^{-1}*K^{-1}$: in (Gao et al. 2016), payback times of less than 10 years were calculated compared to a reference with a double glazing unit and assuming an aerogel cost of 4000 $EUR*m^{-3}$. Nanomaterials in general (including aerogels) could achieve thermal conductivities below 0.004 $W*m^{-1}*K^{-1}$: when the pore diameter in the material is decreased below a certain value (40 nm if the gas contained in it is air), the overall thermal conductivity becomes very low: when the mean free path of the gas molecules is larger than the pore diameter, a gas molecule inside a pore is more likely to hit the pore wall than another gas molecule, thus reducing the conduction of heat in the gas. This is known as the Knudsen effect.

Insulation materials and systems are reaching very low thermal conductivities, and insulated facades tend toward really low U-values. Thus, the unwanted heat flux to or from the exterior environment can be avoided. The importance of thermal insulation for the reduction of heat loss in winter is not to be proven anymore. The improvement of the building shell of existing and new residential buildings offers a huge potential for energy savings in the next decades in Europe, as was shown in (Lechtenböhmer und Schüring 2011), providing a country-by-country bottom up simulation of residential buildings for the whole EU and using strong assumptions. Thermal insulation also offers low payback time (Nyers et al. 2015). Conventional internal and external insulation system also proved their durability over time from the thermal–hygrometric and mechanical point of view (Stazi et al. 2009). However, a building envelope with a very low and constant overall U value also reduces beneficial heat fluxes from or to the exterior, which could lead to overheating and discomfort in the building. In the next chapter, these limitations are detailed, leading to the problem statement.

1.2 Problem statement

A high level of insulation can lead to increased cooling load and overheating risks. (Berger et al. 2016) shows for example that with additional insulation in place, the cooling demand in summer increases as it tends to slow down nocturnal cooling processes. In (McLeod et al. 2013), the author summarizes studies on the overheating risks in passive house buildings:

- the occupants of passive house dwellings often report better thermal comfort in winter than in summer, quoting for example (Mlecnik et al. 2012) and . (Berndgen-Kaiser 2010).
  McLeod give numerous example of northern passive houses showing overheating, for example the study of (Larsen und Jensen 2011): for the Danish passive house dwellings considered in this study, the indoor dry bulb temperature exceeded 26°C 40 % of the time during July 2009 and 60 % of the time in 2010, resulting in "severe overheating". One interesting fact is that this overheating was not predicted by the PHPP (Passive House planning package) model of the certified dwellings, but could afterwards be replicated with a dynamic simulation program.

The risk of overheating in these well insulated buildings is highly dependent upon:

- Solar transmission.
- Internal heat gains due to occupancy, light, computers and other auxiliary equipment.
- The presence of a shading device.
- The glazing to wall ratio.
- The orientation of the glazed areas.
- Thermal mass, which plays a clear role in reducing the overall duration of overheating in the passive house.

Of course, not all well insulated building lead to high overheating in summer: McLeod gives also some examples of studies resulting in high levels of occupant satisfaction under summer conditions, with for example results from Schnieders (Jürgen Schnieders und Andreas Hermelink 2006).

In (Feist et al. 2005), measurement results of passive houses in Kronberg (Germany) are presented: for the house analyzed during a hot summer week (outdoor air temperatures up to 34.5°C), it is stated that "there is nothing to feel inside the house from the very strong diurnal variation of the outside air temperature". However, an augmentation of the room air temperatures in the upper floor from 24.3°C to 27.1°C is observed, and the inner air temperatures for both floors almost never fall below 24°C, also during nighttime.

Based on these previous results, it is clear that the risk of overheating and cooling load peaks in well insulated dwellings exists. Numerous solutions exist to reduce this risk as well

as the cooling loads, as for example shading devices such as e.g. external blinds external blinds (Kuhn 2006b) or glazing solutions with reduced g-values (Wilson 2006). Ventilation and free cooling is also a traditional way to reduce the cooling loads. As soon as external air is led into the building, the issues of filtering, pollution, allergies, etc. must be dealt with. Also, mechanical ventilation can lead to substantial additional consumption of electricity to drive the ventilation fan. Opening windows can be effective but can issue a security problem. Also, reducing the internal heat gains can be a simple solution if possible.

In this thesis and additional way to diminish cooling loads and improve summer comfort in well insulated buildings is presented: façade elements with switchable insulation properties, also called switchable insulation. The aim is to be able to reduce the thermal resistances of the façade element during summer time when it is cooler outside, in order to:

- Accelerate the cooling of the building's mass and so reduce the cooling load.
- Diminish the internal surface temperature of the façade, improving the radiant temperature and so the comfort of the occupants.

Also, depending on the climate, a lower thermal resistance towards the exterior can be of advantage during the heating period to profit from warm exterior temperature or solar irradiances. For the European continental climate, this can be the case during sunny winter days.

The following problem statement is investigated by this thesis: can façade elements with switchable thermal resistance reduce the energy demand (heating, cooling, artificial lighting) of a building significantly?

Additionally, how can the effect of a facade with switchable thermal resistance be quantified? How can numerous variants of such a facade be easily compared?

The author does not only want to analyze the general theoretical potential of these elements, but also to contribute to the development of two new components with switchable insulation properties.

While in this section, the examples found in the literature were somehow centered on passive house buildings due to the abundance of available literature, the results of this study will not be limited to passive houses, but to well-insulated building in general.

The study is focused on but not limited to office buildings. Office buildings are interesting targets for switchable insulations since they have high internal heat gains and large window area, leading to important cooling loads, but residential building will also be discussed.

Concerning the climate, the focus is first given to the European continental climates as defined in (Kuhn et al. 2014), with cold temperatures in winter but also warm summers, average annual solar irradiance levels and important day/night variations during the year.

Within this thesis, the term "switchable" refers in priority to the thermal resistance, but could also refer to the solar heat gain coefficient as a by-product.

To present the building energy simulation results, useful energy demand is used. Useful energy is the portion of final energy which is actually available in the building (for example heat produced by a radiator) after final conversion. Compared to primary energy, useful energy is free from primary energy factors (that can vary from one country or standard to another) or energy conversion coefficients.

The work is structured as follow:

- First, the state of the art of existing switchable insulation solutions is reviewed.
- Then, in chapter 2, a new switchable insulation façade system is presented. First, the potential of this new element is investigated on a building level. Second, the technology is characterized experimentally regarding the optical and thermal properties. For the thermal properties, different geometrical and thermophysical variants are measured. The insulation material is also characterized optically. Then, a detailed physical model is introduced and validated to allow a parametric analysis of the new element.
- In chapter 3, a second innovative switchable insulation is introduced: the new facade element is then investigated at different scale, going from one cavity through the definition of the whole façade element to the building simulation. A prototype is also characterized experimentally, as are the longwave properties of the used film material.
- Chapter 4 summarizes the conclusions and findings as well as the main answers to the problem statement and perspectives.
- Chapter 5 gathers the bibliography.
- Chapter 6 presents the list of the author's publications.
- Chapter 7 under the form of Annexes contains results that were not absolutely necessary to achieve the goals but still interesting from a scientific point of view.
- Chapter 8 is an extended French summary.

1.3 Existing solutions: state of the art

In this paragraph, an overview of existing technologies of switchable insulation is presented.

One way to switch the U-value is to change the gas pressure inside a vacuum insulation panel, as presented for example by (Horn et al. 2000). In (Horn et al. 2000) the system, designed for solar heating purposes, is composed by an evacuated stainless steel panel which is filled with a compressible glass fiber mat. A few grams per m² of metal hydride within the panel permit the release (conducting state) and readsorption of a small amount of hydrogen gas. Electric input of less than 5 W/m² is constantly needed in the conducting state to heat the metal hydride to 400°C and release the hydrogen. The switchable panel is described in details in (Caps et al. 1996).This switchable panel is mounted in front of a massive wall. An absorber is applied on the switchable panel, with a glass pane and an air gap to limit heat losses to the exterior:

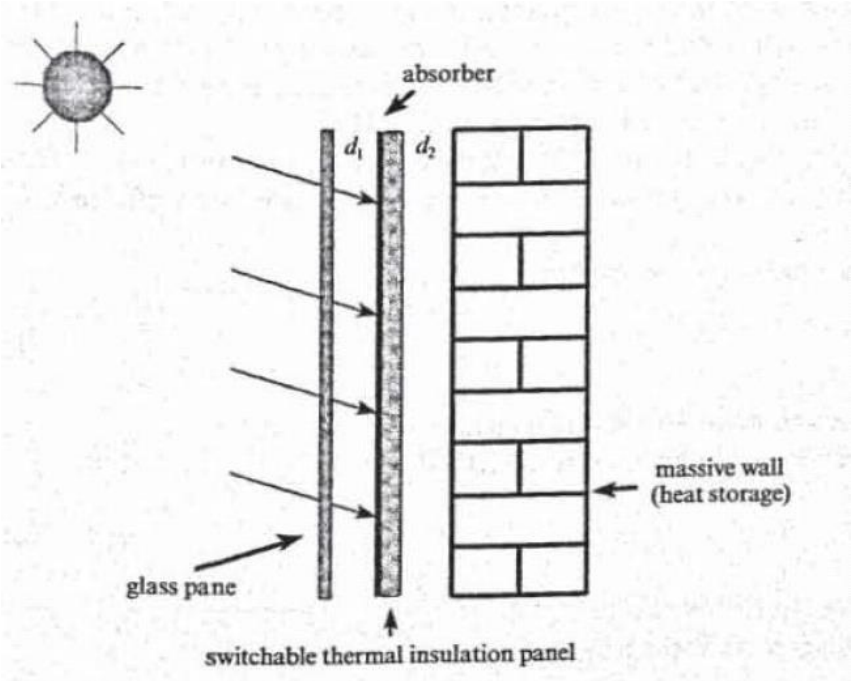

Figure 2 - Switchable thermal insulation panel with metal hydride. Source: (Horn et al. 2000).

The panel is switched to the conductive state either when the difference of temperature between the absorbing surface and the rear surface is superior to a certain value, or when the global solar irradiance incoming at the surface is superior to a given value, in order to maximize the heat gain towards the interior in winter. Taking the weather data of Würzburg, Germany, using the finite-differences method and assuming constant optical properties, the author calculated the heat flux from the wall into the interior at constant temperature of 20°C and recorded it as heat gain over the heating period. The simulation

was performed with the element in front of a 17.5 cm sand-lime bricks wall. From April to September, the panel was kept in insulating state. After optimizing the air gaps thicknesses and using a selective absorber, the influence of the control strategies was investigated. For the temperature-difference based control strategies, the best performance was achieved with the conducting state as soon as $T_{absorber}$-T_{rear}>0, with 136 kWh*m^{-2}. However, if ΔT>25 K is considered, the working hours drop from 1000 hours to 400 hours, while the heat gain only decrease by 9 %. Less working hours could lead to a longer lifetime. With the switching strategy based on irradiance, an identical maximum solar gain of 136 kWh*m^{-2} is reached, if the conductive state is switched on when the irradiance is over 50 W*m^{-2}. Higher limits conduct to important drops in heat gains because larger intensities occur less frequently, while lower limits conduct to heat loss towards the exterior. The limitations of this technology are that 5 W/m² or electrical energy is needed to maintain the conductive state, and the important time of switching process (15 to 60 minutes considered by the author).

(Kimber et al. 2014) presents with a theoretical approach a switchable insulation that is very similar to the concept being investigated in chapter 3. The insulating state is achieved by separating a given air cavity into N smaller air cavities, separated by thin polymer membranes. The conducting state is achieving by physically collapsing the wall and removing the air: the polymer membranes are then compressed into a single layer as shown in following figure:

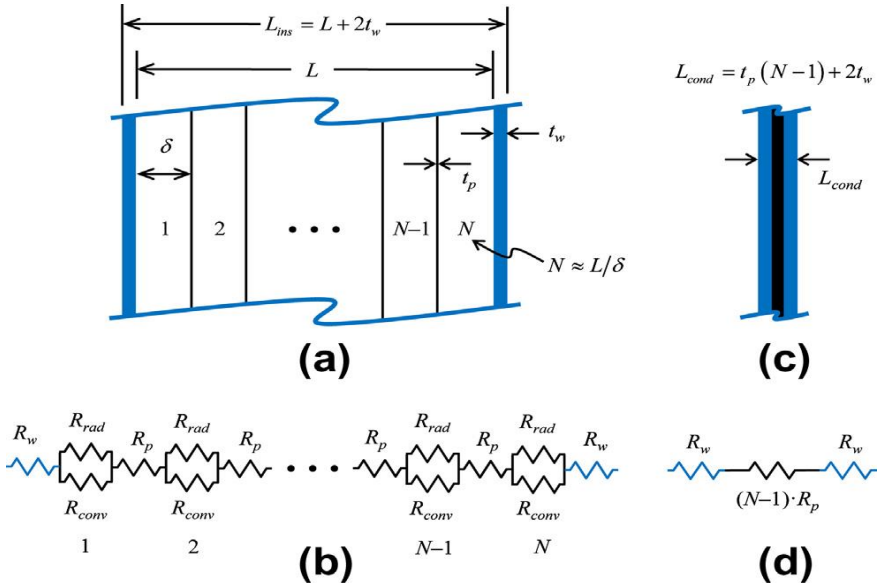

Figure 3 – Schematic drawing of the switchable insulation presented in (Kimber et al. 2014) with N internal air layers: (a) extended wall (insulated) and (c) collapsed wall (conductive) configurations. The corresponding resistance networks used by the author for the heat flow analysis are shown in (b) and (d) for respectively the insulated and conductive configurations. Source: (Kimber et al. 2014).

The presented concept has not been realized yet. The author points out that one of the main fabrication challenges is the actuation method of changing from insulated to

conductive states, and suggest the routing of the ductwork from the HVAC system of the building to inflate the wall for insulation and deflate for conduction purposes.

In (Leppkes und Olbrich 1987, 1988), a transparent cavity can be filled with insulating foam spheres to insulate and for shading purpose. The author advise a bulk density of 100 $kg*m^{-3}$ of foam spheres with a diameter from 4 to 15 mm. An antistatic surface layer is needed on the spheres to allow the complete evacuation of the cavity. Without these antistatic surfaces, the static loads would prevent the complete evacuation. A surface treatment is needed to prevent the antistatic surface layer to lose its efficiency and darken the cavitys' surrounding surfaces by friction. The thermal resistance and shading properties are not specified. Also, no method is given for the filling and emptying of the cavity, and it has most likely to be done manually.

The simplest way of switching insulation is the physical removing of the insulation: in (Sodha et al. 1982), the author presents a solarium which surfaces are covered during off-sunshine hours to prevent heat losses for heating purposes. The sunspace is situated at the south end of the house and is separated from the main house by a thick concrete wall, providing thermal mass. The U-value in the insulating state was assumed as 0.62 $W*m^{-2}*K^{-1}$, and one has to remark that a much lower U-value could be achieved with recent insulation. Taking a single day in January with the weather data of Colorado, U.S.A, the author simulates the thermal behavior of the greenhouse, by applying the Fourier heat conduction equation on the walls and doing an energy balance for the air node of the greenhouse. The author finds out that, if the off-sunshine hours insulation is not applied, the heat flux going from the greenhouse to the main house through the thermal mass decreases by 31 %, and so do the heating gains. Also, the thickness of the massive wall separating the greenhouse from the house's interior had a very important influence on the heat flux to the interior of the house. The advantage of the physical removing of thermal insulation is that it allows the switching between really low U-values to very high U-values comparable to the one of a single-glazing unit. The inconvenient of the physical removing of conventional thermal insulation is that it would need an important mechanical power. Also, the removed insulation has then to be stocked, needing additional room from or next to the building.

In (Shima und Philip 2011), the thermal conductivity of magnetic nanofluids is switched from low to very high values by varying the magnetic field strength and its orientation. Magnetic nanofluids are materials that have the properties of fluid, while having magnetic-dependent properties. However, these technologies are now in an early stage and far away from building-scale applications.

Another method to switch the thermal conductivity is to use nanoporous materials for which even a smaller change in internal pressure produces an important change in the thermal conductivity (Berge et al. 2015). In (Berge et al. 2015), the author states that for materials with small pores below 100 nm, the thermal conductivity changes almost linearly

with a change in the air pressure. This includes aerogels and silica aerogels in particular. However, the thermal conductivities are switched from upper values of about 0.020 $W*m^{-1}*K^{-1}$ for 100 kPa to values to lower values between 0.005 and 0.010 $W*m^{-1}*K^{-1}$ for 1kPa. This upper value is much too low to allow significant cooling or heating of a building through such a surface. Also, no statement is given on the energy consumed by the vacuum pump to create or maintain this low pressure level. The author finally performs a yearly simulation of a well-insulated office building in Sweden with a switchable insulation, using a rough energy balance for each time step. The simulation shows an important decrease of the cooling load with the switchable insulation. However, the U-values used in both the insulating and conducting states are higher than the one achievable with the thermal conductivity measured with the nanoporous materials and variable internal pressure.

In (Stazi et al. 2012), a dynamic insulation, rear-ventilated (naturally) in summer, proved to be the best retrofitting solution for different type of buildings in Italy. The biggest benefits compared to traditional retrofitting solution were the increase in summer comforts:

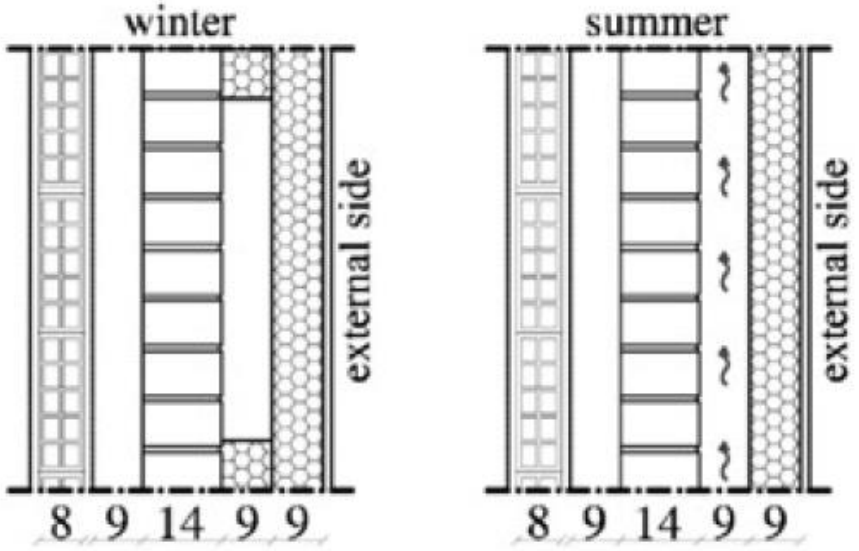

Figure 4 – Dynamic rear ventilated insulation. The internal wall (reference) was a hollow wall brick masonry structure. The numbers indicate thicknesses in centimeters. Source: (Stazi et al. 2012).

Compared to the other retrofitting solutions, it was showed on the basis of dynamic simulation that the variant with rear ventilated insulation produced only 6 % discomfort hours according to the Italian version of (DIN EN 15251:2007), while the external insulation alone showed 37 % discomfort hours and the reference 33 %. The disadvantage of this solution is that the airflow rate and so the cooling rate in the open state varies strongly with wind pressure and temperature difference between massive wall and exterior air. If the wind pressure is superior at the top exit of the cavity, it could counteract the effect of buoyancy and slow down the airflow.

In following table, the precedent studies are summarized and compared:

Year	Reference	Concept	Low U-value [$W*m^{-2}*K^{-1}$]	High U-value [$W*m^{-2}*K^{-1}$]	Experimental or theoretical?	Potential analysis on building level?
1982	(Sodha et al. 1982)	The insulation on the walls and roof is manually removed during nighttime.	0.62	6.02	Theoretical	Yes
1987	(Leppkes und Olbrich 1987)	A cavity can be filled with insulating foam spheres	-	-	Theoretical	No
1996	(Caps et al. 1996; Horn et al. 2000)	Release and absorbtion of hydrogen gas by a metal hydride within a panel	0.3	4.29	Both	Yes
2011	(Shima und Philip 2011)	The thermal conductivity of magnetic nanofluids is varied by applying a magnetic field.	-	-	Experimental	No
2012	(Stazi et al. 2012)	Rear ventilated external insulation	0.26	-	Theoretical	Yes
2014	(Kimber et al. 2014)	Layers separating rectangular air cavities can be collapsed to form a single, conducting solid layer	0.26	3.47	Theoretical, but prototype existing	No
2015	(Berge et al. 2015)	Change of internal pressure in nanomaterial	0.05, assuming a 10 cm thickness	0.2, assuming a 10 cm thickness	Both	Yes

Table 1 – Summary of the different studies on switchable insulations. When only thermal conductivities where given, the U-value was calculated assuming external and internal boundary heat transfer coefficients of respectively 25 and 7.69 $W*m^{-2}*K^{-1}$ (DIN EN 673:2011-04).

Other systems using forced or naturally circulating fluid in the facade exist, but are not the focus of this state of the art since the switching of the thermal resistance is not the purpose of these systems, but rather a by-product: for example, breathable wall, also called dynamic insulation (Taylor et al. 1996) and (Gan 2000), are systems where the air supplied to the room has to go through external porous walls, thus preheating the supplied air. An important group is also mechanically or naturally ventilated facades (Saelens 2012; Poirazis 2008). A comprehensive review of innovative transparent and translucent solar facades, most of them being dynamic, is given in (Quesada et al. 2012). Trombe walls, ventilated or not (Ellis 2003), can be used to increase the solar gains. Building Integrated Solar Thermal (BIST) can be used to produced hot water and influence the g-value and thermal resistances of facade systems (Maurer 2012; Gil-Lopez und Gimenez-Molina 2013; Chow et al. 2010).

To conclude this analysis, it can be seen that switchable insulation is not a completely new concept. However, only a very limited number of systems are ready for the market. Often, experimental data are missing and the analysis is completely done at a theoretical level, as can be seen in Table 1. Also, the potential of these facade systems or new materials has often not been analyzed on a building level. In this thesis, two new switchable insulation façade systems are introduced and investigated, from the building level to the element's level or vice versa. The two elements are also characterized experimentally.

1.4 Performance indicators

Before introducing the new switchable elements in the next chapters, the two main performance indicators used throughout this thesis are presented in this section:

- The U-value, also called U-factor, expressed in $W*m^{-2}*K^{-1}$.
- The g-value, also called solar factor or solar heat gain coefficient (dimensionless).

The U-value, also called U-factor, is the overall heat transfer coefficient that describes how well a building façade element conducts heat. It expresses the rate of heat transfer (in watts) through one square meter of façade element for 1 K temperature difference. The U-value is typically measured with a hot-box apparatus (ISO 8302:1991), and is defined as follow (ISO 15099:2003):

$$U = \frac{1}{R_t} = \frac{1}{\frac{1}{h_e} + \sum R_i + \frac{1}{h_i}}$$

Equation 1

With:

- R_t [m^2*K*W^{-1}] the total thermal resistance of the façade, from the interior (room) to the exterior.
- R_i [m^2*K*W^{-1}] the resistance of the façade's subcomponents such as solid layers, air gaps, etc.
- h_i [$W*m^{-2}*K^{-1}$] the internal boundary heat transfer coefficient between the internal surface of the façade element and the interior environment.
- h_e [$W*m^{-2}*K^{-1}$] the external boundary heat transfer coefficient between the external surface of the façade element and the exterior environment.

In this thesis, values of 7.69 $W*m^{-2}*K^{-1}$ and 25 $W*m^{-2}*K^{-1}$ are used for the characterization of the façade elements, as defined for example in (DIN EN 673:2011-04). This value of 25 $W*m^{-2}*K^{-1}$ for the exterior heat transfer coefficient is very high. In reality, the external heat transfer coefficients that accounts for convective heat transfer (due to buoyancy and/or wind) and longwave radiative heat transfer is often lower. However, this standardized boundary heat transfer coefficients allows the comparison innovative product with traditional window or wall elements, and are therefore used in this thesis. Lower external heat transfer coefficients would result in lower U-values, as the thermal resistance between the façade and the exterior is increased. The impact of lower external boundary heat transfer coefficient is investigated regularly in this thesis.

When solar radiation is considered, or when the resistances of the façade's subcomponent cannot be added like in Equation 1, following definition is more suitable (ISO 15099:2003):

$$U = \frac{q_{int}(I = 0)}{T_{ext} - T_{int}} \qquad \textit{Equation 2}$$

With:

- $q_{int}(I=0)$ [W*m^{-2}] the total heat flux from the interior glass pane towards the room by convection, conduction and longwave radiation, in the absence of solar irradiance.
- T_{ext} [K] the exterior temperature.
- T_{int} [K] the interior temperature.

This definition is further developed in section 2.4.1.2.

The solar heat gain coefficient g is the fraction of the incident solar radiation that enters a room after passing through the building skin. An extensive description of calculation and measurement methods is given in (Kuhn 2015). The g-value is defined as follow (ISO 9050:2003):

$$g = \tau + q_i \qquad \textit{Equation 3}$$

With:

- τ [-] the solar direct transmittance.
- q_i [-] the secondary heat gain, which is the part of incoming solar energy absorbed in the layers of the façade flowing towards the interior of the building by conduction, convection, or longwave infrared radiation.

A more suitable definition for the calculation of façade elements is the following:

$$g = \frac{\tau * I + q_{int} - q_{int}(I = 0)}{I} \qquad \textit{Equation 4}$$

With:

- I [W*m^{-2}] the total irradiance arriving at the element's outer surface
- q_{int} [W*m^{-2}] the total heat flux from the interior glass pane towards the room by convection, conduction and longwave radiation, as defined in Equation 39.
- τ [-] the solar direct transmittance.

If not specified otherwise, the U- and g-values calculated within this thesis are center-of-glazing values which do not take into account the frame effects.

2 Closed movable insulation system

In this chapter, a new way to achieve a switchable insulation is presented and evaluated by simulations and experiments. First, the context as well as the concept of this new façade element is presented. Then, based on first measurement results, the potential of this development is shown on a case study. Numerous thermal and optical measurement results are then presented. Finally, a detailed model of the façade element is presented, validated and used for parametric analysis as well as optimization.

This approach can be perceived as top-down: first, the potential of the new concept is investigated on a building-scale, before going down to the element level. The advantage of the top down method is that a first estimation of the concept's potential on building level could be done in an early stage of the project, before going down to the element level.

2.1 Introduction

The development of the 4 closed movable insulation system took place within the project Wamafat for "Integriertes Wärmemanagement-Fassadenelement" ("Integrated heat-managing façade element"), funded by the BMWi (Germany Federal Ministry for Economic Affairs and Energy) based on a decision by the German Bundestag under the contract ID 03ET1032B. The project partners are BASF, Vinylit (façade providers), LUWOGE consult and Fischer Architekten (Architects), as well as the Fraunhofer ISE. The goal of the project, which started in 2011, was to develop a façade element which could manage the heat in buildings with following goals:

- On cold days:
  - Limit the heat losses
  - Maximize the use of solar gains

- On warm days:
  - Increase Heat transport from inside to outside in comparison with the winter case.
  - Control of solar gains
  - Heat storage

- In the general case: the possibility for active switching of the element between the different modes, depending on the boundary conditions.

During this project, the closed movable insulation system was developed. This basic idea has been filed for a patent (Nestle et al. 2015). The principle of functioning of the façade element is based on controlled convection inside a closed module containing one or several insulating panes. Basically, the element can be in two states, insulating or conducting:

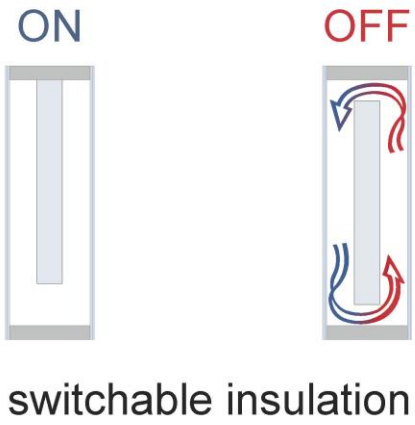

Figure 5 – Translucent switchable facade element in the insulating state (left) and in the conducting state (right).The dimensions are not true to scale. Source: Fischer Architekten.

In the insulating state (left) the insulation panel is at the top. In this state, no large-scale convection around the panel is possible and the element behaves like a system with three insulating layers (two thin air layers and an insulation panel), the convective exchange at the bottom being negligible. This has been shown during the experimental analysis.
In the conducting state (right), the insulation panel is in a vertical middle position, with air gaps at the top and the bottom. In this state, large-scale spontaneous convection around the insulation panes is possible. This large-scale convection is due to the difference of density between the front and back gas column, which results in a driving pressure difference between back and front.

The translucent insulation material used for the test models was Basotect®, which is an insulation and sound absorption material developed by BASF. It is a low-density, open pore melamine foam and has a thermal conductivity at 20°C of 0.035 W/(m*K) (BASF 2014).

2.2 Case study: investigation of the switchable U-value on the building level

To assess energetic benefits achieved with the closed movable insulation system, building-scale simulations were conducted in the building simulation program TRNSYS (TRNSYS 2013). First, the simulation conditions as well as the simplified model are presented, before discussing the simulation results. The case study as well as multiple experimental results have been presented in (Pflug et al. 2015).

2.2.1 Reference: well-insulated office room

The simulation object was a single-room office in Ludwigshafen, Germany.

The office was simulated with a high insulation level, corresponding to the Passive House Standard. In a second step, variants were simulated by replacing part of the facade by our translucent element with switchable U-value.

The simulated office had following geometry:

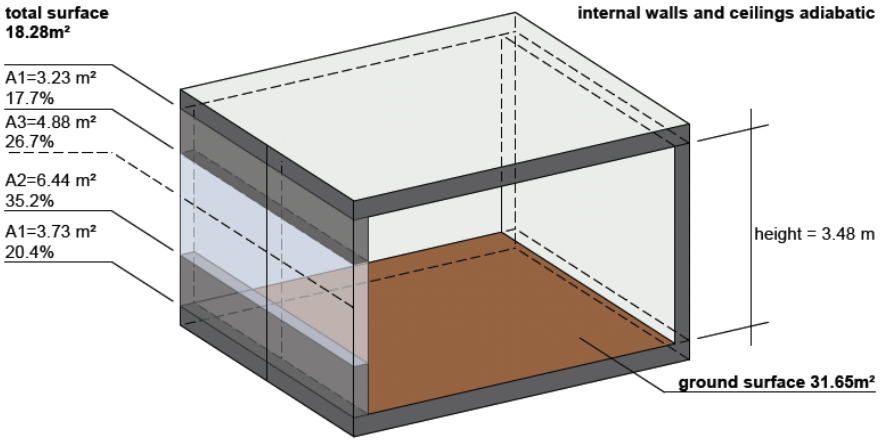

Figure 6 – Simplified geometry of the simulated room. Source: Fischer Architekten.

The external facade is oriented 20° west. The main features of the simulated room are the following:

- All opaque walls (area A1) of the external façade are equipped with insulation, and have a resulting U-value of 0.17 $W*m^{-2}*K^{-1}$. Coldbridges are neglected in this case.
- A2 and A3 are windows with the following features:
  - U_g=1.2 $W*m^{-2}*K^{-1}$
  - g-value=0.42.
  - τ_{vis} =0.71.
  - τ_{sol} =0.39.

- Ratio frame/window=0.3. U_{frame}=2.2 W*m^{-2}*K^{-1}.

The ventilation is equipped with heat recovery (details can be seen in the Appendix).Other simulation conditions are described in the Appendix.

2.2.2 Variants with switchable U-value

Considering the well-insulated reference case, variants were simulated with the new translucent Facade Element with switchable U-value): the upper part of the existing window (starting at 2.2 m from the floor) was replaced by the new translucent element (Area A3 in Figure 6). This represents 4.9 m² and 26.7 % of the external façade. While this part of the façade is only of minor relevance for visual contact to the outside environment, it is highly relevant for the supply of daylight. Scattering elements are advantageous here in the upper part of the facade as they increase light distribution deep into the room.

The solar energy directly transmitted through the façade element was directly calculated as a constant value equals to τ_{sol}*I, with I (W*m^{-2}) being the solar irradiance incoming at the façade and $\tau_{Sol\ the}$ transmittance in the solar range with a value of 0.05. This constant value resulted from the multiplication of the normal-hemispherical transmittance of the three layers (glass, translucent insulation, glass), without taking into account the multiple reflections. A solar transmittance of 0.9 was assumed for glass. For the translucent insulation material, transmittance was taken from the laboratory measurements presented in 2.3.1. This constant value is slightly higher than the value calculated for diffuse incoming solar irradiance or direct solar irradiance at 60° incidence angle, so that it also accounts for direct irradiance at lower altitude angles. In further steps, angle dependent values could be used, as well as the separation of the direct and diffuse light channels.

The heat flux from the element to the interior through convection, conduction and thermal IR radiation, in W/m², is given by:

$$q_{int} = U * (\theta_{ext} - \theta_{int}) + q_i * I \qquad \textit{Equation 5}$$

In the absence of a detailed model of the element at this point, the secondary heat gain q_i was estimated to a constant value of 0.03 in this early stage. This order of magnitude of q_i has been later confirmed by the detailed model (2.4). The parametric study done using the detailed model has shown that the secondary heat gain is almost constant for the different parameters investigated.

The U-values in the insulating and in the conducting states were determined experimentally and depend on the temperature difference between inside and outside. The very extensive and detailed measurement results are detailed in 0. The U-value functions chosen for the simulations were derived from the measurements of the first test models by fitting linear functions to the measurements values:

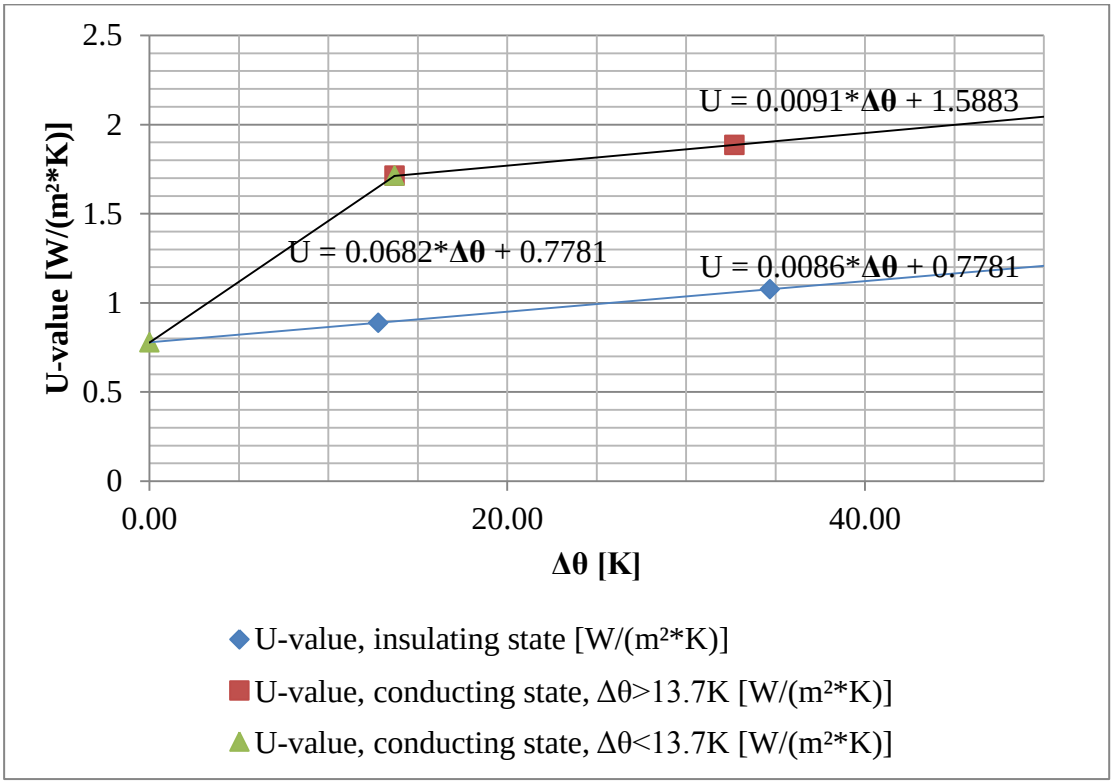

Figure 7 – U=f(ΔT) functions used for the TRNSYS simulations.

These functions were used to calculate the heat transfer through the element for every time step, depending on the temperature difference between room air temperature and exterior air temperature. The influence of the absorbed solar energy on the convective heat transfer has not been considered in this early stage, due to the facts that the absorbed energy in each layer was low and that the high U-value with high temperature differences in summer is mostly activated during night time.

Compared to the reference, following variants have been simulated:

- Variant A: The translucent element has a lower transmission within the solar spectrum, which is 4.5 % instead of 37.7 % for the glazing. The translucent element also has a lower U-value in the insulating state: about 1.0 $W*m^{-2}*K^{-1}$ by a temperature difference of ΔT=25 K instead of U_g=1.2 $W*m^{-2}*K^{-1}$ for the glazing. Thus, without even switching to the high U-value, replacing part of the façade by the translucent element has an influence on the simulation result. This influence is

evaluated with control strategy A, where the U-value is never switched to the high value.

- Variant B: Variant B uses the previously defined U-value functions, with the following control strategy:
    - Heating period :
        - When $T_{ext} > T_{room}$: high U-value.
        - If not, low U-value.
    - Cooling period:
        - When $T_{ext} < T_{room}$: high U-value.
        - If not, low U-value.

  The heating period is defined as the month where the heating load is superior to the cooling load. The rest of the time was then considered as the cooling period.

- Variant C:
  This variant uses the same control strategy as variant B, but 3 $W*m^{-2}*K^{-1}$ is set as a constant value for the high U-value function. This arbitrary value corresponds to non-insulating double glazing. The goal was to simulate the potential of the element, if in the conducting state the convection is optimized or if a small ventilator is used. A small ventilator would allow us to get an U-value quite independent of the difference of temperatures at the boundaries, and would allow us to reach higher U-value due to higher convective heat transfer. This value was not measured in laboratory and is only theoretical.

In order to compare the effect of switching the U-value with a conventional solution: variant A, where the upper part of the window is replaced by the translucent element without switching, was simulated with a free-cooling strategy, in order to compare the effect of free cooling to the switchable U-value. For this variant, the air change rate of the room was raised from 2 to 4 vol/h when the outdoor air temperature was inferior to the indoor temperature. In order not to overcool the building, this strategy is only activated when the outdoor air temperature is above 19°C.

Daylight simulations of the office were made. The outputs of these simulations are the hours in the year where artificial lighting is needed. This output is then read by TRNSYS for every time step. The integration of daylight simulations into thermal simulations allows:

- A much better estimate of the electricity consumption for artificial lighting.
- More realistic values for the heat gains from artificial lighting in the building: when the artificial lighting is need.

For both electricity demand and additional heat gains due to lighting, a constant additional heat gain value of 13 W/m² is assumed as soon as the artificial light is required.

For the daylight simulation, a direct-hemispherical transmission value of τ_{vis}=0.053 was assumed for the façade element, based on the results of optical measurements presented in 2.3.1. To calculate this value, the transmission of glass, translucent insulation and glass were multiplied, without taking into account the multiple reflections and assuming a transmittance of 0.9 for the glass layer in the visible range.

These annual daylight simulations of the reference and the variants were performed using the raytracing software RADIANCE (Building Technologies Department, Lawrence Berkeley Laboratory 2014) in a preliminary step. The hourly outputs where then used in the TRNSYS simulation.

2.2.3 Results and discussion

Reference well-insulated south-oriented room:

The reference room has a low heating demand of 8.1 kWh*m^{-2}*year^{-1}. This corresponds to the Passive-House level. For this well-insulated, south oriented office room, the cooling load then prevails with 28.1 kWh*m^{-2}*yr^{-1}. The room has an office usage with 3 people between 7:00 and 18:00 on working days.

Variants with the translucent element with switchable U-value:

The simulations of the described variants produced following results:

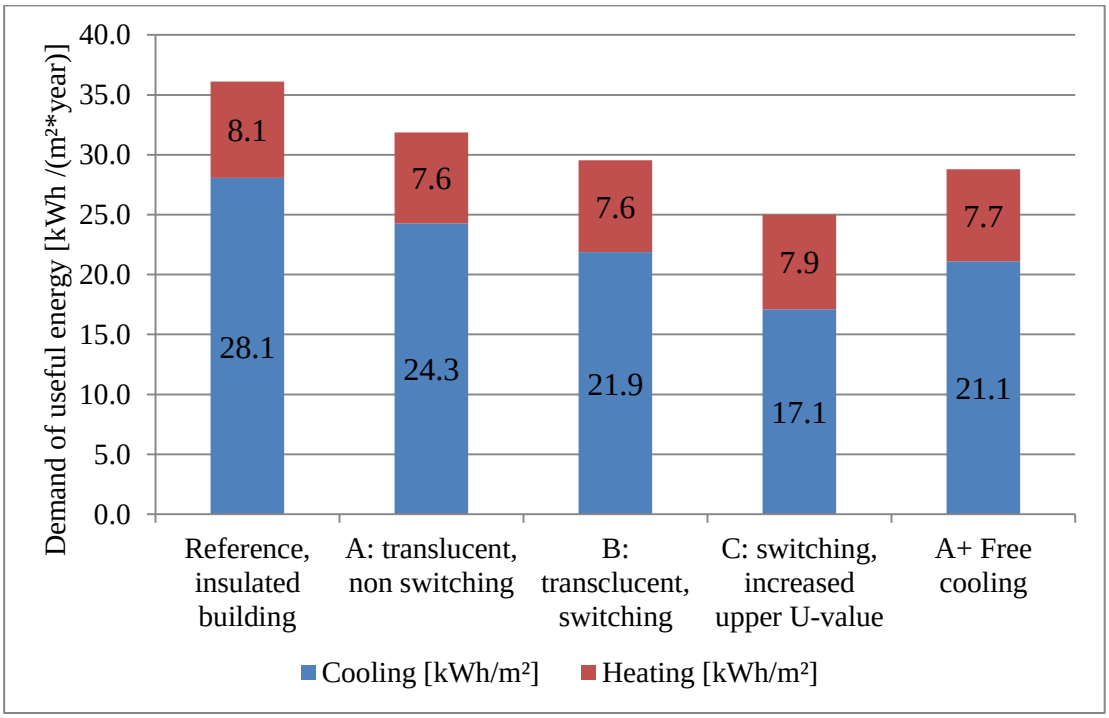

Figure 8 – Annual sum of heating and cooling demands for the insulated reference office and several variants, expressed in useful energy.

The difference between the reference and variant A show us that by replacing part of the glazing by our translucent element without switching, we decrease both the cooling and the heating demand. The decrease of the cooling demand is mainly due to the lower solar transmission, whereas the decrease of the heating demand is mainly due to the higher U-value of the element in the insulated state, compared to the window.

Variant B, where we switched between the high and low U-value, shows a decrease of 9.8 % of the cooling demand compared to variant A. This low reduction of the cooling demand is partly explained by the fact that in Germany, when the outside temperature is lower than the indoor temperature in summer, the difference is often low (under 5 K). According to Figure 7, the U-value is then near to 0.69 W*m^{-2}*K^{-1}, due to the linear

interpolation chosen for this first approach. The assumption is that the heat transfer coefficient of the element with no temperature difference is the same in the insulating and conducting state, because in the conducting state there is no large-scale convection without the driving temperature difference. The consequence is that the heat transfer is low for these small temperature differences. In a further step, the heat transfers in the element have been modeled with a detailed model, showing an important increase of the U-value for low temperature difference.

Variant C, where an element is simulated with forced convection, shows a decrease of 29.6 % of the cooling demand compared to variant A. Compared to the reference, this represents a decrease of 39.1 %. In this case, the high U-value is not temperature dependent.

The comparison of variant A (with translucent element, without switching), variant B (switching U-value) and the free cooling (applied on variant A) shows us that the effect of the switching U-value is comparable with the effect of free cooling with a doubling of the air change rate from 2 to 4 vol*h^{-1}. The savings of cooling demand are respectively 9.8 % and 13 %. In the case of free-cooling, the additional electrical consumption of the fan has to be taken into account. To estimate the additional consumption of the electrical fan, the fan consumption can be estimated at 0.45 W*m^{-3}*h^{-1}, which is the upper limit allowed for a german PassivHaus (Passivhaus Institut 2009). Based on this fan power and on the 1031 hours of functioning of the free cooling function, an additional electrical consumption of 3.2 kWh*$m^{-2*}yr^{-1}$ is calculated. This would more than compensate the thermal gain. To relativize these results, we can point out that the reference air change rate was already quite high (2 vol*h^{-1}).

Concerning the variant B and C, the switch to the high U-value does not occur in the heating period. This is due to the fact than the situation $\theta_{ext}>\theta_{int}$ never occurs during these months for the Ludwigshafen's weather data. During the cooling period, the high U-value is set more than 94 % of the time for variant B and C, so that a biannual control strategy may be considered, with the insulating state during the heating period and the conducting state during the rest of the time. A biannual switching would lead to a slightly variation of the cooling load from 21.89 kWh*m^{-2} to 21.90 kWh*m^{-2} while the heating demand stays the same. Concerning the use of dynamic switching during the cooling period, this is not efficient since when it is warmer outside, the temperature difference to the inside is small, and so the heat transfer coefficient of the element stays low. In this case, a biannual switching seems sufficient.

The influence on comfort has also been calculated, based on the adaptive model of the standard (DIN EN 15251:2007): this standard gives an upper limit for the operative temperature of the room, $\theta_{i\ max}$, depending on the moving average of the external air temperature, θ_{ma}, and includes the fact that the sensibility of people to indoor boundary

conditions depends on the external temperature. This implies that the occupants are able to interact with their environment by opening the windows. Following equations were used:

$$\theta_{\mathrm{i\,max}} = 0.33 * \theta_{\mathrm{ma}} + 18.8 + 3 \qquad \textit{Equation 6}$$

With the moving average θ_{ma} given for a certain day by:

$$\theta_{\mathrm{ma}} = 0.2 * \theta_{\mathrm{ed-1}} + 0.8 * \theta_{\mathrm{am-1}} \qquad \textit{Equation 7}$$

θ_{ma} being the moving average of the external temperature of the day before, and θ_{ed-1} being the mean external temperature of the day before.

In (Kalz und Pfafferott 2014), different adaptive models, including the (DIN EN 15251:2007) model are compared with the Predicted Mean Vote (PMV) static model for eight European buildings. The conclusion were that the comfort requirement are similar in winter, but differ significantly in winter: since with the adaptive model the room temperature setpoints increase with higher ambient temperature, most of the building investigated complied with the limits of the adaptive models, but not with the ones of the static models. Other advantages of adaptive models is that they avoid the strong assumptions which have to be made when using the PMV models, such as the clo and met values, or the local air speed.

In our case, using TRNSYS, following method was used to accurately calculate the inner glass temperature of the façade element and so the operative temperature in the room: the total heat flux to the interior was calculated using Equation 5. Then, this total heat flux was injected for every time step to a virtual window with a very important thermal resistance towards the exterior. The heat flux then integrally flows indoors, and, with the appropriate internal convective and radiative heat transfer coefficients, the correct element surface temperature is calculated. In the conducting state, while this is a good approximation between the two measured U-values, this might lead to differences for the range between no temperature difference and the first measurement point (see Figure 7).

Simulations without cooling have been performed, and the hours of the year where the operative temperature of the room is higher than the limit given by the standard have been summed, as shown in Figure 9 below.

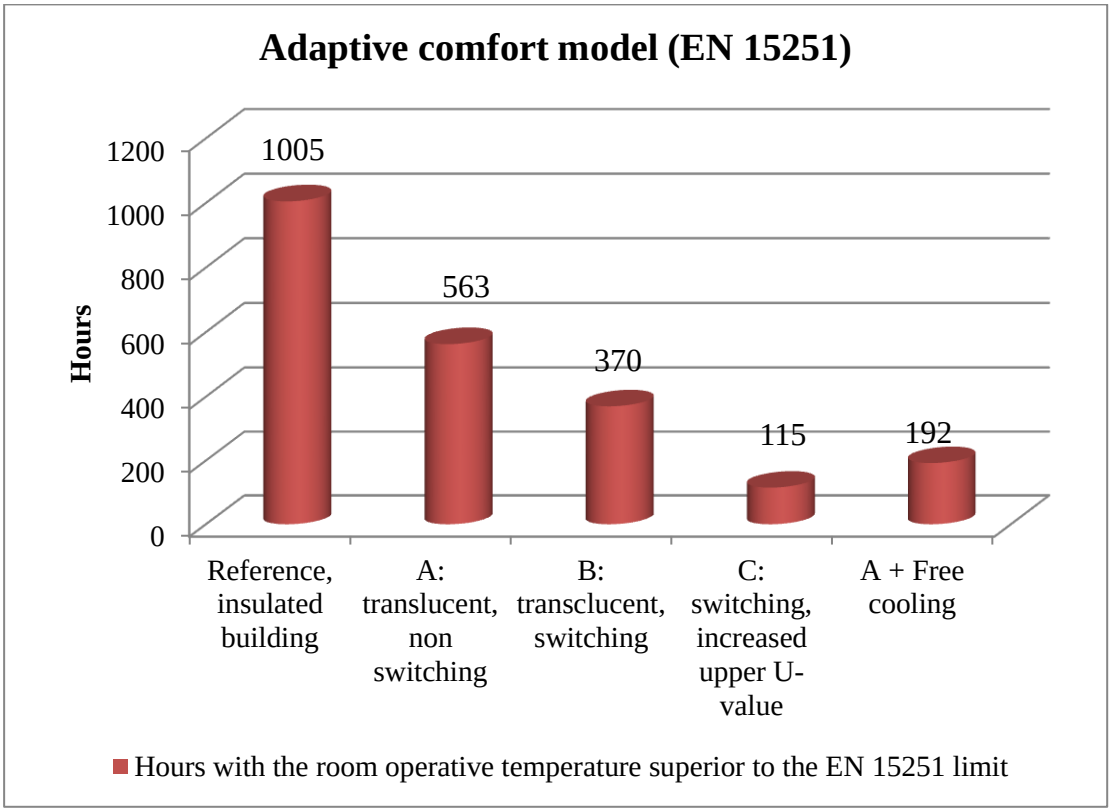

Figure 9 – Hours in the year where the operative temperature is superior to the limit calculated with the DIN EN 15251 standard.

Variant A, where we only replace part of the window by the translucent element without switching to the high U-value, shows a decrease of the hours over variable operative temperature limit. This is due to the lower transmission of the translucent element.

Variant B shows a decrease of more than 193 hours compared to variant A, by switching between the low and high U-value. Variant C shows an even better improvement, with 115 hours of discomfort. Such an element could be even more competitive than a free-cooling strategy. This high impact of the switching on the comfort is due to the high influence of the façade's internal surface temperatures on the operative temperature and on the comfort.

From the daylighting point of view, the replacement of the upper part of the window between the reference and the variants has of course consequences on the artificial lighting demand. Having an element that scatters the incoming light in the upper part of the façade should be of advantage compared to traditional windows since light could be send deeper in the room. However, due to the low visible transmittance of the insulation material, the artificial lighting demand increases from 8.2 $kWh*m^{-2}$ to 13.3 $kWh*m^{-2}$. This overcompensates the positive benefits of the switchable insulation on the cooling load. Possible solutions could be to exchange the translucent insulation material with another with a higher visible transmission, or to reduce the thickness of the insulation layer.

2.3 Experimental study: investigation on the component and material level

In this part, the optical characterization of the translucent insulation material is presented, followed by U-value measurements of different prototypes under difference condition. The goal is to characterize the optical property of the translucent material used, as well as to understand which upper and lower U-values can be reached with the new element as well as the relevant geometrical parameters.

2.3.1 Optical characterization of the translucent insulation material

The translucent insulation material has been characterized optically. The goal was to describe and understand optically this material, as well as too get the inputs needed for the optical calculation done in the case study and for the detailed physical model.

2.3.1.1 Equipment

First, the translucent insulation material has been optically measured with the TAUWIN equipment (Platzer 1987). This equipment is used for angle-dependent direct-hemispherical transmittance measurements. It is used with a 650mm Polytetrafluoroethylene coated integrating sphere with a 100mm diameter opening. The detector is a diode-array spectrometer. The measurement uncertainty for standard (transparent) samples is ±0.01, while the uncertainty of the incidence angle is estimated to ±2°. The RHOWIN equipment is a similar device used for normal-hemispherical reflectance measurement: the sample is then placed within the integrating sphere:

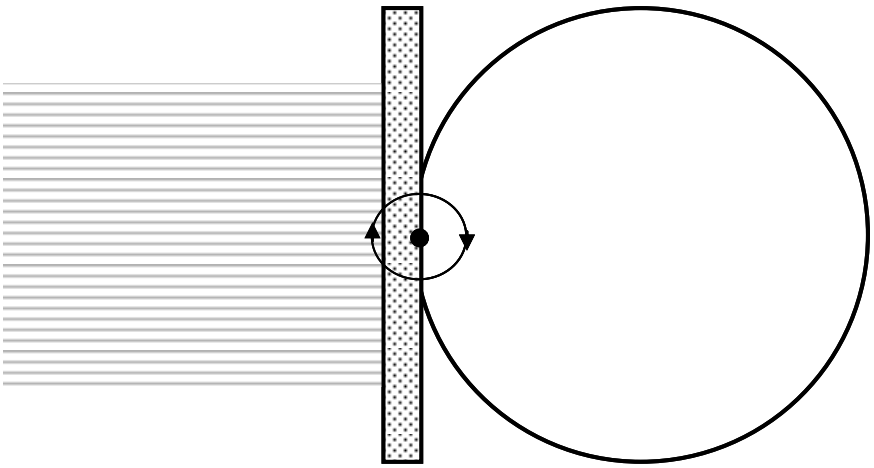

Figure 10 – The "TAUWIN" equipment for measurements of the angle-dependent spectral direct-hemispherical transmittance. The dotted sample is irradiated from the left, transmitted radiation is detected with a spectrometer or broadband sensors on the integrating sphere. Source: (Maurer 2012)

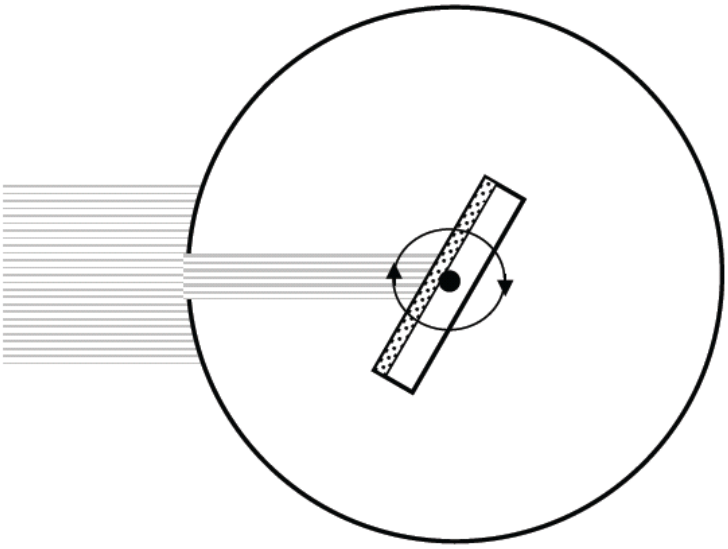

Figure 11 – The "RHOWIN" equipment for measurements of the angle-dependent spectral direct-hemispherical reflectance. The rectangular sample holder is located in the integrating sphere and can be rotated around its center. The back of the sample holder is coated with PTFE and is used for the reference measurements. The detector is a diode-array spectrometer. Source: (Maurer 2012)

2.3.1.2 Measurement issues and uncertainty

By measuring thick, cloudy material, one has to be careful about the material and method used. For the transmittance measurement, using a conventional spectrometer associated with an integrating sphere, like a Lambda900 equipment (also available at ISE), could lead to large underestimating of the transmission values (Wilson et al. 2009).

The Lambda 900 equipment uses a source lamp with a small light ray. The part of the incoming flux going through the sample is integrated into an Ulbricht sphere (also called integrating sphere), where flux sensors are placed.

The crucial point in the case of thick, scattering samples is that a part of the incoming light goes up or down through scattering (A). This part doesn't penetrate the sphere and is not measured by the sensors inside the sphere, which leads to underestimating of the transmission. This effect increases with the thickness of the sample.

The same effect happens with the TAUWIN equipment, but as the incoming irradiance as well as the sample is larger, the part of outgoing flux is compensated by the part entering through the boards of the sample and leaded to the center of the sample through scattering (B).

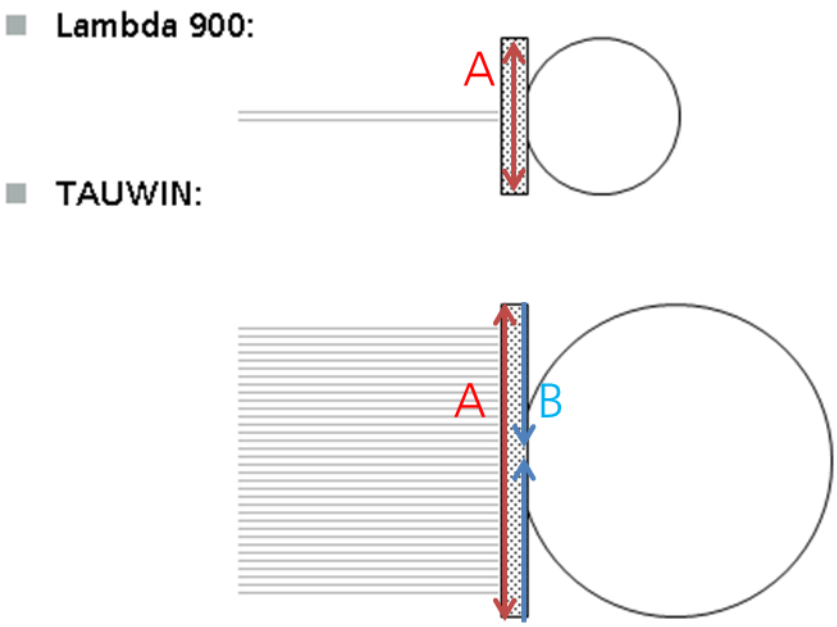

Figure 12 - Differences between Lambda 900 and TAUWIN transmittance measurement equipment. Source: Fraunhofer ISE

Underestimating of the transmission values up to 0.1 have been observed for a 30 mm thick panel of insulation material, measured with Lambda900.

2.3.1.3 Results and discussion

The normal-hemispherical transmittance and reflectance were measured versus the thickness of the insulation layer:

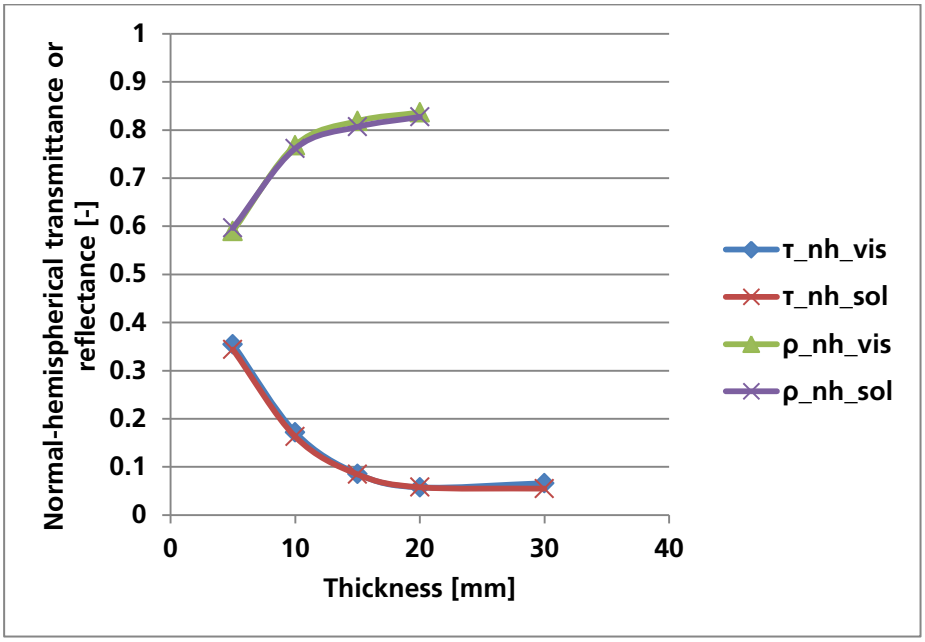

Figure 13 – Normal-hemispherical transmittance and reflectance measured versus the thickness of the transparent insulation layer. Integral values according to EN410. Source: Fraunhofer ISE.

The transmission measurement showed the potential of varying the thickness of the insulation layer in the system to gain daylight: with 5 mm thickness, the Basotect® plate has a visual transmission $\tau_{nh,\,vis}$=0.3548.

For a 15 mm thick translucent insulation layer, the angle-dependent transmittance and reflectance have been measured as well:

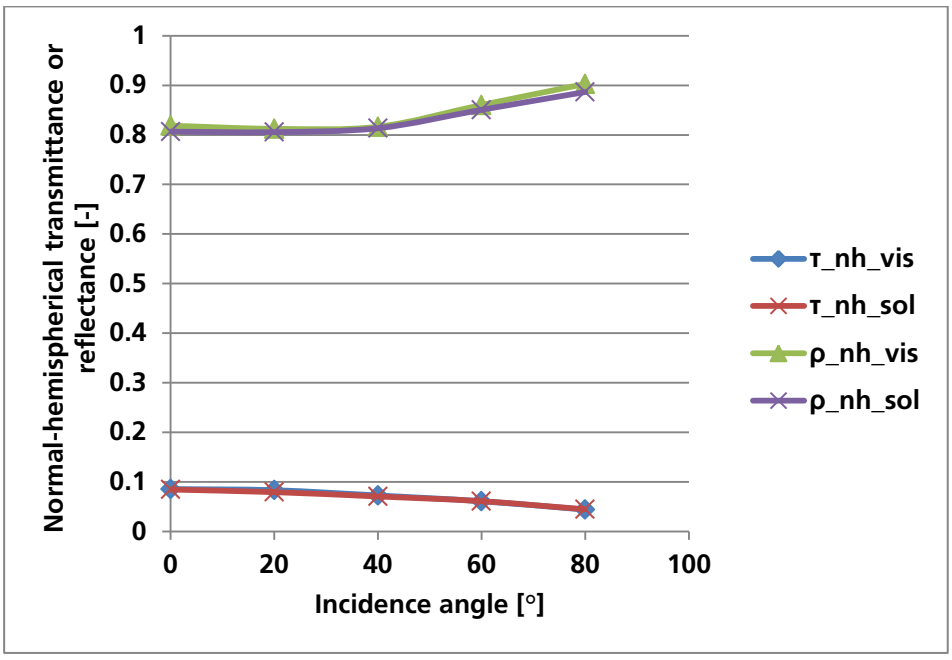

Figure 14 – Normal-hemispherical transmittance and reflectance of the transparent insulation layer measured versus the incidence angle. Integral values according to EN410. Source: Fraunhofer ISE.

The translucent insulation layer used here is very reflective and the transmittance is low. There is a slight angle dependency of these properties, and the reflectance increases strongly after 40° incidence angle. The behavior in the solar and visible spectral ranges is very close. As a matter of comparison, a 10 mm thick granular silica aerogel layer has a normal-hemispherical visible transmittance from 0.43 (for semi-translucent spheres) to 0.85 (translucent fragments), as measured in (Reim et al. 2004).

2.3.2 U-value measurements

Numerous prototypes were designed, built and measured at Fraunhofer ISE. The goal was to assess the potential of this new way of switching U-values as well as to study the impact of different parameter variations.

2.3.2.1 Equipment and uncertainties

The U value was measured in a vertical position in the Taurus equipment (TAURUS instruments – TLP 800 S) at Fraunhofer ISE. The Taurus equipment is a hot plate apparatus in accordance with (ISO 8302:1991). As a difference to the norm, instead of using two samples for each measurement, the second sample was replaced by a reference sample, consisting of a 40 mm thick insulating Styropor plate. The measurement apparatus consists of the test sample and reference sample placed between the electric heater and the two cooling plates. The heat flux leaving the electric heater is measured. The electric heater plates as well as the cooling plates are maintained at constant temperature. Knowing the heat flux leaving the electric heater as well as the two temperature differences at the reference and tested sample and the thermal conductivity of the reference, one can deduct the thermal resistance of the test sample:

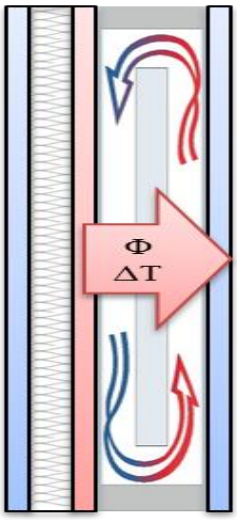

Figure 15 - Schematic drawing of the Taurus apparatus for U-value measurements. From left to right: cooled plate, reference insulating sample, electrical heater, test sample, cooled plate.

The measured values are center of glazing values, the heat flux being measured over a 500*500 mm² central area, and the prototype area being 800*800 mm². For this U-value measurement, the maximal absolute uncertainty was 0.040 $W*m^{-2}*K^{-1}$, the minimal absolute uncertainty was 0.017 $W*m^{-2}*K^{-1}$ and the mean absolute uncertainty was 0.031 $W*m^{-2}*K^{-1}$.

2.3.2.2 Composition of the prototypes

All test models were composed of two 3 mm thick Plexiglas panes, a 20 mm thick PVC frame and a Basotect® pane. The dimensions of the test models are detailed in the result tables:

- A is the thickness of the vertical air layers.
- B is the thickness of the translucent insulation layer.
- C is the dimension of the upper air gap.
- D is the dimension of the lower air gap.

The test models were all measured in a vertical position.

2.3.2.3 Test models with a single insulation pane

The first prototypes were built with a single insulation pane. The test models had no switching mechanism (developed latter), so the models had to be manually modified to switch between insulating and conducting state.

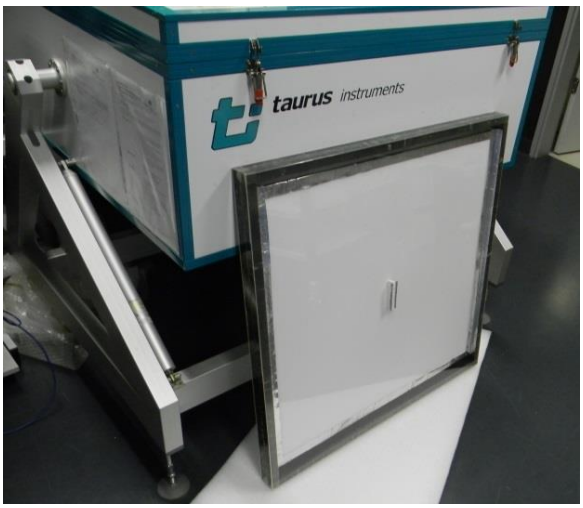

Figure 16 - Test model with a single position pane, in front of the U-value apparatus (in a horizontal position).

This first test model was then measured with two positions of the insulation plate within the test model:

- Translucent insulation pane in the lower position (C=60 mm, D=0 mm).
- Translucent insulation pane in a middle position (C=30 mm, D=30 mm).

Each position was measured with a high (about 35 K) and a low (about 12-15K) temperature difference. The results can be seen in Table 2 below:

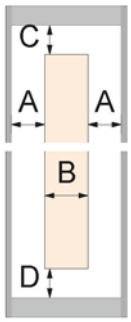

N°	A	B	C	D	ΔT	U-value
-	mm	mm	mm	mm	°C	$W*m^{-2}*K^{-1}$
1I	30	30	60	0	13	0.89
2I	30	30	60	0	35	1.08
3C	30	30	30	30	14	1.71
4C	30	30	30	30	33	1.89

Table 2 – Measurement results of the first test models. I=Insulating state, C= Conducting state.

For the lower temperature difference, a switching of the U-value of +93 % can be observed between the two positions. For the high temperature difference, a switching of the U-value of +75 % can be observed. These measurement values were used for the TRNSYS Simulations.

2.3.2.4 Parameter variation for one plate-test models

New test models were then been built, with a much thinner translucent insulation layer and much thinner total thickness. The goals with these new test models were to have a better translucence and to investigate the influence of several parameters. The direct-hemispherical visible transmittance of a 10 mm Basotect plate, measured with the TAUWIN equipment, is 0.17 (2.3.1.3). The results are presented in Table 3:

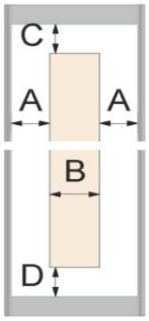

N°	A	B	C	D	ΔT	U-value
-	mm	mm	mm	mm	°C	$W*m^{-2}*K^{-1}$
5I	17.5	10.0	0.0	35.0	15	1.33
6I	17.5	10.0	0.0	35.0	29	1.44
7C	17.5	10.0	17.5	17.5	14	1.72
8C	17.5	10.0	17.5	17.5	29	1.86
9C	30.0	10.0	30.0	30.0	14	1.83
10C	30.0	10.0	30.0	30.0	28	2.03
11C	17.5	10.0	35.0	35.0	14	1.58
12C	17.5	10.0	35.0	35.0	29	1.77
13I	17.5	10.0	0.0	0.0	15	1.31
14I	17.5	10.0	0.0	0.0	34	1.41
15I	17.5	10.0	35.0	0.0	15	1.44
16I	17.5	10.0	35.0	0.0	29	1.57

Table 3 – Measurement results of the second measurement campaign. I=Insulating state, C= Conducting state.

Measurements 5I and 6I are the references in the insulating state: the insulation plate is at the top, with a 35 mm air gap at the bottom. The U-values are 1.33 and 1.44 $W*m^{-2}*K^{-1}$ for respectively the low and the high temperature difference.

Measurements 7C and 8C represent the conducting state, with the insulation panel in the middle. The switching of the U-value represents +29 % for both the low and the high temperature differences. The U-value are respectively 1.72 and 1.86 $W*m^{-2}*K^{-1}$. This decrease in switching compared to the first test models with thicker insulation and thicker air gaps was predictable: indeed, thicker insulation leads to a lower U-value in the insulating state, and in the conducting state, the thermal insulation encourage the temperature difference between the front and back air columns, which is the motor of the convection.

The influence of the thickness of the vertical and horizontal air gaps are investigated with measurements 9C and 10C. Compared to measurements 7C and 8C, the air gaps are now 30 mm thick instead of 17.5 mm. This results in increasing U-value through better large-scale convection between the inner and outer, with U-values of respectively 1.83 and 2.03 $W*m^{-2}*K^{-1}$. More details about these effects are delivered with the detailed model.

The influence of the ratio between the thickness of the horizontal air gap and the thickness of the vertical air gap is investigated with measurements 11C and 12C. In the conducting state, doubling the ratios C/A and D/A results in a diminution of the U-values, with values of 1.58 and 1.77 $W*m^{-2}*K^{-1}$. Compared to measurements 7C and 8C, this represents a decrease of -8 % and -5 %. A possible explanation is that this change of hydraulic diameters causes additional pressure drops, which decrease the airflow rate for the same difference of temperature.

Experiments 13I to 16I were conducted in order to explore the convection effect inside the gap region of the element when switched into the insulating state: compared to measurements 13I and 14I without gaps, the U-value of the element with a gap in the top position (15I and 16I) is about 8 % larger, while the U-value for the gap in the bottom position (5I and 6I) is only 2.5 % larger. Therefore, in the modeling part, the element in the insulating state (with the insulation panel at the top and a small opening at the bottom), it is assumed that the system consists of two closed air cavities and an insulation layer.

2.3.2.5 Test models with two plates

Based on the experiences with the first sets of elements, further test models with two translucent insulation layers were built and measured. A 10 mm additional air gap between the two insulation layers provides additional insulation while not reducing the translucence further.

The results are shown in Table 4:

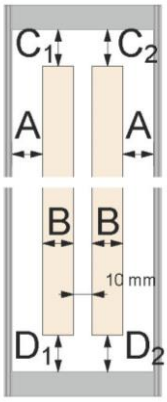

N°	A	B	C_1	C_2	D_1	D_2	ΔT	U-value
-	mm	mm	mm	mm	mm	mm	°C	$W*m^{-2}*K^{-1}$
17I	15	15	30	0	0	30	15	0.71
18I	15	15	30	0	0	30	29	0.80
19C	15	15	15	15	15	15	14	1.44
20C	15	15	15	15	15	15	28	1.60
21I	15	15	0	0	0	0	15	0.72
22I	15	15	0	0	0	0	29	0.80

Table 4 – Measurement results of the test models with two insulation plates. I=Insulating state, C= Conducting state.

Measurements 17I and 18I show the two-plate test model in the insulating state, with the front insulation panel at the top and the back insulation panel to the bottom, to prevent convection. The U-value are respectively 0.71 and 0.80 $W*m^{-2}*K^{-1}$ for the low and high temperature difference. This value can be compared to that of triple glazing.

Measurements 19C and 20C show the two-plate test model in the conducting state, with both insulation panels in a middle position, with air gaps at both ends. The switching of the U-value represents respectively +103 % and +98 % for the low and the high temperature difference. The U-values are then 1.44 and 1.60 $W*m^{-2}*K^{-1}$, which corresponds to a poorly insulating double glazing.

Measurements 21I and 22I where performed using continuous insulation panels, in order to verify that no "slalom" convection occurs in the situation of measurements 17I and 18I. The differences between the two situations are respectively 2.1 % and 1.2 % difference for the low and the high temperature difference.

2.3.2.6 Measurements with CO2

Measurements the elements 17I to 20C were also run with CO_2 instead of air. CO_2 has several advantages compared to air:

- A lower thermal conductivity in the insulating state: 0.0162 $W*m^{-1}K^{-1}$ at 20 °C, 1 atm.
- A lower thermal diffusivity: $105.4*10^{-7}$ m^2*s^{-1}. This favors the convection by carrying the heat away more slowly, allowing the gas to heat. Compared to air, the lower heat capacity (850 $J*kg^{-1}*K^{-1}$ at 20°C) is compensated by a higher density (1.84 $kg*m^{-3}$ at 20°C, 1 atm) and the lower thermal conductivity.
- A lower dynamic viscosity ($14.69*10^{-6}$ Pa*s at 20°C). Compared to air, this also favors the convection.

Particular attention has been paid to the tightness of these test models. Results are shown in Table 5:

N°	A	B	C_1	C_2	D_1	D_2	Cold side	Warm side	ΔT	U-value
-	mm	mm	mm	mm	mm	mm	°C	°C	°C	$W*m^{-2}*K^{-1}$
23	15I	15	30	0	0	30	3.4	18.0	15	0.65
24	15I	15	30	0	0	30	7.4	36.9	30	0.74
25	15C	15	15	15	15	15	4.3	18.0	14	1.45
26	15C	15	15	15	15	15	9.6	37.8	28	1.67

Table 5 – Measurement results with two test models with two insulation panels and CO2. I=Insulating state, C= Conducting state.

Measurements 23I and 24I in the insulating state show a better insulation than the air-filled test models. The difference to measurements 17I and 18I are respectively -8.3 % and -7.5 %, with U-value of 0.65 and 0.74 $W*m^{-2}*K^{-1}$.Measurements 25C and 26C show the two-plate test model in the conducting state, filled with CO_2, with both insulation panel in a middle position and gaps at both ends. The switching of the U-value compared to measurements 23I and 24I represents respectively +123 % and +125 % for the low and the high temperature difference. The U-values are then 1.45 and 1.67 $W*m^{-2}*K^{-1}$.
For the low temperature difference, the value is in the same range as the air value. The better insulation properties counteract the convection-favoring properties. With higher temperature differences, the convection is larger in the CO_2 case, improving the U-value compared to air. So CO_2 showed as expected better performances in both the insulating and the conducting state.

2.4 Detailed physical model: investigation on the component level

Beside the experimental results, a detailed physical model has been developed. The aim was to:

- Test the influence of different parameters.
- Model the thermal behavior of the element depending on the difference of temperature at the boundaries.

2.4.1 Model description

A thermal nodal model is coupled to an airflow model to calculate the U-value and g-value of the element in each case. An optical model was integrated for the calculation of the g-value.

The unknown are the temperatures of each node or solid layer. In case of ventilated gap, three unknown are added: the mass flow rate through the system as well as the mean temperatures of the outer and inner air columns.

The system of equation composed by the thermal and airflow model presented in the next paragraphs was solved using the vba built-in Excel solver.

A schematic description of the physical model for the element in the conducting state is presented on following drawing:

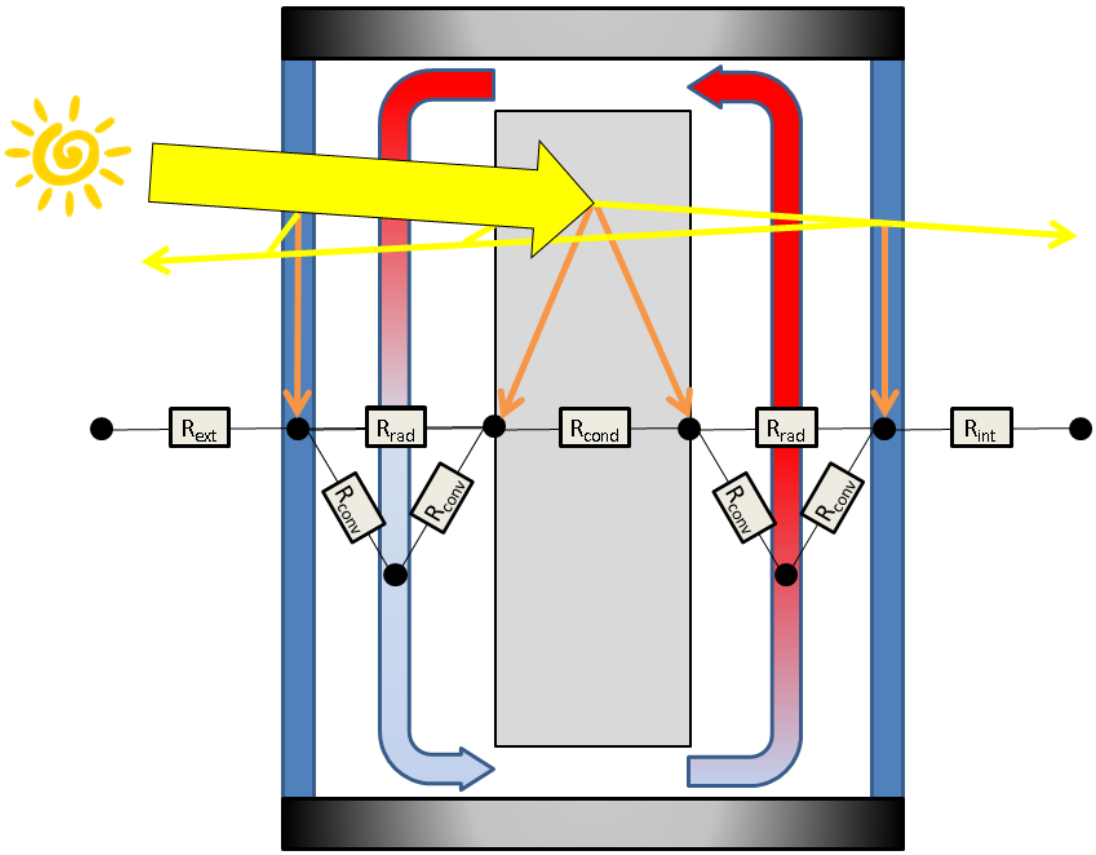

Figure 17 - Schematic drawing of the detailed physical model. The element is in the conducting state. The thermal nodes are represented, as well as the thermal resistance network. The yellow arrows show the solar irradiance which is transmitted or reflected through the system. Multiple reflections are not shown. The orange arrows show the absorbed energy. The thermal resistance are linked to the heat transfer coefficients detailed below by the relation $R=1/h$. The thermal nodes represent, from left to right, the exterior air temperature, the glass temperature, the average fluid temperature of the outer column, the outer and inner surface temperatures of the insulation panel, the average fluid temperature of the inner column, the inner glass temperature and the interior (room) temperature.

A schematic description of the physical model for the element in the insulating state is presented on following drawing:

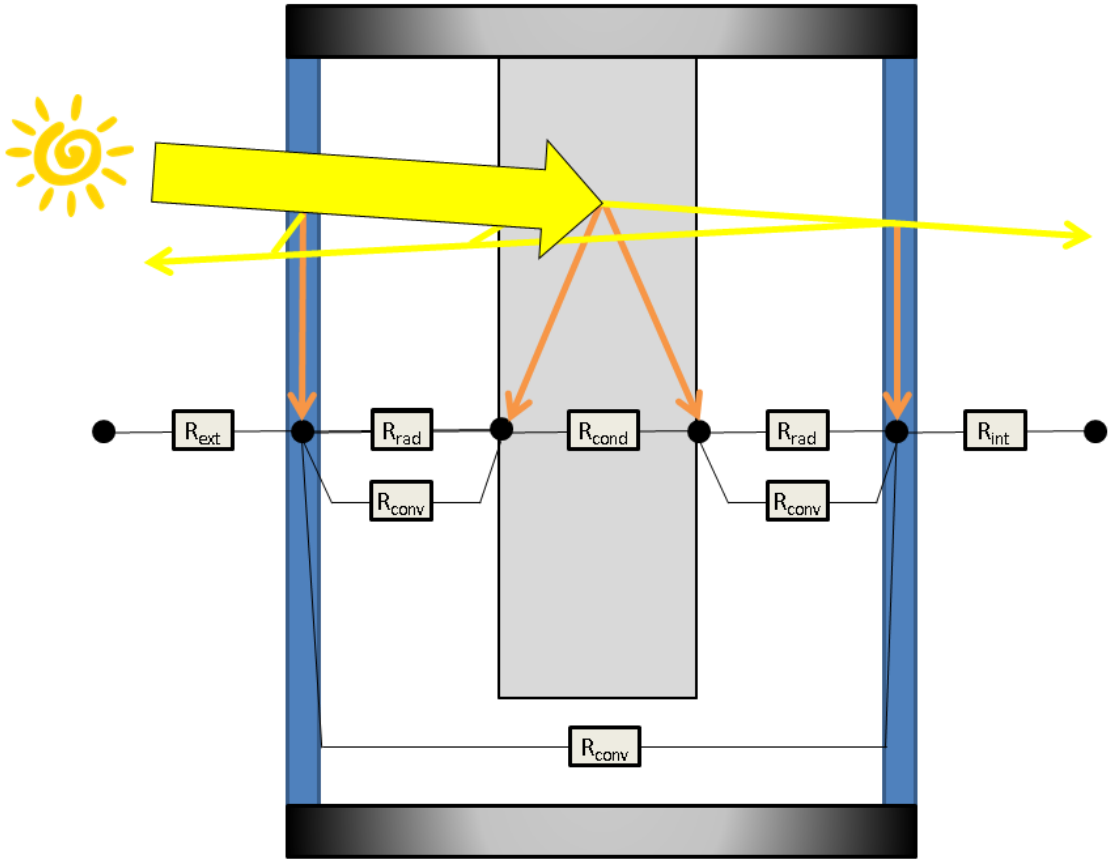

Figure 18 - Schematic drawing of the detailed physical model. The element is in the insulating state. The thermal nodes are represented, as well as the thermal resistance network. The yellow arrows show the solar irradiance which is transmitted or reflected through the system. Multiple reflections are not shown. The orange arrows show the absorbed energy. The thermal resistance are linked to the heat transfer coefficients detailed below by the relation $R=1/h$. The thermal nodes represent, from left to right, the exterior air temperature, the glass temperature, the outer and inner surface temperatures of the insulation panel, the temperature of the internal glass and the interior (room) temperature.

2.4.1.1 Airflow model

For the airflow model, following hypotheses are made:

- Hypothesis 1: the fundamental hypothesis is that the pressure drops in the system are equal to the difference of density (see below) in the system.
- Hypothesis 2: the convection is considered as forced - with the buoyancy force acting as driving pressure- laminar, and hydrodynamically and thermally not fully developed, as detailed below.
- Hypothesis 3: the fluid outlet temperature of one column is the fluid inlet temperature of the other one. In other words, no thermal exchange occurs at the top and bottom horizontal air layers.
- Hypothesis 4: a constant Prandtl number of 0.71 was assumed in the whole system, corresponding to air at 20°C.
- Hypothesis 5: the mass flow is constant in the system, there are no air leakages. During the construction of the prototypes, particular attention was given to airtightness. For convenience, the mass flow rate is converted in airflow rate (m^3*h^{-1}) when presenting results in the following sections.

The nature of the flow (hypothesis 2) has been assessed by verifying following conditions:

- Laminar or turbulent nature of the flow: with a mean Reynolds number of about 300 in the outer air column, the flow is clearly laminar. This calculated value is the mean value of the ten cases in conducting state compared with measurements during validation (2.4.2).

- Forced, natural or mixed convection: the flow can be considered as forced if following condition is verified (Bejan 2013):

$$\frac{\mathrm{Gr}}{\mathrm{Re}^2} \ll 1 \qquad \textit{Equation 8}$$

  With *Gr* the Grashof number in the duct and *Re* the mean Reynolds number in the duct. For the ten cases considered, the mean Gr/Re^2 ratio was 0.11 in the outer air cavity and 0.09 in the inner air cavity. The convection can then be considered as forced for the cases investigated in the validation.

- Thermal and hydrodynamic development of the flow: the flow can be considered as hydraulically developed if following condition is verified (Bejan 2013):

$$L \gg Re * 0.01 * D_h \qquad \textit{Equation 9}$$

With:

- *L* [m] the length of the duct.
- *Re* [- the mean Reynold number in the duct
- D_h [m] the hydraulic diameter of the duct

With a height of the air columns of 0.76 m (for the measured prototypes) and mean *Re**0.01**Dh* values of 0.14 m in both vertical air gaps, the flow pattern cannot be considered as fully hydrodynamically developed.

The flow can be considered as thermally developed if following condition is verified (Bejan 2013):

$$L \gg Pr * Re * 0.01 * D_h \qquad \textit{Equation 10}$$

With a Prandtl number of *Pr*=0.71, it can be concluded that the flow is neither thermally nor hydrodynamically fully developed. This was taken into account for the choice of the correlation to calculate the Nusselt value in the thermal model (2.4.1.2).

The airflow model was built as follows: The main assumption (hypothesis 1) is that the driving pressure difference is equal to the sum of the pressure drops in the system:

$$\Delta P_{driving} = \sum \Delta P_{system} \qquad \textit{Equation 11}$$

The driving pressure of the convection is due to the difference of density between the internal (1) and external (2) vertical air columns, calculated as:

$$\Delta P_{driving} = g * \left| \int_0^H \rho_1(h)dh - \int_0^H \rho_2(h)dh \right| \qquad \textit{Equation 12}$$

With:

- *g*=9.81 [m*s^{-2}] the standard gravity
- *H* [m] the height of the glazed surface
- *h* [m] the height along the vertical axis
- $\rho_1(h)$ and $\rho_2(h)$ [kg*m^{-3}] the density of the fluid in respectively the outer and inner air column at height *h*.

Three types of pressure drops are modelled, with correlations valid for laminar duct flow (Verein Deutscher Ingenieure 2010):

- The pressure drops due to friction with the glass and insulation surface in the vertical columns:

$$\Delta P_{friction} = \frac{\zeta_{gap} * L_{gap} * \rho_{gap} * v_{gap}^2}{2 * D_h} \quad \textit{Equation 13}$$

With:

- ζ_{gap} [-] the drag coefficient in the gap.
- L_{gap} [m] the length of the gap, which can be the height H of the gas columns or the thickness of insulation for the horizontal sections.
- ρ_{gap} [kg*m^{-3}] the density at the gap's mean temperature.
- v_{gap} [m*s^{-1}] the mean velocity in the gap.
- D_h [m] the hydraulic diameter of the gap

ζ_{gap} is given for $Re \leq 2300$ by:

$$\zeta_{gap} = \varphi * \frac{64}{Re} \quad \textit{Equation 14}$$

With:

- Re [-] the Reynolds number in the gas column.
- φ [-] a correcting factor for rectangular ducts instead of round tubes.

For $Re \geq 3000$, ζ_{gap} is calculated by:

$$\zeta_{gap} = 0.3164 * Re^{-\frac{1}{4}} \quad \textit{Equation 15}$$

For Reynolds number between 2300 and 3000, the drag coefficient has been interpolated linearly.

- The pressure drops due to 90° elbows between vertical and horizontal air gaps:

$$\Delta P_{elbow} = \frac{\zeta_{elbow} * \rho_{mean} * v_{elbow,mean}^2}{2} \quad \textit{Equation 16}$$

With the density and velocity taken as the mean between the values before and after the elbow.

ζ_{elbow} has been derivated from (Verein Deutscher Ingenieure 2010):

- If Re_{mean}<1000:

$$\zeta_{elbow} = 10^{29775} * Re_{mean}^{-1.07175} \quad \textit{Equation 17}$$

- If Re_{mean}<1000:

$$\zeta_{elbow} = 0.7 \quad \textit{Equation 18}$$

With Re_{mean} the mean Reynolds number at the elbow.

- The pressure drops due to a reduction or enlargement of cross section between horizontal and vertical gaps, with A_1 and A_2 the sections respectively before and after the change of section, ρ_{mean} as defined above, and v_2 the mean speed after the reduction or enlargement:

  - In case of a sudden widening of section:

$$\Delta P_{widening} = \frac{(\frac{A_1}{A_2} - 1)^2 * \rho_{mean} * v_2^2}{2} \quad \textit{Equation 19}$$

  - In case of a sudden contraction of section:

$$\Delta P_{reduction} = \frac{(\frac{1}{\mu} - 1)^2 * \rho_{mean} * v_2^2}{2} \quad \textit{Equation 20}$$

With:

$$\mu = 0.4924 * (\frac{A_2}{A_1})^2 - 0.105 * \frac{A_2}{A_1} + 0.6066 \quad \textit{Equation 21}$$

2.4.1.2 Thermal model

For the thermal node model, following hypotheses are made:

- Hypothesis 1: the surface temperatures of each layer are assumed uniform over the height and are represented by an energy node. The glass layers are represented by one node, the insulation layer by two surfaces nodes.
- Hypothesis 2: the calculation is steady state (no time-dependency is considered).
- Hypothesis 3: the convective heat transfer coefficients are constant over the height of the glazed and insulation area.
- Hypothesis 4: in the inner and outer air column, the fluid is symmetrically heated by the glass and the insulation, which are at the same mean temperature.
- Hypothesis 5: for the calculation of the g-value, it is assumed that half of the absorbed solar energy in the insulation layer is absorbed at the outer surface and half is absorbed at the inner surface. In reality, more solar energy is absorbed towards the outer surface, which would lead to lower g-values in reality.
- Hypothesis 6: In the insulating case, the two vertical cavities were considered as two closed air columns. The validity of this hypothesis has been shown during the experimental analysis (0), with only 2.5 % difference in the insulating state between the insulation panel at the top and an insulation panel going from the top to the bottom without horizontal air gap.
- Hypothesis 7: the conductive thermal resistance of glass is neglected.
- Hypothesis 8: for the radiative longwave exchange, the hypothesis of infinitely long parallel, grey-diffuse surface is made. The grey-diffuse approximation means, that it is assumed, that the spectral emissivities of the surfaces are independent from the wavelength (grey surface) and the direction of the reflected or emitted radiation (diffuse surface).

The boundary conditions are given by:

- Internal and external air temperatures T_{int} and T_{ext} [K].
- Constant internal and external heat transfer coefficients h_{int} and h_{ext} [W*m^{-2}*K^{-1}] of respectively 7.69 and 25 W*m^{-2}*K^{-1}, as given for example in (DIN EN 673:2011-04).

For simplification purposes, the convective exchange between air and the insulation layer takes place over the whole cavity height, which is slightly higher than the insulation layer height. This hypothesis is justified by the fact that there is more heat flux exchange between glazing and fluid than between insulation and fluid.

Each layer is represented by one or several energy nodes. For each node, an energy balance is performed to determine the temperature of the node. For example, for a one insulation layer façade element in the conducting state, following equations are applied, resulting from the energy balances:

$$\begin{gathered} h_{ext} * \left(T_{outer\ glass} - T_{ext}\right) \\ +h_{rad,outer\ gap} * \left(T_{outer\ glass} - T_{ins.,outer\ surf.}\right) \\ +h_{cv\ vent,outer\ gap} * \left(T_{outer\ glass} - T_{air,outer\ gap}\right) \\ = \alpha_{e,sol,ext.glass} * I \end{gathered} \qquad \textit{Equation 22}$$

This can be written as:

$$\begin{gathered} T_{outer\ glass} = \\ \frac{h_{ext} * T_{ext} + h_{rad,outer\ gap} * T_{ins.,outer\ surf.} + h_{cv,vent,outer\ gap} * T_{air,outer\ gap}}{h_{ext} + h_{rad,outer\ gap} + h_{cv,vent,outer\ gap}} \\ + \frac{\alpha_{e,sol,ext.glass} * I}{h_{ext} + h_{rad,outer\ gap} + h_{cv,vent,outer\ gap}} \end{gathered} \qquad \textit{Equation 23}$$

Or for the outer surface of the insulation layer:

$$\begin{gathered} \frac{\lambda_{ins.}}{d_{ins.}} * \left(T_{ins.,outer\ surf.} - T_{ins.inner\ surf.}\right) \\ +h_{rad,outer\ gap} * \left(T_{ins.,outer\ surf.} - T_{outer\ glass}\right) \\ +h_{cv,vent,outer\ gap} * \left(T_{ins.,outer\ surf.} - T_{air,outer\ gap}\right) \\ = \frac{\alpha_{e,sol,insu.} * I}{2} \end{gathered} \qquad \textit{Equation 24}$$

Or:

$$\begin{gathered} T_{ins.,outer\ surf.} = \\ \frac{\frac{\lambda_{ins.}}{d_{ins.}} * T_{ins.inner\ surf.} + h_{rad,outer\ gap} * T_{outer\ glass}}{\frac{\lambda_{ins.}}{d_{ins.}} + h_{rad,outer\ gap} + h_{cv,vent,outer\ gap}} \\ + \frac{h_{cv,vent,outer\ gap} * T_{air,outer\ gap} + \frac{\alpha_{e,sol,insu.} * I}{2}}{\frac{\lambda_{ins.}}{d_{ins.}} + h_{rad,outer\ gap} + h_{cv,vent,outer\ gap}} \end{gathered} \qquad \textit{Equation 25}$$

With:

- T_{ext} [K] the external boundary air temperature
- $T_{outer\ glass}$ [K] the temperature of the outer glass pane
- $T_{air,outer\ gap}$ [K] the average air temperature of the outer air column
- $T_{ins.,\ outer\ surf.}$ [K] the outer surface temperature of the insulation panel
- h_{ext} [W*m^{-2}*K^{-1}] the external boundary heat transfer coefficient

- $h_{rad,outer\ gap}$ [W*m^{-2}*K^{-1}] the radiative heat transfer coefficient between the outer glass and the outer surface of the insulation layer
- $h_{cv,vent,outer\ gap}$ [W*m^{-2}*K^{-1}] the average convective heat transfer coefficient between the outer air gap and the outer surface of the insulation layer, in case of ventilated cavity, as defined below.
- $\alpha_{e,sol,ext.glass}$*I [W*m^{-2}] the total (or effective) solar energy absorbed in the external glass layer, as calculated in 2.4.1.3.
- $\alpha_{e,sol,insu.}$*I [W*m^{-2}] the total (or effective) solar energy absorbed in the translucent insulation layer, as calculated in 2.4.1.3.
- $\lambda_{ins.}$ [W*m^{-1}*K^{-1}] the thermal conductivity of the insulation layer
- $d_{ins.}$. [W*m^{-1}*K^{-1}] the thickness of the insulation layer

In the conducting case, the hypotheses made above lead to a differential equation resulting in an exponential temperature profile in each column. This method is presented for example in the standard (ISO 15099:2003). For a very thin (infinitely thin) vertical section of the air column, an energy balance is made:

$$\mathrm{h_{cv,vent} * \left(T_S - T_{gas}(z)\right) * 2 * w * dz = \dot{m} * C_p * dT_{gas}} \qquad \textit{Equation 26}$$

With:

- $T_{gas}(z)$ [K] the temperature of the gas at the distance z of the column inlet.
- T_s [K] the mean temperature between the two surrounding surfaces.
- w [m] the width of the glazed area.
- dz [m] the height of the infinitely thin vertical section.
- $\dot{m}$ [kg*s^{-1}] the mass flow rate in the column.
- C_p [J*kg^{-1}*K^{-1}] the specific heat of the gas at the cavity gas temperature T_{gas} (see Equation 30).
- dT_{gas} [K] the temperature difference between the inlet and outlet of the very thin vertical section.

This equation can be written as:

$$\frac{\mathrm{dT_{gas}}}{\mathrm{dz}} = -\frac{\mathrm{h_{cv,vent} * 2 * w}}{\dot{\mathrm{m}} * \mathrm{C_p}} * \mathrm{T_{gas}(z)} + \frac{\mathrm{h_{cv,vent} * 2 * w}}{\dot{\mathrm{m}} * \mathrm{C_p}} * \mathrm{T_S} \qquad \textit{Equation 27}$$

To solve this linear differential equation, the following initial condition is used:

$$\mathrm{T_{gas}(z = 0) = T_{gas,inlet}} \qquad \textit{Equation 28}$$

$T_{gas,inlet}$ being the gas entrance temperature. For the outer air column, it is the outlet air temperature of the inner air column and vice-versa.

The solution is then:

$$T_{gas}(z) = \left(T_{gas,inlet} - T_S\right) * e^{-\frac{2*h_{cv,vent}*w}{\dot{m}*C_p}*z} + T_S \qquad \textit{Equation 29}$$

The thermal equivalent temperature of the gas cavity is calculated by:

$$T_{gas} = \frac{1}{H}\int_0^H T_{gas}(z)dz = T_S - \frac{\dot{m} * C_p}{2 * h_{cv,vent} * w * H} * \left(T_{gas,outlet} - T_{gas,inlet}\right) \qquad \textit{Equation 30}$$

With $T_{gas,\ outlet}$ [K] the cavity gas outlet temperature, equal to $T_{gas}(H)$.

The convective heat transfer coefficient is given by:

$$h_{cv,vent} = \frac{Nu * \lambda}{D_h} \qquad \textit{Equation 31}$$

With:

- *Nu* [-] the Nusselt number in the gap.
- λ [W*m^{-1}*K^{-1}] the thermal conductivity of the gas at the cavity gas temperature T_{gas} (see Equation 30).
- D_h [m] the hydraulic diameter of the gap.

In the open, conducting case, the vertical air columns enclosed between the insulation panels and the glass panes are considered as a ventilated duct. The Nusselt number in the gap, characterizing the convective heat transfer between the air and the two limiting surfaces, is calculating using following correlation for laminar forced convection in the entrance region of a parallel-plate duct (Bejan 2013) with uniform temperature:

$$Nu = 7.55 + \frac{0.024 * (Re * Pr * \frac{D_h}{H})^{1.14}}{1 + 0.0358 * (Re * Pr * \frac{D_h}{H})^{0.64} * Pr^{0.17}} \qquad \textit{Equation 32}$$

With:

- *Pr* [-] the Prandtl Number of the fluid.
- *H* [m] the height of the vertical air channel.
- *Re* [-] the Reynold Number in the gap.

The laminar and forced nature of the flow has been investigated in 2.4.1.1. During the validation process, the validity of the symmetrical heating hypothesis is discussed.

For the ventilator-driven cases simulated, the Gnielinski correlation was used for Reynolds number superior to 2300 (Bejan 2013):

$$\mathrm{Nu} = \frac{\mathrm{f}}{2} * (\mathrm{Re} - 1000) \; * \; \frac{\mathrm{Pr}}{1 + 12.7 * (\mathrm{Pr}^{\frac{2}{3}} - 1) * (\frac{\mathrm{f}}{2})^{0.5}} \qquad \textit{Equation 33}$$

With the friction factor *f* defined as:

$$\mathrm{f} \; = \; (1.74 \; * \; \log(\frac{\mathrm{D_h}}{\mathrm{k_s}}) \; + \; 2.28)^{-2} \qquad \textit{Equation 34}$$

The factor k_s=0.003 [m] being the grain size with regards to the pipe's roughness.

In the insulating case, the two vertical cavities were considered as two closed air columns. Following correlation is then used (Wright 1996):

$$\mathrm{h_{cv,closed}} = \frac{\mathrm{Nu} * \lambda}{\mathrm{d}} \qquad \textit{Equation 35}$$

$$\begin{gathered} \mathrm{Nu} = \max(Nu_1, Nu_2) \\ \text{if } \mathrm{Ra} > 5 * 10^4\text{:} \;\; \mathrm{Nu_1} = 0.0673838 * \mathrm{Ra}^{\frac{1}{3}} \\ \text{if } 10^4 < \mathrm{Ra} \leq 5 * 10^4\text{:} \;\; \mathrm{Nu_1} = 0.028154 * \mathrm{Ra}^{0.4134} \\ \text{if } \mathrm{Ra} \leq 10^4\text{:} \;\; \mathrm{Nu_1} = 1 + 1.7596678 * 10^{-10} * \mathrm{Ra}^{2.2984755} \\ \mathrm{Nu_2} = 0.242 * (\frac{\mathrm{Ra}}{\mathrm{A_r}})^{0.272} \end{gathered} \qquad \textit{Equation 36}$$

With:

- *d* [m] the thickness of the gas cavity.
- *Ra* [-] the Rayleigh number in the gas cavity.
- $A_r = \frac{H}{d}$ [-] the aspect ratio of the gas cavity.

For the elements with two insulation layer separated by a thin vertical air column, this air column was also considered as a closed cavity, both in the conducting and insulating state.

Finally, following correlation was used to calculate the radiative longwave heat transfer coefficients between two infinite parallel, grey-diffuse surfaces (Duffie und Beckman 2006):

$$h_{rad} = \sigma * \left(\frac{1}{\frac{1}{\varepsilon_1} + \frac{1}{\varepsilon_2} - 1} \right) * \frac{T_1^4 - T_2^4}{T_1 - T_2} \qquad \textit{Equation 37}$$

With:

- σ= 5.67*10-8 [W*m^{-2}*K^{-4}] the Stefan-Boltzmann constant.
- ε_1, ε_2 [-] the longwave emissivities of both surfaces.
- T_1, T_2 [K] the temperature of both surfaces.

After solving the system of equations, the U-value was calculated as follow (ISO 15099:2003):

$$U = \frac{q_{int}(I = 0)}{(T_{ext} - T_{int})} \qquad \textit{Equation 38}$$

$q_{int}(I=0)$ [W*m^{-2}] being the total heat flux from the interior glass pane towards the room by convection, conduction and longwave radiation, in the absence of solar irradiance, defined as:

$$q_{int} = h_{int} * (T_{inner\ glas} - T_{ext}) \qquad \textit{Equation 39}$$

With:

- h_{int}=7.69 [W*m^{-2}*K^{-1}] the internal boundary heat transfer coefficient, as defined for example by (DIN EN 673:2011-04)
- $T_{inner\ glass}$ [K] the inner glass pane temperature
- T_{int} [K] the interior air temperature
- T_{ext} [K] the exterior air temperature

For the purpose of the parametric analysis, the U-value with the constant boundary heat transfer coefficients to the interior and exterior environment allows the comparison between different variants. Of course, for the purpose of building simulation, the convective and radiative parts have to be dealt with in a more detailed way.

2.4.1.3 Optical model

In this part, the calculation procedure of the solar energy absorbed in each layer is detailed, as well as the total transmitted solar energy and the calculation of the g-value. Following hypotheses were used:

- Hypothesis 1: For the purpose of the parametric analysis, we assume that the incoming solar energy is completely diffuse. The consequence is that hemispherical-hemispherical transmittance and reflectance values can be used for the glass and translucent insulation layers. This could correspond to a cloudy day. Also, the hemispherical-hemispherical transmittance and reflectance values of the outer glass pane are near to the direct-hemispherical values at an incidence angle of 60° (Roos et al. 2001): $\rho_{dir\text{-}h,\ glass,\ 60°}$=0.143, $\rho_{hh,\ glass}$= 0.136, $\tau_{dir\text{-}h,\ glass,\ 60°}$=0.749, $\tau_{hh,\ glass}$=0.753 (values in the solar spectrum taken for 3 mm clear glass from (Lawrence Berkeley National Laboratory 2015)). Also, for the translucent insulation material, the measured $\tau_{dir\text{-}h,\ trans.\ insu.,\ 60°}$ value of 0.061 is near to the calculated $\tau_{hh,\ trans.insu.}$ value of 0.067. The calculated g-value for diffuse incoming light could then be extended to a case with completely direct solar irradiance with high incidence angle (as for example in a clear-sky summer day).
- Hypothesis 2: In the absence of angle-dependent measurement data for translucent insulation material with thicknesses different from 15 mm, the ratio between the direct-hemispherical values measured at 60° (see 2.3.1) and the hemispherical-hemispherical values is assumed constant for all thicknesses. To calculate the hemispherical-hemispherical transmittance and reflectance values of the translucent insulation layer with different thicknesses, the angle-dependent transmittance and reflectance values of the 15 mm translucent insulation layer have been used, as detailed in this chapter.
- Hypothesis 3: The integral values according to (EN 410:2011) have been used, assuming that the optical properties do not strongly vary with the wavelength. To get a slightly better accuracy, wavelength-dependent value could be used.

To calculate the part of incoming diffuse solar energy absorbed in each layer, as well as the overall transmittance of the element, different state of the art methods are available: these methods go from raytracing over multiplication of matrixes containing optical information towards simplified models. Raytracing, using for example Radiance (Larson und Shakespeare 1998), e.g. enables to simulate complex blind geometries, display shadows in the room or the repartition of daylight, etc. at the cost of heavy computational requirement. The Bi-directional Scattering Distribution Functions (Klems 1994a, 1994b) are a simplified way to represent the optical properties of layers or systems in matrixes. They are also several simplified models to calculate the absorbed energy in each layer as well as the g-value of fenestration systems. In following table, a summary of this simplified model is exposed:

Reference and purpose	**Thermal heat transfer and optical calculation**	**Hypotheses**
(ISO 15099:2003) Thermal performance of windows, doors and shading devices – Detailed calculations U-value, g-value (not directly) optical properties and solar transmittance	Thermal heat transfer: Nodal model: for each layers, 4 unknown: the front and back temperatures, the front and back radiosities. Optical calculation: Wavelength-dependent if wavelength-dependent data are available for each layer. A method is proposed based on a balance for each layer I+/I- for each layer (based on ISO9050) For blinds, equations are proposed to determine the optical properties of slat type blinds, but the view factors are missing. It is then distinguished between the three channels dir/dir, dir/dif, dif/dif.	Isothermal layers Heat transfer coefficients constant over the height Solar energy absorbed in center of layer For slats: the reflected radiation is diffuse
(EN 410:2011) Determination of luminous and solar characteristics of glazing g-value Optical properties	Thermal heat transfer: For the calculation of the secondary heat gain, the energy absorbed in each layer is used as well as an overall constant heat transfer coefficient between glazing calculated with EN673. Optical calculation: If wavelength dependent data are available, the overall transmittance and reflectance, as well as the energy absorbed in each glazing can be calculated. This is based correlations derived from multiple reflections between glazings. For glass layers, procedures to determine wavelength-dependent properties are given in	Constant overall heat transfer coefficients between glazings

	appendix.	
(DIN EN 673:2011-04) Glass in building - Determination of thermal transmittance (U value) - Calculation method U-value	Thermal heat transfer: The U-value/overall heat transfer coefficient is calculated in a simplified way by adding thermal resistances in series. For glazings with more than one gas cavity, an iterative process is proposed to determine the difference of temperature at each cavity and so the thermal resistance of each cavity. Optical calculation: No model	For multiple gas cavity, it is assumed that all gas cavity have a mean temperature of 283 K (see Appendix) Isothermal layers Heat transfer coefficients constant over the height
(DIN EN 13363-1:2007-09) Solar protection devices combined with glazing – Calculation of solar and light transmittance – Part 1: Simplified method; g-value	Thermal heat transfer: A rough method is proposed to calculate the g-value of glazings with external, internal and integrated blinds. The U-value of the glazing is an input and the overall heat transfer coefficient between glazing layers is constant. Optical calculation: The visible and solar transmission can be calculated with simplified correlation using multiple reflections	Constant thermal resistances between blind and glazing and glazing and environment
(DIN EN 13363-2:2005-06) Solar protection devices combined with glazing – Calculation of total solar and light transmittance – Part 2: Detailed calculation method; g-value Optical properties	Thermal heat transfer: Similarly to ISO 15099, energy balances are made for each layer, and the resulting equation system is then solved to get the temperatures and heat fluxes. Optical calculation: First, the optical properties of each layer have to be defined with EN 410. For each layer, a radiative wavelength-dependent energy balance is made. Solving this equation system results in overall optical properties as well as energy absorbed in each layer. If no wavelength-dependent are available,	Diffuse incoming light is considered as beam Lamella systems/blinds are considered as homogenous materials with equivalent optical properties, which can be dependent of the angle of

	integrated values can be used with the according risks.	incidence.
(EN 14500:2008) Blinds and shutters – Thermal and visual comfort – Test and calculation methods Optical properties	Thermal heat transfer: No model Optical calculation: For the optical properties of venetian blinds, this norm refers to EN 13363-2. For fabrics and other products with rotationally symmetric transmittance ($\tau_{d\text{-}h}$ does not change in case of a fixed angle of incidence when the relative orientation of the fabric to the incident irradiation is changed), a method is proposed to calculate $\tau_{h\text{-}h}$ from $\tau_{d\text{-}h}$ measurements (integration method). Another method is proposed for venetian blinds and other products with transmittance with profile angle symmetry (τdir-h does not change in case of a fixed profile angle when the azimuth angle is varied)	The constant heat transfer coefficients between environment and blind and blind and window are chosen in a conservative way for the cooling load calculation.
(Kuhn et al. 2011) Total heat flux going from the fenestration system towards the interior, for building simulation.	Thermal heat transfer: Every glazing system, independently of its complexity, is represented by a two layer/nodes system. The solar energy absorbed in the two layers as well as the thermal resistance separating the two nodes are calculated using only following inputs: - Angle dependent overall optical transmittance and g-values. - U-values total reflectance (optional) Optical calculation: The angle dependent g-values and solar transmittances are inputs to this model.	The complex fenestration can be represented by a two-layer system, with a constant thermal resistance between the two layers.
(Kuhn 2006a) g=f(azimuth, altitude, tilt angle (or switching state in general)) of facade with solar control	Thermal heat transfer: Similar to EN13363-1 Optical calculation: The whole glazing is treated as one layer and the blind as another.	Profile angle symmetry for the diffuse properties calculation: the properties of the

systems	The model presents an extension of the Roos model for glazing to calculate the transmission and reflection of the glazing (only glass) for incidence angle other than 0°. For venetian blinds or other layers with profile angle symmetry. A correlation to determine the diffuse properties is presented. Finally, a series of correlations, based on multiple reflections, is presented to calculate the g-value in the case of internal and external blinds.	blind depend only on the profile angle The diffuse radiation is isotropic Constant overall heat transfer coefficients between the layers, but temperature dependent U-value of the glazing.
(ISO 9050:2003) Glass in building — Determination of light transmittance, solar direct transmittance, total solar energy transmittance, ultraviolet transmittance and related glazing factors g-value, optical properties	Thermal heat transfer: Similar to EN410 Optical calculation: Similar to EN410. In addition, the method is generalized to calculate the absorbed energy in each layer for glazing with more than 3 layers (N-layers). The problem is solved by iteration and decomposing it in N-1 sub-problems.	Constant overall heat transfer coefficients between the layers

Table 6 – Comparison of simplified models to calculate the optical properties of glazings as well as g-values.

Among the different models exposed, the (EN 410:2011) standard proposed an analytical solution for the solar energy transmitted through a façade element composed by three layers, taking into account the multiple reflection between layers. For the purpose of the parametric calculation, the goal was to calculate the part of incoming diffuse light which was absorbed in every layer, as well as the solar radiation being transmitted inside. If one would for example need the spatial distribution of the irradiance towards the indoor environment, the BSDF method would be more suited. Consequently, the EN410 model was chosen to calculate the part of incoming diffuse solar irradiance transmitted to the interior and absorbed in each layer (glass, insulation, glass) of our system.

This results in following equations for the total transmitted and absorbed solar energy:

$$\tau_{h-h} = \frac{\tau_{h-h,glass} * \tau_{h-h,trans.insu.} * \tau_{h-h,glass}}{\left(1 - \rho_{h-h,glass} * \rho_{h-h,trans.insu.}\right) * \left(1 - \rho_{h-h,trans.insu.} * \rho_{h-h,glass}\right) - \tau^2_{h-h,trans.insu.} * \rho^2_{h-h,glass}} \quad \textit{Equation 40}$$

$$\alpha_{e,sol,ext\ glass} = \alpha_{h-h,glass} + \frac{\tau_{h-h,glass} * \alpha_{h-h,glass.} * \rho_{h-h,trans.insu.} * \left(1 - \rho_{h-h,trans.insu.} * \rho_{h-h,glass}\right)}{\left(1 - \rho_{h-h,trans.insu.} * \rho_{h-h,glass}\right)^2 - \tau^2_{h-h,trans.insu.} * \rho^2_{h-h,glass}} \quad \textit{Equation 41}$$

$$+ \frac{\tau_{h-h,glass} * \tau^2_{h-h,trans.insu.} * \alpha_{h-h,glass.} * \rho_{h-h,glass}}{\left(1 - \rho_{h-h,trans.insu.} * \rho_{h-h,glass}\right)^2 - \tau^2_{h-h,trans.insu.} * \rho^2_{h-h,glass}}$$

$$\alpha_{e,sol,trans.insu.} = \frac{\tau_{h-h,glass} * \alpha_{h-h,trans.insu.} * \left(1 - \rho_{h-h,trans.insu.} * \rho_{h-h,glass}\right)}{\left(1 - \rho_{h-h,trans.insu.} * \rho_{h-h,glass}\right)^2 - \tau^2_{h-h,trans.insu.} * \rho^2_{h-h,glass}} \quad \textit{Equation 42}$$

$$+ \frac{\tau_{h-h,glass} * \tau_{h-h,trans.insu.} * \alpha_{h-h,trans.insu.} * \rho_{h-h,glass}}{\left(1 - \rho_{h-h,trans.insu.} * \rho_{h-h,glass}\right)^2 - \tau^2_{h-h,trans.insu.} * \rho^2_{h-h,glass}}$$

$$\alpha_{e,sol,int\ glass} = \frac{\tau_{h-h,glass} * \tau_{h-h,trans.insu.} * \alpha_{h-h,glass}}{\left(1 - \rho_{h-h,trans.insu.} * \rho_{h-h,glass}\right)^2 - \tau^2_{h-h,trans.insu.} * \rho^2_{h-h,glass}} \quad \textit{Equation 43}$$

With:

- $\tau_{h\text{-}h,glass}$: the hemispherical-hemispherical transmittance value of float glass. A value of 0.753 was assumed (Lawrence Berkeley National Laboratory 2015).
- $\tau_{h\text{-}h,\ trans.insu.}$: the hemispherical-hemispherical transmittance value of the translucent insulation layer. This thickness-dependent value was calculated as explained above
- $\rho_{h\text{-}h,glass}$: the hemispherical-hemispherical reflectance value of float glass. A value of 0.136 was assumed (Lawrence Berkeley National Laboratory 2015).
- $\rho_{h\text{-}h,\ trans.insu.}$: the hemispherical-hemispherical reflectance value of the translucent insulation layer. This thickness-dependent value was calculated as explained above.
- $\alpha_{e,sol,ext\ glass}$: the part of incoming solar energy that is absorbed in the external glass layer.

- $\alpha_{e,sol,trans.insu.}$: the part of incoming solar energy that is absorbed in the translucent insulation layer.
- $\alpha_{e,sol,int\ glass}$: the part of incoming solar energy that is absorbed in the internal glass layer.
- $\alpha_{h\text{-}h,glass}$: the hemispherical-hemispherical absorptance of glass. It was assumed that: $\alpha_{h\text{-}h,glass}=1-\tau_{h\text{-}h,\ glass}-\rho_{h\text{-}h,glass}$.
- $\alpha_{h\text{-}h,trans.insu.}$: the hemispherical-hemispherical absorptance of the translucent insulation layer. It was assumed that: $\alpha_{h\text{-}h,\ trans.insu.}=1-\tau_{h\text{-}h,\ trans.insu.}-\rho_{h\text{-}h,\ trans.insu.}$

It has been assumed that the ratio between the direct-hemispherical values measured at 60° (see 2.3.1) and the diffuse-hemispherical values is constant for all thicknesses. Following ratios have been used:

Incidence angle [°]	$\rho_{dir\text{-}h,vis}$	$\rho_{dir\text{-}h,sol}$	$\tau_{dir\text{-}h,vis}$	$\tau_{dir\text{-}h,sol}$
0	0.819	0.807	0.086	0.085
15	0.814	0.806	0.084	0.081
20	0.812	0.806	0.083	0.079
30	0.814	0.809	0.078	0.075
40	0.816	0.813	0.073	0.071
45	0.827	0.823	0.070	0.068
60	0.860	0.851	0.061	0.061
75	0.892	0.877	0.048	0.049
80	0.903	0.886	0.044	0.045
86.25	0.916	0.898	0.039	0.040
Diffuse-hemispherical	0.840	0.832	0.068	0.067
Ratio 0°/Hem	0.975	0.970	1.252	1.262

Table 7 – Calculated direct-hemispherical reflectance and transmittance values for the 15 mm thick translucent insulation layer. Calculated ratio between measured direct, angle-dependent values at 60° incidence angle and calculated diffuse-hemispherical values. The grey values have been interpolated.

The hemispherical values have been integrated assuming rotationally symmetric optical properties. This means that the optical property does not change in case of a fixed angle of incidence when the relative orientation of the material to the incident irradiation is changed. The following formula, taking into account the solid angle for each measured values, is for example proposed in (Kuhn 2006a) and used in (EN 14500:2008):

$$\tau_{h-h} = \sum_{k=0}^{6} a_k * \tau_{dir-h}(15° * k) \qquad \textit{Equation 44}$$

With:

- $\tau_{h\text{-}h}$: the hemispherical-hemispherical transmittance. These highlighted values for 15° angle intervals have first been interpolated linearly from the values for 20° incidence angle interval.
- $\tau_{dir\text{-}h}$: the angle-dependent direct-hemispherical transmittance.
- a_k: the geometrical coefficients:
    - $a_0 = 0.0170$
    - $a_1 = 0.1294$
    - $a_2 = 0.2241$
    - $a_3 = 0.2588$
    - $a_4 = 0.2241$
    - $a_5 = 0.1294$
    - $a_6 = 0.0170$

The hemispherical-hemispherical transmittance and reflectance values of the translucent insulation layer for thicknesses other than 15 mm where then calculated:

- Using the direct-hemispherical measured values at 0° incidence angle for different thicknesses.
- Assuming the same ratio between direct-hemispherical at 0° incidence angle and hemispherical-hemispherical values than for the 15 mm sample.

Thickness [mm]	$\rho_{h\text{-}h,sol}$	$\tau_{h\text{-}h,sol}$
5	0.615	0.272
10	0.785	0.129
15	0.832	0.067
20	0.853	0.046
30	0.854	0.043

Table 8 – Calculated hemispherical-hemispherical transmittance and reflectance values for different thicknesses of the translucent insulation layer.

The near normal transmittance value for 30 mmm was not measured and was extrapolated using the fitted function $\rho_{nh,sol}$=0.8286*(1-exp(-0.2533*t)), t being the thickness in mm. The R^2 coefficient between this fitted function and the measured values was equal to 0.99993.

Finally, following thickness-dependent values were calculated for the whole façade element:

Thickness of the transparent insulation layer [mm]	$\tau_{h\text{-}h}$	$\alpha_{e,sol,ext\ glass}$	$\alpha_{e,sol,trans.insu.}$	$\alpha_{e,sol,int\ glass}$
5	0.184	0.168	0.096	0.027
10	0.092	0.185	0.074	0.014
15	0.048	0.189	0.087	0.007
20	0.033	0.192	0.087	0.005
30	0.032	0.192	0.088	0.005

Table 9 – Calculated optical properties of the facade element.

While the part of total solar irradiance absorbed in each layer doesn't vary much with the thickness – with a maximum difference of 0.024 for the external glazing between 5 mm and 30 mm insulation thickness-, the thickness of the insulation layer has a major impact on the solar transmission. Concerning the direct solar irradiance, the direct-hemispherical transmittance at incidence angle lower than 60° should be slightly higher than these hemispherical-hemispherical values since then the transmittance of the external glazing is higher.

The g-value can then be calculated as follow:

$$g = \frac{\tau_{h-h} * I + q_{int} - q_{int}(I = 0)}{I} \qquad \textit{Equation 45}$$

With:

- I [W*m^{-2}] the total irradiance arriving at the element's outer surface
- q_{int} [W*m^{-2}] the total heat flux from the interior glass pane towards the room by convection, conduction and longwave radiation, as defined in Equation 39.
- $\tau_{h\text{-}h}$ [-] the hemispherical-hemispherical transmittance as defined above.

2.4.2 Validation

For the validation, the measurements presented in 0 have been used, with the Taurus equipment. For the validation process, the model's boundary conditions were adapted to the Taurus measurement procedure: the internal and external boundary heat transfer coefficient, h_{int} and h_{ext}, were set to infinitely high values, resulting in constant temperatures boundary conditions. Also, since the Taurus equipment measures center-of-glazing U-values, the definition of q_{int} presented in Equation 39 was adapted to following formulation in the conducting case:

$$\begin{aligned} q_{int} &= h_{cv,vent,inner\ gap} \\ &* \left(T_{gas,inner\ gap}\left(\frac{H}{2}\right) - T_{inner\ glass}\right) \\ &+ h_{rad,inner\ gap} * (T_{ins.,inner\ surf.} \\ &- T_{inner\ glass}) \end{aligned} \qquad \textit{Equation 46}$$

And following correlation was used in the insulating case:

$$\begin{aligned} q_{int} &= (h_{cv,closed,inner\ gap} + h_{rad,inner\ gap}) \\ &* (T_{ins.,inner\ surf.} - T_{inner\ glass}) \end{aligned} \qquad \textit{Equation 47}$$

With:

- $T_{gas,\ inner\ gap}(H/2)$ [K] the temperature at middle height in the inner air column, as defined in 2.4.1.2.
- $h_{cv,\ vent,\ inner\ gap}$ [W*m^{-2}*K^{-1}] the convective heat transfer coefficient in the inner vertical gap in case of ventilated cavity, as defined in 2.4.1.2 .
- $h_{cv,\ closed,\ inner\ gap}$ [W*m^{-2}*K^{-1}] the convective heat transfer coefficient in the inner vertical gap in case of closed cavity as defined in 2.4.1.2 .
- $h_{rad,\ inner\ gap}$ [W*m^{-2}*K^{-1}] the longwave radiative heat transfer coefficient in the inner vertical gap, as defined in 2.4.1.2 .
- $T_{inner\ glass}$ [K] the inner glass pane temperature.
- $T_{ins.,\ inner\ surf.}$ [K] the inner surface temperature of the insulation panel

The U-value was then calculated as follow:

$$U = \frac{1}{\frac{q_{int}(I=0)}{(T_{ext} - T_{int})} + \frac{1}{h_{int}} + \frac{1}{h_{ext}}} \qquad \textit{Equation 48}$$

With:

- h_{int}=7.69 [W*m^{-2}*K^{-1}] the internal boundary heat transfer coefficient, as defined for example by (DIN EN 673:2011-04).
- h_{ext}=25 [W*m^{-2}*K^{-1}] the external boundary heat transfer coefficient, as defined for example by (DIN EN 673:2011-04).
- T_{int} [K] the interior air temperature.
- T_{ext} [K] the exterior air temperature.

In this part, "inner" refers to the warm, heated side and "outer" refers to the cold side.

For each geometrical configuration and two temperature differences at the boundary, the model has been compared with the measurements:

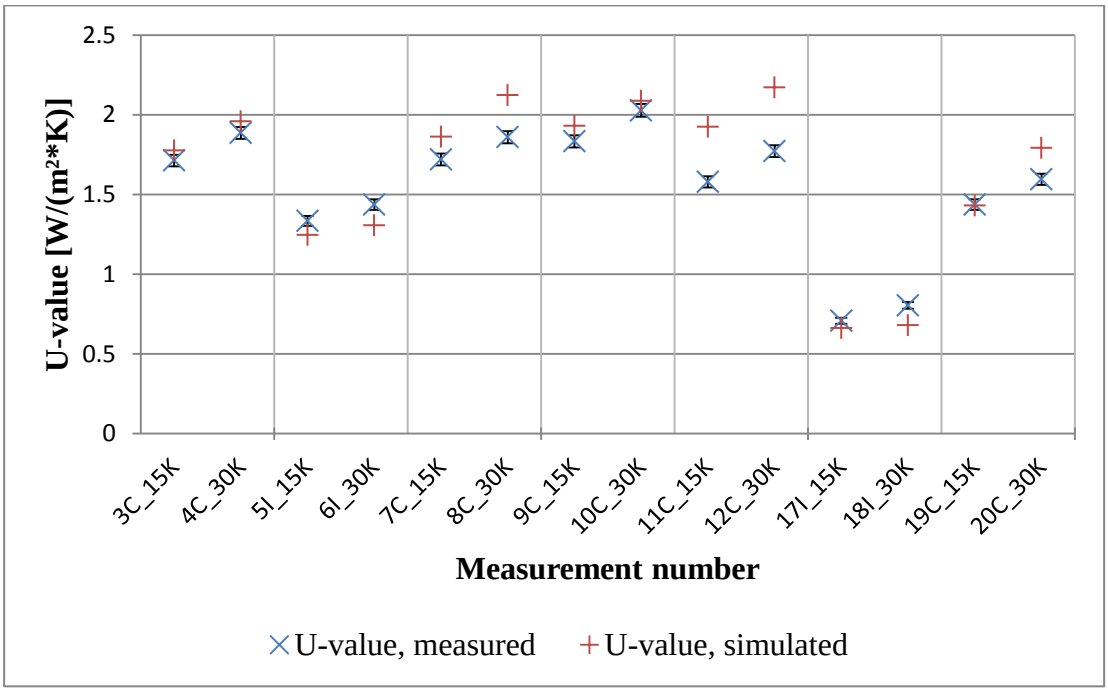

Figure 19 – Comparison between the measured and modelled U-value for 14 different cases.

For this 7 different geometries and insulating state, the mean difference is 9.5 %, mainly due to cases 7C, 8C, 11C and 12C. Without cases 11C and 12C, the mean difference drops to 6.3 %.

The laminar flow conditions are still largely verified in the conducting state, with Reynolds numbers in the vertical gaps going from 203 to 412 and airflow going from 4.1 to 9.5 m³/h for the 10 cases in the conducting state.

Cases 7C, 8C and 19C, 20C show an overestimation of the U-value which increases with the temperature difference. These four cases in the conducting case have the lowest

thickness of vertical air gaps, with thicknesses of 17.5 mm for cases 7C and 8C and 15 mm for cases 19C and 20C. For these four cases 7C, 8C, 19C and 20C, the relative difference is respectively of 8.3 %, 14.2 %, 0.4 % and 12.4 %. These differences are explained further in this section.

Cases 11C and 12C show the most important differences between measurements and model, with respectively 21.1 % and 21.5 % relative differences. For these two cases, the height of the horizontal air gap (35 mm) at the top and bottom of the element is twice larger than the thickness of the vertical air gaps (17.5 mm). However, the model is capable to simulate larger horizontal air gaps with a high accuracy, if the hydraulic diameters of the horizontal air gaps and the vertical air gaps are the same, as shown by cases 3C, 4C, 9C and 10C. It appears than that the difference appearing for cases 11C and 12C are a consequence of this change of hydraulic diameter between the vertical and horizontal air gaps. Despite the fact that Equation 19 and Equation 20 were introduced to capture this effect, these equations seem to underestimate the pressure drop in this case.

The model results 3C, 4C, 9C and 10C show good agreement with the measurements, with a maximum relative difference of 3.3 % for measurement 11C. These measurements have a thickness of the vertical air gaps of 30 mm, and the insulation panel is either 10 mm or 30 mm thick.

The cases in the insulating state (5I, 6I and 17I, 18I) are modelled with a good accuracy, the maximum relative difference being 15.5 % for case 18I. The slight underestimation can be explained by the fact that the model in the insulating state consider the vertical cavities as completely closed with no mass-transfer between the outer and inner cavities, while in reality it is probable that a low mass transfer occur at the bottom of the element.

The cases with two insulation panels (17I, 18I, 19C, 20C) are the same prototype in insulating and conducting state. It is composed by an outer and inner vertical air gap of 15 mm, two insulation panels of 15 mm and an "insulating" air gap of 10 mm in the middle between the two insulation panels. For this geometry with two insulation panel and thin vertical air gaps, the same conclusions can be drawn than for the single insulation layer prototypes: the model slightly underestimates the U-value in the insulating case, and slightly overestimates it in the conducting case.

A second measurement campaign was performed on a single-panel prototype, covering differences of temperatures between the outer pane and the inner pane between 1 and 30 K. For this second measurement campaign, the prototype was equipped with a single insulation panel in a conducting state. From outside to inside, there was a 15 mm vertical air layer, a 15 mm insulation layer and again a 15 mm vertical air layer. The height and width of the glazed area was 760*760 mm². The height of the insulation panel was 730 mm, and the height of the top and bottom air gaps were 15 mm. The measurement

results of this prototype in the conducting case are compared against the detailed model in Figure 20:

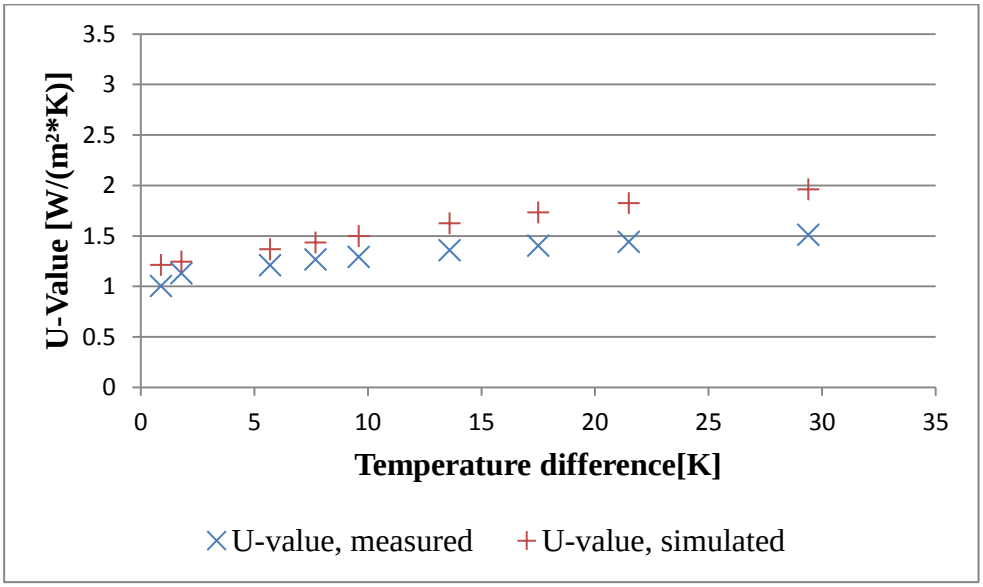

Figure 20 – Comparison between the measured and modelled U-value for 9 differences of temperatures at the boundary.

For those 9 different temperature differences at the boundary, the mean relative difference between model and measurement is 19 %. For this geometrical configuration, the model is overestimating the heat transfer and the difference increases with the difference in temperature, with a maximal relative difference of 29.9 % for a temperature difference of 29.4 K. 4 PT100 temperature sensors were also used to measure at middle vertical height the air temperature in the vertical outer and inner air channel, and the inner and outer surface temperatures of the insulation panel.

The results for the inner, warm air gap are shown in following figure:

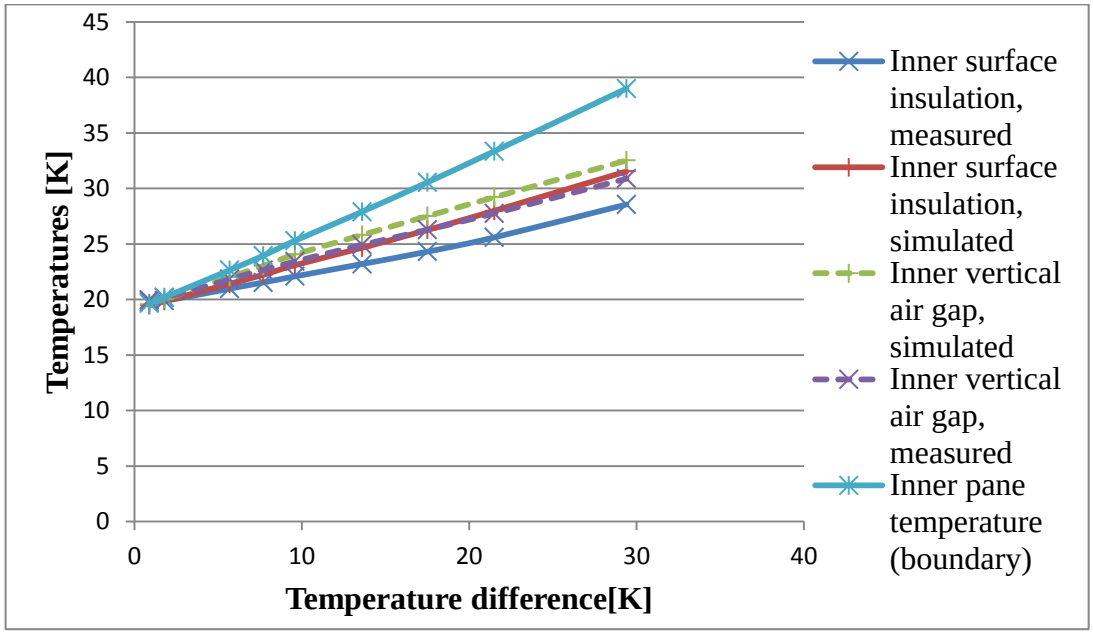

Figure 21 – Simulated and measured inner air gap temperature at middle vertical height (warm side) and insulation layer inner surface temperature versus temperature difference between inner and outer boundary temperatures. The inner pane temperature is also plotted for informative purpose.

While the model shows good agreement with the measurement for the outer air gap and outer surface of the insulation layer, the model overestimates the air temperature in the inner, warm air gap. As a consequence, the temperature of the inner surface of the insulation layer is also overestimated. The difference increases with temperature. This difference in the air gap temperature for high temperature differences explains the overestimating of the U-value.

Taking for example the inner, warm air gap, it can be observed that for this measurement with thin insulation thickness (15 mm), the air in the inner gap is heated from the Plexiglas side and cooled from the insulation side. For example, for a temperature difference of 29.4 K applied at the boundaries of the prototype, a temperature difference between air at middle vertical height and Plexiglas of -8.1 K can be observed (the air is heated), while the temperature difference between the air and the insulation inner surface is of 2.3 K (the air is cooled). The hypothesis that the fluid is heated from both surrounding parallel plates at a uniform temperature (see 2.4.1.2) is no longer true since the air is cooled from one side and slightly heated from the other.

In the above cases 7C, 8C, 11C, 12C, 13C, 14C, the heat transfer coefficient between insulation and fluid is high due to the low thickness of vertical air gaps and low hydraulic diameters, and the temperature of the insulation surface is nearer to the average fluid temperature. Also, for cases 7C and 8C, as well as the measured case with multiple

temperature difference, the low thickness of the insulation layer increases the effect, because the transmission through the insulation decreases the insulation inner surface temperature, which is then even nearer to fluid temperature, or below. For example, for case 8C with 17.5 mm thick vertical air gaps and insulation layer, the results of the detailed model, assuming symmetric heating, shows us that the convective heat flux going from the insulation inner surface towards the air column is of 8.8 $W*m^{-2}$, while the convective heat flux going from the inner Plexiglas towards the air column is of 60.2 $W*m^{-2}$, showing a very strong asymmetrical heating situation. In the cases 3C, 4C with more important thicknesses of the vertical air gaps and larger insulation thickness, the insulation surface temperature in the inner gap is warmed by the inner cover pane by longwave radiation. For example, in case 4C, the convective heat flux insulation-fluid in the inner gap is of 25.0 $W*m^{-2}$, while the convective heat flux fluid-Plexiglas is of 53.9 $W*m^{-2}$ and the radiative heat flux between the two surfaces 43.8 $W*m^{-2}$. In these cases there is a good agreement between simulation and measurements. The hypothesis of symmetric heating seems to be sufficient for the cases with large insulation thickness and/or large hydraulic diameter, but leads to and overestimation of the convective heat transfers in cases with low hydraulic diameters and low insulation thickness.

In reality, the air columns are in a situation of asymmetrical heating or cooling. For the last measurement with several temperature differences, the inner air column is even heated at the Plexiglas side and slightly cooled at the insulation side. In the case of asymmetric heating, the Nusselt numbers and so the heat transfer coefficients are different at both sides of the duct. In (Gloriant et al. 2015), it is stated that for this case the only result found in literature to calculate different convective heat transfer coefficients at both sides of the duct was presented in (Shah und London 1978), and further investigated by (Nield 2004)(corrected by (Nield 2008)). However, the method presented by (Shah und London 1978) is only valid for constant heat flux boundaries. For $380<Re<2900$, (Schwab 2002) proposes a correlation to determine the Nusselt number at both sides of an asymmetrically heated parallel-plate ducts, based on experiments with different aspect ratios, different Reynolds numbers and different temperatures at both surfaces. A similar correlation is proposed for ducts cooled on one side and heated on the other side. Unfortunately, the detailed models showed us that we are often below the range of Reynolds numbers, and thus these results cannot be used here. A better approach, as presented in (Gloriant et al. 2015), would be to calculate the convective heat transfer coefficients at both sides of the air columns with a CFD calculation. This could however not be done within the framework of this thesis.

For the purpose of the parametric analysis, it has been chosen to continue with the hypothesis of symmetrical heating due to the good accuracy of the model in most cases, but being aware that the model overestimates the U-value for low hydraulic diameters and low insulation thicknesses, and that the difference increases with the temperature difference at the boundary.

2.4.3 Results and discussion

2.4.3.1 Parametric analysis

The goal of the parametric analysis was to investigate the impact of the thermophysical and geometrical parameters on the element's performance. For simplification purpose, this study was conducted only on façade elements with one insulation layer. The method used is One-At-a-Time (OAT): while one parameter is varied, the others are maintained constant.

For this parametric analysis, a summer situation was chosen, with following boundary conditions:

- Room air temperature: 26°C
- Exterior air temperature: 16°C
- Interior boundary heat transfer coefficient: 7.69 $W*m^{-2}*K^{-1}$.
- Exterior boundary heat transfer coefficient: 25 $W*m^{-2}*K^{-1}$.
- Solar irradiance incoming at the element's outer surface:
    - For the calculation of the g-value: 500 $W*m^{-2}$ direct irradiance on the façade with 60° incidence angle or diffuse irradiance.
    - For the calculation of the U-value: no radiation (night case).

For each variation of parameter: two cases are calculated: a case with solar irradiance and a case without solar irradiance. The monitored values for the case with solar irradiance are the g-value and the element's internal glass pane temperature. For the case without solar irradiance, the U-value is monitored. The results are displayed for the element in the insulating state and conducting state.

The reference, with 30 mm thick vertical air layers and insulation layer, was chosen as a starting point since the validation showed a low relative difference of about 3 % on the U-value between model and simulation. This was also the geometry simulated in the building simulation.

Following parameters were investigated:

Name	Unit	Range	Step	Reference value
Height of the glazed area and of the vertical air gap	m	[0.4-5]	0.1	0.76
Width of the glazed area	m	[0.4-5]	0.1	0.76
Thickness of the insulation layer	m	[0.005-0.03]	0.005	0.030
Thickness of the vertical air gaps	m	[0.01-0.10]	0.002	0.030
Thermal conductivity of the insulation layer	$W*m^{-1}*K^{-1}$	[0.005-0.25]	0.005	0.035
Longwave emissivity of the outer glass, inner surface	-	[0-1]	0.02	0.84
Longwave emissivity of the inner glass, outer surface	-	[0-1]	0.02	0.84

Table 10 – Parameters investigated within the parametric analysis.

The hydraulic diameter of the vertical and horizontal air gaps is always identical. The g-value is given with three decimal numbers to show slight differences between variants, but this is no indication of the accuracy of the model.

Height of the glazed area and vertical air gap:

For these simulations, the height of the glazed area, which is also the height of the vertical air gaps, is varied. The height of the horizontal layers is kept constant (3 cm), and so the height of the insulation layer varies accordingly to the one of the glazed area (minus 6 cm).

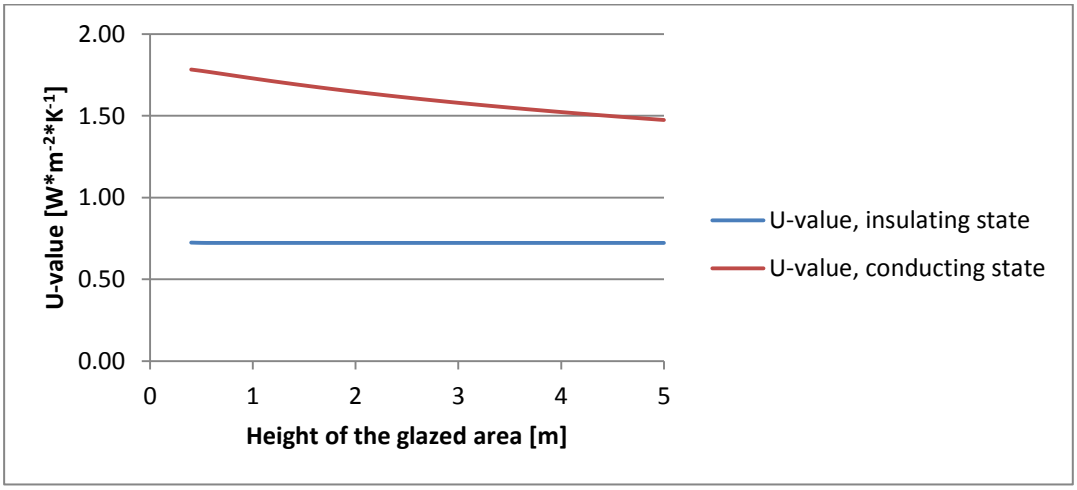

Figure 22 – U-value versus height of the glazed area and vertical air gaps, without solar irradiance.

In the conductive case, while the airflow increases from 3.1 to 19.1 m^3*h^{-1} due to the chimney effect, the airflow rate relative to the glazed surface area decreases from 10.1 to 5.0 $m^3*h^{-1}*m^{-2}$, and so the U-value diminishes. When the height increases, the façade element is less efficient per m^2 to evacuate the heat from the room.

For the case with irradiance, the airflow rate is slightly lower, as can be seen in Figure 23:

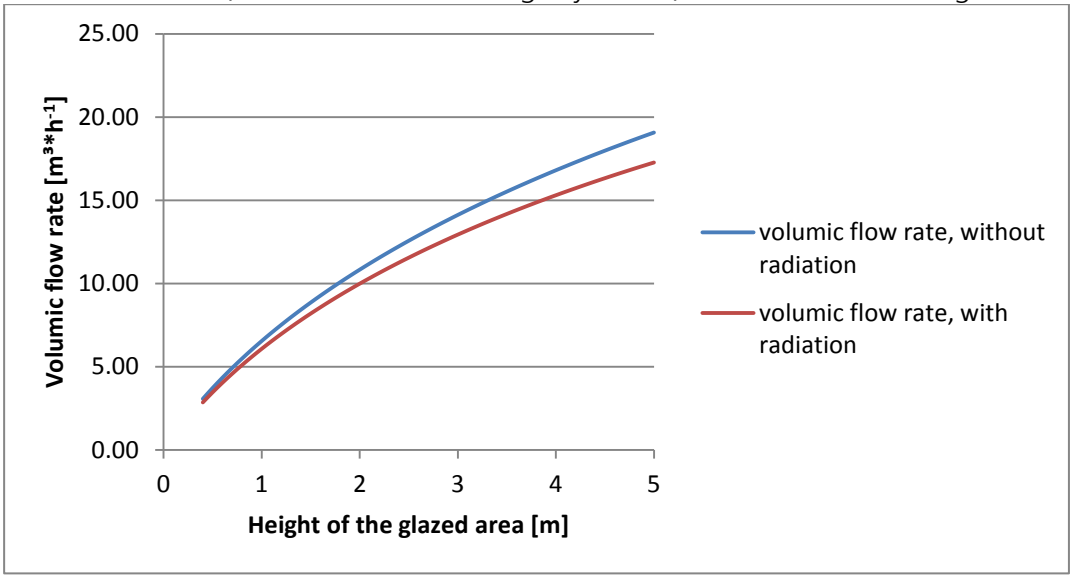

Figure 23 – Airflow rate versus height of the glazed area and vertical air gaps, with and without solar irradiance, for the conducting case.

Due to absorbed solar energy, the difference of temperature between inner glass temperature and outer glass temperature is lower since more solar energy is absorbed at the outer glass layer and outer surface of the insulation layer. For example, for 5 m height, the inner and outer glass temperatures are respectively 27.6°C and 21.2°C with solar irradiance and 24.1 °C and 16.7°C without solar irradiance. With solar irradiance, the airflow rate increases from 2.9 to 17.3 m^3*h^{-1}. The relative increase of the airflow rate with or without irradiance is about the same, and so is the variation of the internal glass pane temperature. This explains an almost constant g-value of about 0.086 when the height of the glazed area is increased.

In the insulating case, the U-value remains constant around 0.72 $W*m^{-2}*K^{-1}$ in the case without solar irradiance. The vertical air gaps are not large enough to allow a large scale internal convection, due to the height to thickness ratio. With solar irradiance, the g-value is also almost constant at 0.082.

For this insulation thickness of 3 cm, the hemispherical-hemispherical solar transmittance calculated for the element was 0.032 (see 2.4.1.3).

For important heights of the glazed area, the hypothesis of constant surface temperatures may be far from reality, in particular for the insulation material with low thermal conductivity.

Width of the glazed area and vertical air gap:

Here, the width of the glazed area is varied between 0.4 and 5 m. Varying the width of the glazed area has no significant influence on the main outputs: in the conductive state, the width has only little influence on the U-value, which has an almost constant value of about 1.75 $W*m^{-2}*K^{-1}$. With solar irradiance, the g-value keeps the same value of 0.086. In the insulating state, both the U-value and the g-value are constant at respectively 0.72 $W*m^{-2}*K^{-1}$ and 0.082.

Thickness of the translucent insulation layer:

For this variation of the insulation layer's thickness, the absorbed solar energy in case of solar irradiance has been calculated according to section 2.4.1.3, based on the optical measurements. The thickness of the vertical air gaps is constant (3 cm)

The U-value is of course strongly dependent of the thickness of the insulation layer:

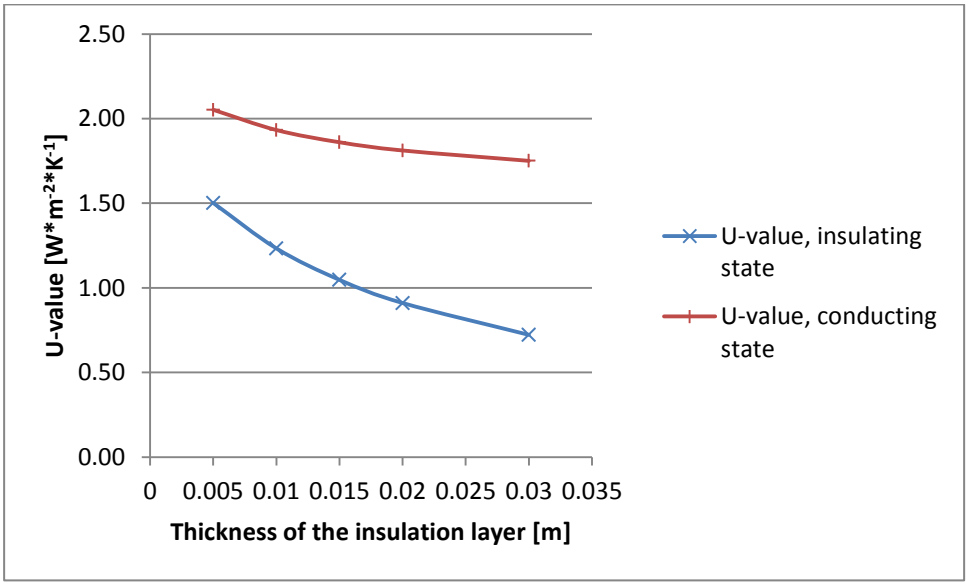

Figure 24 – U-value in the insulating and conducting state versus thickness of the insulation layer, without solar irradiance.

It can be observed that the difference between insulating and conducting state increases: the thicker is the insulation layer, the higher is the difference of temperature between the inner and outer vertical air column. In the conducting state, this has as a consequence a slight increase of the airflow rate from 4.7 m^3*h^{-1} to 5.3 m^3*h^{-1} which compensates the higher thermal resistance of the insulation.

The influence of the insulation's thickness on the g-value is the following:

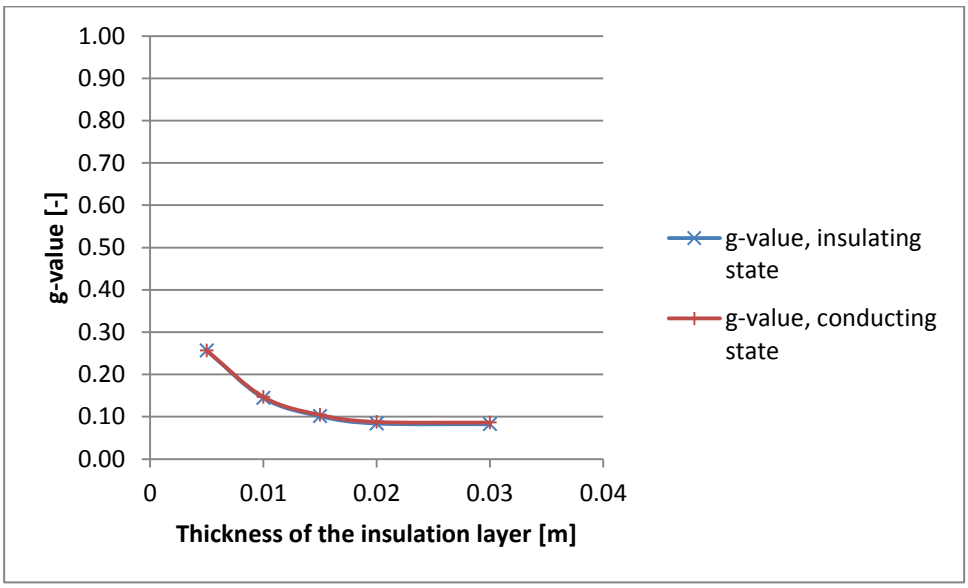

Figure 25 – g-value in the insulating and conducting state versus thickness of the insulation layer

The g-value varies strongly with the thickness of the insulation layer. It can be observed that the g-value in insulating and conducting state are almost equal. The g-value in the conducting state is only very slightly higher. An important part of the incoming solar irradiance is absorbed in the outer glass pane and the outer surface of the insulation, increasing their temperature. The consequence is that the temperature difference between inner and outer air column is lower, and so is the driving force for the airflow rate in the conducting state. In the conducting state, the airflow rate is then lower with solar irradiance. This explains why the difference in g-value is so low compared to the insulating state.

Thickness of the vertical air gaps:

In this part, the thickness of the outer and inner air columns is varied. The dimension of the horizontal air gaps is identical.

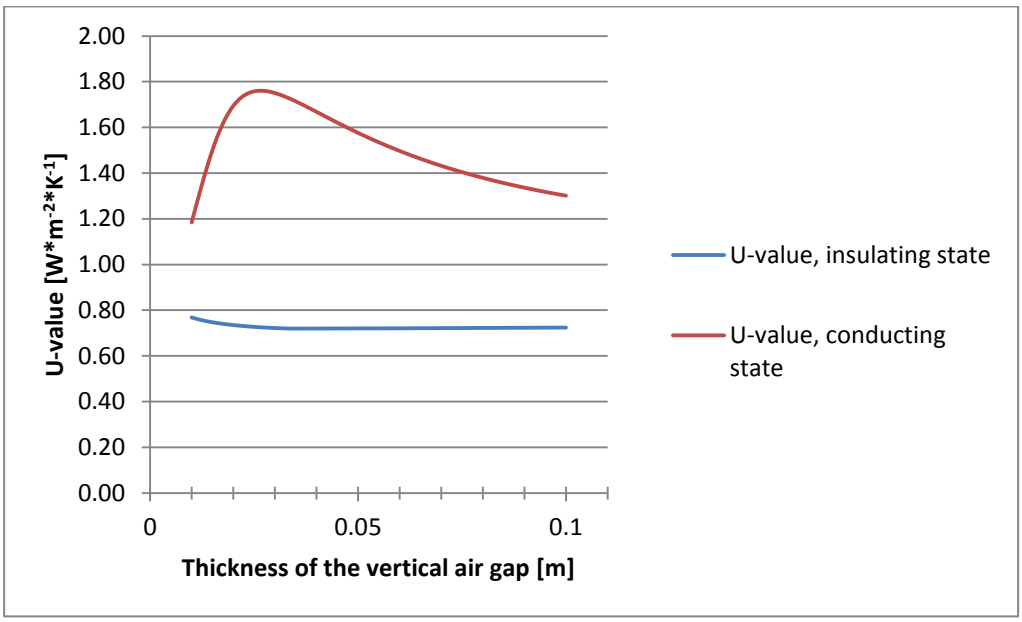

Figure 26 – U-value in the insulating and conducting state versus thickness of the vertical air columns, without solar irradiance.

In the conducting state, without irradiance, the Reynolds number increases with the thickness of the gaps, going from 57 for 1 cm to 479 for 10 cm in the outer gap for example. However, the convective heat transfer coefficients decrease from 9.9 $W*m^{-2}*K^{-1}$ for 1 cm to 1.4 $W*m^{-2}*K^{-1}$ for 10 cm due to the augmentation of the hydraulic diameter. The U-value then reaches a maximum of 1.76 $W*m^{-2}*K^{-1}$ for a thickness of 2.6 cm, corresponding to a good compromise between airflow rate and CHTCs.

In the insulating case, the U-value decreases to reach a minimum value of 0.72 $W*m^{-2}*K^{-1}$ for 3.6 cm, before increasing very slowly again: before this value, there is no convection in the vertical air gaps, and the thermal resistance increase with the thickness. Around 2.8 cm, the convection starts slowly, with for example a Nusselt number in the outer cavity of 1.02 for 2.8 cm. After 3 cm, the convection increases, until a Nusselt number of 3.8 is reached in the outer vertical air gap for 10 cm thickness.

The ratio between U-value in the conducting case and U-value in the insulating case reaches a maximum of 2.4 for a gap thickness of 2.8 cm, with a U-value in the insulating case of 0.72 $W*m^{-2}*K^{-1}$, and a U-value in the conducting case of 1.76 $W*m^{-2}*K^{-1}$. However, the validation has shown that the model tends to overestimate the U-value for thin air gaps, so this ratio may be lower in reality, although the overestimating effect is lower for low temperature differences.

Also, for air gaps thicker than 3 cm, the free convection in the vertical air gaps, between the two surrounding surfaces, is not negligible anymore compared to the forced convection, since the condition $Gr/Re^2<<1$ is not verified anymore. For 3 cm, this ratio equals 0.11, while for a thickness of 10 cm for example, this ratio equals 1.24. For important thicknesses, Computational Fluid Dynamics could help to understand the interactions between internal convection within the vertical air gaps between the two surrounding surfaces, and large scale convection between the inner and outer vertical air gap.

The g-value in the conducting case is almost constant around 0.085 and slightly higher than in the insulating case.

The influence of the thickness of the vertical and horizontal air gaps has also been investigated with measurements 9C and 10C. Compared to measurements 7C and 8C, the air gaps were 30 mm thick instead of 17.5 mm. The insulation thickness was 10 mm. Also here, an increase of the U-value was observed, with U-values of respectively 1.83 and 2.03 $W*m^{-2}*K^{-1}$ for 14 K and 29 K temperature differences and 30 mm gaps, instead of 1.72 and 1.86 $W*m^{-2}*K^{-1}$ for 14 K and 28 K temperature differences and 17.5 mm gaps.

Thermal conductivity of the insulation layer:

The thermal conductivity of the insulation layer is varied. It is assumed that the optical properties remain constant:

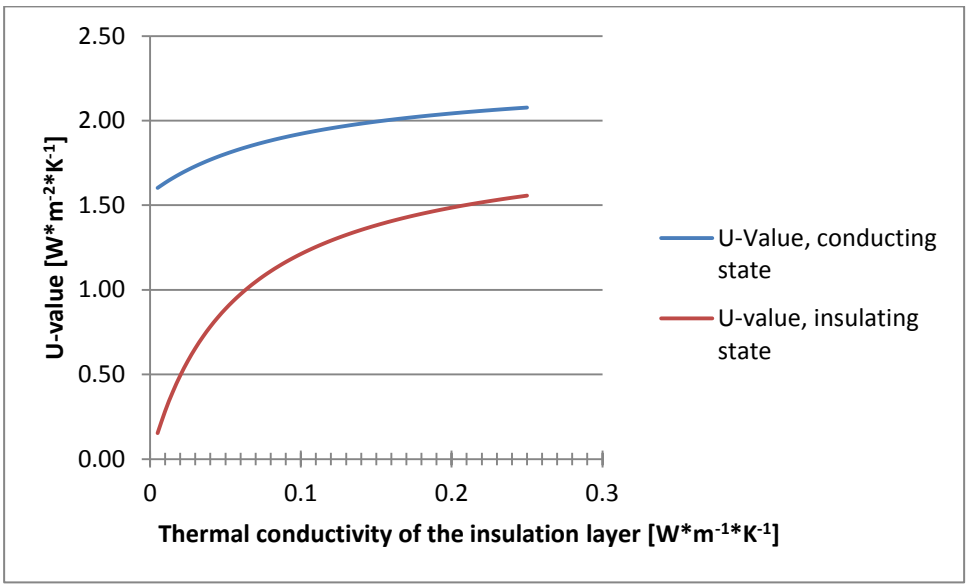

Figure 27 - U-value in the insulating and conducting state versus thermal conductivity of the insulation layer, without solar irradiance.

In the conducting case, the lower the thermal conductivity of the insulation layer, the higher is the airflow rate: since the temperature difference between the outer and inner air column is higher, the difference of density which is the driving force of the convection is higher, with a maximum airflow rate in the outer air gap of 5.6 m^3*h^{-1} for 0.005 $W*m^{-1}*K^{-1}$. This compensates partly the decrease of conduction through the insulation and leads to an U-value of 1.60 $W*m^{-2}*K^{-1}$ for a thermal conductivity of 0.005 $W*m^{-1}*K^{-1}$. This thermal conductivity value corresponds for example to vacuum insulation and results in the highest U-value ratio of 10.5 between conducting and insulating states, with an U-value of 0.09 $W*m^{-2}*K^{-1}$ in the conducting state. It seems to be very advantageous to have a very low thermal conductivity for the insulating layer.

Longwave emissivity of the inner surface of the external glass pane:

The longwave emissivity of the internal side of the external glass pane is variated:

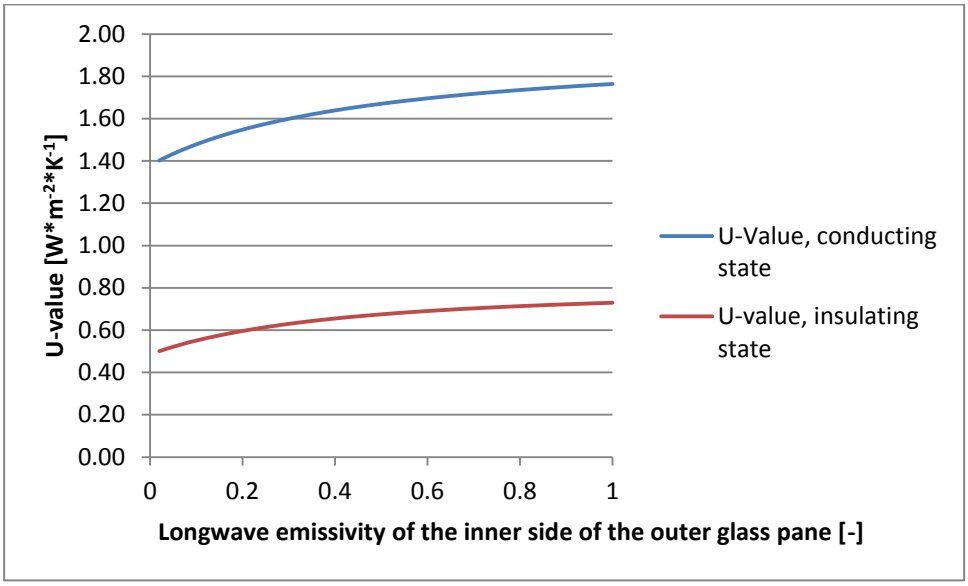

Figure 28 – U-value in the insulating and conducting state versus longwave emissivity of the inner side of the outer glass pane, without solar irradiance.

Without solar irradiance, in the insulating case, the U-value diminishes with the emissivity since the radiative exchanges in the outer air column are lowered. In the conductive case, the lower emissivity of the internal surface of the external glass pane has as a consequence that the outer surface of the insulation layer has a higher temperature, since the radiative exchange with the colder glass pane is reduced. The consequence is that the outer air column is warmer and the driving pressure difference lower, as is the airflow rate.

The longwave emissivity of the internal side of the outer glass pane has also a moderate impact on the g-value:

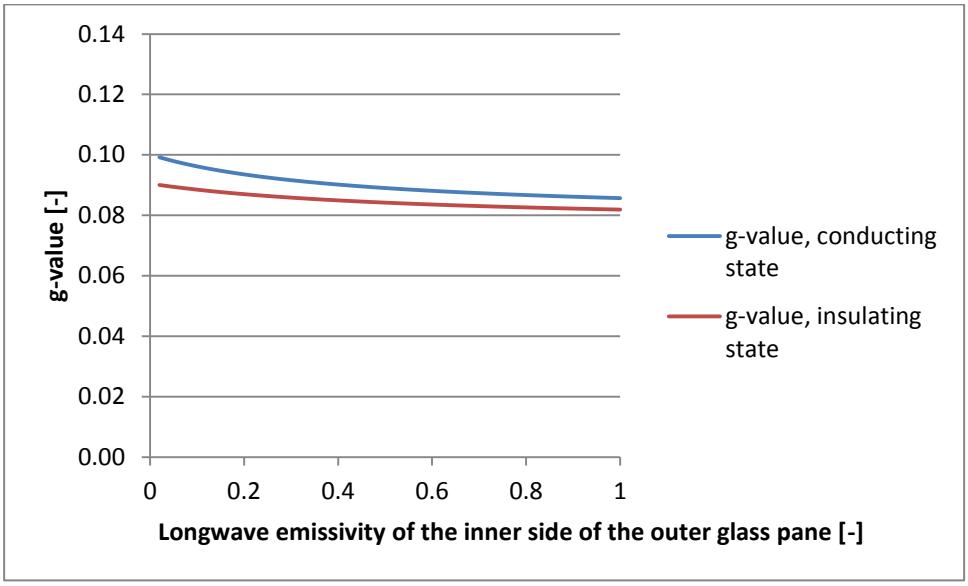

Figure 29 – g-value in the insulating and conducting state versus longwave emissivity of the inner surface of the outer glass pane.

In both states, the g-value increases when the emissivity decrease: due to the high external boundary heat transfer coefficient of 25 $W*m^{-2}*K^{-1}$, most of the solar energy absorbed in the external glazing flows towards the exterior anyway. When the longwave emissivity of the outer glass pane diminishes, the solar energy absorbed at the insulation layer tends to flow toward the interior since the radiative exchange with the outer glass is much lower. With a lower boundary heat transfer coefficient, the g-value would be higher. For example, if the external heat transfer coefficient is set equal to the internal one (7.69 $W*m^{-2}*K^{-1}$), a g-value of 0.102 instead of 0.090 is obtained in the insulating case for an emissivity of 0.02.

Longwave emissivity of the outer surface of the internal glass pane:

The longwave emissivity of the external surface of the internal glass pane is variated. For the case without solar irradiance, the U-value results are very close to the above section, with a minimum U-value of 0.49 $W*m^{-2}*K^{-1}$ in the insulating case and 1.40 $W*m^{-2}*K^{-1}$ in the conducting case for a longwave emissivity of 0.02 and a maximum U-value of 0.73 $W*m^{-2}*K^{-1}$ in the insulating case and 1.76 $W*m^{-2}*K^{-1}$ in the conducting case for a longwave emissivity of 1.

With solar irradiance, the g-value is strongly dependent on the longwave emissivity of the internal glazing:

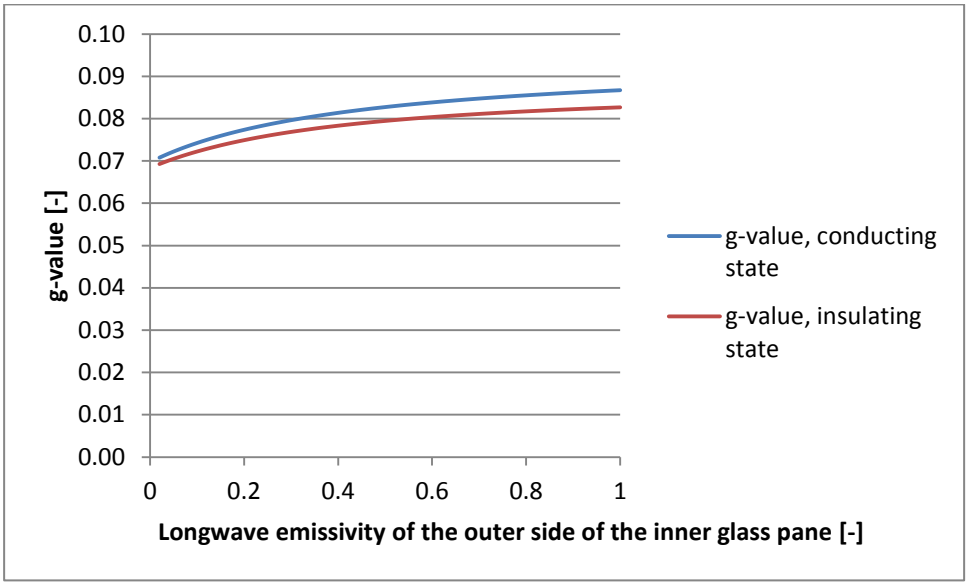

Figure 30 – g-value in the insulating and conducting state versus longwave emissivity of the outer surface of the inner glass pane.

In the conducting case, the lower the longwave emissivity of the internal glass pane, the more energy absorbed at the insulation back surface is given to the circulating fluid instead of being exchanged by longwave radiation with the inner glass pane. This is of course affected by the hypothesis that half of the energy absorbed in the translucent insulation layer is absorbed at the inner surface of the layer. In really, more energy is absorbed at the outer surface, which would result in lower U-values.

In the insulating case, when the longwave emissivity of the internal glass pane is very low, the secondary heat gain is linked only to the convective exchange in the inner vertical air gap. For a longwave emissivity of 0.02, considering a total hemispherical-hemispherical solar transmittance of 0.032, the secondary heat gain is equal to 0.039, while it is equal to 0.055 for a longwave emissivity of 1.

2.4.3.2 Alternative translucent insulation

Using the results of the parametric analysis, a first optimization step was achieved: in order to reach a higher visible transmittance and a lower U-value in the insulating state, the translucent insulation material has been replace by aerogel. Aerogel can have a thermal conductivity of about 0.013 $W*m^{-1}*K^{-1}$ (Cuce et al. 2014) as well as visible direct hemispherical transmittance between 0.43 ± 0.04 and 0.85 ± 0.04 for a 10 mm thick layer, depending on the sample structure (Reim et al. 2004). Also, low-e layers with thermal

emissivities of 0.03 have been applied to the internal surface of the external glazing and the outer surface of the internal glazing. This was a one-insulation-layer construction.

The vertical height (0.76 m), the height of the horizontal air gaps (0.03 m) and the thickness of the insulation layer (0.03 m) have been taken over from the parametric analysis.

Using identical boundary conditions as in the parametric analysis, the thickness of the vertical air gaps has then been optimized:

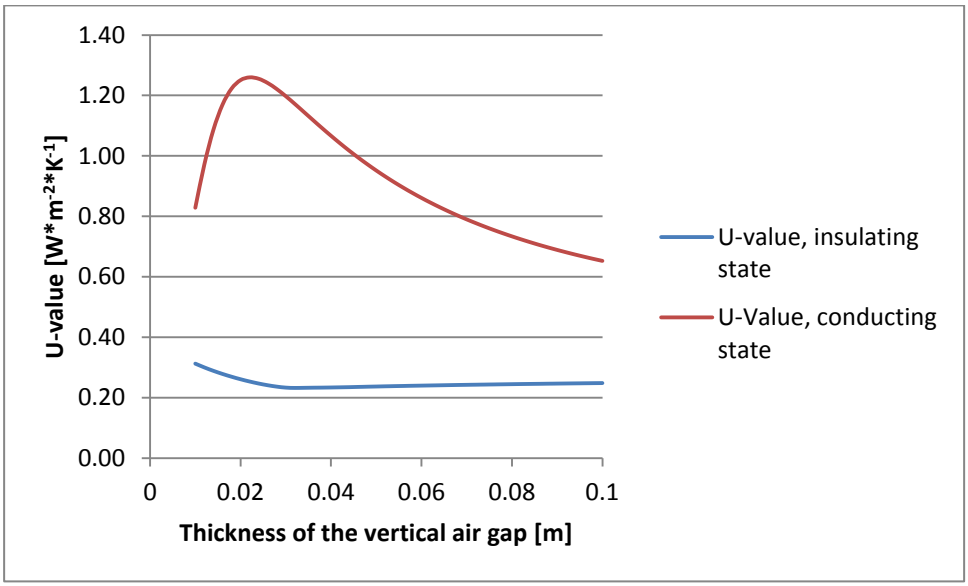

Figure 31 – U-value in the insulating and conducting state versus thickness of the vertical air columns, without solar irradiance. Element with aerogel and two low-e layers

The U-value in the insulating state is really low and near to the one of insulated opaque walls. The best ratio of 5.2 between U-value in the conducting and insulating state is found for 2.8 cm thickness, with values, with values of 0.24 $W*m^{-2}*K^{-1}$ in the insulating case and 1.22 $W*m^{-2}*K^{-1}$ in the conducting state. The analysis of the physical behavior is the same than for the variation of the air gap's thickness in the parametric variation, with the same model limitation.

Using a thickness of the vertical air gap of 2.8 cm, the properties of the façade element have been calculated versus the difference of temperature the room and the exterior. The average between external air and room air temperature was constant at 21°C, while the difference of temperature was varied with a 1 K step from 1 K to 30 K:

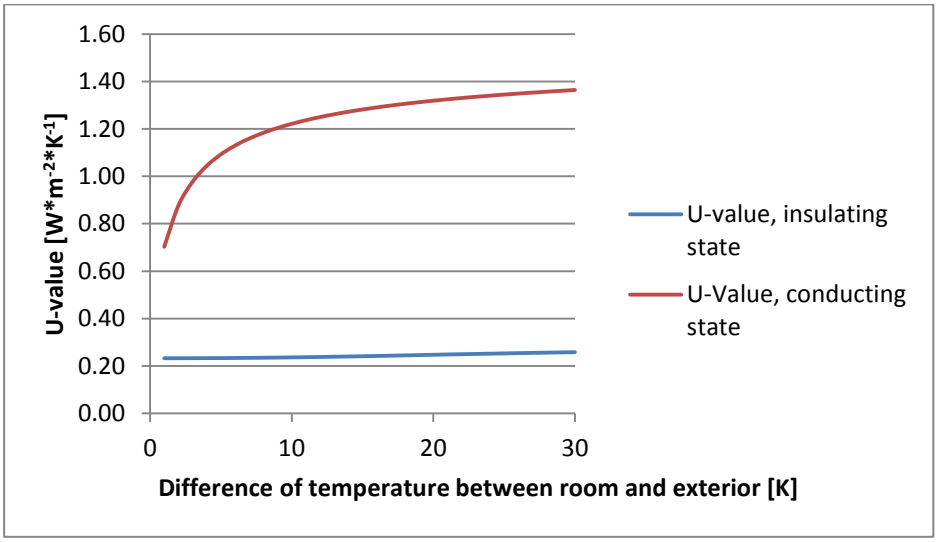

Figure 32 – U-value in the insulating and conducting state versus difference of temperature between room air and exterior air, without solar irradiance. Element with one aerogel layer and two low-e layers on the glass covers.

In the conducting state, the airflow rate increases from 1.4 m^3*h^{-1} for 1 K temperature difference to 7.5 m^3*h^{-1} for 30 K, resulting in an increase of U-value from 0.70 to 1.36 $W*m^{-2}*K^{-1}$. For higher temperature difference, the increase in U-value is slower, following the increase of airflow rate. The increase of airflow rate is dampened by the increase of pressure drop, which are proportional to the square of the air speed.

In the insulating state, the U-value increases slowly, and the internal convection in the columns is dampened by the 3 cm thicknesses of the vertical air gaps and the relatively low temperature difference between insulation and glass, due to the important thermal resistance of the insulation: for a temperature difference of 30 K, the Nusselt number in the outer column is equal to 1.46.

The first prototype built, measured and simulated had a U-value of 0.89 $W*m^{-2}*K^{-1}$ in the insulating state and 1.71 $W*m^{-2}*K^{-1}$ in the conducting state (for a temperature difference of about 15 K applied at the Plexiglas' surfaces). The element with aerogel and two low-e layers show a low U-value of 0.24 $W*m^{-2}*K^{-1}$ in the insulating state, but only 1.31 $W*m^{-2}*K^{-1}$ in the conducting state for a temperature difference of 15K. However, the use of these materials could lead to a visible transmittance near to the one of conventional windows, and consequently avoid the increase of the artificial lighting demand. For the comparison with the measurement, the results with a difference of temperature between interior air and exterior air resulting in a difference of temperature between inner glass and outer glass of about 15 K where chosen.

2.4.3.3 Forced convection

To achieve the reduction of cooling loads showed with the building simulation, a fan could be used to create forced convection. The configuration chosen was the one defined with aerogel in the previous section. To model forced convection in turbulent flow, the Gnielinski correlation has been chosen (Bejan 2013) , as detailed in the description of the thermal model. In this case, the buoyancy force is neglected, and the mass flow rate is imposed. This fan-driven configuration has not been validated by measurements. For these simulations, the interior temperature was 26°C while the exterior air temperature was 16°C.

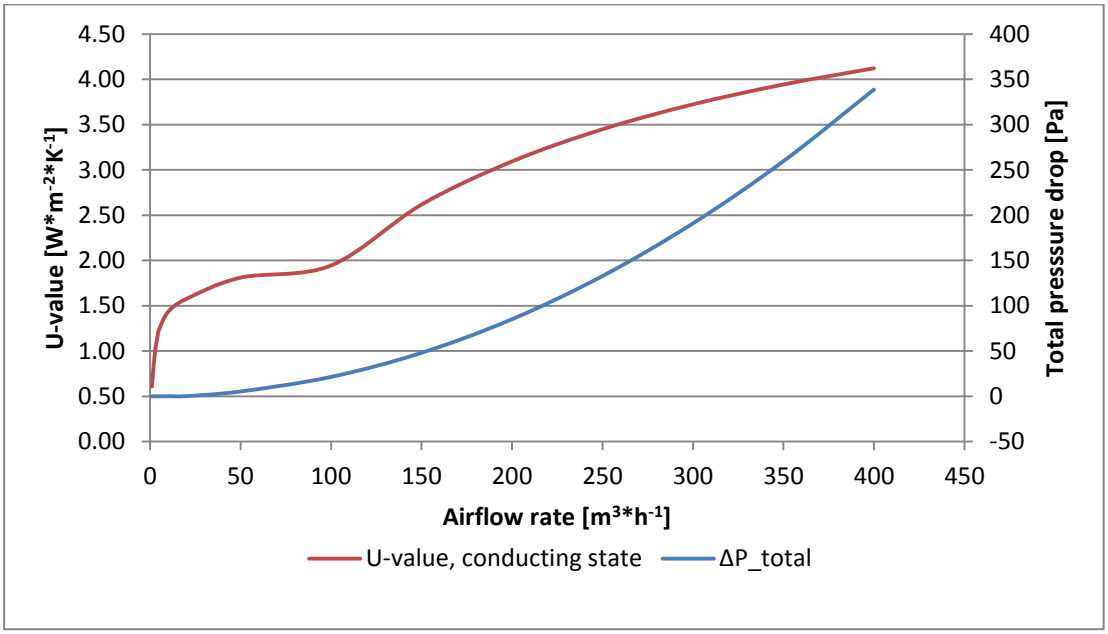

Figure 33 – U-value and total pressure drop in the system, depending on the airflow rate with forced convection. Element with aerogel and two low-e layers.

It can be observed that the fastest increase in U-value happens from 1 to 5 m^3*h^{-1}, which corresponds to the range of airflow rate also achieved with buoyancy driven convection. The angle around 100 m^3*h^{-1} corresponds to the transition between laminar and turbulent regime. The pressure drops in the system are linked through a power law to the air speed in the system, and thus to the airflow rate.

The targeted U-value of 3 $W*m^{-2}*K^{-1}$ can be achieved with a very high airflow rate of about 200 m^3*h^{-1}, at the cost of high pressure drops of 85 Pa. These airflow and pressure drop values are in the range of commercial building HVAC System and would imply high electricity consumption, not speaking about the issue of placing such fans in the façade element or controlling noise.

2.5 Conclusion: closed movable insulation system

After presenting the concept of the closed movable insulation system, a case study has been conducted to show its potential as an energy efficiency strategy. This is done by simulating an office at passive house level in Ludwigshafen within the TRNSYS simulation environment. Compared to this reference, a variant using the first measured prototype has been simulated in the upper part of the facade, showing a reduction due to the switching of the U-value of about 10 % of the cooling demand and large improvement in the summer operative temperature. It has been shown that an optimized element with switchable an upper U-value of 3 $W*m^{-2}*K^{-1}$ could lead to a reduction of about a third of the cooling demand, showing the potential of switching thermal resistances in the facade. Compared to the traditional free-cooling solution, even the non-optimized element is competitive since free cooling strategies imply additional fan electrical consumptions. Due to the very low visible transmittance of the insulation material used in this project, which was characterized optically, the reduction of cooling load is compensated by the increase of artificial lighting demand, when the upper part of the façade is replaced by the closed movable insulation system.

U-value measurements of different geometrical variations of the façade element with switchable U-value have been presented. The influence of the dimension of the air gaps has been investigated. Test models with one and two insulation plates have been designed, built and characterized experimentally. A factor of two between the U-value of the insulating and of the conducting state has been reached with the first prototypes, proving that it is possible to switch U-values with this technology. Different geometrical configurations have been measured to assess the impact on the performance. It has been shown that in the insulating state, the vertical air columns can be considered as closed cavities if the insulation layer is in the top position. One test model has additionally been measured with CO2 in the cavity, leading to a lower U-value in the insulating state and a higher U-value in the conducting state.

A detailed model has been developed and validated using these measurements: the calculated and measured U-values of different cases have been compared, with a mean relative difference of 9.5 % for the 7 geometries considered. The model shows larger difference for thinner air gaps and high temperature differences. The parametric study showed us that, despite of the chimney effect, it is not advantageous to increase the height of the element. The width has no significant influence on the thermal properties. The analysis also showed that there is an optimal vertical layer thickness to get the maximum U-value in the conductive case, which should be searched for every new configuration. The presence of solar irradiance, by increasing the temperature of the outer air column, slows down the convection in the conductive case. Between the conductive and insulating cases, the g-values did not show important variations, which is due to the low secondary heat gain and the reduced airflow rate in conducting case. During daytime, switching the

element will not help to reduce the g-value. Changing the thickness of the insulation layer, and using calculated thickness-dependent optical properties showed that the g-value could be increased up to 0.26 for 5 mm thickness, both in the insulating and conducting case. Decreasing the thermal conductivity of the insulation layer as well as changing the longwave emissivities of the insulation facing surface of both glazing showed an important impacts.

Using the detailed model, a variant with aerogel was calculated, with the hope of high visible transmittance and better thermal properties instead of the previous translucent insulation material. With two low-e layers, a U-value in the insulating case of 0.24 $W*m^{-2}*K^{-1}$ can be achieved, almost competing with insulated opaque walls. Compared to the prototype used in the building simulation, this would lead to lower heating demands due to higher thermal insulation in winter. However, the U-value in the conductive case is then lower than the one of the first prototype. Ventilator-driven convection is not an option for this configuration with aerogel and low-e due to the high mass flow rates required to achieve important U-values. The next step would be to link the detailed model to find for each transparent insulation material the best geometrical configuration considering:

- the heating demand in winter
- the reducing of the cooling demand in summer
- an optimized translucency, considering that high translucency implies low artificial lighting demand but more important solar gains

3 Removable insulation system

In this chapter, the second innovative switchable insulation technology is investigated. The goals are:

- To investigate the physical phenomenon of heat transfers at different levels in order to optimize the new component.
- To analyze the potential of the new switchable insulation in the building context.

To achieve these goals, contrarily to the previous chapter, where a top-down approach was used in the beginning, a bottom-up method was used: first, the new concept was characterized on the element level, via measurements and modelling. Then, the element was simulated on a building-scale to assess its potential.

3.1 Introduction

In this section, the new switchable insulation presented in this chapter is introduced, as well as the context of this study.

The switchable insulation concept behind this chapter has been invented by Mr. Sergej Kvasnin, owner of the company I[n]solation UG. The patented concept ((Kvasnin 2013) and (Kvasnin 2014)) consists of a series of vertical parallel films that can be winded up or down around a drum. The drum is similar to the ones used for conventional roller blinds. The system can be mounted in front of an existing window as a traditional roller blind system, or in front of a massive opaque wall. Two positions are possible:

- In the insulating state, the films are rolled down, creating N closed air cavities in series, which leads to a high thermal resistance, or a low U-value.
- In the conducting state, the films are rolled up, achieving a low thermal resistance between the cover pane and the existing window or wall. Also, depending on the chosen front and back cover panes, a high solar transmittance can be achieved for the element.

The concept can be applied in front of a window (Figure 34) or a massive wall (Figure 35):

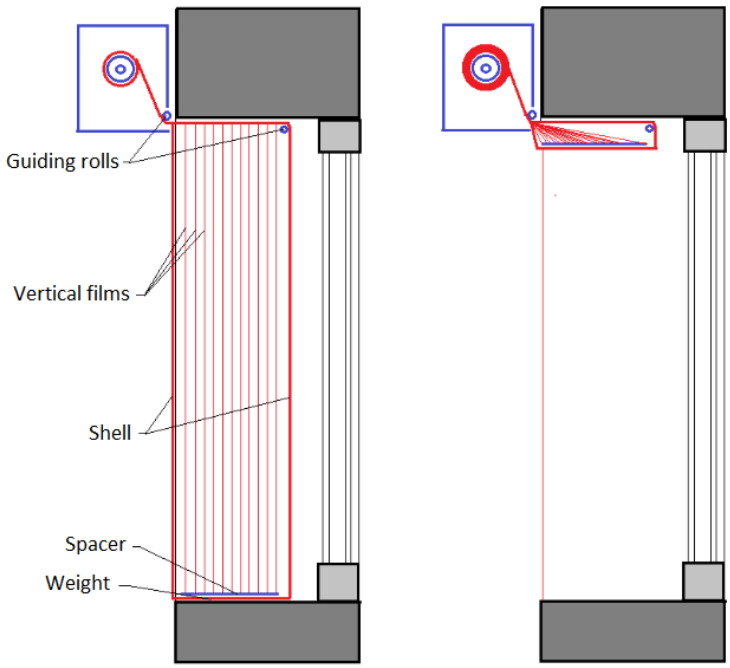

Figure 34 - Scheme of the removable switchable insulation in front of a double glazing, in the insulating (left) and conducting (right) position. Source: S. Kvasnin.

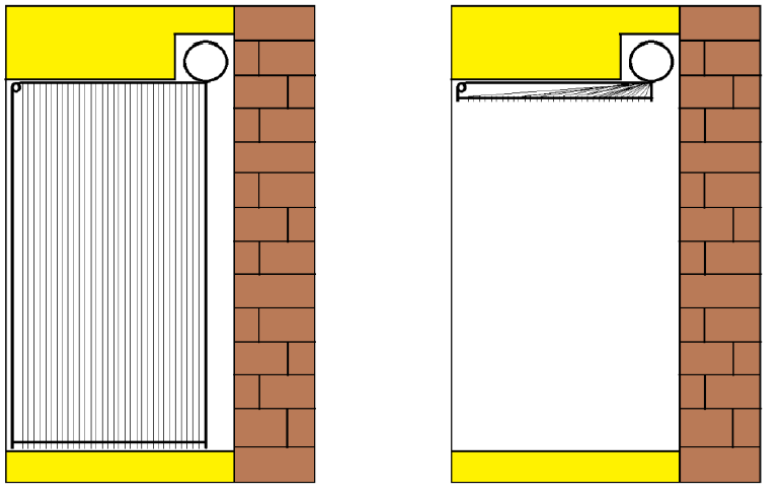

Figure 35 - Scheme of the removable switchable insulation in front of a massive opaque wall, in the insulating (left) and conducting (right) position. Source: S. Kvasnin.

The application in front of a massive wall allows the direct heating or cooling of the building's thermal mass. The outer surface of the wall can be coated with a black paint or a selective coating, in order to increase solar gains during the heating period.

For the first prototypes, the films used were very thin Polyethylene terephthalate (PET) layers, metallized on one side with an Aluminum coating. The films are described and characterized in the experimental part of this study.

3.2 Investigation of an individual component

In this part, the goals are to:

- Assess the thermal and optical properties of the element that can be achieved with the given concept, such as U-value or g-value.
- Assess the impact of different parameters on the performance, and fix the design by choosing:
    - The thickness of the cavity in the conducting state (films retracted), corresponding to the total thickness of the façade element.
    - The thickness of each cavity in the insulating state.
    - The number of cavity in the insulating state.
    - The longwave properties of the films
    - The longwave and solar properties of the outer and inner cover.
- Finally, based on the previous results, select the variants to be simulated on a building level.

To achieve these goals, the films as well as first prototypes are characterized experimentally. Then, the study focuses on a single cavity, before investigating the whole element.

3.2.1 Experimental study

This section focuses on the U-value measurements of the first prototype, as well as the characterization of the longwave properties of the films used.

3.2.1.1 U-value measurement

A first prototype was measured at Fraunhofer ISE. The Taurus apparatus used for this paragraph is described in section 2.3.2.1. The measured prototype consisted of:

- A 2 cm thick wooden frame, with a width of 95 mm and an area of 797*797 mm².
- 10 parallel vertical films, separated by air gaps of about 9 mm, fixed on horizontal lamellas. In this version for testing purpose, the films and lamellas are not removable. The metallized PET films were all oriented in the same direction, with the metallized sides facing the cold plate of the U-value apparatus.
- Two 3 mm wide Plexiglas layers, which act as inner and outer cover. In total, there are consequently 11 air gaps.

Figure 36 - External view of the tested sample.

This prototype has been measured with three different average temperatures and two different temperature differences. The boundary conditions as well as the measurement results are presented in following table:

N°	Temperature of the cold surface [°C]	Temperature of the warm surface [°C]	Temperature difference [K]	Mean temperature [K]	U-value [$W*m^{-2}*K^{-1}$]
1	5.0	14.9	9.9	10.0	0.35 ± 0.03
2	14.7	24.6	9.8	19.7	0.40 ± 0.03
3	24.4	34.2	9.8	29.3	0.44 ± 0.04
4	16.9	21.8	4.9	19.4	0.35 ± 0.03
5	10.3	30.0	19.8	20.1	0.45 ± 0.04

Table 11 - Measurement results of the first removable insulation prototype, measured with the Taurus U-value apparatus.

To compare this value with the one of conventional insulation, the U-value of a 95 mm thick conventional insulation panel with an arbitrary chosen thermal conductivity of 0.035 $W*m^{-1}*K^{-1}$ would be equal to 0.35 $W*m^{-2}*K^{-1}$.

The thermal resistance variates both with the average temperature and the temperature difference. With gap dimensions of less than 1 cm, such a variation is not expected since the convection should not be possible, and IR longwave radiation is limited by the low-e layers in the gaps. This is further detailed in section 3.2.2. The thermal behavior of the measured prototype is explained during the model validation, in section 3.2.3.

3.2.1.2 Measurement of infrared properties

In order to characterize the films used in the first prototypes, the infrared properties where measured at the ISE facility. General information about infrared heat exchange are given in section 3.2.2.1.1.

The film consists of a polyethylene terephthalate (PET) substrate which is metallized on one side with aluminum. The film was produced by the company Tenolan® and has the product number OAM0112. The thickness of the film is 12 µm. The measured sample had an area of about 100*100 mm².

The "cold" and "warm" surfaces in this report refer to the previous U-value measurements, where one side of the film insulation system was electrically heated and the other side kept at a constant temperature. They refer respectively to the aluminum and PET surfaces.The spectral hemispherical reflectance for near-normal incidence (8 ° angle of incidence) of the sample was measured over the IR spectral range from 1.5 µm to 25 µm. A highly sensitive Fourier spectrometer, model IFS 66 from the Bruker company, was used. The spectrometer is equipped with a diffusely reflecting, gold-coated integrating sphere for measurements in the medium infrared range. Diffusely reflecting standards from NIST and NPL are used as references below 17 µm.

First, the measured wavelength-dependent normal-hemispherical transmittance and reflectance of both sides of the sample have been extrapolated from 25 µm to 50 µm, assuming the value measured at 25 µm to be constant until 50 µm, based on the measured evolution of the spectral properties below 25 µm.

Then, the normal thermal emissivity of both surfaces of the sample was determined from the normal-hemispherical transmittance $T_{nh}(\lambda)$ and near-normal-hemispherical reflectance measurements in the infrared range: the normal emissivity $E_{nh}(\lambda)=(1-T_{nh}(\lambda)-R_{nh}(\lambda))$ was weighted with the Planck blackbody radiation spectrum for temperatures of 283.15 K (10°C), 288.15 K (15°C), 293.15 K (20°C) and 298.15 K (25°C), over the spectral range from 1.5 µm to 50 µm.

Similarly, the normal-hemispherical thermal transmittance of the sample and the reflectance of both surfaces were determined by weighting respectively $T_{nh}(\lambda)$ and $R_{nh}(\lambda)$ with the Planck blackbody radiation spectrum for the temperatures above.

For the emissivity, a corrected thermal emissivity according to (DIN EN 12898:2001) has been calculated from the normal emissivity to take into account the angular dependence of the thermal emissivity in the geometrical configuration of the parallel-film insulation, which is comparable to that within an insulating glazing unit. This corresponds to multiply the normal-hemispherical emissivity by a correcting factor to get the hemispherical-hemispherical (or corrected) emissivities needed to use the radiosities calculation method.

The total absolute measurement uncertainty was less than ±0.02.

The measurement results are showed in following tables:

Name	Surface	$\varepsilon_{n,}$ 283.15 K	$\varepsilon_{corr,}$ 283.15 K	$\varepsilon_{n,}$ 288.15 K	$\varepsilon_{corr,}$ 288.15 K	$\varepsilon_{n,}$ 293.15 K	$\varepsilon_{corr,}$ 293.15 K	$\varepsilon_{n,}$ 298.15 K	$\varepsilon_{corr,}$ 298.15 K
Thermal emissivity	**Al surface (cold side)**	0.025	0.030	0.025	0.030	0.025	0.031	0.025	0.031
	PET surface (warm side)	0.471	0.475	0.474	0.477	0.476	0.479	0.478	0.481

Table 12 - Thermal emissivity values (ε) weighted with the Planck blackbody radiation spectrum at different temperatures, either normal (n) or with the DIN EN 12898 correction (corr). Only the second decimal place is significant. The third decimal place is used only to indicate small relative differences.

Name	Surface	nh, 283.15 K	nh, 288.15 K	nh, 293.15 K	nh, 298.15 K
IR reflectance	**Al- surface (cold surface)**	0.975	0.975	0.975	0.975
	PET surface (warm surface)	0.529	0.526	0.524	0.522
IR transmittance	**-**	1E-04	1E-04	1E-04	1E-04

Table 13 - Normal-hemispherical thermal reflectance and transmittance values weighted with the Planck blackbody radiation spectrum at different temperatures. Only the second decimal place is significant. The third decimal place is used only to indicate small relative differences.

The thermal emissivity of about 0.03 on the metallized side corresponds to the values of conventional low-e coatings. The reported results show that the thermal transmittance of the film is negligible and below the uncertainty of measurements.

For the PET surface, an emissivity of about 0.9 is expected for a thicker PET layer, but the measured emissivity for the PET surface is about 0.48. Due to the very small thickness of the PET layer (the overall thickness of the film is 12 µm), the transmittance of the PET layer is non-negligible, and the radiation transmitted through the PET layer is reflected back by the aluminium layer which has a thermal reflectance of about 0.975. Thus, the total reflected value for the PET surface is higher than expected, and the emissivity lower:

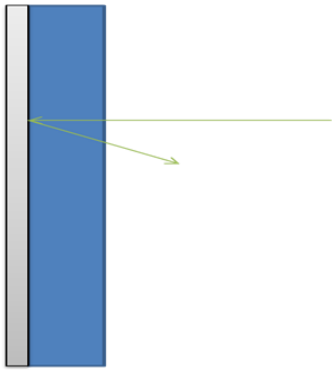

Figure 37 - Radiation transmitted through the thin PET layer and reflected back by the aluminum layer through the PET layer.

It can be observed that the choice of the temperature for weighting using the Planck blackbody radiation spectrum has only a slight influence on the calculated values. For the theoretical investigation and building simulation, the values for a temperature of 293.15 K are chosen. The corrected emissivities of 0.031 and 0.479 for respectively the metallized and PET sides are then used, and the thermal transmittance is assumed to be negligible. IR reflectances of 1-0.031 and 1-0.479 are then used for respectively the metalized and PET sides.

3.2.1.3 Solar properties

The same measured spectral values were also averaged for the solar and visual spectral range according to (ISO 9050:2003). The transmission value was again below the measurement uncertainty of ±0.02, and is therefore neglected, while the reflectance and so the absorptances vary:

	$\rho_{nh,sol}$	$\rho_{nh,vis}$
Al-surface (cold surface)	0.896	0.888
PET surface (warm surface)	0.859	0.854

Table 14 - Solar properties of the foil.

It can be concluded that the films are highly reflective in also the solar and visible spectral area.

3.2.2 Theoretical investigation

In this part, the goals are:

- To detail the physical phenomenon at stake and investigate them, with a particular focus on the convection and longwave radiation heat exchanges within the cavities.
- To assess the impact of thermophysical and geometrical parameters as well as choose the thermophysical and geometrical properties of the element, such as:
    - The thickness of the cavity in the conducting state (films removed), corresponding to the total thickness of the façade element.
    - The thickness of each cavity in the insulating state.
    - The number of cavities in the insulating state.
    - The IR properties of the films.
    - The longwave and solar properties of the outer and inner cover.
- To compare the variants in order to choose the most promising variants to be simulated within the building simulation environment.

To achieve these goals, the element is investigated without the building context:

- First a single cavity is investigated. The analysis is divided in two parts: first the analysis of the convective part, then the analysis of the radiative part and finally the combination of both.
- Then, the whole façade element is studied, consisting of 2 cover panes and several cavities in series.

First, the modeling approach is presented and the required theoretical background is introduced, before producing and discussing the results in a second step.

3.2.2.1 Modeling approach

In this part, the modeling approach used for the analysis of a single cavity and then for the investigation of the whole façade element is detailed.

3.2.2.1.1 Analysis of a single cavity

The heat transfer in a single cavity can be decomposed in two parts:

- The heat transfer through conduction or convection within the gas.
- The heat transfer through longwave infrared radiation between the two surrounding surfaces.

In the optimization done in (Kimber et al. 2014) for a stack of air cavities, the thickness of the polymer layer of 2 mm separating the cavities affects the results and conclusions: the number of layers then reduces the effective space available for insulating air for a given total thickness of the whole element. In our case, the thickness of the films is 12 µm and is

therefore not a constraint: the thermal resistance of the films due to heat conduction within the film can therefore be neglected in our case, since if we assume a thermal conductivity of 0.2 $W*m^{-1}*K^{-1}$, the thermal resistance of the film would be equal to $6*10^{-5}$ $m^2*K^1*m^{-2} \approx 0$.

For the convective problem, an important dimensionless number is the Nusselt number. The Nusselt number can be interpreted as the ratio of convective to conductive heat transfer across a fluid thickness. A Nusselt number of 1 can be interpreted as gas conduction only, while a Nusselt number superior to 1 indicates convection within the cavity:

$$\mathrm{Nu} = \frac{h_{cv} * \lambda}{d}$$ *Equation 49*

With:

- *Nu* [-] the Nusselt number in the cavity.
- λ [$W*m^{-1}*K^{-1}$] the thermal conductivity of the gas at the cavity mean gas temperature.
- *d* [m] the thickness of the cavity.

The Nusselt number depends on the Rayleigh number in the cavity. The Rayleigh number, defined for free convection, is also an indicator of convection: the convection starts above a certain case-dependent critical Rayleigh number, and increase with the Rayleigh number:

$$\mathrm{Ra} = \frac{g * \beta * \Delta T * d^3}{\alpha * \nu}$$ *Equation 50*

With:

- *g=9.81* [$m*s^{-2}$] the standard acceleration due to gravity
- β [K^{-1}] the thermal expansion coefficient, equal to *1/T* for ideal gases.
- ΔT [K] in our case, the difference of temperature between the surrounding surfaces.
- *d* [m] the thickness of the cavity.
- α [m^2*s^{-1}] the thermal diffusivity of the gas, as detailed below.
- ν [m^2*s^{-1}] the kinematic viscosity of the gas.

The thermal diffusivity of a gas represents its capacity to conduct energy away compared to its capacity to store it:

$$\alpha = \frac{\lambda}{\rho * C_p}$$ *Equation 51*

With:

- λ [$W*m^{-1}*K^{-1}$] the thermal conductivity of the gas.

- ρ [kg*m^{-3}] the density of the gas.
- C_p [J*kg-1*K-1] the specific heat capacity of the gas.

The different correlations for the Nusselt number used for closed-cavity convection are summarized for example in (Manz 2003), where they are used by the author to validate a CFD approach of the problem. The correlations were the following:

- (Yin et al. 1978), based on experiments:

$$\mathrm{Nu} = 0.23 * \mathrm{A}^{-0.131} * \mathrm{Ra}^{0.269} \qquad \textit{Equation 52}$$

  Valid for $10^3 \leq Ra \leq 5*10^6$ and $4.9 \leq A \leq 78.7$
  With:

  - d [m] the thickness of the gas cavity.
  - Ra [-] the Rayleigh number in the gas cavity.
  - A [-] the aspect ratio of the gas cavity.

- (ElSherbiny et al. 1982), based on experiments:

$$\mathrm{Nu}_1 = 0.0605 * \mathrm{Ra}^{\frac{1}{3}}$$
$$\mathrm{Nu}_2 = \left[1 + \left(\frac{0.104 * \mathrm{Ra}^{0.293}}{1 + \left(\frac{6310}{\mathrm{Ra}}\right)^{1.36}}\right)^3\right]^{1/3} \qquad \textit{Equation 53}$$
$$\mathrm{Nu}_3 = 0.242 * \left(\frac{\mathrm{Ra}}{\mathrm{A}}\right)^{0.272}$$
$$\mathrm{Nu} = \max(\mathrm{Nu}_1, \mathrm{Nu}_2, \mathrm{Nu}_3)$$

  Valid for $5 \leq A \leq 110$ and a range of Rayleigh number depending on the aspect ratio and presented in Appendix.

  With this correlation, only Nu_3 depends on the aspect ratio and Nu_3 only affects Nu if $A<25$, as stated in (Wright 1996).

- (Wright 1996), based on existing experimental data from other authors:

$$\mathrm{Nu} = \max(Nu_1, Nu_2)$$
$$\mathrm{Ra} > 5 * 10^4: \ \mathrm{Nu}_1 = 0.0673838 * \mathrm{Ra}^{\frac{1}{3}}$$
$$10^4 < \mathrm{Ra} \leq 5 * 10^4: \ \mathrm{Nu}_1 = 0.028154 * \mathrm{Ra}^{0.4134}$$
$$\mathrm{Ra} \leq 10^4: \ \mathrm{Nu}_1 = 1 + 1.7596678 * 10^{-10} * \mathrm{Ra}^{2.2984755}$$
$$\mathrm{Nu}_2 = 0.242 * (\frac{\mathrm{Ra}}{\mathrm{A}})^{0.272}$$

Equation 54

For low aspect ratios, the Wright model uses the Aspect ratio dependent result from ElSherbiny. These correlations were based on measurements up to Rayleigh numbers of about 10^6, but Wright states based on a theoretical analysis that the correlations should be valid well beyond this limit, that's why no upper Rayleigh number limit is given for the first equation.

- (DIN EN 673:2011-04). In this standard, it is not stated whereas the correlation is based on experimental or theoretical results:

$$\mathrm{Nu} = \max(0.0365 * \mathrm{Ra}^{0.38}, 1)$$

Equation 55

The validity range is not stated in the standard. Note that the standard also proposes correlations for horizontal and 45° inclined cavities.

The difference between the models comes not only from different boundary conditions during measurements, but also from the mathematical fitting of the proposed correlations to this measurements or theoretical results. In (Manz 2003), the Yin model showed the most important difference with the CFD calculation and the other models, with a larger Nusselt number and a transition from conduction to convection regime happening with lower Rayleigh numbers. (Wright 1996) states that the critical value of *Ra* at which the flow leaves the conduction regime is a function of the aspect ratio, and that the convective flow leaves the conduction regime at lower *Ra* values in cavity with lower aspect ratios. This is in accordance with the correlation which depends on aspect ratios. Wright also explains that if *Ra* is increased sufficiently, a turbulent boundary layer flow appears. In the turbulent regime, *Nu* increases faster with *Ra*. The critical *Ra* value for the transition from laminar to turbulent regime is a function of the aspect ratio, and the flow in enclosures with more important aspect ratios becomes turbulent at lower *Ra* values.

Although for a given thickness of cavity the temperature difference has the biggest impact, the convective resistance is of course very slightly dependent of the average cavity temperature (mean temperature between the surrounding surfaces): for 2.5 cm thickness, 15K temperature difference and 20°C average temperature, we obtain with the Wright

model Nu=1.83 and R_{conv}=0.53 m²*K*W⁻¹, while for an average temperature of 0°C Nu=2.11 and R_{conv}=0.49 m²*K*W⁻¹, resulting in 1 % difference. This is due to the variation of the Rayleigh number from 25*10³ for 20°C to 34*10³ for 0°C. This increase of the Rayleigh number is mainly due to the increase of the thermal expansion coefficient 1/($T_{average}$) by 7 %, and an increase of the square of the density by 15 %.

For the radiative part, following correlation was used to calculate the radiative longwave heat transfer coefficients between two infinite parallel, grey-diffuse surfaces (Duffie und Beckman 2006):

$$\mathrm{h_{rad}} = \sigma * \left(\frac{1}{\frac{1}{\varepsilon_1} + \frac{1}{\varepsilon_2} - 1} \right) * \frac{\mathrm{T_1^4} - \mathrm{T_2^4}}{\mathrm{T_1} - \mathrm{T_2}} \qquad \textit{Equation 56}$$

With:

- σ= 5.67*10-8 [W*m⁻²*K⁻⁴] the Stefan-Boltzmann constant.
- ε_1, ε_2 [-] the longwave emissivities of both surfaces.
- T_1, T_2 [K] the temperature of both surfaces.

Note that this equation can of course be linearized: if we assume that $T_1 \approx T_2 \approx T_{average}$, then we obtain:

$$\mathrm{h_{rad}} = \sigma * \left(\frac{1}{\frac{1}{\varepsilon_1} + \frac{1}{\varepsilon_2} - 1} \right) * \frac{(\mathrm{T_1} - \mathrm{T_2}) * (\mathrm{T_1} + \mathrm{T_2}) * (\mathrm{T_1^2} + \mathrm{T_2^2})}{\mathrm{T_1} - \mathrm{T_2}} \qquad \textit{Equation 57}$$

$$\mathrm{h_{rad,linearized}} = \sigma * \left(\frac{1}{\frac{1}{\varepsilon_1} + \frac{1}{\varepsilon_2} - 1} \right) * 4 * \mathrm{T_{av}^3}$$

With T_{av} [K] the average temperature between the surrounding surfaces

This linearization is accurate for the range of temperature differences encountered usually within fenestration systems: for T_1-T_2=15K, $h_{rad,\ linearized}$=4.67 W*m²*K⁻¹ and h_{rad} =4.68 W*m²*K⁻¹, while for T_1-T_2=60 K, $h_{rad,\ linearized}$=4.67 W*m²*K⁻¹ and h_{rad} =4.72 W*m²*K⁻¹, showing only 1 % difference. Here, we can also observe that the influence of temperature difference on the longwave heat transfer coefficient is very low.

For the radiative part, (Kimber et al. 2014) assumes that the two limiting layer of a cavity have identical emissivities and zero transmissivities. The relation above, translated into a thermal resistance can then be written as:

$$R_{rad} \approx \frac{2 - \varepsilon}{4 * \varepsilon * \sigma * T_{av}^3} \qquad \textit{Equation 58}$$

With:

- ε [-] the longwave emissivity of the two surfaces
- σ [W*m^{-2}*K^{-4}] the Stefan–Boltzmann constant
- T_{av} [K] the average temperature between the two surfaces

During the analysis of the convective and radiative heat transport in one cavity, the top, bottom and side surfaces of the cavity are assumed to be adiabatic. This assumption is justified by the high aspect ratios of the cavity (typically around 80 for glazings): the back and front surfaces surrounding the cavity are much larger than the top, bottom and side surfaces.

3.2.2.1.2 Analysis of several cavities and whole system

For the thermal analysis of the whole element (from outer pane to inner pane over the stack of cavities), the nodal model presented in (ISO 15099:2003) is used. This model was designed for the calculation of the layer to layer heat transfer through fenestration system. One of the main advantages of this model is that it can easily be extended to a varying number N of cavities, and implemented to a programming code. It is included in numerous building and façade simulation programs, such as EnergyPlus (Crawley et al. 2001) or WINDOW (Lawrence Berkeley National Laboratory 2015).

The main hypotheses are:

- Hypothesis 1: the surface temperatures of each layer are assumed uniform over the height and width. The layers can then be represented by one-dimensional energy nodes. The glass layers are represented by one node, the insulation layer by two surfaces nodes.
- Hypothesis 2: the calculation is steady state (no time-dependency is considered). This is justified by the very low mass (and so thermal capacity) of the films.
- Hypothesis 3: the convective heat transfer coefficients are assumed constant and equal to the average value over the height of the glazed and insulation area. The edge effects at the top and the bottom of the cavity can be neglected with regard to the total heat transferred through the cavity.

The inputs are the geometrical and thermophysical description of the glazing system.
The main outputs are the heat flux toward the room and the temperatures of the layers.

For each node or layer, the energy balance results in following equations:

$$q_i = h_{cv.i} * (T_{ft.i} - T_{b.i}) + J_{ft.i} - J_{b.i} \quad \textit{Equation 59}$$

$$q_i = S_i + q_{i+1} \quad \textit{Equation 60}$$

$$J_{ft,i} = \varepsilon_{ft,i} * \sigma * T_{ft,i}^4 + \tau_i * J_{ft,i+1} + \rho_{ft,i} * J_{b,i-1} \quad \textit{Equation 61}$$

$$J_{b,i} = \varepsilon_{b,i} * \sigma * T_{b,i}^4 + \tau_i * J_{b,i-1} + \rho_{b,i} * J_{ft,i+1} \quad \textit{Equation 62}$$

$$T_{b,i} - T_{ft,i} = \frac{t_{gv,i}}{2 * \lambda_{gv,i}} * (2 * q_{i+1} + S_i) \quad \textit{Equation 63}$$

With:

- $T_{ft,i}$ [K] the front surface temperature of the layer.
- $T_{b,i}$ [K] the back surface temperature of the glazing layer.
- $J_{ft,i}$ [W*m^{-2}] the total longwave radiosity leaving the front surface of the glazing layer.
- $J_{b,i}$ [W*m^{-2}] the total longwave radiosity leaving the back surface of the glazing layer.
- q_i [W*m^{-2}] the total heat flux leaving the layer i towards the layer i-1.
- S_i [W*m^{-2}] the solar irradiance absorbed in the layer.
- $t_{gv,i}$ [m] the thickness of the layer.
- $\lambda_{gv,i}$ [W*m^{-1}*K^{-1}] the thermal conductivity of the layer.
- ε,τ,ρ [-] the infrared longwave properties of the layer.

Here, the method used for the IR longwave heat transfer between the layers is the radiosity method, where the longwave heat fluxes are explicitly calculated. The advantage of this method is that it can be used to model infrared transparent layers.

Within the European project INSPIRE, the ISO15099 thermal model for window has been implemented in the programming language python 3.4 by the author. A comparison of the implementation towards the WINDOW 7.2 software and a validation of the model for ventilated window using experimental data from the company Gruppo TOSONI has been done in (Braesch 2015) under the supervision of the author.

3.2.2.2 Results and discussion

In following section, the calculation results for the analysis of one single cavity are presented, before extending the results to several cavities and the whole element. Finally, the designs to be simulated at building level are defined.

3.2.2.2.1 Analysis of a single cavity

In this part, the different properties of a single air cavity are investigated. The goals are to understand the physical process at work as well as to determine the recommended thickness of the cavity and the infrared properties required to get the best insulating properties. First, the convection only is analyzed. Then, the IR longwave heat transport alone is analyzed. Finally, the cavity is analyzed with both phenomena combined.

If only convection is considered, in the insulating case the Rayleigh number has to be the lowest possible to minimize or prevent convection, by having the Nusselt number as near as possible to 1. Different models for closed-cavity convection where compared, for a cavity mean temperature of 20°C, and two temperature differences between the surrounding surfaces of 5K and 15K, using isothermal boundary conditions. These temperature differences are already very high for the insulating state: for example, for 10 cavities, this would result in respectively 50 K and 150 K temperature difference over the whole element. The fixed cavities' height was 0.76 m as a starting point, corresponding to the prototype of switchable insulation measured in laboratory. The convective thermal resistances and the Nusselt number, dependent on the cavity thickness (and on the aspect ratio), are shown in respectively Figure 38 and Figure 39 below.

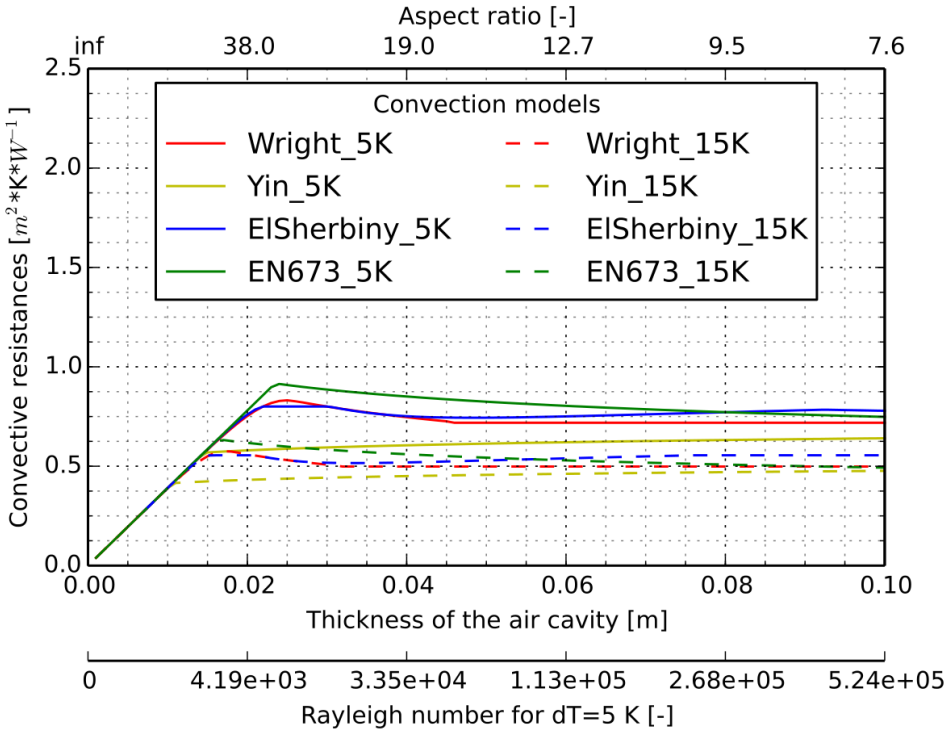

Figure 38 - Convective thermal resistance of a single cavity, calculated with different models for the Nusselt number, with 5 K and 15 K temperature difference at the boundaries. When the curve is outside the validity range of the correlation the points are not plotted.

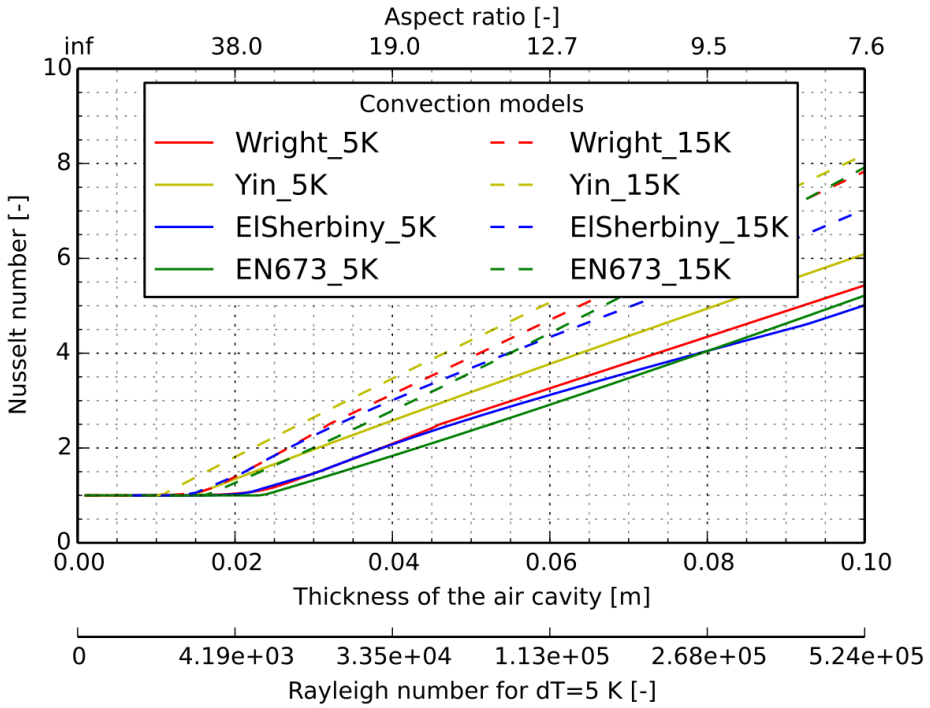

Figure 39 - Nusselt number calculated with different models with 5 K and 15 K temperature difference at the boundaries. When the curve is outside the validity range of the correlation the points are not plotted.

The Nusselt number is equal to 1 until a certain thickness is reached, after which convection becomes significant. After that, the convection compensates the potential additional insulation provided by the additional air thickness, and the convective resistance is more or less constant, as observed also in (Wright 1996). For 5 K temperature difference the thickness after which convection starts is about 1.8 cm, with Nusselt numbers of 1.02 and 1.01 for the Wright and ElSherbiny models. With the Yin model, the start of the convection is predicted earlier, with a Nusselt number of 1.03 for 1.5 cm, while for the EN673, it is predicted later with a Nusselt number of 1.03 for 2.4 cm. After the start of the convection, the convective resistance reaches a maximum for values around 2.5 cm for the 5K temperature difference and the Wright or ElSherbiny correlations. The maximum is slightly higher with EN673. The Yin correlation predicts a significantly higher Nusselt number and lower resistance, and does not predict a maximum for the resistance. For a higher temperature difference of 15 K, the convection starts with a smaller thickness of about 1.2 cm, with Nusselt numbers of 1.02 and 1.01 for respectively the Wright and ElSherbiny models. The maximum resistances are lower than in the 5 K difference case due to higher Rayleigh numbers, and are reached earlier for a thickness of about 1.7 cm.

In the insulating state, the goal is to have the highest thermal resistance for each cavity. To achieve that from the convective point of view, a Nusselt number of 1 (only conduction) should be aimed for. For the already high temperature differences of 5 K and 15 K, a thickness of 1 cm is low enough to stay in the "full" conduction range. It has been checked (graphs visible in Annex), that for other heights (0.5 m and 2m), the convection doesn't start earlier. Even for the Ying model that predicts convection for the lowest thickness among all models, for 50 cm height and 15 K temperature difference, the 1 cm thickness is still in the conductive range. A lower thickness would results in an unnecessary additional number of films. Therefore, the thickness of 1 cm is chosen.

Concerning the choice of the convection model, (Kimber et al. 2014), modelling also a succession of air cavity in series, choses the correlation presented in (Wright 1996). The choice of convection model is only relevant for the "conducting" case, without films and a large air cavity. The Wright model is also the approach from the standard (ISO 15099:2003). The Wright correlations were based on measurements up to Rayleigh numbers of about 10^6, but Wright states based on a theoretical analysis that the correlations should be valid well beyond this limit. (Wright 1996) also proposes that the correlations of (ElSherbiny et al. 1982) may be used for aspect ratio below 40. The Wright model is then very practical to use, covering a large range of Rayleigh numbers and aspect ratios. From the accuracy point of view, Wright doesn't indicate an uncertainty range, but the correlation is for example partially based on results from ElSherbiny, which had an experimental uncertainty of ±3 % on Nu (Wright 1996). The statistical error due to the fitting of the Wright correlation to these measurement data is not given.

In a second step, the longwave radiative exchange only is analyzed. In our case, the emissivities of the two surfaces limiting a cavity are different: one surface is the metalized

side of the layer, with a thermal emissivity of 0.03, and can be considered as a low-e layer. The PET surface has an emissivity of 0.48. The infrared longwave transmittance is negligible (see measurement results), as is the variation of the emissivity with temperature (see 3.2.1.2). To calculate the radiative heat transfer coefficient, Equation 37 can be used assuming infinite parallel and isothermal surfaces. The influence of the temperature difference is negligible, as shown later in this section. In following graph, the influence of the average temperature is investigated for a constant difference of temperature of 5K, and for different infrared properties, as for example an emissivity of float glass of 0.84 for the opposite surface (DIN EN 673:2011-04):

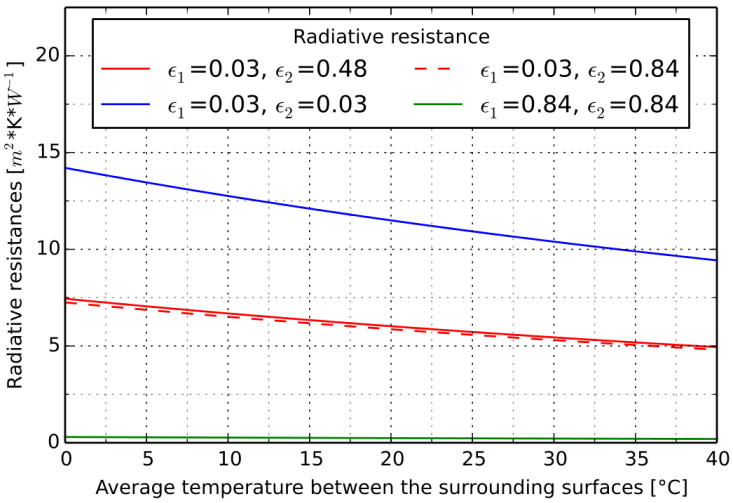

Figure 40 – Radiative resistances as a function of the average temperatures of the surrounding surfaces, with different longwave properties.

There is an important dependence of the radiative resistance on the average temperature. For several cavities in series, if one would assume a constant radiative heat transfer coefficient at the mean temperature between the external and internal boundary layer, this would then lead to overestimate the resistances towards the colder boundary and underestimate the resistance towards the warmer one. Globally, even if the total resistance may be near to the reality, the temperature calculation within the system may show differences.

The starting point is the real used layers, with one surface with an emissivity of 0.03 seeing an opposite surface with an emissivity of 0.48. If the opposite layer would be glass (with ε = 0.84), the difference with the previous case would be very low. On the contrary, if a low-e layer would be applied to the other side, the thermal resistance could be significantly improved. These conclusions are only valid without air.

To conclude on the single cavity problem, taking the real infrared properties of the films used in the prototype, with emissivities of 0.03 on the one side and 0.48 on the other side, we can remark that R_{rad}>>R_{conv}. Without low-e layer, both resistances are much closer. The total thermal resistance (convective and radiative) of the gap is most influenced by the

lowest resistance, due to both resistances acting in parallel. This is also underlined by following graphic, where the equivalent resistance of the two resistances in parallel is shown, as a function of the thickness of the air gap, for temperature differences of 5 K and 15 K and a mean temperature of 20°C. It must be noted that, for low aspect ratios, the infinitely long parallel plate assumption may not be valid anymore. The Wright model was used for convection:

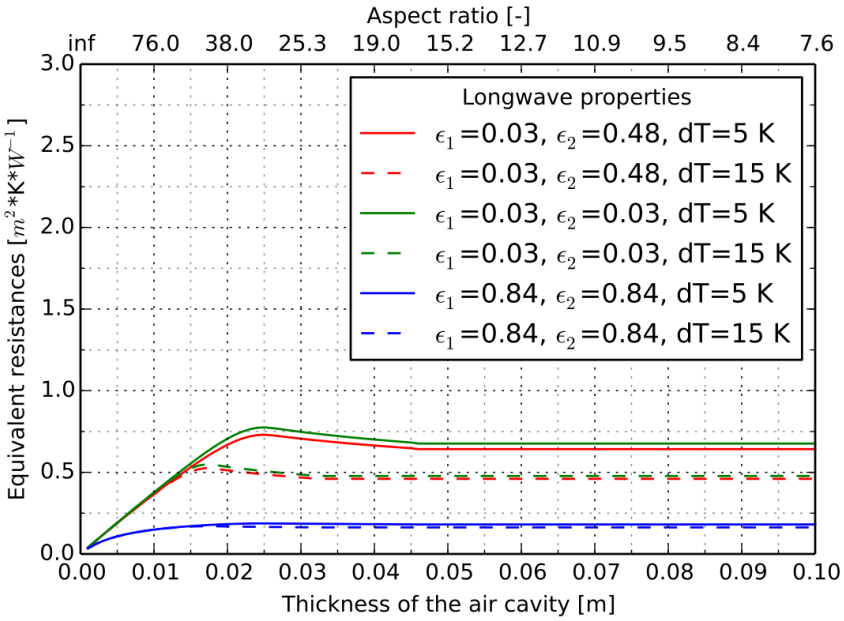

Figure 41 - Equivalent thermal resistance of a single cavity, calculated with different infrared longwave properties, with 5 K and 15 K temperature difference at the boundaries, 20°C average temperature.

Without low-e layer, the radiative heat transfer has an important effect, and after about 2 cm thickness the equivalent resistance doesn't vary much with the thickness. In this case, the equivalent resistance is independent of the temperature difference. As soon as there is a low-e layer in the cavity, the equivalent resistance is dominated by the convective effect, a maximum is reached around 2 cm thicknesses, and the results are temperature dependent. Note that adding then a second low-e layer only improves very slightly the equivalent resistance due to the dominating effect of the convective resistance.

The conclusion of this single cavity analysis is that that the cavity thickness should be chosen in order to stay in the "purely" conductive range. For the following analysis of a stack of cavity, a thickness of 1 cm is chosen. Also, with the actual film, if we divide one large cavity, which thickness is already below the convection limit, into several cavities with an even lower thickness, this will not affect the convective part, since the Nusselt number was already equal to 1, but will add radiative resistances. However, the benefice of doing that is really low, because the maximum resistance we can get is the one from the cavity with two low-e layers. In other words, the chosen film, with low-e layer on one surface and PET on the other is sufficient to get almost the maximum possible thermal resistance for one cavity.

3.2.2.2.2 Analysis of several cavities and whole system

In this part, the whole façade element is investigated without the building context. The impact of the thermal mass is then not analyzed here, but will be investigated within the building simulation: in case of the wall variant, the internal wall behind the element is treated as an internal isothermal boundary. Based on the conclusions from the previous conclusions, the properties of a stack of cavities together with different boundary layers are analyzed in this chapter. The goals are to:

- Investigate the impact of the cavity's thickness in the conducting state (films retracted), corresponding to the total thickness of the façade element and to a certain number of cavities in the insulating state, with a fixed thickness of 1 cm for each cavity.
- Investigate the effect of different IR longwave and solar properties of the outer and inner cover on the performance indicators.
- Finally, select the variants to be simulated on a building level.

The whole system is delimited by a glazing or a wall at the interior side, and an external cover glazing. Between the two cover layers, the multilayer insulation is rolled down (insulating state) or up (conducting state). From the previous section we know that an optimum thickness of the gap between two films is 1 cm. This optimum has been chosen in order to make sure that the heat transfer between two films is in the conduction regime which ensures the most efficient insulation function. The measured IR longwave properties of the films (see 3.2.1.2) were performant enough and these films will also be used in this part. This corresponds to a thermal emissivity of 0.031 for the metallized side of each film, and 0.479 for the PET side. As a convention, for the stack of cavities, all metallized surfaces are facing the exterior. It has been checked that the facing direction of the metallized surfaces does not affect the performance indicators significantly, both sides having about the same optical properties in the solar range (see 3.2.1.3).

In this investigation, following properties are aimed for:

- In the insulating case: the lowest possible U-value and g-value, to respectively reduce heat loss during the night in the heating period and overheating during the day in the cooling period.
- In the conducting case:
    - A high U-value already for low temperature differences, to favor the evacuation of heat in the night of the cooling period.
    - A high g-value to maximize the solar gains during the sunny days in the heating period.

The approach defined in the standard (ISO 15099:2003) and described in the modeling approach was used as a basis for the calculations. The boundaries for the calculations of the thermal resistances, U-values and g-values were:

- The external air temperature and exterior constant boundary heat transfer coefficient of 25 $W*m^{-2}*K^{-1}$, as given for example in (DIN EN 673:2011-04). This allows the comparison with U-values traditional glazing and wall components.
- The room air temperature and interior constant boundary heat transfer coefficient of 7.69 $W*m^{-2}*K^{-1}$

The definition of the U-values and g-values used in this calculation are similar to respectively 2.4.1.2 and 2.4.1.3. For the calculation of the g-value, the part of incident solar irradiance absorbed in each part of the system has been calculated using the software WINDOW7.2 (Lawrence Berkeley National Laboratory 2015).

The influence of the total thickness of the element on the U- and g-values in the insulating and conducting state has been investigated, for different inner and outer cover panes. In the insulating state, the thickness of each cavity is fixed (1 cm) for following cover panes:

Name of variant	Outer cover		Inner cover		Application
SB	Solar glass	ID=4337 τ_{sol}=0.910 $\rho_{sol,1}$=0.079 $\rho_{sol,2}$=0.079 τ_{vis}=0.916 ε_1=0.84 ε_2=0.84	Black painted metal plate with high solar absorptance	ID=274 τ_{sol}=0 $\rho_{sol,1}$=0.055 $\rho_{sol,2}$=0.069 τ_{vis}=0 ε_1=0.90 ε_2=0.93	Wall
SB+low-e	Solar glass	ID=4337 τ_{sol}=0.910 $\rho_{sol,1}$=0.079 $\rho_{sol,2}$=0.079 τ_{vis}=0.916 ε_1=0.84 ε_2=0.84	Black painted metal plate with high solar absorptance + low-e	ID=274+low-e τ_{sol}=0 $\rho_{sol,1}$=0.055 $\rho_{sol,2}$=0.069 τ_{vis}=0 ε_1=0.03 ε_2=0.84	Wall
SS	Solar glass	ID=4337 τ_{sol}=0.910 $\rho_{sol,1}$=0.079 $\rho_{sol,2}$=0.079 τ_{vis}=0.916 ε_1=0.84 ε_2=0.84	Solar glass	ID=4337 τ_{sol}=0.910 $\rho_{sol,1}$=0.079 $\rho_{sol,2}$=0.079 τ_{vis}=0.916 ε_1=0.84 ε_2=0.84	Window
KS	K-glass, 4 mm thick	ID=4140 τ_{sol}=0.704 $\rho_{sol,1}$=0.106 $\rho_{sol,2}$=0.118 τ_{vis}=0.825	Solar glass	ID=4337 τ_{sol}=0.910 $\rho_{sol,1}$=0.079 $\rho_{sol,2}$=0.079 τ_{vis}=0.916	Window

		ε_1=0.837 ε_2=0.173		ε_1=0.84 ε_2=0.84	
SK	Solar glass	ID=4337 τ_{sol}=0.910 $\rho_{sol,1}$=0.079 $\rho_{sol,2}$=0.079 τ_{vis}=0.916 ε_1=0.84 ε_2=0.84	K-glass, 4 mm thick	ID=4140 τ_{sol}=0.704 $\rho_{sol,1}$=0.106 $\rho_{sol,2}$=0.118 τ_{vis}=0.825 ε_1=0.173 ε_2=0.837	Window

Table 15 - Different configuration tested, glazing properties taken from (Lawrence Berkeley National Laboratory 2015). The optical properties are given for 0° incidence angle. The indices 1 and 2 indicate respectively "facing the exterior" and "facing the interior".

The solar glass is a very performant glass, with high transmittance both in the solar and visible range. The opaque black painting is absorbing in the solar range, and is for example used for solar collectors. The opaque selective black painting has the same absorptance in the solar range (hypothesis), but a low thermal emissivity in the infrared range. The term "selective" refers to these different properties for different wavelength.

For the window application, K-glass is used instead of a low-e layer. The reason is that the façade element cannot be completely air-tight (sealed glass unit), since this would cause dilatation issues that could damage the coatings or glazings. If the element is not sealed, the air entering from the exterior brings humidity, which would damage the low-e coating. The K-glass has a higher thermal emissivity than a low-e coating, with values around 0.17 instead of 0.03, but is resistant to humidity.

First, the U-value where calculated. In the conducting state, when insulation is removed, then the outer glass pane delimiting the system forms a cavity with the internal glazing, and we return to the situation of the previous section. In the insulating case, the thermal resistance must be guaranteed in the worst case, which is for an important temperature difference, since the overall resistance decreases with temperature difference due to the augmentation of the Rayleigh number in the cavities. That is why in the insulating case, the element is simulated with a temperature difference of 25 K at the boundary. Also, in the insulating state, the temperature difference has only little difference on the thermal resistance since we are insured that convection within the 1 cm gaps is avoided.

For the calculation of the U-value, the element average temperature was 21°C, and two differences of temperature were simulated. In the case of the wall application, the thermal resistance and mass of the wall are ignored (stationary calculation). For the building simulation, these parameters are taken into account. The results for the application on the wall are showed in following picture:

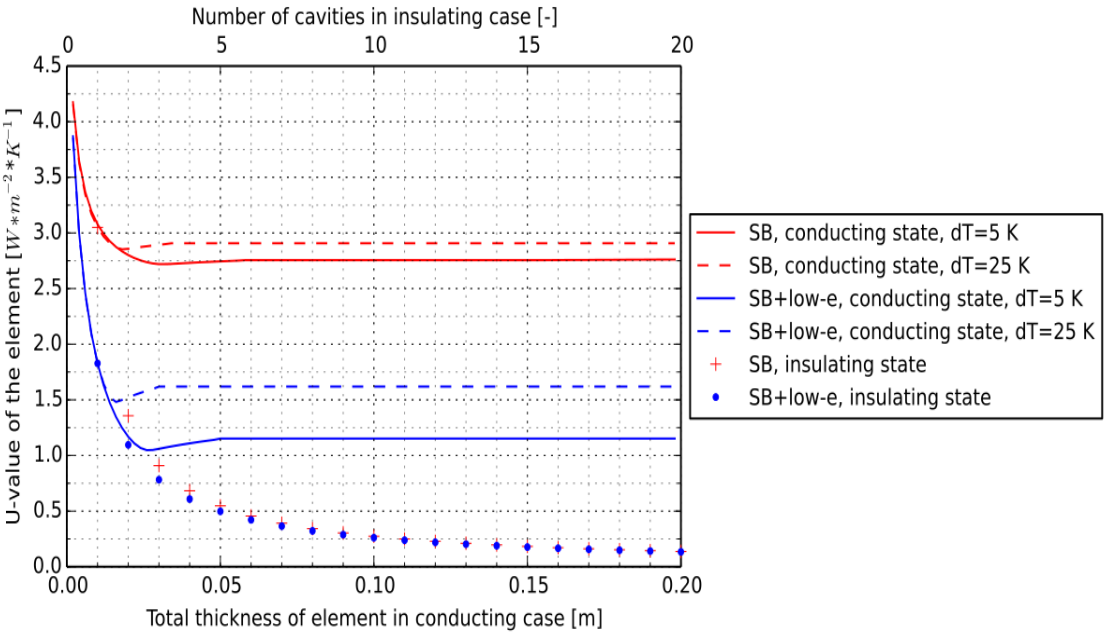

Figure 42 - U-value calculated as a function of the total thickness of the element and the number of cavities in the insulating case, for different inner and outer panes for the application on the wall. The thickness of the cavities in the insulating case is fixed (1 cm).

In the insulating case, the additional selective painting (SB+low-e) has an impact for a low number of cavities, since the relative importance of the innermost cavity's resistance increases. For 15 cavities, a U-value of about 0.18 $W*m^{-2}*K^{-1}$ is reached, while for 20 cavities (and 20 cm overall thickness), the U-value decreases to about 0.14 0.18 $W*m^{-2}*K^{-1}$. It is interesting to note that this value is below the passive house requirement for opaque walls.

In the conductive case, the transition in the convection regime is achieved in the first centimeters. For more important distances between the two cover panes, an almost constant U-value is reached, which depends on the temperature: the additional insulating air thickness compensates the increasing closed-cavity convection, as shown in the previous section. The use of a selective painting decreases the U-value in the conducting case by a factor of about 2, depending on the temperature difference. This has mainly an influence in the summer night case, where the lower U-value in conducting case will diminish the cooling of the thermal mass. It can also be observed that the U-value in the conducting case varies more with the selective painting, since then the part of convection in the total thermal resistance is more important.

Then, the results for the window application were calculated:

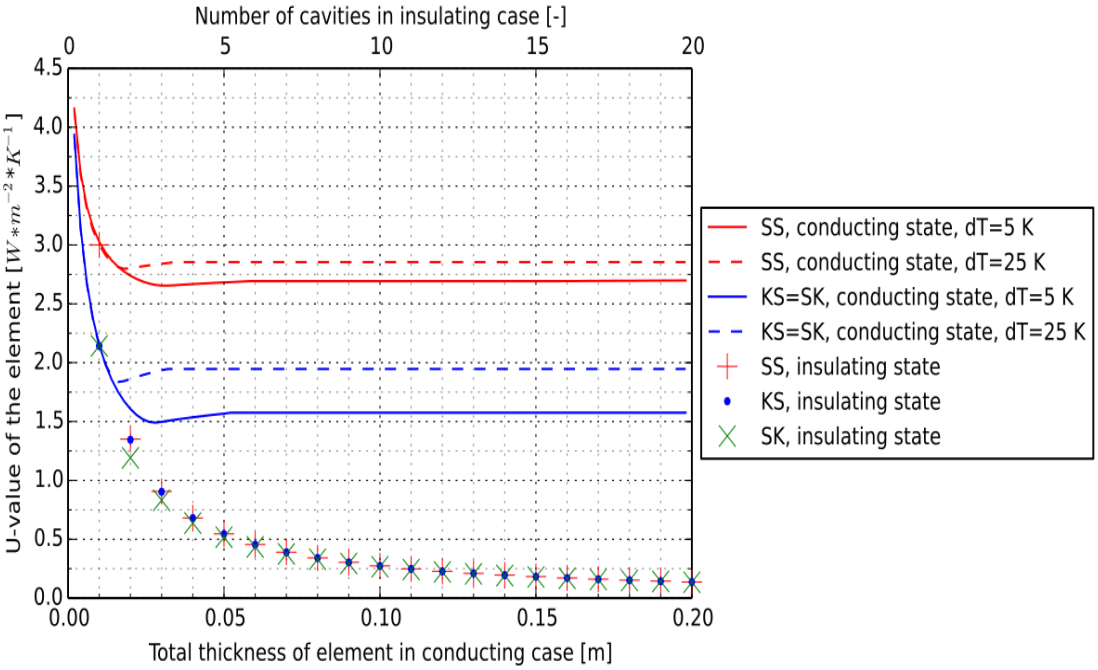

Figure 43 - U-value calculated as a function of the total thickness of the element and the number of cavities in the insulating case, for different inner and outer panes for the window application. The thickness of the cavities in the insulating case is fixed (1 cm).

The solar glass-solar glass solution offers the highest U-value in the conducting state of about 2.75 $W*m^{-2}*K^{-1}$. In the conducting state, the cases SK and KS are identical with lower values due to lower infrared exchange. Also, the dependence on the temperature difference increases due to the higher importance of the convective resistance relatively to the infrared thermal resistance.

In the insulating case, with a number of cavities between 2 and 5, the SK variant has the lowest U-value. This is due to the fact that in the innermost cavity, the K-glass, facing a PET surface, diminishes the longwave exchange. For the KS surface, in the outermost cavity the K-glass doesn't bring much benefit since it is facing the low-e surface of the exterior film, while in the innermost cavity there is nothing to diminish the Infrared exchange. For a more important number of cavities, the differences in U-value are much lower.

Based on this U-value results, it seems reasonable to have an important number of cavities or overall thickness, since after the first 5 cm the U-value in the conducting state doesn't diminish anymore, while the U-value in the insulating case continue to decrease, thus increasing the ratio between the U-value in conducting and insulating state.

In a second step the g-values have been calculated. In the insulating case, with the insulation layers rolled down, it can be assumed that the g-value is null by applying a rapid energy balance to the system: it is assumed that the direct solar irradiance arrives at the outer film with 0° incidence angle: for an incidence angle superior to 0°, more irradiance would be reflected at the cover glazing and the g-value would be lower. To estimate the part of incoming solar energy absorbed at the film's surface, it is assumed that the PET surface is facing the exterior, which induce a more important solar absorbed energy than the metallized side due to a lower solar reflectance of $\rho_{nh,sol}$=0.859. The portion of solar irradiance absorbed at the outer film is then assumed to be 1- $\rho_{nh,sol}$=0.141. The solar absorptance absorbed in the outer solar glass pane is neglected.

The total heat transfer coefficient between this outer film and the exterior is given by:

$$h'_{ext} = \frac{1}{\frac{1}{h_{ext}} + R_{cavity,1\ cm}}$$ *Equation 64*

With:

- h_{ext} [W*m^{-2}*K^{-1}] the boundary exterior heat transfer coefficient of 25 W*m^{-2}*K^{-1}.
- $R_{cavity,\ 1cm}$=0.366 [m^2*K*W^{-1}] the thermal resistance of a 1 cm cavity as calculated in the analysis of a single cavity for a temperature difference of 5 K. This is to take into account the resistance between the outer film and the outer glazing. To be conservative, it is this time assumed that the metallized side is facing the glazing, to have a higher thermal resistance and a higher g-value as more energy will flow towards the interior.

The total heat transfer coefficient between this outer film and the room is given by:

$$h'_{int} = \frac{1}{\frac{1}{U} - \frac{1}{h'_{ext}}}$$ *Equation 65*

With:

- U [W*m^{-2}*K^{-1}] the U-value of the element. An U-value of 0.137 W*m^{-2}*K^{-1} is assumed for the element in the insulating case, corresponding to 20 cavities of 1cm thickness each, plus the boundary heat transfer coefficients.
- h'_{ext} [W*m^{-2}*K^{-1}] the total heat transfer coefficient between the outer film and the exterior as defined above.

A simple energy balance then gives following result with the definition of the g-value given previously and taking into account that the solar transmission of the films is null:

$$g = \frac{h'_{int} * \alpha_{sol,outer\ film}}{h'_{int} + h'_{ext}}$$ *Equation 66*

With $\alpha_{sol,outer\ film}$ the part of incoming solar energy absorbed at the outer film.

Applying the above equations shows that the g-value in the insulating state is below 0.001 and can be considered as negligible. This is partially due to the high exterior heat transfer coefficient of 25 $W*m^{-2}*K^{-1}$. With a low external boundary heat transfer coefficient of for example 1 $W*m^{-2}*K^{-1}$, the g-value would increase to about 0.02, which is still very low. This is of course due to the high thermal resistance provided by the stack of cavities.

For the calculation of the g-value in the conductive case, winter boundary conditions were chosen, with a mean temperature between room air and exterior air of 10°C, and a direct solar irradiance of 500 $W*m^{-2}$ incoming at the façade with 0° incidence angle. The amount of solar energy absorbed in each layer has been calculated using WINDOW 7.2 (Lawrence Berkeley National Laboratory 2015).

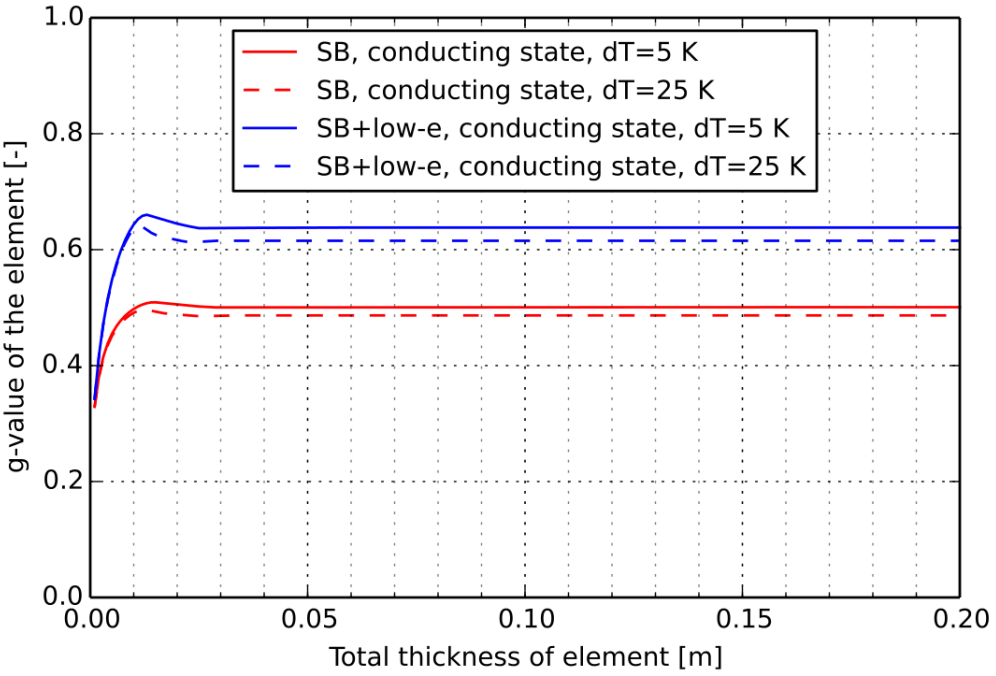

Figure 44 – g-value calculated as a function of the total thickness of the element, for different inner and outer panes for the application on the wall.

For this calculation, it has been assumed that the selective painting has the same optical properties in the solar range than the standard black painting.

A high g-value in the conducting state is of advantage since it allows gathering more solar energy when there is enough solar irradiance in the heating period.

The variation of the g-value with the total thickness follows the trend of the thermal resistance of one air gap detailed in the investigation of a single air gap. The more important is the thermal resistance between the glazings, the less absorbed solar energy

flows towards the exterior. For the same reason, the variant with selective painting shows a more important g-value. The maximum of the g-value corresponds to the maximum of the convective thermal resistance.

For the case with selective painting, the difference between the two temperature differences is more important than in the case with standard black painting. This is due to the fact that in the selective painting case, the convective heat transport has more importance.

For the case without selective painting, where the influence of longwave radiation in the cavity is slightly higher due to the absence of low-e layer, it has been checked that the influence of the average temperature is very low.

The g-value is also calculated for the window application, also in conducting state:

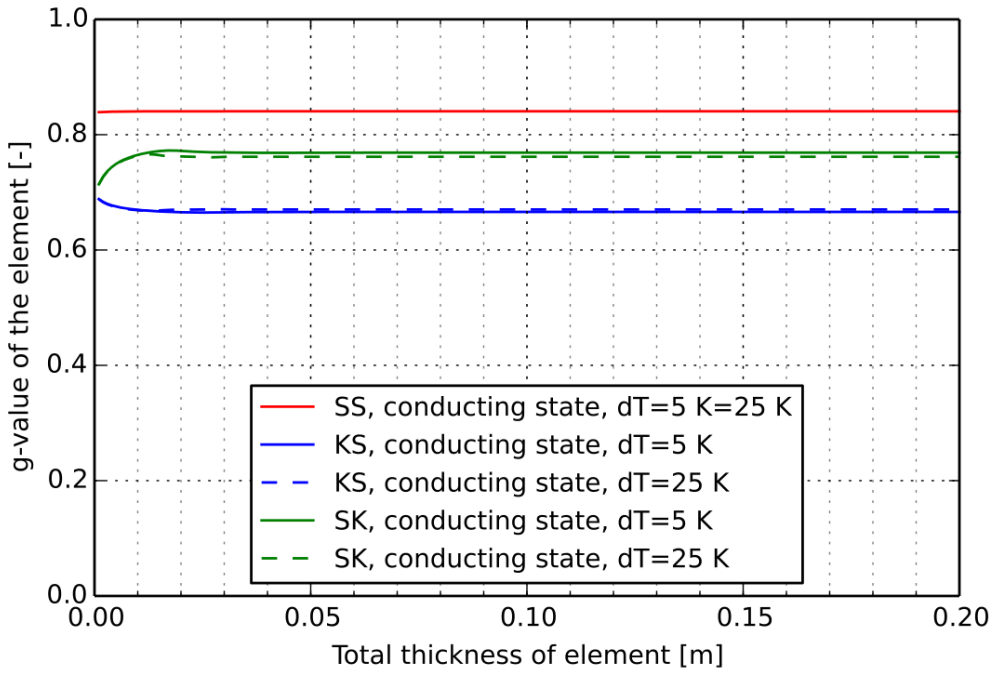

Figure 45 - g-value calculated as a function of the total thickness of the element, for different inner and outer panes for the application on the window.

For the case with two solar glasses, the absorbed energy and so the secondary heat gain are very low, and consequently there is no variation with temperature or total thickness.

For the case with K-glass at the outer cover, more solar energy is absorbed at this outer pane. A thickness of the air gap between the cover panes below 1 cm implies a lower convective resistance, and more absorbed energy flows towards the interior. For the SK variant, it is the opposite since the K-glass is at the inner position.

It can be remarked that the external heat transfer coefficient of 25 $W*m^{-2}*K^{-1}$ used in this preliminary calculations and given for example by the standard (DIN EN 673:2011-04) is high. In reality, this external heat transfer coefficient is often lower. The consequence would be a lower U-value, but also a lower g-value, as more absorbed energy flows toward the exterior. For the building simulation, a variating external heat transfer coefficient based on wind-dependent correlation will be used.

The results are summarized in following table for a total thickness of 20 cm in the conductive state and 20 cavities (20 cm) in the insulating state. The U-value is given for 25 K temperature difference in the insulating case and for 5 K temperature difference in the conductive case to have conservative results. For the same reason, the g-value was calculated with a 25 K temperature difference and 10 °C average temperature:

For 20 cm thickness in the conducting state and 20 cavities in the insulating state, the results are the following:

Name of variant	U-value, insulating state	U-value, conducting state	g-value, conducting state	Application
Unit	$W*m^{-2}*K^{-1}$	$W*m^{-2}*K^{-1}$	-	
SB	0.137	2.762	0.487	Wall
SB+low-e	0.134	1.152	0.615	Wall
SS	0.137	2.699	0.840	Window
KS	0.137	1.576	0.670	Window
SK	0.135	1.576	0.762	Window

Table 16 - Summary of the calculated properties of different variants, for a total thickness of 20 cm in the conducting state and 20 cavities in the insulating state. The number of digits is not an indication of the accuracy of the model but is rather to show small relative differences. The U-value is calculated with 25 K temperature difference in the insulating case and for 5 K temperature difference in the conductive case to have conservative results. For the same reason, the g-value was calculated with a 25 K temperature difference and 10 °C average temperature.

In all cases, adding low-e properties to the covers doesn't affect the U-value in the insulating case (with the insulation rolled down) since they are already 13 other insulating cavities at work.

For the wall application, having an IR-selective painting on the wall allows to increase the g-value from 0.59 to 0.62, but the U-value in the conducting case decreases dramatically from 2.76 to 1.15. Consequently, for the building simulation, the variant without low-e is chosen. In reality, a layer could be added between the wall and the painting to prevent the condensed humidity to penetrate the wall.

For the window application, replacing one of the two glazings by a K-glass with lower emissivity only lowers both the U-value in the conducting case and the g-value in the conducting case, bringing no benefit. Consequently, for the building simulation the variant with two solar glasses is chosen.

Similar results are presented for a thickness of 15 cm or 15 cavities:

Name of variant	U-value, insulating state	U-value, conducting state	g-value, conducting state	Application
Unit	$W*m^{-2}*K^{-1}$	$W*m^{-2}*K^{-1}$	-	
SB	0.183	2.755	0.487	Wall
SB+low-e	0.177	1.152	0.615	Wall
SS	0.183	2.693	0.840	Window
KS	0.182	1.575	0.670	Window
SK	0.179	1.575	0.762	Window

Table 17 – Summary of the calculated properties of different variants, for a total thickness of 15 cm in the conducting state and 15 cavities in the insulating state. The number of digits is not an indication of the accuracy of the model but is rather to show small relative differences. The U-value is calculated with 25 K temperature difference in the insulating case and for 5 K temperature difference in the conductive case to have conservative results. For the same reason, the g-value was calculated with a 25 K temperature difference and 10 °C average temperature.

While the results in the conducting case are very near to the case with 20 cm/20 cavities, there is a significant increase in the U-values in the insulating state. For heating dominated climates, it is then of advantage to have 20 cavities of 1 cm each in the insulating case, corresponding also to an overall thickness of 20 cm between the two cover panes in the conducting case.

To summarize, for the building simulation, following elements are chosen with 20 cavities and 20 cm overall thickness:

- The solar glass-black painting (not selective) variant for the wall application
- The solar glass-solar glass variant for the window application.

3.2.2.2.3 Investigation on the U-value and g-value

In order to calculate easily the U-value and g-value of the façade element in all situations, it is interesting to check the dependence of:

- The U-value to the temperature difference between the room air temperature and the exterior air temperature, as well as the average temperature between room and exterior air temperature.
- The g-value to:
    - The angle of incidence of direct irradiance.
    - The total amount of incoming irradiance.
    - The temperature difference between the room air temperature and the exterior air temperature.
    - The average temperature

In this part, a secondary goal is also to establish polynomial fits of the U- and g- functions. To assess the accuracy of this polynomial fit, the R^2 value is used. The coefficient of determination R^2 shows how well the polynomial values fit to the calculated ("true") values. R-square ranges from 0 to 1. If R^2 is close to 1, the polynomial fit explains all the variability of the calculated values around its mean; on the contrary if R^2 gets closer to 0 the polynomial fit is unable to represent the variability of the calculated values around its mean.

Only the SS (window) configuration selected for the building simulations is investigated, in the insulating and conducting cases. For this SS case, the internal and external boundary heat transfer coefficients were identical to the previous analysis.

First, the dependence of the SS (solar glass – solar glass covers) on the temperature difference between inside and outside air was tested:

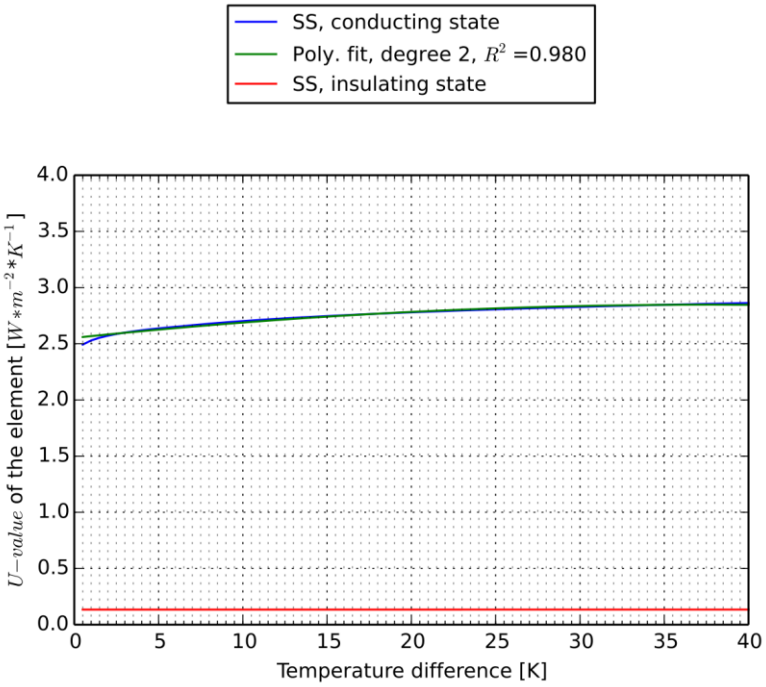

Figure 46 - SS case, U=f(dT) in the insulating and conducting case, for an average temperature between room and exterior air of 15°C.

In the insulating state, the U-value is constant with a value of 0.134 $W*m^{-2}*K^{-1}$. In the conducting case (only two solar glasses separated by 20 cm of air), the U-value varies with the temperature difference as expected from the previous analysis, and a first degree polynomial is not enough to represent the U-value with a R^2 value of 0.900. This is mainly due to the domain below 5 K where the U-value varies strongly with the temperature difference, caused by the start of the convection in the 20 cm air gap. A second degree polynomial is a better approximation, with significant differences only for a temperature difference below 2 K.

For the same façade configuration, the dependence of the U-value on the average temperature between room and exterior air has been tested:

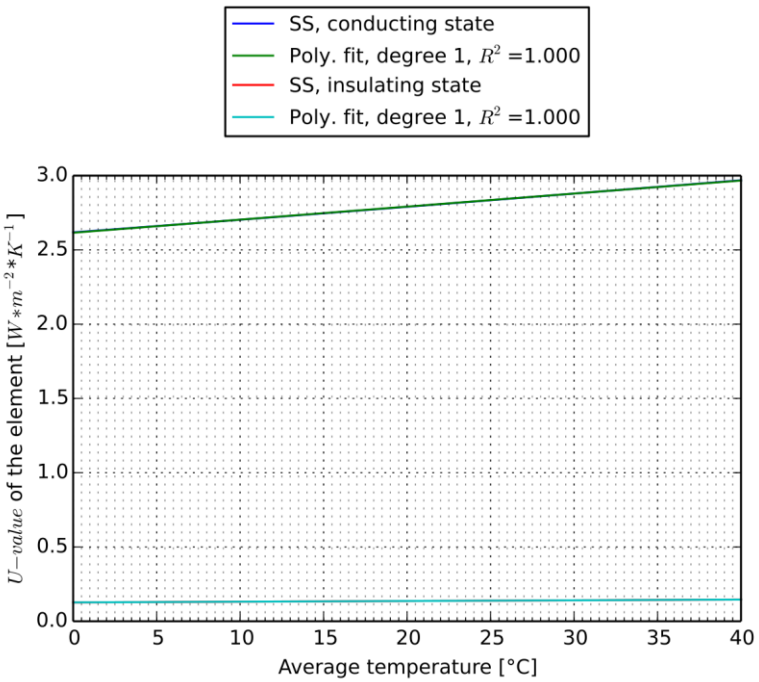

Figure 47 - SS case, U=f($T_{average}$) in the insulating and conducting case, for a temperature difference between room and exterior air of 15 K.

These results are in accordance with the results of the analysis of a single cavity:

- In the conducting case, with the absence of low-e layer, the thermal resistance and so the U-value varies linearly with the average temperature, due to the variation of the longwave infrared heat transfer coefficient.
- Also, in the insulating case and for the same reason, the variation is linear but with lower absolute values going from 0.127 $W*m^{-2}*K^{-1}$ for 0°C to 0.146 $W*m^{-2}*K^{-1}$ for 40°C.

In a second step, the g-value was investigated: first, the dependence of the g-value on the angle of incidence was tested assuming winter conditions, with a direct solar irradiance of 500 W*m^{-2}, a temperature difference of 10 K and an average temperature of 10°C. The part of incident energy absorbed in each layer was calculated with the software WINDOW 7.2 (Lawrence Berkeley National Laboratory 2015).The g-value was only investigated in the conducting case, since it was proven in the previous section that the g-value in the insulating case is negligible. The dependence of the g-value on the angle of incidence is shown on following graph for the SS case:

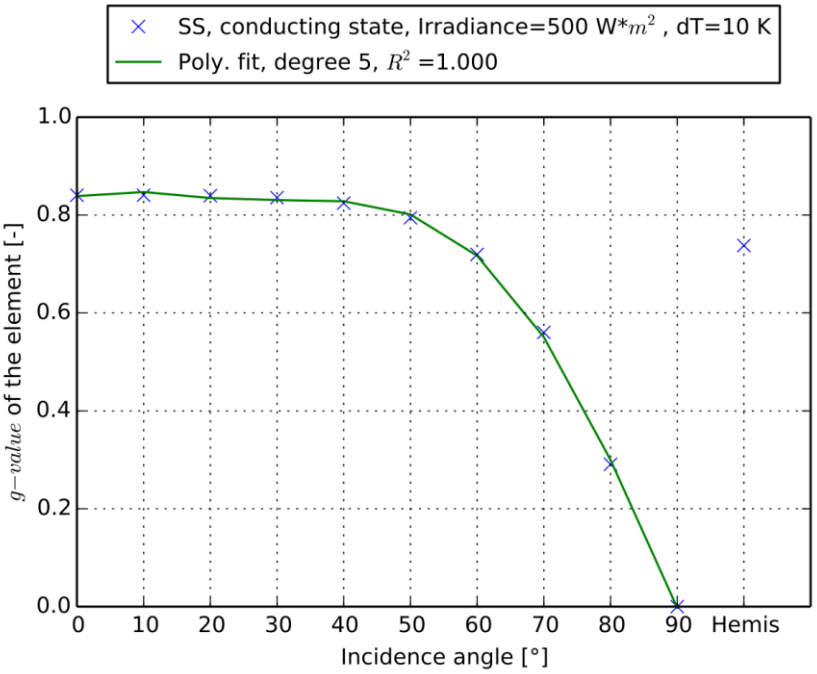

Figure 48 - SS case, g=f(incidence angle) in the conducting state, for a temperature difference between room and exterior air of 10 K, an average temperature of 10°C and an irradiance level of 500 W*m^{-2}. The hemispherical value for diffuse incoming light is showed as well. The value for hemispherical incoming irradiance is also plotted.

As expected, the g-value varies strongly with the angle of incidence, since more irradiance is reflected from the glazings with higher incidence angles.

In the SS case, the dependence of the g-value on the temperature difference and the average temperature is negligible, with a constant value of about 0.84. The reason is that for the SS variant, the secondary heat gain is always very low, because a very low amount of incoming solar irradiance is absorbed in the glazings. For example, for 0° angle of incidence, 1 % of the incoming energy is absorbed at the outer glazing and 1 % at the inner glazing. The theoretical maximum of the secondary heat gain is then 2 %, but a large part of the absorbed energy flows toward the exterior.

In the SS case, the dependence on the irradiance is negligible. This is due to a very low secondary heat gain generally but also to the fact that the order of magnitude of absorbed energy in the two layers is the same and the temperature difference between the two layers is not increased by the additional absorbed energy.

For the purpose of the advanced control strategies that will be used in the building simulation, one could reasonably assume constant U- and g-values. For the U-value in the conductive case, the constant values of Table 16 are assumed for both the SB and SS cases. These values were calculated in the previous section for a conservative temperature difference of 5 K (a higher temperature difference resulting in a higher, better U-value in this state). For example, in the SS case, if the temperature difference is then 30 K, an error of about 7 % is made on the U-value. However, a temperature difference of 30 K is unlikely and the error would more likely be much lower. The U-values in the conductive case presented in Table 16 were calculated with an average temperature of 21°C, corresponding to a summer situation. If the average temperature drops to 0°C, an error of about 6 % is made, but situations with such a low average temperature are also rare. Identically, in the insulating case, the same assumption of constant U-values is made.

For the g-value, the dependence on the angle of incidence is strong in both configurations and should be taken into account. However, the hemispherical values could be used as a simplifying approximation that provides better results than the value for 0° incidence angle: by takin the hemispherical value, when the irradiance is diffuse, the g-value is predicted accurately. When the irradiance is direct, the error is acceptable for incidence angles below 60° (corresponding to winter and mid-season situations), and gets important for incidence angles above 70°, for which the g-value is overestimated. In the SS case, the dependence on irradiance level, temperature difference and temperature average is very low and can be neglected, due to the low secondary heat gain in general.

3.2.3 Comparison between measurement and ISO 150999 model

In this section, the prototype built is compared with the ISO 15099 calculation. The prototype and the measurements are described in the experimental study.

To construct virtually the element, following assumptions were made:

- Isothermal boundary conditions at the outer and inner Plexiglas cover pane, taken directly from the measurements.
- For the Plexiglas outer and inner pane, a thermal emissivity of 0.9 and a thermal conductivity of 0.19 $W*m^{-1}*K^{-1}$ were assumed.
- Concerning the longwave properties of the films, the measured thermal emissivities weighted for a Planck spectrum at 293.15 K were chosen, corrected with the DIN EN 12898 to take into account the angular response. This corresponds to a value of 0.031 for the aluminum "cold" side and a value of 0.479 for the PET "warm" side. Since the transmittance in the infrared spectral range is negligible, we assume that the thermal reflectivity is equal to 1-ε.
- The frame effect is neglected, since the U-value measurement device measures center-of-glazing values.

In following figure, the measured values are plotted versus the calculated ones. Measurements 1 to 3 refer to measurement with the same temperature difference at the boundary but different average temperatures. Measurements 4 and 5 are with the same average temperature and temperature differences of respectively 4.9 K and 19.8 K:

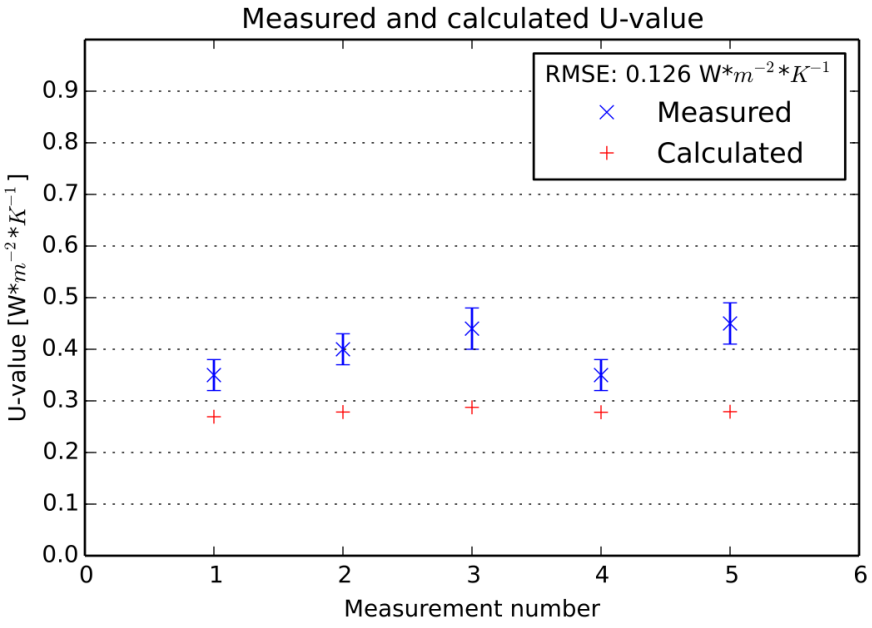

Figure 49 - Measured against calculated value for the first prototype.

As the heat flux are measured in a 500*500 mm² central area, thermal bridges through the wooden frame are unlikely to explain this difference. However, for this prototype, the films were not fixed to the wooden frame, and the connection to the frame was loose. Consequently the airtightness assumed during modeling was not realized. Thus, convection and mass transfer is possible between two adjacent cavities, leading to a lower overall thermal resistance. From the mechanical point of view, one design point is then to optimize this airtightness at the sides, top and bottom while still allowing the films to be rolled up and down, in order to reach the optimum shown by the model. At the end of this thesis, this airtight prototype was not build yet.

For the building simulation, the optimal element as calculated by the model will be simulated, before taking into account the higher U-value of the existing prototype in the insulating state and assessing its impact on the overall performance of the element.

3.3 Evaluation of the element in a building application

In this part, the goal is to assess the potential of the new element on a building level. First, the modeling approach is detailed. Then, variants are defined with the new elements and control strategies are proposed. Finally, the results of the variants are compared to the reference case based on the building energy demand (heating, cooling, artificial lighting).

3.3.1 Modeling approach

First, the building simulation environment and the implementation of the façade element are presented, before choosing a climate and a reference building. Finally, the variants with the new façade element are introduced as well as the control strategies to operate it.

3.3.1.1 Simulation environment

For the building simulation, the simulation program EnergyPlus (Crawley et al. 2001) has been used, using the ISO15099 for the thermal modelling of façade elements. EnergyPlus is a building energetic calculation tool which can calculate the heating and cooling loads as well as artificial lighting load, process loads. EnergyPlus has many ready-to-use submodels for different physical problems or components.

To model the window application, the element in the conducting state has been represented by a conventional double pane window. The switching to the insulating state has then been handled using the Energy Management System (EMS). The EMS can among other things be used to switch dynamically façade element based on inputs or building variables. In the insulating state, with the films rolled down, the element has been implemented with (from the exterior towards the interior) an equivalent layer, one film and the inner glazing, allowing to calculate accurately the inner temperature of the element which is important for comfort. The equivalent layer was an opaque layer with an equivalent thermal resistance, so that the total thermal resistance of the system was represented accurately.

To model the wall component, the Trombe approach has been used. This approach has been developed and validated in (Ellis 2003). The Trombe wall cavity is represented by a thermal zone in which the internal convection is handled by the (Wright 1996) correlations. In our case, this approach is valid for the conducting state, when the films are rolled up and there is only one cover pane within a certain distance of the massive wall. However, it is then not possible to model the insulating case, since the important air cavity cannot be cancelled. In our case, the thickness of the Trombe wall zone has been set to a very low value, so that the exterior surface of the wall is in perfect thermal contact with the interior surface of the window. The windows are then switched using the EMS approach.

3.3.1.2 Choice of climate

Following criteria's where considered for the choice of the climate:

- Heating-dominated, to justify the need of insulation in winter, but with still an important part of cooling needs.
- At least average yearly irradiance value, to be able to use irradiance in winter and have cooling loads in summer.
- Important temperature variation between day and night, to benefit from the ability to switch on or off the thermal resistance of the façade.

The European climatic conditions have been analyzed in depth within the European project INSPIRE (Kuhn et al. 2014). An analysis considering air temperature ranges, heating and cooling degree days as well as humidity in Europe allowed the differentiation of seven different climates:

- Southern Dry
- Mediterranean
- Southern continental
- Continental
- Oceanic
- Norther continental
- Nordic

The climates are represented by following map:

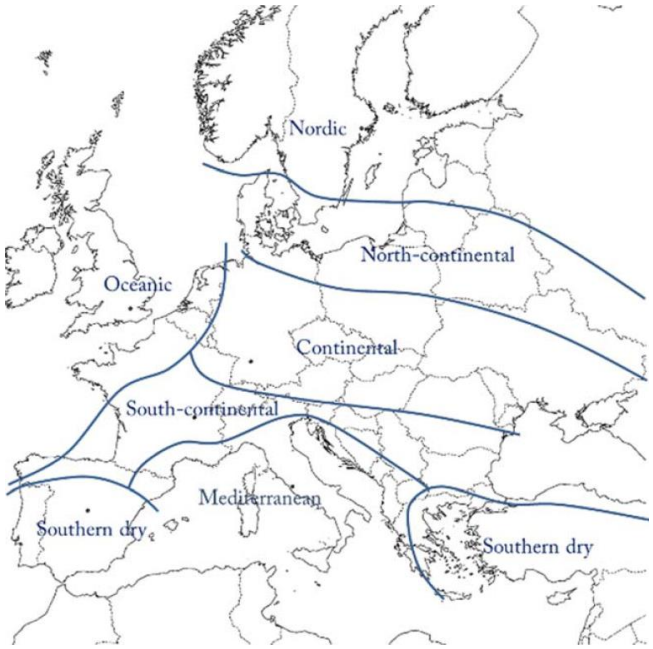

Figure 50 - European climate classification. Source: (Kuhn et al. 2014).

Based on the criteria mentioned above, the continental climate has been selected for the purpose of this study. The continental climate represented by the city of Stuttgart, is described as "Inner land climate zone with high yearly temperature amplitudes between cold winters and hot summers. It includes Central Europe (Germany, Austria, Czech Republic, Slovakia, Hungary, etc.) as well as parts of Ukraine, Poland and Romania".

In the INSPIRE report (Kuhn et al. 2014), is it stated that for the climate of Stuttgart, "the repartition of the temperatures over the year is quite spread out, with an amplitude of 43°C between the extreme summer and winter temperatures. During more than 10 % of the year, the ambient air temperature is negative". This is illustrated by following graphs:

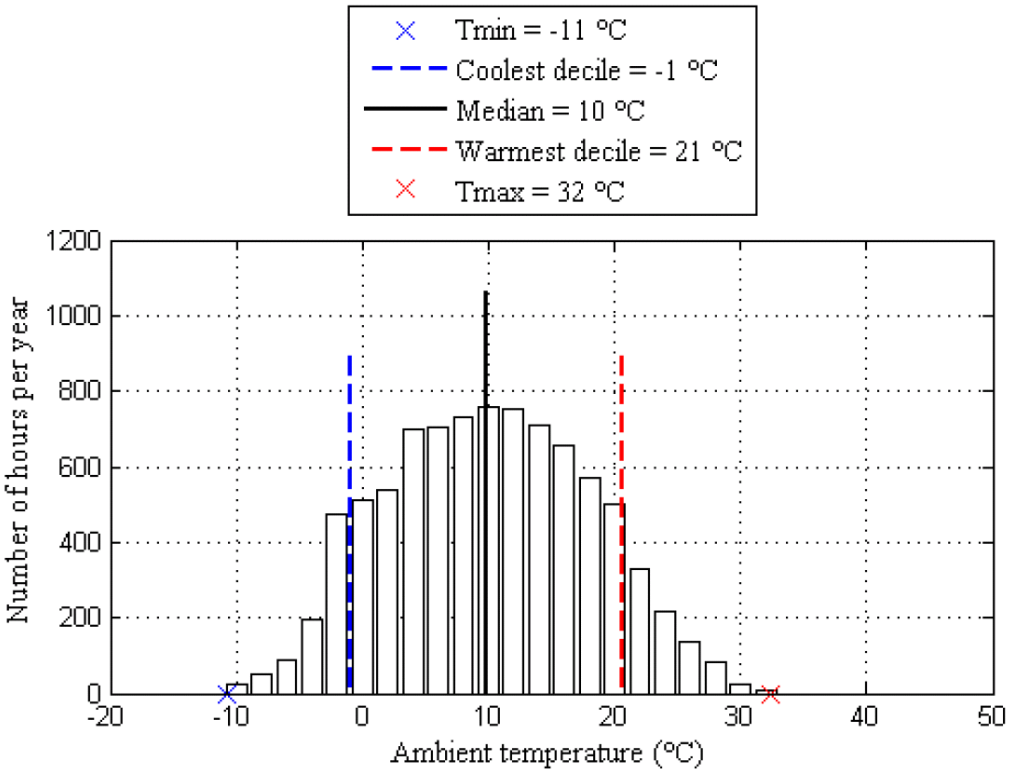

Figure 51 - Repartition of the ambient air temperature in Stuttgart over a year. Source: (Kuhn et al. 2014).

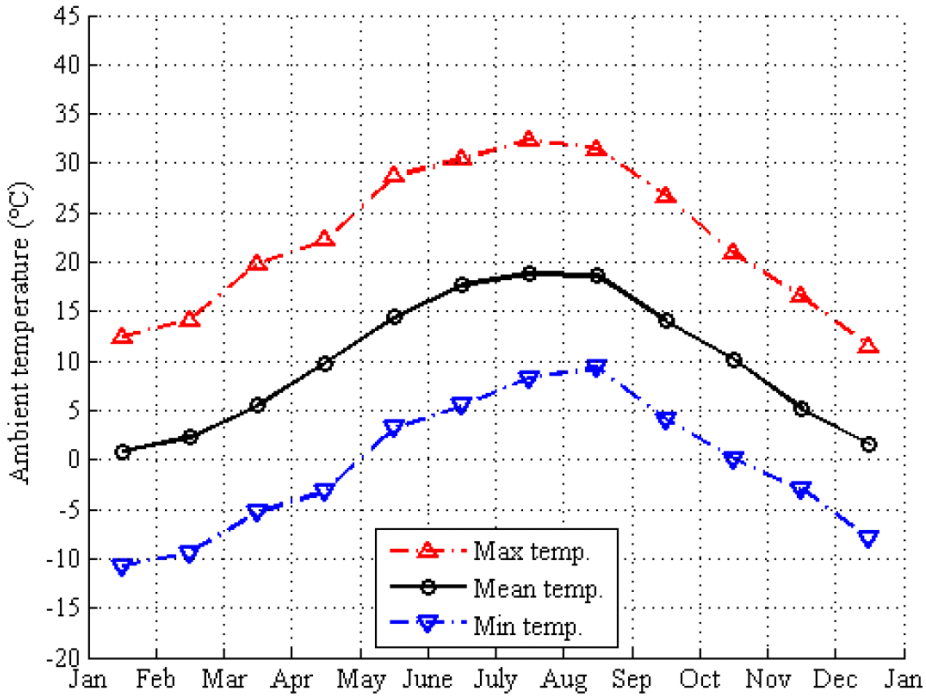

Figure 52 - Monthly ambient air temperatures in Stuttgart. Source: (Kuhn et al. 2014).

It can be observed that even in summer, the minimum air temperature during the night stays below 10°C, which should allow us to cool down the building.

Alternatively, the southern continental climate, represented by the city of Lyon also fits to the criterions above. This climate is described as "Climate zone with summer as warm as Mediterranean summers, but with winters much colder. It includes most part of France, North Italia, Slovenia, Serbia and Bulgaria". This type of climate would produce more cooling load and less heating load for the same reference building. The potential of the switchable façade element to reduce the cooling load would still be important due to important variation during day and night in summer. The potential of reducing the heating load is diminished by the lower heating load, but increased again by the additional solar irradiance.

Compared to the continental climate, the switchable façade element is likely to show less potential for a northern climate: the cooling loads are lower in summer, reducing the potential of switching to the conducting state during the night. Also, during the heating period, the lower irradiance and very low external temperatures strongly diminish the switching potential and potential heat gains. In a Mediterranean climate, lower insulation levels are needed due to higher external temperatures and solar irradiance level. However, the window application could still be used to lower the g-values of windows and diminish solar gains.

For the purpose of this study, the climate of Stuttgart (Germany) is then chosen.

3.3.1.3 Reference building

After the choice of the climate, a reference building is chosen. The reference building is well insulated. To simplify the problem, a shoebox geometry is simulated. The simulated room has one exterior façade and five adiabatic walls (three vertical internal walls, one roof and one ceiling). The room had the following interior dimensions:

- Floor and ceiling: 4*5=20 m² each.
- Exterior south wall and north adiabatic wall: 4*3=12 m² each.
- Adiabatic east and west walls: 5*3=15 m² each.
- The middle third of the south exterior wall was occupied by the window (about 3.5 m² glazed area and 0.50 m² frame): 4 m².

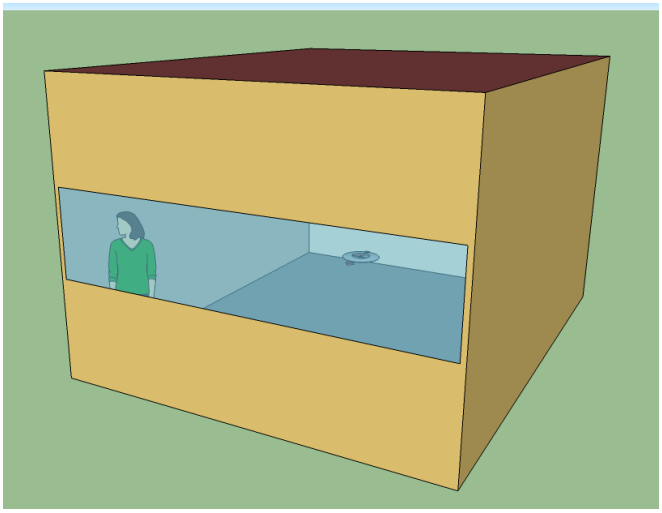

Figure 53 - Simplified representation of the simulated room (interior dimensions).

The orientation of the exterior façade was south. The south orientation produces an important cooling load due to the high solar gains. These solar gains can also be used in winter to diminish the heating load with the switchable element. In a second step, other orientations will be investigated.

The external façade was defined as follow (from the exterior towards the interior):

Name	Thickness	Conductivity	Density	Specific heat	Source
-	M	$W*m^{-1}*K^{-1}$	$kg*m^{-3}$	$J*kg^{-1}*K^{-1}$	-
Polyurethan	0.2	0.031	40	2090	(TRNSYS 2013)
Concrete	0.15	2.100	2400	1000	(TRNSYS 2013)

Table 18 - Detail of the external wall (Reference building), from outside towards inside.

The U-value of this external wall is 0.149 $W*m^{-2}*K^{-1}$. This is compatible with the Passive House standard.

The adiabatic internal walls, floor and ceiling are composed of 15 cm of concrete:

Name	Thickness	Conductivity	Density	Specific heat	Source
-	M	$W*m^{-1}*K^{-1}$	$kg*m^{-3}$	$J*kg^{-1}*K^{-1}$	-
Concrete	0.15	2.100	2400	1000	(TRNSYS 2013)

Table 19 - Detail of the internal walls, floor and ceiling (Reference building), from outside towards inside.

The impact of this important thermal mass on the reference case is discussed in the results section.

The selected triple glazing window with Argon and two low-e layers is detailed below:

Name	U-value	g-value	τ_{sol}	τ_{vis}	Area	Source
Unit	$W*m^{-2}*K^{-1}$	-	-	-	m^2	-
Glazing: Saint-Gobain SGG PLANITHERM LUX	0.75	0.61	0.51	0.73	3.5	http://exprover.saint-gobain-glass.com/product/351/sgg-planitherm-lux#tabs-2
Frame: reinforced aluminum and wood frame, 5 cm wide	0.85	-	-	-	0.5	http://www.wiegand-info.de/waermebruecken/download.php?download=69
Window	0.76	0.601	0.51	0.73	4.0	-

Table 20 -Description of the overall properties of the reference triple glazing window.

This window complies with the passive house standard.

To avoid glare and overheating, the window was equipped with an external horizontal venetian blind. The blind went down when the irradiance on the external surface exceeded 150 $W*m^{-2}$. The slat angle between the normal to the horizontal blind and the normal to the glazing was then 25°.

In the room, the artificial daylight was turned on and modulated if the illuminance in the room was below 500 lux (DIN V 18599-10:2007). When the light was on, an additional heat gain of 10 $W*m^{-2}$ was assumed in the room.

The room was assumed to be occupied by two people between 7:00 and 18:00 during weekdays (DIN V 18599-10:2007). The total heat gain due to people including convective, radiant, and latent was assumed to be 150 W per person (seated, light work, typing) (ISO 7730:2005), half of it being sensible heat.

The internal gains through auxiliary are equal to 15 $W*m^{-2}$ when the office is occupied (DIN V 18599-10:2007).

The heating setpoint was 21°C between 5:00 and 18:00 during weekdays, and 17°C otherwise (DIN V 18599-10:2007). The cooling setpoint was 24°C between 5:00 and 18:00 during weekdays, and 28°C otherwise (DIN V 18599-10:2007). To simplify the problem, a perfect heating and cooling system was assumed: for example, during a heating period, if the predicted room temperature was below the setpoint temperature, the room temperature was set to the setpoint temperature and the calculated energy to be provided to the room air node is then calculated as heating load.

Concerning the ventilation, the exterior airflow rate per person was 40 m^3*hr^{-1} (DIN V 18599-10:2007). Heat recovery with a recovery rate of 75 % was active whenever useful. The infiltration rate was 0.2 $vol*hr^{-1.}$

These hypotheses and parameters had as a consequence that the building had a heating and cooling demand corresponding to a passive house, as will be seen in the result section.

3.3.1.4 Simulated variants

After the reference building was defined, different variants were introduced with the new switchable element:

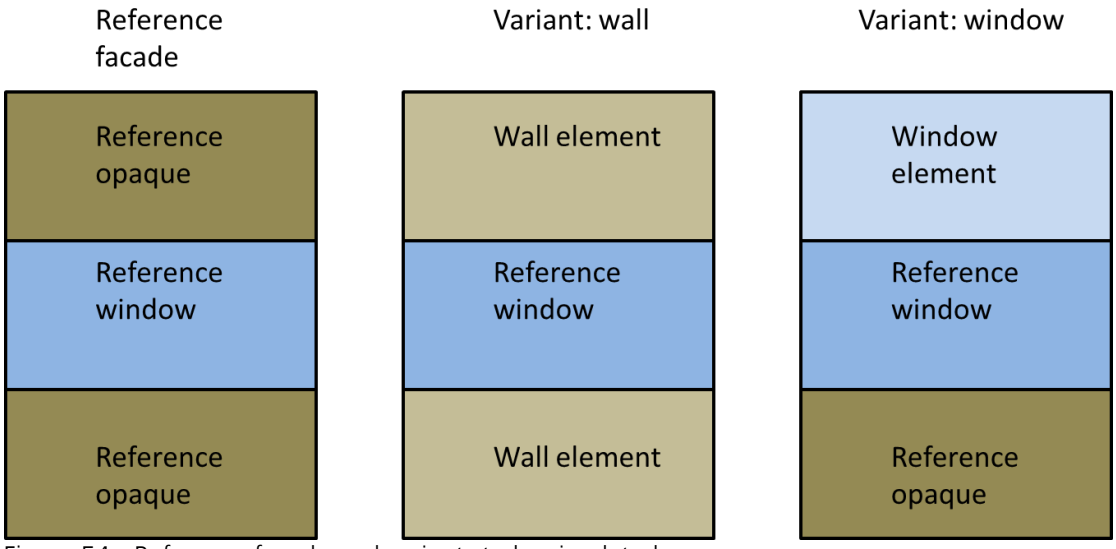

Figure 54 - Reference facade and variants to be simulated.

The reference façade is divided in three parts: one window part in the vertical middle (1m to 2m height), and two insulated opaque areas. For the wall application, the external insulation in front of the opaque surface is replaced by the switchable element. For the window application, the entire upper part of the wall (insulation and concrete) is replaced by the switchable element. Only the upper part is replaced, because, from the daylighting point of view, the benefit of having a transparent element in the lower third (1m) of the façade is low.

The ratio between window area and frame area is the same than for the reference window. The U-value of the frame is also the same (0.85 $W*m^{-2}*K^{-1}$). At the moment of the writing of this thesis, no complete frame with integrated mechanism to roll up or down the foil was designed and the design of the frame was not developed yet.

3.3.1.5 Control strategies

After defining the reference room and different façade variants with the switchable element, different control strategies are now proposed:

- A simple control strategy that is easy to implement.
- An advanced control strategy.

3.3.1.5.1 Simple control strategies

These simple control strategies do not consider daylight. The priority is on the thermal energy demand. Different control strategies are proposed for the window and wall application. We have two modes: a heating-dominated mode and a cooling-dominated mode. We decide in which case we are based on the mean temperature over the last 24 hour. Compared to a strategy based on the legal heating and cooling period for a location, this strategy is more performant during mid-season where there are periods with alternatively heating and cooling demands.

Name of the control strategy	Inputs			Controlled variables
	$T_{ext,24}$ <T_{switch}	T_{ext}>T_{int}	I>150 W*m^{-2}	Insulating (0) or conducting (1) state
Heating	1	1	-	1
		0	1	1
		0	0	0
Cooling	0	0	0	1
		0	1	0
		1	-	0

Table 21 - Simple control strategy for the window application.

With:

- $T_{ext,24}$ [K] the mean exterior air temperature over 24 h.
- I [W*m^{-2}] the total (direct+diffuse) energy arriving at the vertical façade.
- T_{switch} [K] an arbitrary temperature above which we switch from the heating mode to the cooling mode.

The limit of 150 W*m^{-2} is meant to prevent overheating in summer, and to switch to the conducting state only when there is enough sun in winter. The influence of this limit will be investigated. As we only replace the upper third of the façade, glare is not taken into consideration in these control strategies.

Hereunder is the control strategy for the application on the wall. The interior temperature is replaced by the outer surface temperature of the wall with thermal mass, $T_{wall,out}$ (at the connection with the switchable element). The reason is that, due to the thermal mass, this

surface temperature is more meaningful than the inner temperature to decide if the element is switched to the conducting or insulating state.

Name of the control strategy	Inputs			Controlled variables
	$T_{ext,24} < T_{switch}$	$T_{ext} > T_{wall,out}$	$I > 150\ W*m^{-2}$	Insulating (0) or conducting (1) state
Heating	1	1	-	1
		0	1	1
		0	0	0
Cooling	0	0	0	1
		0	1	0
		1	-	0

Table 22 - Simple control strategy for the wall application.

During the testing of these control strategies, the influence of the switching temperature between heating and cooling mode as well as the influence of the limit on the global irradiance on the façade will be investigated.

The advantage of this control strategy is that the four inputs are easy to measure and need only to be compared logically to each other or to a fixed limit.

3.3.1.5.2 Advanced control strategy: optimized heat transfer

Here, we try to predict what will happen in the current time step if we open the element. To do so, we predict the total heat flux through the back of the element, composed of:

- The directly optically transmitted solar radiation
- The secondary heat gain
- The heat flux due to the temperature difference between the external air temperature and the room air temperature or the temperature of the back of the element for respectively the window or wall application.

This total heat flux is defined by:

$$q_{tot,in} = q_{solar} - q_{thermal} \quad \textit{Equation 67}$$

With:

- $q_{thermal}$ [W*m^{-2}] the heat loss due to temperature difference, defined as:

$$q_{thermal} = U(I = 0) * (T_{int} - T_{ext}) \quad \textit{Equation 68}$$

- q_{solar} [W*m^{-2}] the heat gain due to solar irradiance, defined as:

$$q_{solar} = g * I \quad \textit{Equation 69}$$

For the window application, we then have following control strategy:

Name of the control strategy	Controlled variables		
	$T_{ext,24} < T_{switch}$	$q_{tot,in}>0$ (conducting state)	Insulating (0) or conducting (1) state
Heating	1	1	1
		0	0
Cooling	0	0	1
		1	0

Table 23 - Advanced control strategy with prediction of the total heat flux towards the back of the element for the window application, if the element would be in a conducting state.

For the calculation of the heat flow through the back of the element in the wall application, the temperature difference $deltaT' = T_{ext} - T_{wall,out}$ is taken. Doing that, and using U' and g' defined below allow us to calculate the heat flux that leaves the back of the element towards the massive wall. For example, during a cold winter day, even if the interior air is warmer than the exterior air, we may warm up the wall if the wall outer temperature is lower than the exterior air temperature.

The advantage of this control strategy is that we take advantage of every situation where the heat flux could be favorable. This control strategy could be easily adapted to other climate. Only the switching limit between the heating and cooling mode has to be adapted to the new climate. One alternative solution is to set the heating mode during the entire legal heating period for a location, and set the cooling mode otherwise.

The U- and g-values of the wall and window elements (respectively SB and SS configurations) have been calculated in 3.2.2.2.2. The influence of different boundary conditions has been investigated in 3.2.2.2.3. Here, the U- and g values are considered constant. Following values have been taken to predict the total heat flux towards the interior in the conducting case:

- U=2.70 $W*m^{-2}*K^{-1}$ for the window (SS) configuration, corresponding to the value of Table 16.
- U'=4.40 $W*m^{-2}*K^{-1}$ for the wall (SB) configuration. The value is superior to the one from Table 16 because the interior boundary heat transfer coefficient has been set to a very high value, so that the heat flux predicted with the advanced control strategy is the heat flux going from the façade element to the massive wall. This is why U' is used instead of U. The outer wall temperature is then considered as an isothermal boundary condition for the prediction of the total heat flux towards the wall.
- g=0.74 for the window (SS) configuration. This value is different from the value in Table 16, since it corresponds to the hemispherical value. The consequence is that for direct irradiance and low incidence angle (winter situations), the g-value is slightly underestimated, while for high incidence angles the g-value is overestimated. The g-value is modelled correctly for diffuse incoming solar irradiance.
- g'=0.76 for the wall (SB) configuration, also corresponding to the hemispherical value (and an isothermal internal side boundary condition).

3.3.2 Results and discussion

In the following section, the building simulation results are presented. The goal is to assess the potential of the new switchable façade element on the building level. After introducing the modeling approach, choosing the climate, the reference building, the variants as well as the control strategies to be simulated, the simulations are conducted as follow:

- First, the simulation results of the reference alone are presented.
- Then, the results of the window variant are presented, with the new switchable element replacing the upper part of the façade.
- The results for the wall variant are then shown, were the opaque areas are equipped with the new element.
- The impact of the difference between the properties of the theoretical façade elements and the measured element on the building simulation is investigated.
- Finally, the influence of thermal mass is investigated, as well as other orientations

3.3.2.1 Reference building and thermal mass

The building simulation results for the reference building are shown on following graph. Along to the reference case, three other cases are shown:

- the same room with a lower thermal mass (5 cm concrete instead of 20 cm for each wall, roof and ceiling)
- the same room without thermal insulation
- the same room without thermal insulation and a lower thermal mass

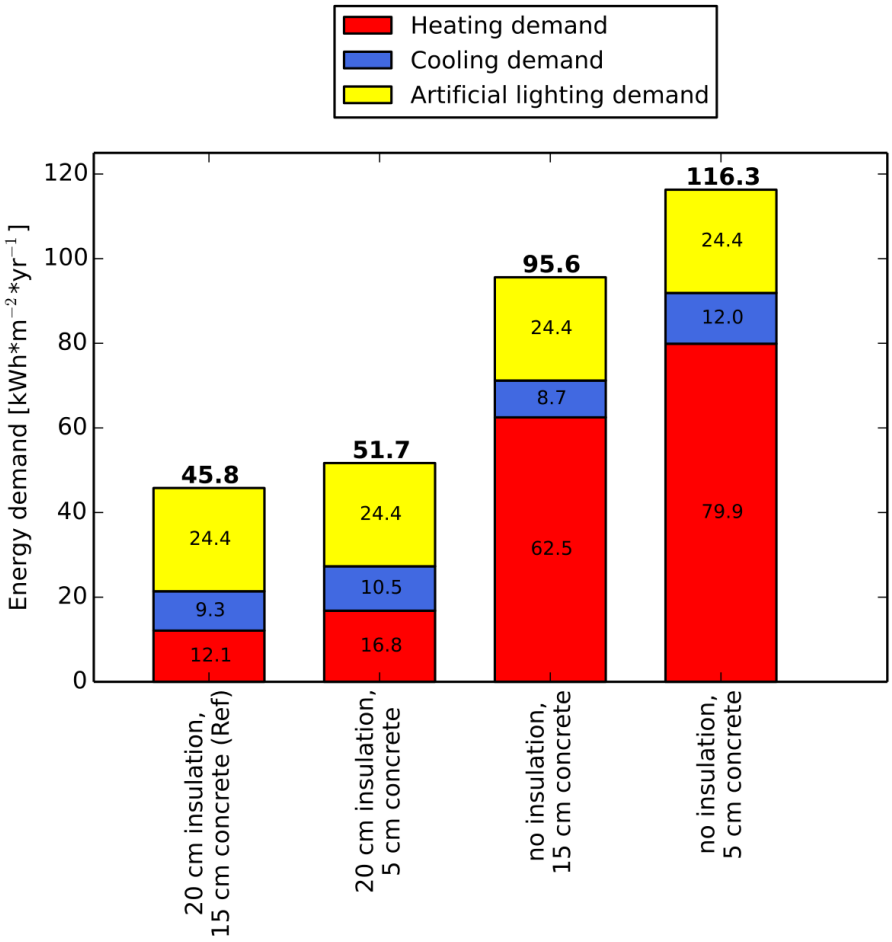

Figure 55 - Simulation results: reference and influence of thermal mass as well as influence of the insulation level of the external wall. Results expressed in useful energy.

The reference room has a passive house like energy demand, with heating and cooling demands below 15 kWh*m^{-2}. The artificial lighting demand is high, due to the high illuminance setpoint of 500 lux in the room as well as the quite high light consumptions of 10 W*m^{-2}.

Thermal mass generally as well as the position of thermal mass compared to the position of the insulation for the exterior facades are important criteria for the reduction of the building heating and cooling demand as shown in (Kossecka und Kosny 2002), (Aste et al. 2009) or (Long und Ye 2015). In (Kossecka und Kosny 2002), analyzing different six different US climates and different wall configurations, the authors show that the best performance in terms of heating and cooling demand is achieved with concrete layers at the inside and insulation layers at the outside. In (Aste et al. 2009), the author comes to the same conclusion simulating a south room in Milan and several external wall configuration, and also shows the importance of thermal mass since the highest energy demand results from a light weight wall configuration with no significant thermal mass layers.

In our case, compared to the reference, the same room with a lower thermal mass has a higher energy: thermal mass absorbs the peaks of room loads, tempering overheating in summer and helping storing solar gains during winter days.

Without insulation, besides the obvious important increase of heating demand, it is interesting to remark that the cooling demand slightly decreases compared to the case with insulation. This is the effect that is aimed for in summer with the switchable element. However, it can also be remarked that with the low thermal mass, this effect is reversed: the effect of the switchable element is then also very likely to be dependent on thermal mass.

3.3.2.2 Window variant

In following section, the simulation results for the window variant are shown:

- First, the upper portion of the exterior south wall is replaced by the switchable façade element, but with the switching state always insulating.
- Then, a second simulation is done with the element always in the conducting state.
- Then, the element is simulated with the simple control strategy defined previously.
- Finally, the element is simulated with the advanced control strategy defined previously.

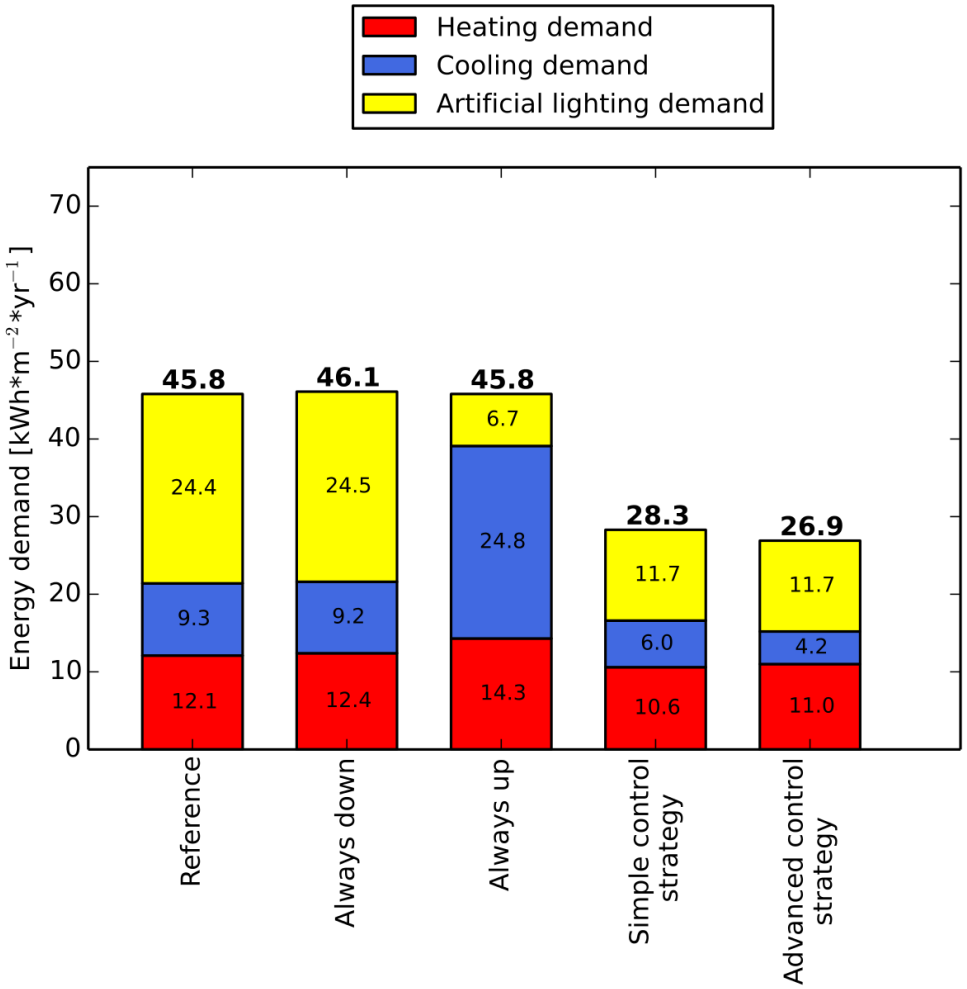

Figure 56 - Building simulation results: window application. Results expressed in useful energy.

The difference between variant always down and the reference is the much lower thermal mass in the upper part of the facade, which is compensated by a slightly lower U-value of 0.137 instead of 0.149 $W*m^{-2}*K^{-1}$ for the reference opaque wall.

When the switchable element is always in conducting state, the diminution of artificial lighting demand is compensated by the additional cooling demand due to solar gains and by the additional heating demand due to higher thermal losses in winter, not compensated by the additional solar gains.

With the simple control strategy and compared to the reference, there is a reduction by 22 % (4.8 kWh*m^{-2}) of the sum of heating and cooling demands: the cooling demand can be reduced by 3.3 kWh*m^{-2} (36 %) and the heating demand can be reduced by 1.5 kWh*m^{-2} (12 %). Due to the replacement of an opaque area with the switchable element with a high transparency in conducting state, the artificial lighting is diminished by 12.7 KWh*m^{-2} (52 %). For the simple control strategy, the system was in insulating state 47 % of the time.

With the advanced control strategy and compared to the reference, the reduction of the sum of the heating and cooling demands reaches 29 % (6.2 kWh*m^{-2}): the cooling demand can be reduced by 5.1 kWh*m^{-2} (55 %) and the heating demand can be reduced by 1.1 kWh*m^{-2} (11 %). For the advanced control strategy, the system was in insulating state 58 % of the time during the year. The advanced control strategy is very effective during the cooling period, but is slightly less effective than the simple control strategy during the heating period. The assumptions of constant U- and g-values could explain these differences.

To understand more in detail the reductions of the heating and cooling energy demand, the variation of different temperatures and variables is shown for two winter days, for the simple control strategy:

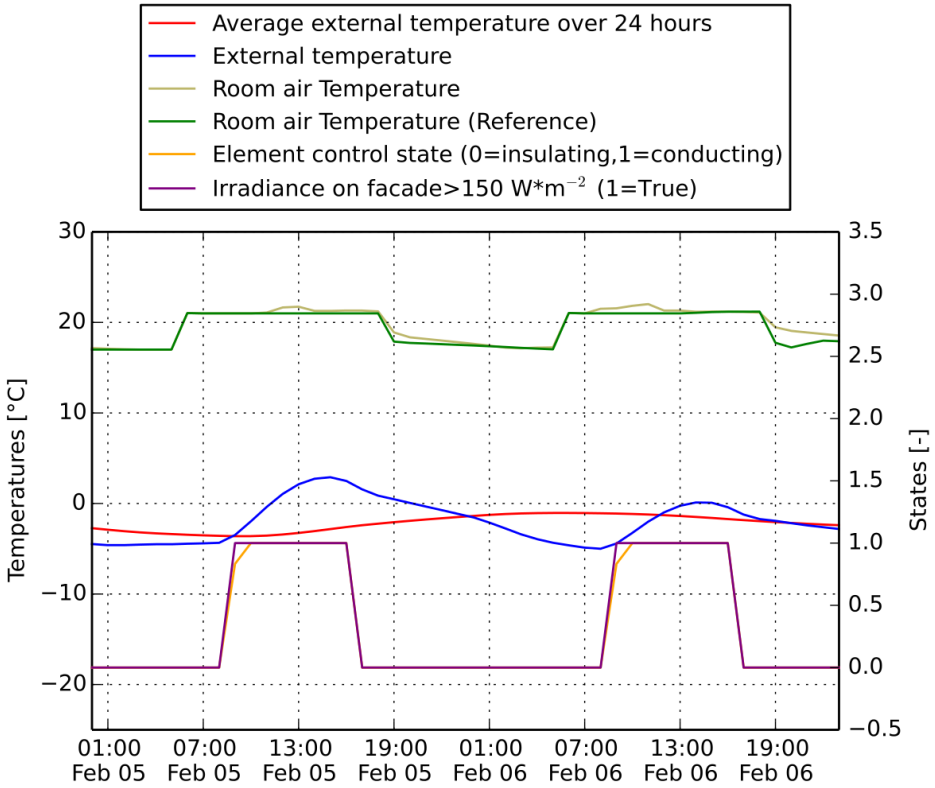

Figure 57 –Temperatures, irradiance condition and control state for the simple control strategy during two winter days. The indoor air temperature of the reference is also plotted.

During this two sunny winter days, the irradiance on the façade is superior to 150 W*m^{-2} during daytime. Consequently, the façade element is switched to the conducting state: this conducts to a warming of the building's internal mass and internal air temperature: the temperature rises over the lower limit of 19°C when the room is occupied. The additional solar gains are stored in the building's mass is then released when there is not enough solar irradiance anymore and the element is switched to the insulating state. Thus, the internal air temperature decreases slower than the one of the reference case.

The same analysis is performed for two summer days:

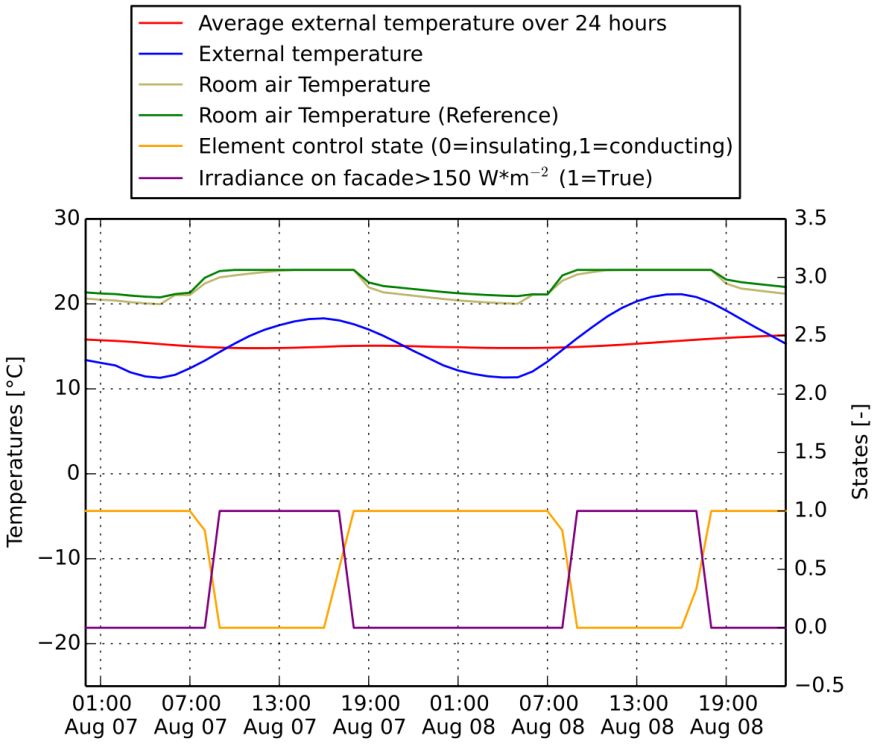

Figure 58 – Temperatures, irradiance condition and control state for the simple control strategy during two summer days. The indoor air temperature of the reference is also plotted.

During these two summer days, the switching to the conducting state during nighttime allows to cool down the thermal mass. Consequently during daytime, when the element is switched to the insulating state, the increase of the internal room air temperature is more attenuated in the variant than in the reference.

For the simple and advanced control strategies, one important factor is the switching temperature which decides whether the system is operating in heating mode or in cooling mode. In a preliminary step, this switching temperature has been optimized:

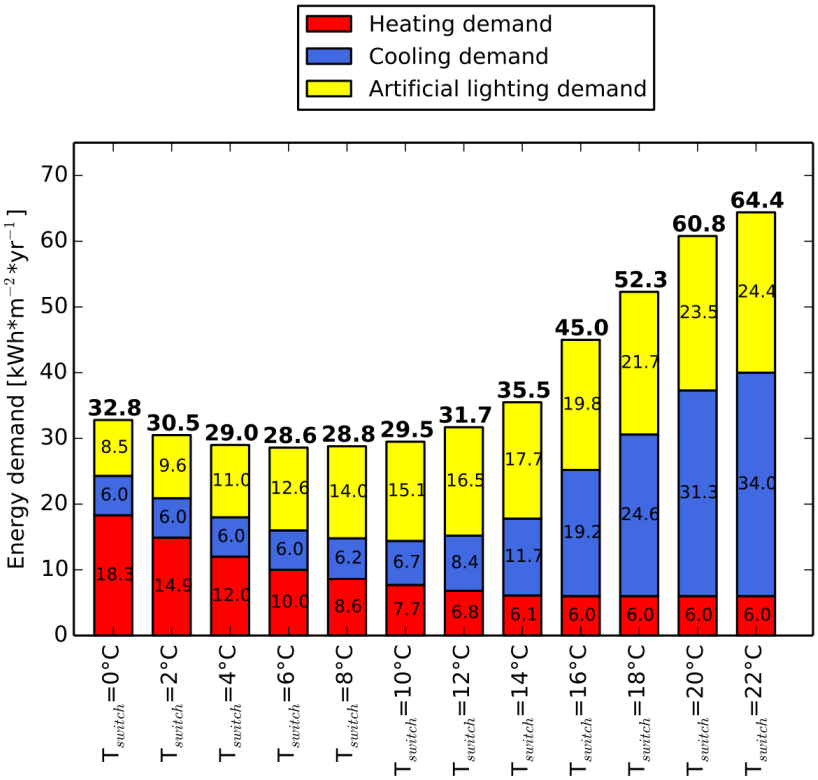

Figure 59 - Building simulation. Window application: influence of the switching temperature with a limit on the irradiance of 150 W*m^{-2}, with the simple control strategy. Results expressed in useful energy.

A high switching temperature favors the heating demand, while a low one favors the cooling demand, as the corresponding control strategies are activated more frequently. A low switching value, by having more cooling control strategy, also lowers the artificial lighting demand. The optimum was found for 5.2°C. This value is also the optimum for the advanced control strategy.

Also, for the simple control strategy, the influence of the irradiance limit has been checked: the same simulation has been conducted with an irradiance limit of 300 W*m^{-2} instead of 150 W*m^{-2}: the results, visible in Appendix, show for the same switching temperature an overall higher energy demand: the cooling energy demand is higher, since more solar gains are allowed in summer before switching to the insulating state. The heating energy decreases slightly, since in winter, the system is not switched to the conducting state anymore for low solar irradiance level below 300 W*m^{-2}. Another improvement step to this control strategy would be to have two different conditions on the incoming irradiance for the cooling and heating periods. The advanced control strategy based on the calculation of the total heat flux to the interior is not dependent of such considerations.

3.3.2.3 Wall variant

In following section, the simulation results for the wall variant are detailed:

- First, the upper portion and lower of the exterior insulation is replaced by the switchable façade element, but with the switching state always insulating.
- Then, a second simulation is done with the element always in the conducting state.
- Then, the element is simulated with the simple control strategy defined previously.
- Finally, the element is simulated with the advanced control strategy.

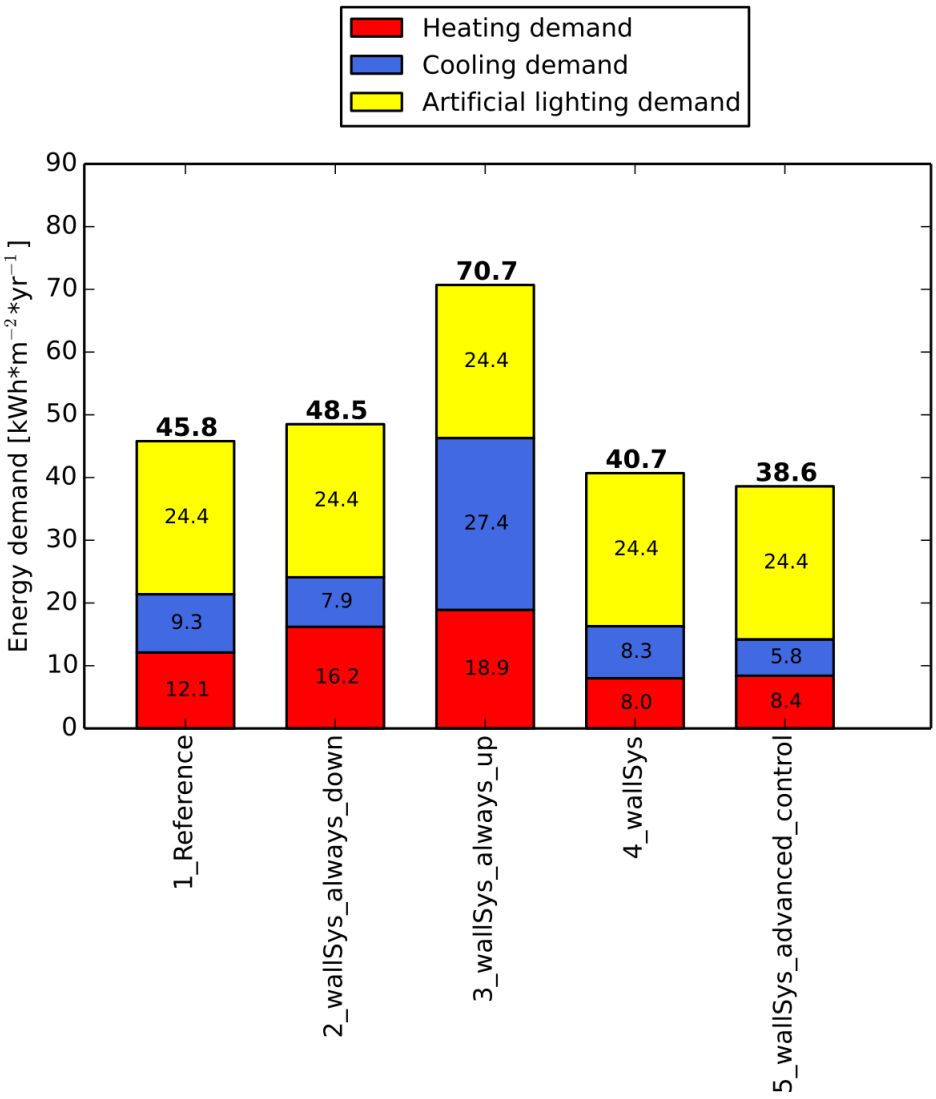

Figure 60 - Building simulation results: wall application. Results expressed in useful energy.

Although the switchable element in insulating state (element down) has a slightly better thermal resistance than the insulation it is replacing, the frame of the switchable element

has a much lower thermal resistance: it was assumed that the U-value of the frame is the same as the one of a good window frame, equal to 0.85 $W*m^{-2}*K^{-1}$. After weighting with their respective areas, the U-value of the total element area (with frame) in insulating state is 0.23 $W*m^{-2}*K^{-1}$, while the reference external façade has an U-value of 0.15 $W*m^{-2}*K^{-1}$. Consequently, when the external insulation is replaced by the switchable element in the "always down" position, the heating demand increases while there is a slight decrease of cooling demand.

When the element is always in a conducting state (up), it acts as a Trombe wall: the absorbed energy at the absorbing paint on the wall external surface increases the cooling demand dramatically. The additional heating gains in winter are not compensated by the additional heat loss due to the higher U-value of the element in conducting state with a 20 cm air cavity.

With the simple control strategy, compared to the reference, the sum of heating and cooling demands is reduced by 24 % (5.1 $kWh*m^{-2}$): the cooling demand is reduced by 1.0 $kWh*m^{-2}$ (11 %) and the heating demand by 4.1 $kWh*m^{-2}$ (34 %). However, if we compare the switching element to the case of the element always in insulating case ("Always down"), it can be observed that a reduction of about half the heating demand can be achieved. However, the cooling energy demand slightly increases, which is due to the optimization of the switching temperature detailed below.

The advanced control strategy produces the best results with a reduction of the sum of heating and cooling demands by 34 % (7.2 $kWh*m^{-2}$) compared to the reference: the cooling demand is reduced by 3.5 $kWh*m^{-2}$ (38 %) and the heating demand by 3.7 $kWh*m^{-2}$ (31 %) compared to the reference. To assess the true potential of switching the insulation, the variant with advanced control strategy is compared to the "always down" case: a reduction by 41 % (9.9 $kWh*m^{-2}$) of the sum of the heating and cooling demand is then achieved.

To underline the importance of the frame effect, the "window" frame of the wall element, with an U_f-value of 0.85 $W*m^{-2}*K^{-1}$, is insulated at the same level than the opaque walls of the reference (U=0.15 $W*m^{-2}*K^{-1}$). Then, the reduction of the sum of heating and cooling demand compared to the reference increase to 34 % (7.3 $kWh*m^{-2}$) instead of 31 %.

Again, particular days are taken investigated for the simple control strategy:

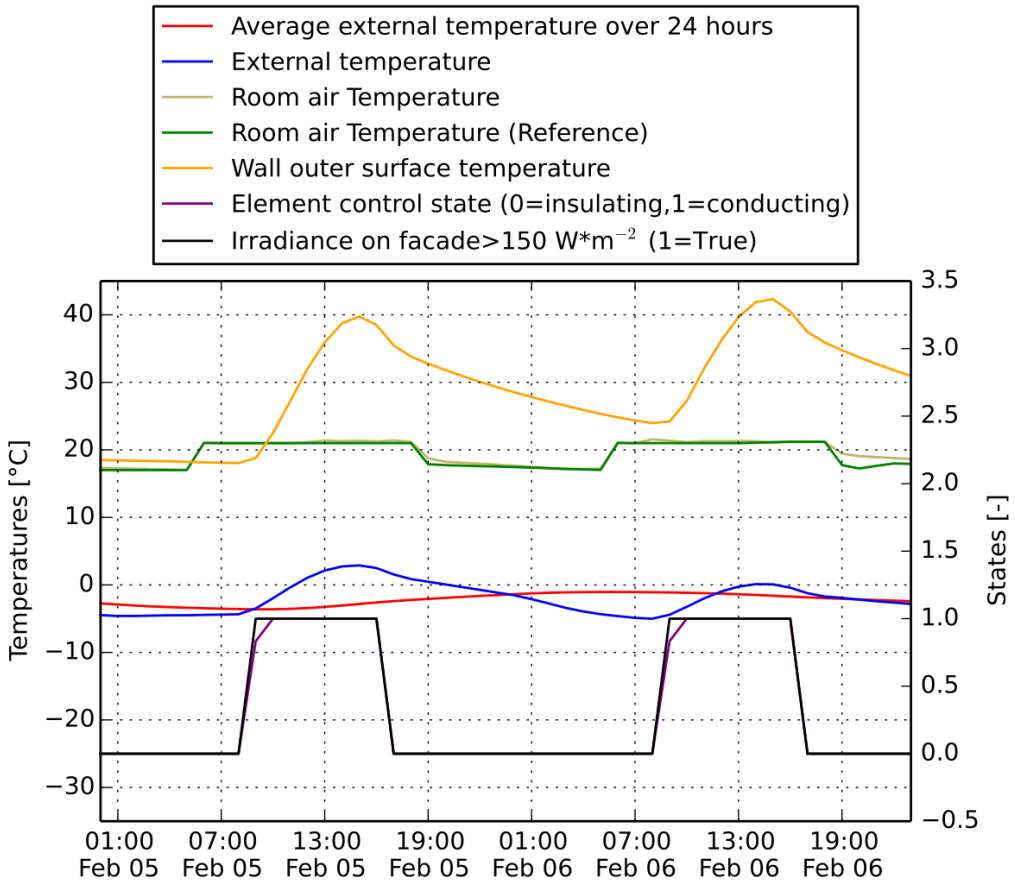

Figure 61 - Temperatures, irradiance condition and control state for the simple control strategy during two winter days. The indoor air temperature of the reference is also plotted.

During these sunny winter days, the wall outer surface temperature, coated with the absorbing painting, reaches a high surface temperature above 40°C, despite the fact that the external temperature is below 5°C. The consequence is a direct heating of the thermal mass. During nighttime, this heat is delivered to the room, whose internal temperature is higher than the one of the reference room.

During the cooling period, the mass of the external wall is directly cooled down during nighttime, while the element acts as a standard exterior insulation during daytime. However, with the actual simple control strategy, this effect is not emphasized, as shown during the optimization of the switching temperature below.

For the wall element, the switching temperature between heating and cooling mode has also been optimized:

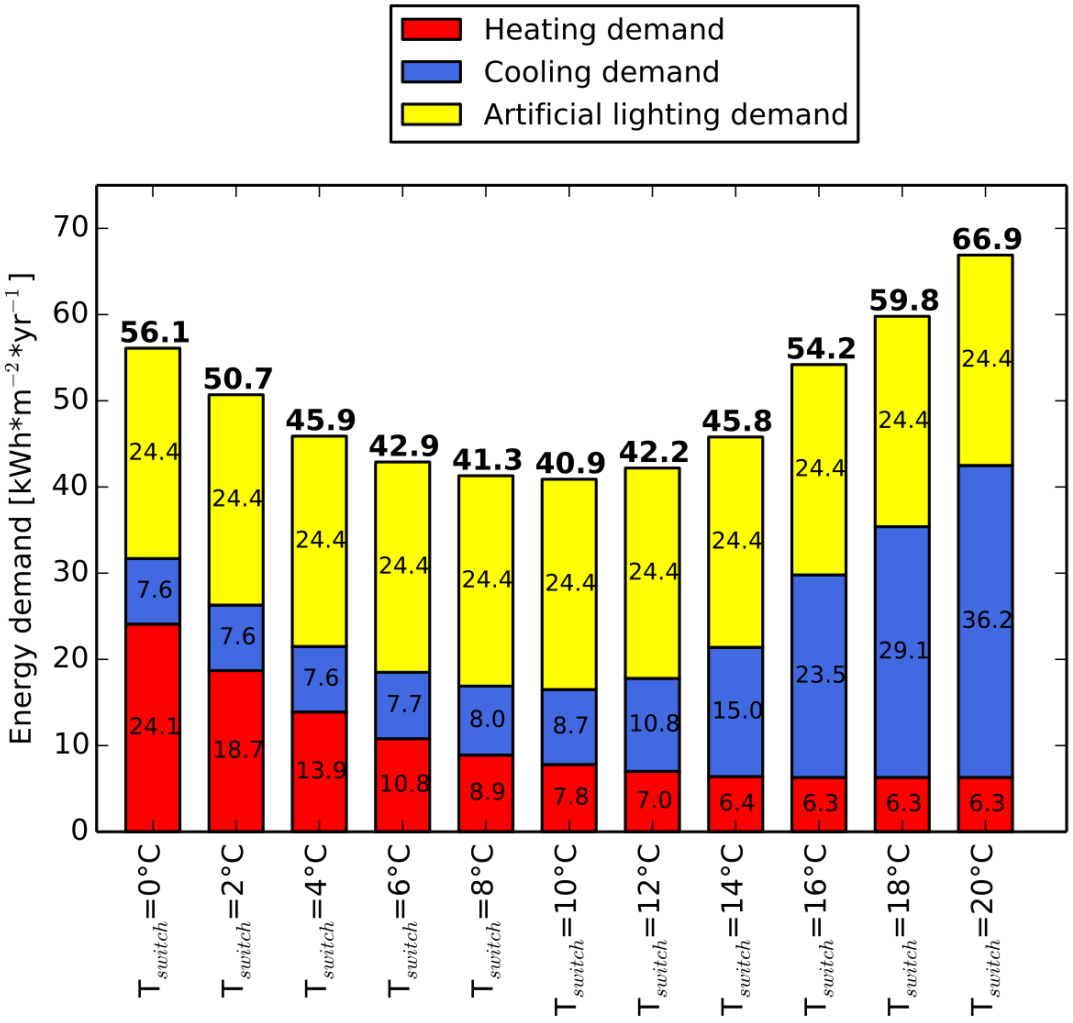

Figure 62 - Building simulation. Wall application: influence of the switching temperature with a limit on the irradiance of 150 W*m^{-2} for the simple control strategy.

The trend is the same than for the window element. The optimum is higher than for the window element and was found to be 9.6°C (also for the advanced control strategy), with a total annual energy demand of 40.7 kWh*m^{-2}. The difference with the window element is that the control strategy has no influence on the artificial lighting demand here. Towards this optimum, the slight increase in cooling demand is overcompensated by the important decrease of heating demand.

The influence of the solar irradiance limit followed the same trend as for the window element, as can be seen in Appendix.

3.3.2.4 Measured prototype versus theoretical values

The previous results have been simulated using the U- and g- values calculated with the theoretical model in section 3.2.2.2. However, during the comparison between the ISO15099 model and the experimental measurement of a prototype, it has been shown that the prototype has a higher U-value than predicted by the model in the insulating state. In this section, the impact of this difference on the building simulation is assessed.

From the five U-value measurements presented in 3.2.1.1, the case with the highest U-value has been chosen ("worst case"), with an U-value of 0.45 $W*m^{-2}*K^{-1}$, measured with an average temperature of 20.1°C and a difference of temperature of 19.8 K. Since the U-value measurement was done with 11 cavities of about 9 mm, the equivalent thermal conductivity of the element has been calculated. This thermal conductivity has then be used to calculate the thermal resistance of a "real" element of 20 cm overall thickness, which has been implemented in the building simulation model. The U-value of this "real" 20 cm element is then 0.22 $W*m^{-2}*K^{-1}$ to be compared to the value of 0.14 $W*m^{-2}*K^{-1}$ of the theoretical calculation.

For the window element, replacing the theoretical U-values with this measured value leads to a very small increase of the heating demand from 11.0 $kWh*m^{-2}*yr^{-1}$ to 11.2 $kWh*m^{-2}*yr^{-1}$ in the variant with the advanced control strategy. For the wall element, the heating demand increases from 8.4 $kWh*m^{-2}*yr^{-1}$ to 8.7 $kWh*m^{-2}*yr^{-1}$. The cooling demand remained unchanged for both the wall and window configurations. With the real measured thermal properties, the performance of the switchable insulation is not affected in a significant way. The reason is that this higher U-value is compensated by the solar gains achieved during the heating period with the switching process.

3.3.2.5 Influence of thermal mass

In this section, the impact of thermal mass on the performance of the switchable insulation is investigated.

In our case, the well-insulated reference building has 15 cm concrete on all internal and external walls (see also 3.3.1.3). The reference case has already been simulated with a lower thermal mass (see 3.3.2.1).The influence of the thermal mass on the variant with the window element and the advanced control strategy is shown on following graph:

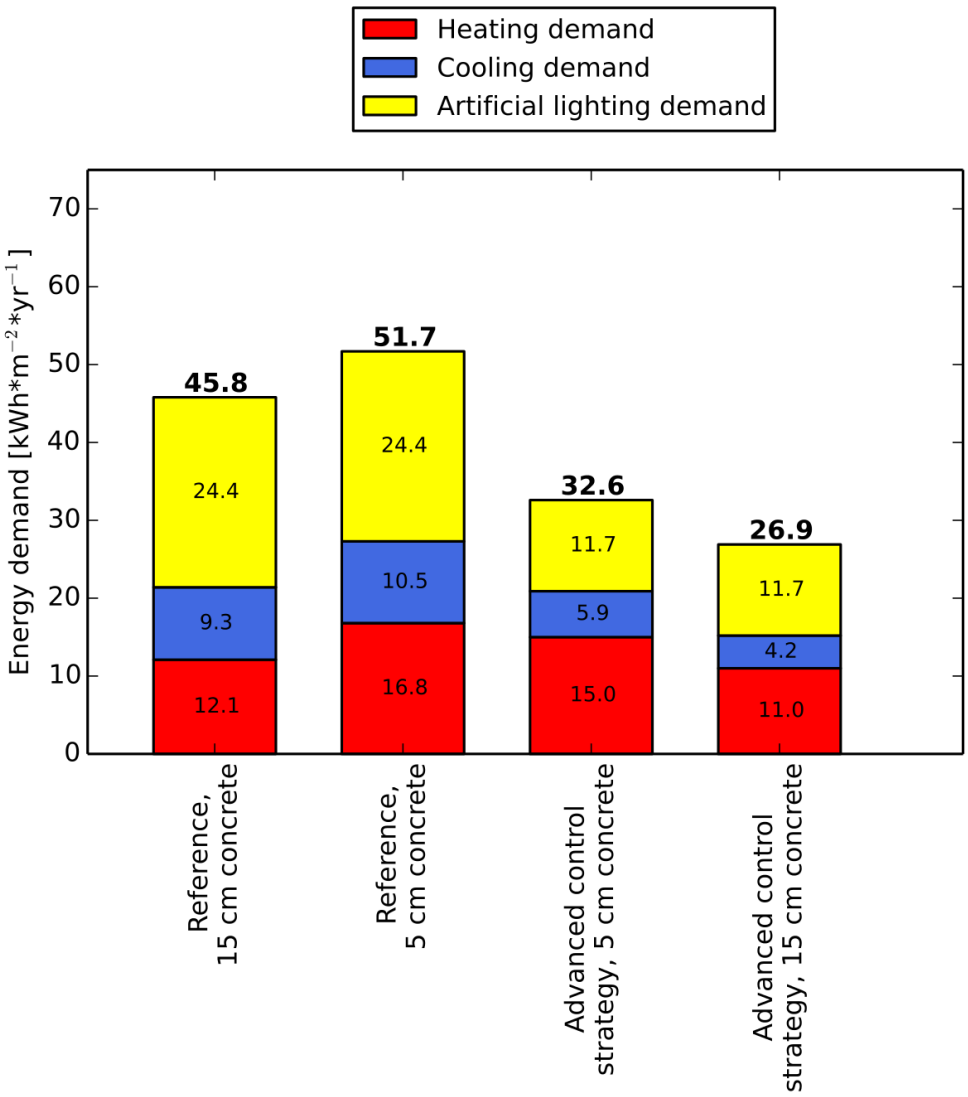

Figure 63 – Influence of the thermal mass on the window variant with advanced control strategy. Results expressed in useful energy.

The thermal mass has an important impact on the performance: for the case with 15 cm, the sum of the heating and cooling demand was reduced by 29 % (6.2 kWh*m^{-2}) compared to the reference, as shown previously. With 5 cm concrete, the reduction due to

the switchable insulation drops to 23 % (6.4 kWh*m^{-2}), compared to the reference with only 5 cm concrete: in winter the thermal mass allows to store the solar gains when the element is in the conducting state, while during the cooling periods the thermal mass can be cooled down during nighttime and dampen the effect of internal gains and solar radiation during daytime.

For the wall variant, the conclusion is similar: the reduction of heating and cooling demand drops from 34 % (7.2 kWh*m^{-2}) for the 15 cm case to 17 % (4.6 kWh*m^{-2}) for the case with 5 cm concrete. It has also been checked that the optimal switching temperature for the control strategies did not change with another level of thermal mass.

3.3.2.6 Other orientations

In this section, the potential of the switchable insulation is investigated for other orientations than the original south orientation, with the advanced control strategy.

The whole room was rotated so that the orientation of the external surface went from south to west, north and east.

The reference building has an external blind over the triple glazing window in the central area (see also 3.3.1.3). The blinds goes down when the total irradiance above 150 W*m^{-2}, in order to prevent glare and overheating during the cooling period. This control strategy is the same for all four orientations, and the consequence is that for example for the south façade, the blind is down 1859 hours over the year while for the north façade it is only down 534 hours. The consequence is that for the reference building the solar gains to the room are quite similar for the four orientations, leading to very close energy demands.

For the window variant, the best reduction of the sum of heating and cooling demands is for the south façade, with 29 % (6.2 kWh*m^{-2}) compared to the reference. The west, north and east façade show reductions of respectively 17 % (3.8 kWh*m^{-2}), 8 % (1.7 kWh*m^{-2}) and 19 % (4.3 kWh*m^{-2}): while the reduction of the cooling demand is still important (but lower, especially for the North façade), there is no reduction of the heating demand: one reason is the lower level of solar irradiance incoming at the façade for other orientations, with less solar gains during the heating period. The other reason is due to the optimization of the switching temperature between heating and cooling mode (see also 3.3.1.5), which focus on the sum of heating, cooling and lighting demand. If the optimization is based on heating and cooling only, a higher switching temperature is taken and a more important reduction of heating and cooling can be achieved.

For the wall variant, the switchable element does not impact the artificial lighting. For the south orientation, it was showed in the previous sections that a reduction of the sum of the heating and cooling demand by 34 % (7.2 kWh*m^{-2}) compared to the reference could be achieved. For other orientations, the reduction is less important. For the west and east

orientations, the reduction of the sum of heating and cooling demand is respectively 15 % (3.4 kWh*m^{-2}) and 13 % (3.0 kWh*m^{-2}), while this reduction is only of 3% (0.7 kWh*m^{-2}) for the north facade. Relatively to the variant with the element always in an insulating state, the reduction is again higher, since the frame with low insulation is then present in both cases. For the wall variant, it is interesting to remark that the optimal switching temperature between heating and cooling mode (average external temperature over 24 hours) changes significantly for other orientations: for the west and north orientation, the optimum switching temperature is respectively 10.0°C and 13.4 °C instead of 9.6°C for the south and east orientations.

3.4 Conclusion: removable insulation system

In this chapter, a new façade element with switchable thermal properties has been presented. A first prototype has been built and measured in a hotbox apparatus. The optical solar and infrared properties of the films have also been characterized experimentally.

The element has then been investigated from the theoretical point of view, first on the single cavity level: the convective and radiative heat transports in one cavity have been detailed: in particular, the effect of the choice of IR properties and cavity thickness has been investigated. For a single cavity, as soon as there is a low-e layer in the cavity, the equivalent resistance is dominated by the convective effect. A maximum is reached around 2 cm thicknesses, and the results are temperature dependent. Adding then a second low-e layer in the cavity only improves very slightly the equivalent resistance due to the dominating effect of the convective resistance. The cavity thickness should be chosen in order to stay in the "purely" conductive range. For this purpose, and in order to keep a limited number of films, a thickness of 1 cm is chosen. It has also been shown that the film used for the first prototype, with a low-e layer on one side and PET on the other, is sufficient to get almost the maximum possible thermal resistance for one air cavity and a given thickness.

In a second step, several air cavities in series and the whole façade element have been analyzed using the model introduced in (ISO 15099:2003). The influence of the number of insulating cavities in the insulating state and the influence of the total cavity's thickness in the conducting state has been investigated, for different front and back covers. Finally, two systems have been selected for the building simulation with 20 cavities and 20 cm overall thickness:

- The solar glass-black painting (not selective) variant for the wall application. A switching of the U-values from about 0.14 to 2.76 $W*m^{-2}*K^{-1}$ was obtained as well as a switching from none to 0.49 for the g-value.
- The solar glass-solar glass variant for the window application. The switching range is from about 0.14 to 2.70 $W*m^{-2}*K^{-1}$ for the U-value and from none to 0.84 for the g-value.

The influence of the difference between the room air temperature and the exterior air temperature, as well as the average temperature between room and exterior air temperature on the U-value has been investigated, as well as the influence of the angle of incidence of direct irradiance, the total amount of incoming irradiance, the temperature difference and average temperature on the g-value.

A comparison between the measurement of the U-values and the calculated values show a higher U-value than predicted, the suspected reason being air tightness at the connection

between films and frame. From the mechanical point of view, one design point is then to optimize this airtightness at the sides, top and bottom of the element while still allowing the films to be rolled up and down, in order to reach the optimum shown by the model.

A well-insulated building was simulated. Two different control strategies where developed. The buildings simulations results showed that for the window configuration, a reduction of the sum of the heating and cooling demands by 29 % (6.2 $kWh*m^{-2}$) could be achieved with the advanced control strategy: the cooling demand can be reduced by 5.1 $kWh*m^{-2}$ (55 %) and the heating demand can be reduced by 1.1 $kWh*m^{-2}$ (11 %). As an opaque surface is replaced by a transparent (switchable) element, the artificial lighting is diminished by 12.7 $KWh*m^{-2}$ (52 %). For the wall element, a reduction of the sum of heating and cooling demands by 34% (7.2 $kWh*m^{-2}$) could be achieved compared to the reference: the cooling demand is reduced by 3.5 $kWh*m^{-2}$ (38 %) and the heating demand by 3.7 $kWh*m^{-2}$ (31 %) compared to the reference. It is important that the "true" potential of switching the insulation is higher, but dampened by the frame of the element. Building simulations results showed us the importance of having a high thermal resistance for the frame of the element in order to keep the benefits from the switching of the U-value.

The influence of thermal mass is very high on the reduction of heating and cooling demands: for example, in a building with a lower thermal mass, the wall variant with the advanced control strategy would only reduce the heating and cooling demand by 17 % (instead of 34 %).

The best potential was found (for this Stuttgart climate) for a South orientation, with important solar gains causing cooling loads in summer and possible heat gains in winter.

4 Conclusion and perspectives

4.1 General conclusion

In this thesis, two new concepts of switchable insulation have been introduced and developed.

For the first system, the closed movable insulation system, an extensive experimental campaign was performed: the translucent insulation material was characterized optically which allowed to parametrize a theoretical model. Numerous U-value measurements permitted to investigate the impact of different thermophysical parameters on the performance of this façade element. A detailed physical model was developed, showing a good agreement with measurements. The detailed model was used to perform a parametrical analysis and understand the range of possibilities that could be achieved with this first concept. The model also allowed us to characterize in detail the thermal behavior of the façade element. A building simulation based on the first U-values measured for the prototype showed that important reductions of the cooling demand could be achieved with the new switchable element as well as an important improvement of the summer comfort. An optimized element could even compete with free cooling solutions, both from the energetic and comfort point of view.

For the second system, the removable insulation system, the focus was on the theoretical analysis on different levels: the convective and radiative heat transfers of a single air cavity have been investigated in detail, showing the impact of the different thermophysical parameters. Using an existing standard model, the properties of different variants were calculated, as well as the influence of the most relevant thermophysical parameters and boundary conditions. On the building level, an extensive simulation campaign was done to assess the potential of the two variants of this removable insulation system. The influence of control strategy, orientation and thermal mass was also shown.

If the closed movable insulation system is compared to the removable insulation system, it can be concluded that:

- For the U-value, the highest switching range is offered by the removable insulation system, with low U-values of about 0.14 $W*m^{-2}*K^{-1}$ and high U-values of about 2.70 $W*m^{-2}*K^{-1}$. However, the detailed model presented in chapter 2 showed that with the use of a vacuum insulation panel, the closed movable insulation system could reach an even lower U-value in the insulating state, at the expense of a lower U-value in the conducting state. In the case study on the closed movable insulation system, a variant vas simulated with a "virtual" higher U-value of 3 $W*m^{-2}*K^{-1}$, producing an important reduction of the heating and cooling energy demand as well as important improvements in the summer comfort. It is interesting to remark

that, even if this virtual U-value value could not be reached with the first system, the value is close to the 2.70 $W*m^{-2}*K^{-1}$ reachable with the removable insulation system.
- The translucent closed movable insulation system has a very low overall solar transmittance and g-value, due to the translucent insulation material used. This could be solved by the use of a high-performance translucent insulation material, such as aerogel. However, the system should then be equipped with an external blind to reduce the unwanted solar gains in summer.
- The removable insulation system needs an important thickness of 20 cm to achieve these thermal properties. The closed translucent system could be a good compromise if for architectural reasons the thickness is limited.
- Concerning the costs, the removable insulation system is likely to be the cheapest system of both, since it is using a technology to retract the films that already exists for conventional roller blinds, and the much less expensive insulating material air.
- The mechanically moving parts of both technologies could be a barrier to the market penetration, due to the added complexity. However, such mechanized parts are already accepted in the blind industries.

Concerning the potential of switchable insulation, both systems showed an important potential of reduction of the heating and cooling energy demand in buildings for the continental climate investigated. The thermal mass of the building is a decisive factor for the performance of switchable insulation, and the best orientation is south. The numerous building simulations performed in section 3.3 showed potential of reducing the heating and cooling demand by about 30 %, achieved not only by deactivating the insulation during the cooling period, but also by using solar gains during the heating period, without consuming any electricity to run pumps and fans, without exterior air to filter and noiseless.

4.2 Perspectives

Within this research, new scientific challenges appeared which can be addressed in future research on switchable insulation:

- What is the potential of switchable insulation for other climates?
- What is the potential of switchable insulations system for a residential building?
- How cost-effective are the different new technologies that were introduced?

After demonstrating the potential of switchable insulations with building simulations and numerous laboratory measurements, the next step would be apply the technologies in a first commercial building project. Outdoor measurement results on a test building could also help the market penetration of these new products.

With measurements of the airflow rate within the closed movable insulation element presented in chapter 2 and a modelling of the airflow with a Computational Fluid Dynamic software, the detailed physical model could be extended to more complex geometries which may offer even higher switching factors.

5 References

Aste, Niccolò; Angelotti, Adriana; Buzzetti, Michela (2009): The influence of the external walls thermal inertia on the energy performance of well insulated buildings. In: *Energy and Buildings* 41 (11), S. 1181–1187. DOI: 10.1016/j.enbuild.2009.06.005.

Baetens, Ruben; Jelle, Bjørn Petter; Thue, Jan Vincent; Tenpierik, Martin J.; Grynning, Steinar; Uvsløkk, Sivert; Gustavsen, Arild (2010): Vacuum insulation panels for building applications: A review and beyond. In: *Energy and Buildings* 42 (2), S. 147–172. DOI: 10.1016/j.enbuild.2009.09.005.

BASF (2014): Marketinginformation: Basotect® - Der vielseitige Schaumstoff aus Melaminharz. Available online at www.basotect.de, checked online the 01.01.2014.

BASF (2016): Neopor Anwendungsbroschüre: Wanddämmung - Bauen und modernisieren mit Neopor®. Available online at http://basf.com/group/corporate/de/literature-document:/Marke%20Neopor-Brosch%C3%BCre--Bauen%20und%20modernisieren%20mit%20Neopor-Deutsch.pdf, checked online the 09.05.2016.

Bejan, Adrian (2013): Convection Heat Transfer, Fourth Edition: John Wiley & Sons, Inc.

Berge, Axel; Hagentoft, Carl-Eric; Wahlgren, Paula; Adl-Zarrabi, Bijan (2015): Effect from a Variable U-Value in Adaptive Building Components with Controlled Internal Air Pressure. In: *Energy Procedia* 78, S. 376–381. DOI: 10.1016/j.egypro.2015.11.677.

Berger, Tania; Amann, Christof; Formayer, Herbert; Korjenic, Azra; Pospichal, Bernhard; Neururer, Christoph; Smutny, Roman (2016): Impacts of external insulation and reduced internal heat loads upon energy demand of offices in the context of climate change in Vienna, Austria. In: *Journal of Building Engineering* 5, S. 86–95. DOI: 10.1016/j.jobe.2015.11.005.

Berndgen-Kaiser, Andrea (2010): Leben im Passivhaus. Baukonstruktion, Baukosten, Energieverbrauch, Bewohnererfahrungen. Dortmund: ILS, Institut für Landes- und Stadtentwicklungsforschung gGmbH (ILS-Forschung, 2010, 2).

Braesch, Cosima (2015): Modeling, validation and simulation of a ventilated window. Diploma thesis (confidential until 2020). INSA de Strasbourg, Strasbourg. Available online at http://eprints2.insa-strasbourg.fr/1932/.

Building Technologies Department, Lawrence Berkeley Laboratory (Hg.) (2014): The RADIANCE 4.2 Synthetic Imaging System. Available online at http://radsite.lbl.gov/radiance/refer/.

Caps, R.; Hetfleisch, J.; Fricke, J. (1996): [DE] Vakuumwärmedämmpaneel. Patent applied by Bayerisches Zentrum für Angewandte Energieforschung eV, 97074 Würzburg, DE the 18.11.1996. Registration number: 19647567. Publication number: DE 196 47 567 C 2.

Chow, Tin-tai; Li, Chunying; Lin, Zhang (2010): Innovative solar windows for cooling-demand climate. In: *Solar Energy Materials and Solar Cells* 94 (2), S. 212–220. DOI: 10.1016/j.solmat.2009.09.004.

Crawley, Drury B.; Lawrie, Linda K.; Winkelmann, Frederick C.; Buhl, W. F.; Huang, Y.Joe; Pedersen, Curtis O. et al. (2001): EnergyPlus. Creating a new-generation building energy simulation program. In: *Energy and Buildings* 33 (4), S. 319–331. DOI: 10.1016/S0378-7788(00)00114-6.

Cuce, Erdem; Cuce, Pinar Mert; Wood, Christopher J.; Riffat, Saffa B. (2014): Toward aerogel based thermal superinsulation in buildings: A comprehensive review. In: *Renewable and Sustainable Energy Reviews* 34, S. 273–299. DOI: 10.1016/j.rser.2014.03.017.

DIN EN 12898:2001: Glass in building - Determination of the emissivity; German version.

DIN EN 13363-1:2007-09: Solar protection devices combined with glazing – Calculation of solar and light transmittance – Part 1: Simplified method;German version.

DIN EN 13363-2:2005-06: Solar protection devices combined with glazing - Calculation of total solar energy transmittance and light transmittance - Part 2: Detailed calculation method; German version.

DIN EN 15251:2007: Indoor environmental input parameters for design and assessment of energy performance of buildings addressing indoor air quality, thermal environment, lighting and acoustics; German version.

DIN EN 673:2011-04: Glass in building –Determination of thermal transmittance (U value) – Calculation method; German version.

DIN V 18599-10:2007: Energy efficiency of buildings – Calculation of the net, final and primary energy demand for heating, cooling, ventilation, domestic hot water and lighting – Part 10: Boundary conditions of use, climatic data.

Duffie, John A.; Beckman, William A. (2006): Solar Engineering of Thermal Processes, Third Edition: John Wiley & Sons, Inc.

Ellis, Peter Graham (2003): Development and validation of the unvented Trombe wall model in EnergyPlus. Master Thesis. Graduate College of the University of Illinois at Urbana-Champaign.

ElSherbiny, S. M.; Raithby, G. D.; Hollands, K.G.T. (1982): Heat transfer by natural convection across vertical and inclined air layers. In: *Journal of Heat Transfer* 104 (1), S. 96–102.

EN 14500:2008: Blinds and shutters - Thermal and visual comfort - Test and calculation methods.

EN 410:2011: Glass in building – Determination of luminous and solar characteristics of glazing;

EnEV 2009 (2009): Energieeinsparverordnung für Gebäude - Verordnung über energiesparenden Wärmeschutz und energiesparende Anlagentechnik bei Gebäuden (Energieeinsparverordnung – EnEV 2009). In: *Bundesgesetzblatt*.

European Parliament (2010): Directive 2010/31/EU of the European Parliament and of the council of 19 May 2010 on the energy performance of buildings (recast). In: *Official Journal of the European Union*.

Feist, Wolfgang; Peper, Søren; Kah, Oliver; Oesen, Matthias von (2005): Klimaneutrale Passivhaussiedlung Hannover-Kronsberg: Bau und Messung. Kurzfassung aus der Zusammenführung der CEPHEUSBerichte Nr. 18 und Nr. 19. Passiv Haus Institut.

Gan, Guohui (2000): Numerical evaluation of thermal comfort in rooms with dynamic insulation. In: *Building and Environment* 35 (5), S. 445–453. DOI: 10.1016/S0360-1323(99)00034-7.

Gao, Tao; Ihara, Takeshi; Grynning, Steinar; Jelle, Bjørn Petter; Lien, Anne Gunnarshaug (2016): Perspective of aerogel glazings in energy efficient buildings. In: *Building and Environment* 95, S. 405–413. DOI: 10.1016/j.buildenv.2015.10.001.

Gil-Lopez, Tomas; Gimenez-Molina, Carmen (2013): Influence of double glazing with a circulating water chamber on the thermal energy savings in buildings. In: *Energy and Buildings* 56, S. 56–65. DOI: 10.1016/j.enbuild.2012.10.008.

Gloriant, François; Tittelein, Pierre; Joulin, Annabelle; Lassue, Stéphane (2015): Modeling a triple-glazed supply-air window. In: *Building and Environment* 84, S. 1–9. DOI: 10.1016/j.buildenv.2014.10.017.

Horn, Ronny; Rene Neusinger; Michael Meister; Jörg Hetfleisch; Roland Gaps; Jochen Fricke (2000): Switchable thermal insulation. results of computer simulations for optimisation in building applications. In: *High Temperatures-High Pressures* 32, S. 669–675.

ISO 15099:2003: Thermal performance of windows, doors and shading devices - Detailed calculations.

ISO 7730:2005, 2005: Ergonomics of the thermal environment - analytical determination and interpretation of thermal comfort using calculation of the PMV and PPD indices and local thermal comfort criteria, edition 2005.

ISO 8302:1991: Thermal insulation - Determination of steady-state thermal resistance and related properties - Guarded hot plate apparatus.

ISO 9050:2003: Glass in building — Determination of light transmittance, solar direct transmittance, total solar energy transmittance, ultraviolet transmittance and related glazing factors.

Jelle, B. P.; Gustavsen, A.; Baetens, R. (2010): The path to the high performance thermal building insulation materials and solutions of tomorrow. In: *Journal of Building Physics* 34 (2), S. 99–123. DOI: 10.1177/1744259110372782.

Jelle, Bjørn Petter (2011): Traditional, state-of-the-art and future thermal building insulation materials and solutions – Properties, requirements and possibilities. In: *Energy and Buildings* 43 (10), S. 2549–2563. DOI: 10.1016/j.enbuild.2011.05.015.

Jürgen Schnieders; Andreas Hermelink (2006): CEPHEUS results: Measurements and occupants' satisfaction provide evidence for Passive Houses being an option for sustainable building. In: *Energy Policy* 34, S. 151–171.

Kalz, Doreen E.; Pfafferott, Jens (2014): Thermal Comfort and Energy-Efficient Cooling of Nonresidential Buildings. Cham, s.l.: Springer International Publishing (SpringerBriefs in Applied Sciences and Technology).

Kimber, Mark; Clark, William W.; Schaefer, Laura (2014): Conceptual analysis and design of a partitioned multifunctional smart insulation. In: *Applied Energy* 114, S. 310–319. DOI: 10.1016/j.apenergy.2013.09.067.

Klems, J. H. (1994a): New method for predicting the solar heat gain of complex fenestration systems - I. Overview and derivation of the matrix layer calculation. In: *ASHRAE Transactions* 100 (1), S. 1065–1072.

Klems, J. H. (1994b): New method for predicting the solar heat gain of complex fenestration systems - II. Detailed description of the matrix layer calculation. In: *ASHRAE Transactions* 100 (1), S. 1073–1086.

Kossecka, Elisabeth; Kosny, Jan (2002): Influence of insulation configuration on heating and cooling loads in a continuously used building. In: *Energy and Buildings* 34 (4), S. 321–331. DOI: 10.1016/S0378-7788(01)00121-9.

Kuhn, Tilmann E. (2006a): Solar control: A general evaluation method for facades with venetian blinds or other solar control systems. In: *Energy and Buildings* 38 (6), S. 648–660. DOI: 10.1016/j.enbuild.2005.10.002.

Kuhn, Tilmann E. (2006b): Solar control: Comparison of two new systems with the state of the art on the basis of a new general evaluation method for facades with venetian blinds or other solar control systems. In: *Energy and Buildings* 38 (6), S. 661–672.

Kuhn, Tilmann E. (2015): Design, Development and Testing of Innovative Solar-Control Facade Systems. PhD Thesis. In: *National and Kapodistrian University of Athens,* checked online the 09.05.2016.

Kuhn, Tilmann E.; Herkel, Sebastian; Frontini, Francesco; Strachan, Paul; Kokogiannakis, Georgios (2011): Solar control. A general method for modelling of solar gains through complex facades in building simulation programs. In: *Energy and Buildings* 43 (1), S. 19–27. DOI: 10.1016/j.enbuild.2010.07.015.

Kuhn, Tilmann; Fath, Karoline; Bales, Chris; Nouvel, Romain; Fedrizzi, Roberto (2014): Deliverable 2.3 RES availability survey and boundary conditions for simulations. Project INSPIRE. Available online at http://www.inspirefp7.eu/wp-content/uploads/2015/01/WP2_D2.3_20141118_P5_RES-Availability-Survey-and-Boundary-Conditions-for-Simulations_WEBSITE.pdf.

Kvasnin, Sergej (2013): [DE] Isolationsvorrichtung für Fenster[EN] Isolation device for window e.g. skylight window of building, has cover that is arranged at deflecting element, and plastic foil webs whose thickness is dimensioned much smaller than thickness of shell side portions and fastener. Patent applied by Kvasnin, Sergej, 33647, Bielefeld, DE the 24.01.2013. Registration number: 102013001176. Publication number: DE102013001176A1.

Kvasnin, Sergej (2014): [DE] Isolationsvorrichtung für Fenster oder Fassaden. Patent applied by Kvasnin, Sergej, 33647, Bielefeld, DE the 23.01.2014. Registration number: 202014000533. Publication number: DE202014000533U1.

Larsen, Tine Steen; Jensen, Rasmus Lund (2011): Comparison of measured and calculated values for the indoor environment in one of the first danish passive houses. In: *Proceedings of Building Simulation 2011: 12th Conference of International Building Performance Simulation Association, Sydney, 14-16 November.*

Larson, Greg W.; Shakespeare, Rob A. (1998): Rendering with Radiance: The Art and Science of Lighting Visualization. San Francisco: Morgan Kaufmann Publishers.

Lawrence Berkeley National Laboratory (2015): WINDOW. Version 7.2. Available online at https://windows.lbl.gov/software/window/window.html, checked online the 2015.

Lechtenböhmer, Stefan; Schüring, Andreas (2011): The potential for large-scale savings from insulating residential buildings in the EU. In: *Energy Efficiency* 4 (2), S. 257–270. DOI: 10.1007/s12053-010-9090-6.

Leppkes, Reinhard; Olbrich, Helmut (1987): [DE] Polystyrol-Schaumstoffkugeln für die variable Wärmedämmung und Beschattung von transparenten Gebäudeteilen. Patent applied by BASF AG, 6700 Ludwigshafen, DE the 08.09.1987. Registration number: 3730023. Publication number: DE000003730023C2.

Leppkes, Reinhard; Olbrich, Helmut (1988): [EN] Use of polystyrene foam beads for mobile heat insulation and shadowing of transparent parts of buildings. Patent applied by BASF AG, DE the 03.09.1988. Registration number: 88114434. Publication number: EP000000306877A2.

Long, Linshuang; Ye, Hong (2015): Effects of Thermophysical Properties of Wall Materials on Energy Performance in an Active Building. In: *Energy Procedia* 75, S. 1850–1855. DOI: 10.1016/j.egypro.2015.07.161.

Manz, Heinrich (2003): Numerical simulation of heat transfer by natural convection in cavities of facade elements. In: *Energy and Buildings* 35 (3), S. 305–311. DOI: 10.1016/S0378-7788(02)00088-9.

Maurer, Christoph (2012): Theoretical and experimental analysis and optimization of semi-transparent solar thermal façade collectors. Stuttgart: Fraunhofer-Verl.

McLeod, Robert S.; Hopfe, Christina J.; Kwan, Alan (2013): An investigation into future performance and overheating risks in Passivhaus dwellings. In: *Building and Environment* 70, S. 189–209. DOI: 10.1016/j.buildenv.2013.08.024.

Mlecnik, E.; Schütze, T.; Jansen, S.J.T.; Vries, G. de; Visscher, H. J.; van Hal, A. (2012): End-user experiences in nearly zero-energy houses. In: *Energy and Buildings* 49, S. 471–478. DOI: 10.1016/j.enbuild.2012.02.045.

Nestle, Nikolaus; Pflug, Thibault; Daiss, Andreas; Hahn, Klaus; Kuhn, Tilmann; Maurer, Christoph et al. (2015): Construction element having a controllable heat-transfer coefficient U. Registration number: 14701321.

Nield, D. A. (2004): Forced convection in a parallel plate channel with asymmetric heating. In: *International Journal of Heat and Mass Transfer* 47 (25), S. 5609–5612. DOI: 10.1016/j.ijheatmasstransfer.2004.07.006.

Nield, D. A. (2008): Erratum to. "Forced convection in a parallel plates channel with asymmetric heating" [Int. J. Heat Mass Transfer 47 (2004) 5609–5612]. In: *International Journal of Heat and Mass Transfer* 51 (7-8), S. 2108. DOI: 10.1016/j.ijheatmasstransfer.2007.09.044.

Nyers, Jozsef; Kajtar, Laszlo; Tomić, Slavica; Nyers, Arpad (2015): Investment-savings method for energy-economic optimization of external wall thermal insulation thickness. In: *Energy and Buildings* 86, S. 268–274. DOI: 10.1016/j.enbuild.2014.10.023.

Passivhaus Institut (2009): Anforderungen und Prüfverfahren zur energetischen und schalltechnischen Beurteilung von Passivhaus-Lüftungsgeräten<600 m³/h für die Zertifizierung als "Passivhaus geeignete Komponente".

Passivhaus Institut (2015): Kriterien für den Passivhaus-, EnerPHit- und PHI-Energiesparhaus-Standard. Available online at http://www.passiv.de/de/02_informationen/02_qualitaetsanforderungen/02_qualitaetsanforderungen.htm, zuletzt aktualisiert am 6/30/2015, checked online the 04.05.2016.

PassivHaus Institute (2015): Passive House Planning Package PHPP. http://passivehouse.com/04_phpp/04_phpp.htm#PH9.

Pflug, Thibault; Kuhn, Tilmann E.; Nörenberg, Ralf; Glück, Andre; Nestle, Nikolaus; Maurer, Christoph (2015): Closed translucent façade elements with switchable U-value—A novel option for energy management via the facade. In: *Energy and Buildings* 86, S. 66–73. DOI: 10.1016/j.enbuild.2014.09.082.

Platzer, Werner J. (1987): Solar transmission of solar insulation material. In: *Solar Energy Materials and Solar Cells* 16, S. 275–287.

Poirazis, Harris (2008): Single and Double Skin Glazed Office Buildings, Analyses of Energy Use and Indoor Climate. PhD Thesis. Department of Architecture and Built Environment, Faculty of Engineering LTH, Division of Energy and Building Design, Lund University.

Quesada, Guillermo; Rousse, Daniel; Dutil, Yvan; Badache, Messaoud; Hallé, Stéphane (2012): A comprehensive review of solar facades. Transparent and translucent solar facades. In: *Renewable and Sustainable Energy Reviews* 16 (5), S. 2643–2651. DOI: 10.1016/j.rser.2012.02.059.

Reim, M.; Reichenauer, G.; Körner, W.; Manara, J.; Arduini-Schuster, M.; Korder, S. et al. (2004): Silica-aerogel granulate – Structural, optical and thermal properties. In: *Journal of Non-Crystalline Solids* 350, S. 358–363. DOI: 10.1016/j.jnoncrysol.2004.06.048.

Roos, Arne; Polato, Pietro; van Nijnatten, Peter A.; Hutchins, Michael G.; Olive, Francois; Anderson, Charles (2001): Angular-dependent optical properties of low-e and solar control windows—. In: *Solar Energy* 69, S. 15–26. DOI: 10.1016/S0038-092X(01)00019-6.

RT2012 (2012): Décret n° 2012-1530 du 28 décembre 2012 relatif aux caractéristiques thermiqueset à la performance énergétique des constructions de bâtiments. In: *Journal officiel de la république francaise*.

Saelens, Dirk (2012): Energy performance assessment of single storey multipleskin facades. PhD Thesis. K.U. Leuven, Leuven, Belgium.

Schwab, Armin (2002): Zur Wärmeübertragung bei Mischkonvektion in luftdurchströmten Bauteilen. In: *Bauphysik* 24 (6).

Shah, R. K.; London, A. L. (1978): Laminar flow forced convection in ducts. A source book for compact heat exchanger analytical data. New York: Academic Press (Advances in heat transfer. Supplement, 1).

Shima, P. D.; Philip, John (2011): Tuning of Thermal Conductivity and Rheology of Nanofluids Using an External Stimulus. In: *The Journal of Physical Chemistry C* 115 (41), S. 20097–20104. DOI: 10.1021/jp204827q.

Sodha, M. S.; Nayak, J. K.; Bansal, N. K.; Goyal, I. C. (1982): Thermal performance of a solarium with removable insulation. In: *Building and Environment* 17 (1), S. 23–32. DOI: 10.1016/0360-1323(82)90006-3.

Stazi, F.; Di Perna, C.; Munafò, P. (2009): Durability of 20-year-old external insulation and assessment of various types of retrofitting to meet new energy regulations. In: *Energy and Buildings* 41 (7), S. 721–731. DOI: 10.1016/j.enbuild.2009.02.008.

Stazi, Francesca; Vegliò, Ambra; Di Perna, Costanzo; Munafò, Placido (2012): Retrofitting using a dynamic envelope to ensure thermal comfort, energy savings and low environmental impact in Mediterranean climates. In: *Energy and Buildings* 54, S. 350–362. DOI: 10.1016/j.enbuild.2012.07.020.

Taylor, B. J.; Cawthorne, D. A.; Imbabi, M. S. (1996): Analytical investigation of the steady-state behaviour of dynamic and diffusive building envelopes. In: *Building and Environment* 31 (6), S. 519–525. DOI: 10.1016/0360-1323(96)00022-4.

TRNSYS. software homepage (2013). Available online at http://www.trnsys.com/.

Verein Deutscher Ingenieure (2010): Heat Atlas. 2nd ed. Berlin, New York: Springer (VDI-buch).

Verein MINERGIE (2014): Reglement zur Nutzung der Qualitätsmarke MINERGIE®. Available online at

http://www.minergie.ch/tl_files/download/Reglemente/Nutzungsreglement_Minergie_2014-dt.pdf, checked online the 04.05.2016.

Wilson, Helen Rose (2006): Solar Control Coatings for Windows. In: K. Grassie, E. Teuckhoff,G. Wegner,J. Hausselt,H. Hanselka (Hg.): Functional Materials, Bd. 13.

Wilson, Helen Rose; Hutchins, Michael G.; Kilbey, N. B.; Anderson, Charles (2009): Intercomparison of Transmittance and Reflectance Measurements of Light-Scattering and Patterned Glass with Spectrophotometers and Integrating Spheres (Report). INTERNATIONAL COMMISSION ON GLASS - TECHNICAL COMMITTEE 10 Optical properties of Glass and Coated Products.

Wright, John L. (1996): Correlation to quantify convective heat transfer between vertical window glazings. In: *ASHRAE Transactions* 102 (1). Available online at http://www.scopus.com/inward/record.url?eid=2-s2.0-0029697557&partnerID=40&md5=c086ea4a7f3ad9cf7745969f8d662af5.

Yin, S. H.; Wung, T. Y.; Chen, K. (1978): Natural convection in an air layer enclosed within rectangular cavities. In: *International Journal of Heat and Mass Transfer* 21 (3), S. 307–315. DOI: 10.1016/0017-9310(78)90123-0.

6 List of publications

International patent:

Nestle, Nikolaus; Daiss, Andreas; Hahn, Klaus; **Pflug, Thibault**; Kuhn, Tilmann; Maurer, Christoph; Wienold, Jan; Glück, Andre; Nörenberg, Ralf; Szeifert, Johann Martin; Khazova, Elena; Löffler, Achim (2015): Construction element having a controllable heat-transfer coefficient N°: 14701321, 2015

Peer-reviewed journal paper:

Pflug, Thibault; Kuhn, Tilmann E.; Nörenberg, Ralf; Glück, Andre; Nestle, Nikolaus; Maurer, Christoph: Closed translucent façade elements with switchable U-value—A novel option for energy management via the facade. In: Energy and Buildings 86, S. 66–73. DOI: 10.1016/j.enbuild.2014.09.082, 2015

Peer-reviewed international conference papers:

Pflug, Thibault; Di Lauro, Paolo; Kuhn, Tilmann E.; Maurer, Christoph (2013): Evaluation of a simplified model for façade collectors. In: Building Simulation Conference, IBPSA, Chambéry, France, 25–28 August 2013

Maurer, Christoph; **Pflug, Thibault**; Di Lauro, Paolo; Hafner, Joze; Knez, Friderik; Jordan, Sabina; Hermann, Michael; Kuhn, Tilmann E. (2012): Solar Heating and Cooling with Transparent Façade Collectors in a Demonstration Building. In: Energy Procedia 30, S. 1035–1041. DOI: 10.1016/j.egypro.2012.11.116, 2012

Maurer, Christoph; Gasnier, Damien; **Pflug, Thibault**; Plešec, Primož; Hafner, Jože; Jordan, Sabina; Kuhn, Tilmann E. (2014): First Measurement Results of a Pilot Building with Transparent Façade Collectors. In: Energy Procedia 48, S. 1385–1392. DOI: 10.1016/j.egypro.2014.02.156, 2014

Peer-reviewed national conference papers:

Pflug, Thibault; Siroux, Monica; Nestle, Nikolaus; Maurer, Christoph (2015b): Présentation d'un modèle détaillé d'isolation commutable. In: Congrès de la Société Française de Thermique, La Rochelle, France, 2015

Nestle, Nikolaus; Daiss, Andreas; Nörenberg, Ralf; Szeifert, Johann Martin; Wolf, Erwin; Schneider, Frank; Glück, Andre; Wehnl, Antonio; **Pflug, Thibault**; Kuhn, Tilmann; Maurer, Christoph (2014): Wärmedämmung - auch mal abschalten? In: Conference proceedings:EnOB Symposium 2014, Essen, Germany, 2014

7 Appendix

A. Simulation details of the well-insulated office

In this appendix, the simulation details of the well-insulated office presented in chapter 2 are detailed:

Internal walls:

The internal walls are composed of:

- Light partition wall: 39.3 m².
- Concrete internal wall: 21.5 m²
- Concrete ceiling: 63.3m²

Ventilation:

A heat recovery system was implemented, with an efficiency of 75 % and four different cases:

- Heating: 75 % heat recovery.
- Heating: 0-75 % heat recovery: it is not advisable to introduce air with more than 20°C in winter, because this could lead to cooling loads in winter.
- Cooling: No heat recovery
- Cooling: 75 % recovery.

The ventilation rate is constant at 2 $vol*h^{-1}$.

Occupation:

3 Persons between 7:00 and 18:00 on working days.

Cooling:

Cooling temperature: 24°C between 5:00 and 18:00 on working days, 28°C otherwise. Unlimited cooling power.

Heating:

Heating temperature: 20°C between 5:00 and 18:00 on working days, 16°C otherwise. Unlimited cooling power.

Infiltration:

The new infiltration is 0.1 vol*h^{-1}.

Internal gains by occupation and computers:

The internal gain through occupation were calculated with the Norm ISO 7730 (seated, light work, typing). The internal gains through computers are equal to 3*150 W when the office was occupied.

B. Range of application of the correlation from ElSherbiny

In this section, the range of application of the correlation from ElSherbiny introduced in (ElSherbiny et al. 1982) is presented graphically:

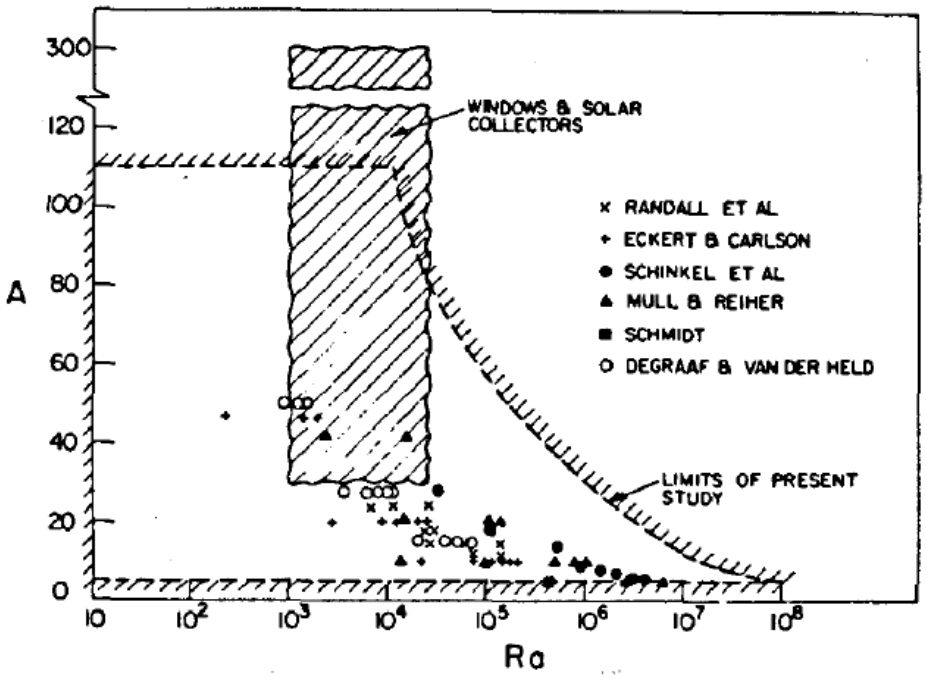

Figure 64 - Parameter range for the correlation presented by ElSherbiny for closed cavity convection. Source (ElSherbiny et al. 1982).

The ElSherbiny correlation is used in section 3.2.2.1.1.

C. Building simulation: influence of the switching temperature for a higher limit on the irradiance for the window and wall configuration

In following graphs, the influence of the switching temperature as defined in the control strategies on the energy demand for the window and wall configurations is presented, for a limit on the irradiance of 300 W*m^{-2} (see also 3.3.2):

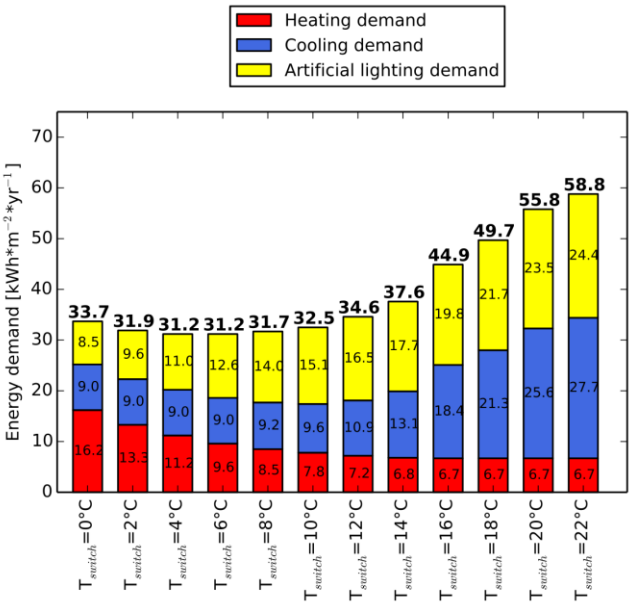

Figure 65 - Building simulation. Window application: influence of the switching temperature with a limit on the irradiance of 300 W*m-2.

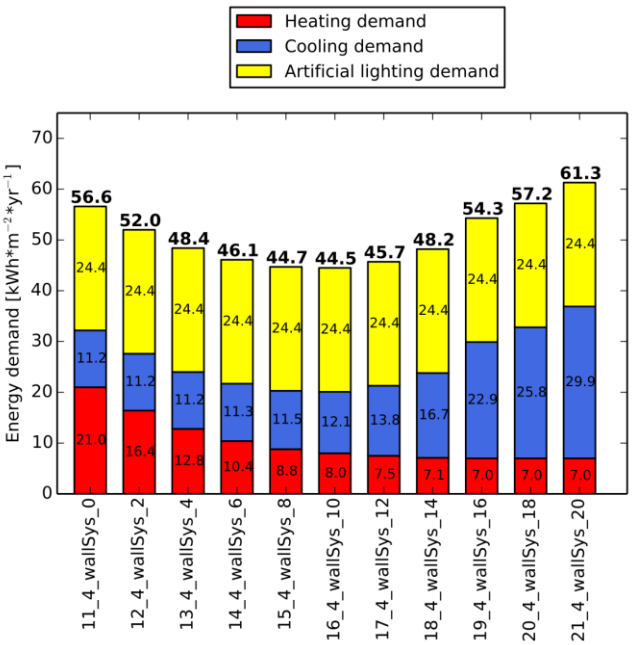

Figure 66 - Building simulation. Wall application: influence of the switching temperature with a limit on the irradiance of 300 W*m^{-2}.

8 Résumé étendu

Les nouvelles réglementations européennes et nationales concernant les besoins énergétiques des bâtiments impliquent des épaisseurs d'isolations toujours plus importantes. Pour le climat continental européen, ces importantes épaisseurs d'isolations ont pour conséquence, en hiver, des besoins de chauffage toujours plus bas. Par contre, en été, ces épaisseurs importantes d'isolations (parfois au-delà de 20 cm) ont parfois pour conséquence une surchauffe des pièces, due aux gains solaires et aux apports internes (personnes, équipements, etc.) : du fait de l'épaisseur importante d'isolant, ces flux de chaleur ne peuvent être évacués à travers les parois la nuit, ou quand les températures extérieures sont favorables, et la masse du bâtiment ne peut être refroidie.

Les moyens traditionnels d'évacuer cette chaleur sont notamment la ventilation nocturne (mécanique ou naturelle). Dans le cadre de cette thèse, un autre moyen d'optimiser les flux de chaleur entre l'intérieur et l'extérieur du bâtiment est proposé : l'isolation commutable. Une isolation commutable est une isolation dont on peut varier la résistance thermique en fonction des conditions.

Pour arriver à déterminer le potentiel de tels éléments de façade, cette thèse aborde la question scientifique suivante : les isolations commutables peuvent t-elles réduire les besoins en énergie d'un bâtiment (chauffage, refroidissement, éclairage artificiel) de manière significative ?

L'étude se concentre sur les bâtiments de bureaux : les bâtiments de bureaux sont des cibles intéressantes pour les isolations commutables car ils ont des gains de chaleur internes élevés et une grande surface vitrée, ce qui conduit à des charges de refroidissement importantes.

En ce qui concerne le climat, l'accent est d'abord donné aux climats continentaux européens, avec des températures froides en hiver, des étés chauds, des niveaux annuels d'ensoleillement moyens et d'importantes variations de température entre le jour et la nuit.

Des isolations commutables existent déjà, et ont été présentés dans un état de l'art. Un résumé est présenté dans le tableau suivant :

Année	Référence	Concept	Valeur de U basse [$W*m^{-2}*K^{-1}$]	Valeur de U haute [$W*m^{-2}*K^{-1}$]	Etude expérimentale ou théorique?	Analyse du potentiel au niveau du bâtiment ?
1982	(Sodha et al. 1982)	L'isolation sur les murs et le toit est retirée manuellement pendant la nuit.	0.62	6.02	Théorique	Oui
1987	(Leppkes und Olbrich 1987)	Une cavité peut être remplie de sphères de mousse isolante.	-	-	Théorique	Non
1996	(Caps et al. 1996; Horn et al. 2000)	Libération et absorption d'hydrogène gazeux par un hydrure métallique dans un panneau.	0.3	4.29	Les deux	Oui
2011	(Shima und Philip 2011)	La conductivité thermique de nanofluides magnétiques est variée par application d'un champ magnétique.	-	-	Expérimentale	Non
2012	(Stazi et al. 2012)	Isolation extérieure ventilée	0.26	-	Théorique	Oui
2014	(Kimber et al. 2014)	Les films séparant des cavités d'air verticales peuvent être déplacés pour former une seule couche conductrice solide	0.26	3.47	Théorique, mais un prototype existe	Non

2015	(Berge et al. 2015)	Changement de pression interne dans un nanomatériau	0.05, en supposant une épaisseur de 10 cm	0.2, en supposant une épaisseur de 10 cm	Les deux	Oui

Table 24 - Résumé des différentes études sur les isolations commutables.

L'isolation commutable n'est pas un concept totalement nouveau. Toutefois, seul un nombre très limité de systèmes sont prêts pour le marché. Souvent, il n'y a pas d'étude expérimentale et l'analyse est entièrement théorique. En outre, le potentiel de ces systèmes de façade ou de ces nouveaux matériaux n'a souvent pas été analysé au niveau du bâtiment. Dans cette thèse, deux nouveaux systèmes d'isolation commutable sont introduits et étudiés, de l'échelle de l'élément de façade à l'échelle du bâtiment. Les deux éléments font également l'objet d'une étude expérimentale.

Les indicateurs de performances utilisés au niveau de l'élément de façade dans cette thèse sont :

- Le coefficient de transmission thermique U, exprimé en $W*m^{-2}*K^{-1}$, qui décrit à quel point un élément de façade conduit la chaleur de l'intérieur à l'extérieur du bâtiment. Il exprime le taux de transfert de chaleur (en watts) à travers un mètre carré de l'élément de façade pour 1 K différence de température.
- Le facteur solaire g (sans unité), qui représente la fraction du rayonnement solaire incident qui pénètre dans le bâtiment après son passage à travers l'élément de façade.

Le premier système d'isolation commutable consiste en un double vitrage, composé de deux lames d'air verticales séparées par un panneau d'isolation translucide. Le panneau d'isolation peut se déplacer verticalement :

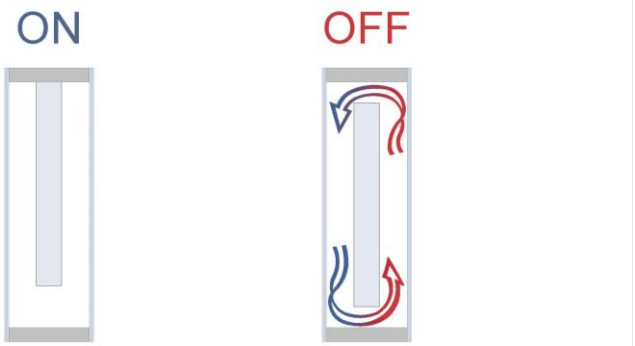

Figure 67 – Elément de façade commutable dans l'état isolant (à gauche) et conducteur (à droite). Source : Fischer Architekten.

Deux états sont possibles :

- L'état isolant (à gauche) : quand le panneau isolant est en position haute, la convection entre les lames d'air avant et arrière est très limitée. En pratique, on a une lame d'air isolante, un panneau d'isolation et une autre lame d'air.
- L'état conducteur (à droite) : le panneau d'isolant est cette fois en position médiane, et les deux ouvertures au sommet et à la base permettent une convection entre les deux lames d'air : la résistance thermique de l'élément est fortement diminuée.

Des simulations sur un bâtiment réel ont été réalisées avec un modèle simplifié :

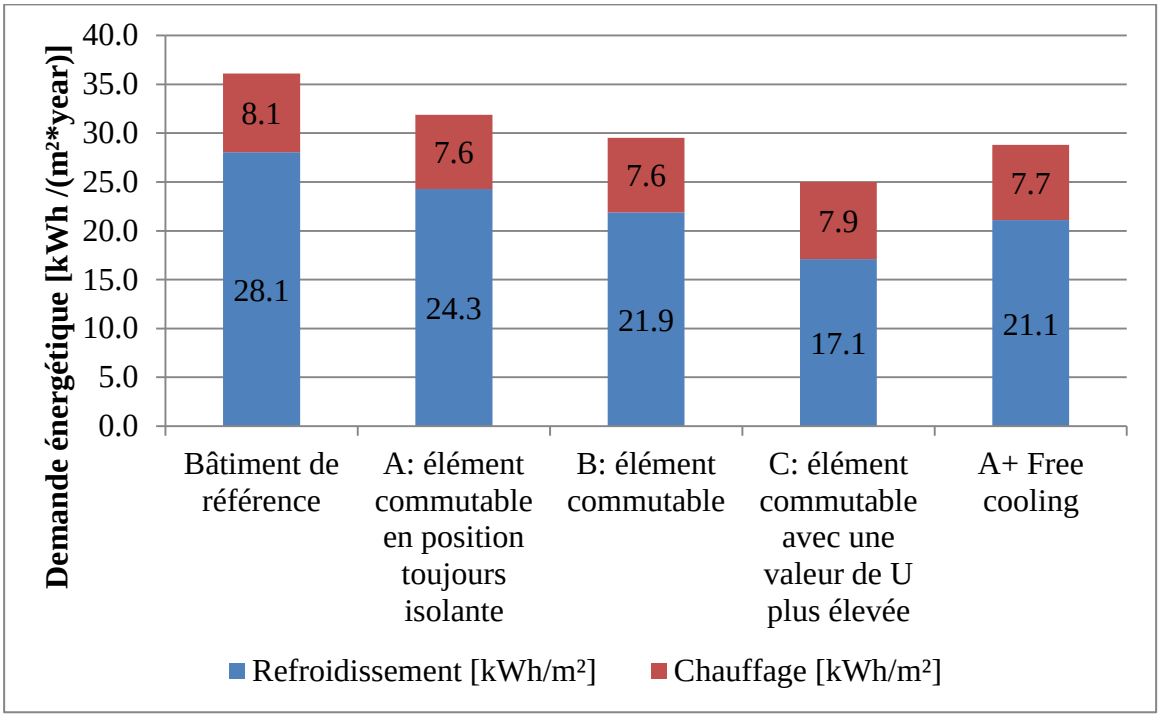

Figure 68 – Sommes annuelles des besoins énergétiques en chauffage et refroidissement pour le bâtiment de référence ainsi que différentes variantes.

La différence entre la référence et la variante A où la partie supérieure de la façade de référence est remplacée par l'isolation commutable nous montre qu'en remplaçant une partie du vitrage par l'élément translucide sans commutation, on diminue à la fois les besoins de refroidissement et de chauffage, le tout s'en commuter l'élément entre la position isolante et conductrice : La diminution des besoins de refroidissement est principalement due à la transmission solaire plus faible, alors que la diminution des besoins de chauffage est principalement due à un coefficient de transmission thermique U plus élevé de l'élément à l'état isolé, par rapport à la fenêtre.

Quand l'élément est commuté (variante B), une baisse des besoins de refroidissement de l'ordre de 10 % est observée par rapport à la variante A.
La variante C correspond au même élément commutable mais avec une valeur virtuelle de U plus élevée dans l'état conducteur (3 $W*m^{-2}*K^{-1}$). Une diminution des besoins de refroidissement de l'ordre de 29.6 % par rapport à la variante A peut alors être atteinte. Par rapport à la référence, cela représente une diminution de 39.1 %.

La comparaison des variantes B et C avec la dernière colonne, où le bâtiment est refroidi en augmentant le débit de ventilation pendant les nuits d'été (« free cooling ») nous montre que l'élément commutable est très compétitif par rapport à cette solution traditionnelle, surtout si il pouvait être optimisé avec une valeur de U plus élevée dans l'état commuté.

Le nouvel élément d'isolation commutable a aussi fait l'objet d'une vaste campagne expérimentale : le coefficient de transmission thermique U de différents prototypes a été mesuré en laboratoire:

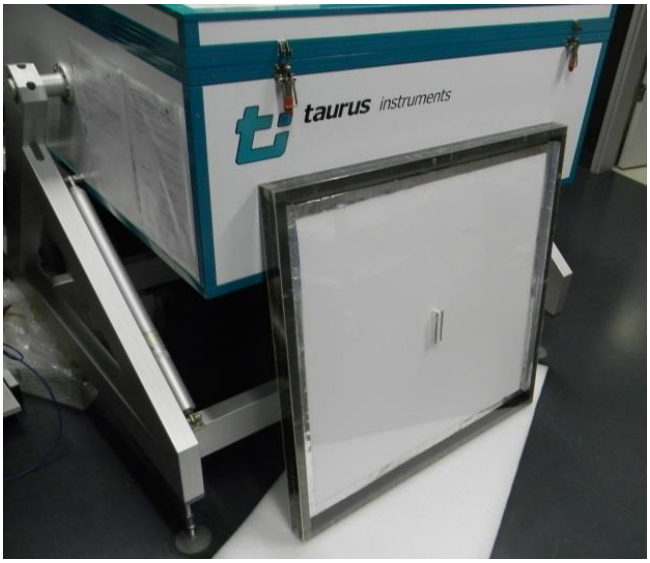

Figure 69 – Prototype devant l'appareil de mesure « hot box » Taurus utilisé pour les mesures de la valeur du coefficient de transmission thermique U.

Les premiers prototypes ont par exemple montré qu'il était possible de commuter entre une valeur de 0.89 $W*m^{-2}*K^{-1}$ en position isolante (correspondant à un double vitrage performant) et une valeur de 1.71 $W*m^{-2}*K^{-1}$ en position conductrice (correspondant à un double vitrage).

Ont aussi été mesurées :

- L'influence de l'épaisseur des lames d'air verticales.
- L'influence du ratio entre lames d'air verticales et horizontales.
- L'influence de l'épaisseur d'isolant.
- L'influence du gaz utilisé, en remplaçant l'air par du CO2 dans l'élément, ce qui conduit à un élément légèrement plus performant avec une valeur de U inférieure à l'état isolant et une valeur plus élevée dans l'état conducteur.

Il a été démontré que, dans l'état isolant, les colonnes d'air verticales peuvent être considérées comme des cavités fermées si la couche d'isolation se trouve dans la première position.

Les propriétés optiques de l'isolation translucide utilisée ont aussi été caractérisées expérimentalement en laboratoire:

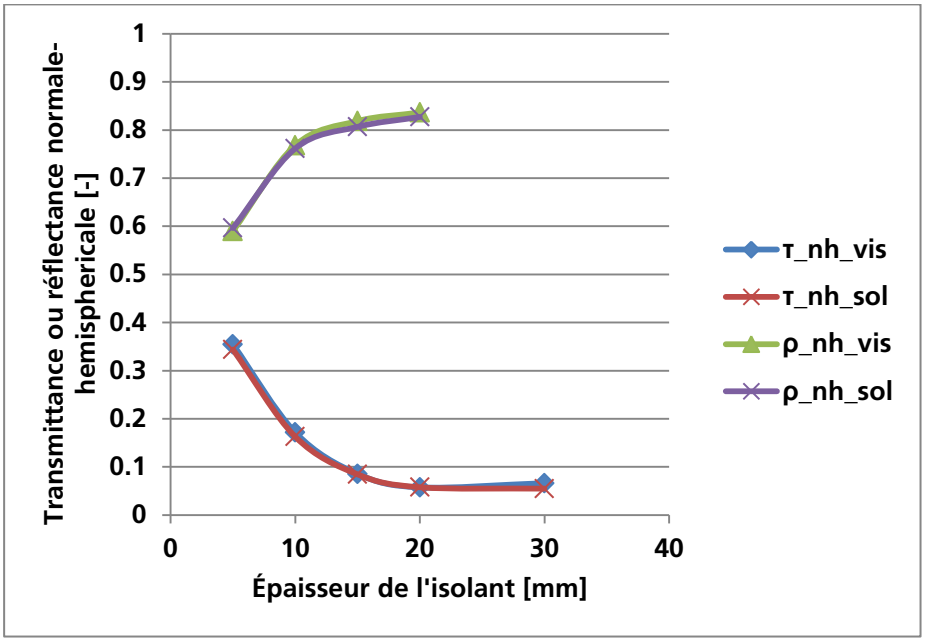

Figure 70 – Transmittance ou réflectance normale-hémisphérique en fonction de l'épaisseur d'isolant translucide.

Du fait de la faible transmittance solaire de l'isolant pour des épaisseurs importantes, il n'est pas possible d'avoir à la fois une bonne isolation et une baisse de l'éclairage artificiel avec cet isolant.

Un modèle détaillé de l'élément a été développé: ce modèle nodal est composé d'un modèle thermique, d'un modèle aéraulique et d'un modèle optique. Une description schématique du modèle de l'élément à l'état conducteur est présentée sur le schéma ci-dessous:

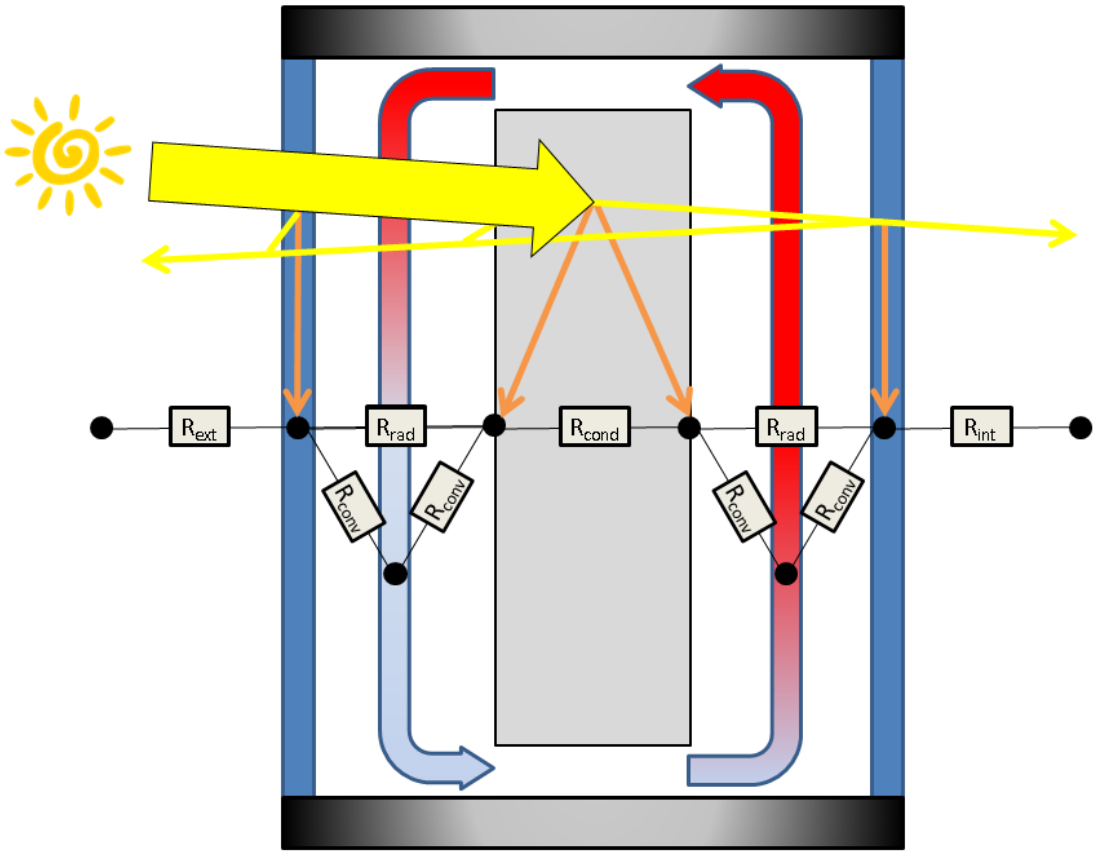

Figure 71 - Schéma du modèle physique détaillé. L'élément est à l'état conducteur. Les noeuds thermiques sont représentés, ainsi que le réseau de résistances thermiques. Les flèches jaunes indiquent le rayonnement solaire qui est transmis ou réfléchi par le système. Les réflexions multiples ne sont pas représentées. Les flèches orange montrent le rayonnement absorbé. Les nœuds représentent, de gauche à droite, la température de l'air extérieur, la température du vitrage extérieur, la température moyenne du fluide de la colonne d'air extérieure, les températures de surface de part et d'autre du panneau d'isolation, la température moyenne du fluide de la colonne d'air intérieure, la température du vitrage intérieur et la température de l'air intérieur (pièce).

Une description schématique du modèle pour l'élément dans l'état isolant est présenté sur le dessin ci-dessous:

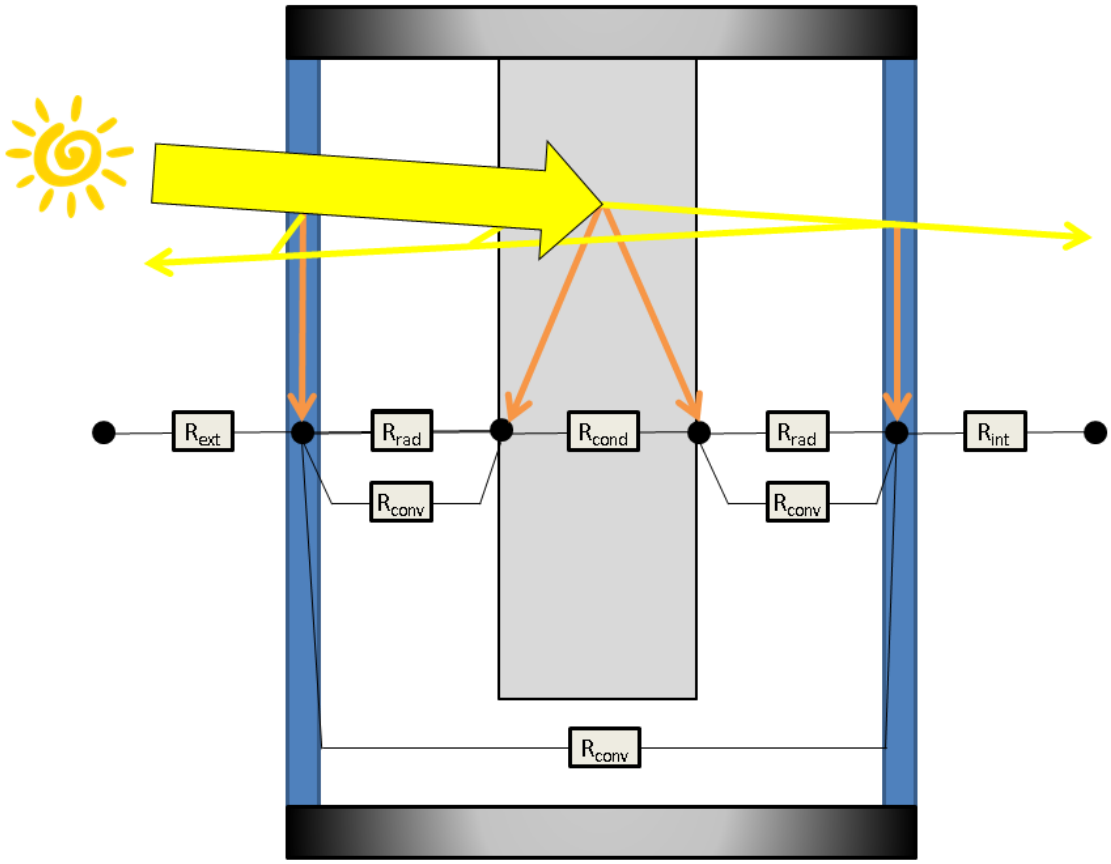

Figure 72 - Schéma du modèle physique détaillé. L'élément est à l'état isolant. Les nœuds thermiques sont représentés, ainsi que le réseau de résistances thermiques. Les flèches jaunes indiquent le rayonnement solaire qui est transmis ou réfléchi par le système. Les réflexions multiples ne sont pas représentées. Les flèches orange montrent le rayonnement absorbé. Les nœuds représentent, de gauche à droite, la température de l'air extérieur, la température du vitrage extérieur, les températures de surface de part et d'autre du panneau d'isolation, la température du vitrage intérieur et la température de l'air intérieur (pièce).

Le modèle a été validé à l'aide de l'étude expérimentale : pour chaque configuration géométrique et deux différences de température aux limites par géométrie (15 et 30 K), le modèle a été comparé aux mesures:

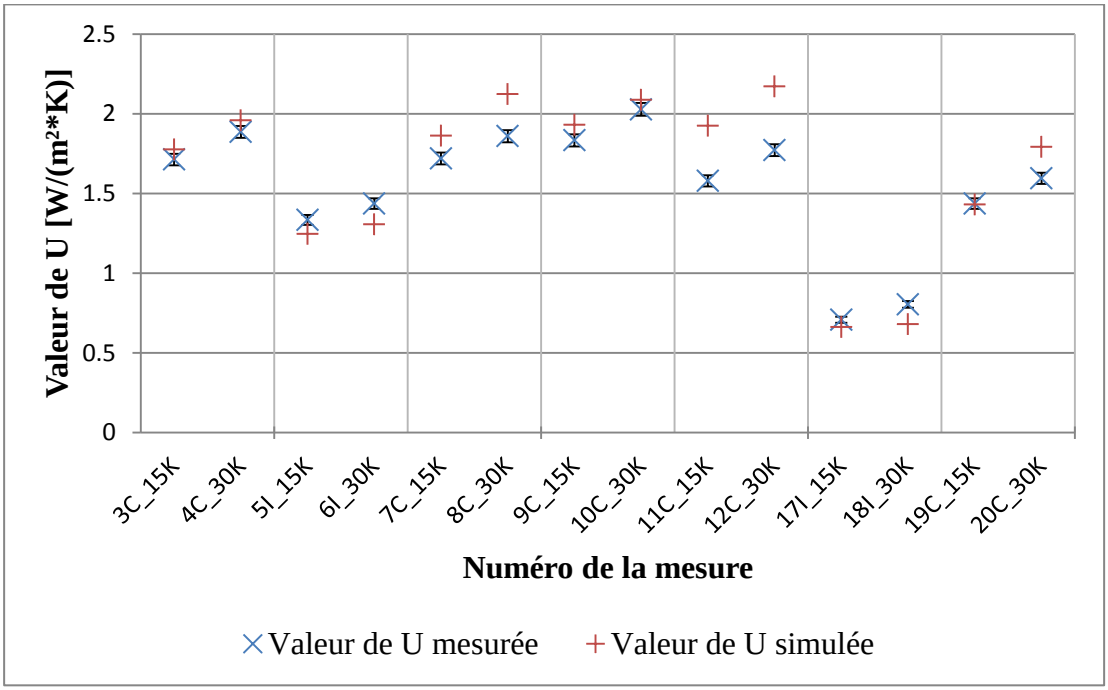

Figure 73 – Comparaison entre modèle et mesures pour 14 mesures différentes.

Pour ces 7 cas différents, l'écart moyen est de 9.5 %. Des mesures de températures supplémentaires ont permis d'expliciter les différences entre modèle et mesures.

Le modèle a ensuite été utilisé pour réaliser une étude paramétrique, qui a permis de montrer l'influence des paramètres les plus importants sur les valeurs de U et g. Par exemple, l'impact de la conductivité thermique sur la valeur de U a été calculé :

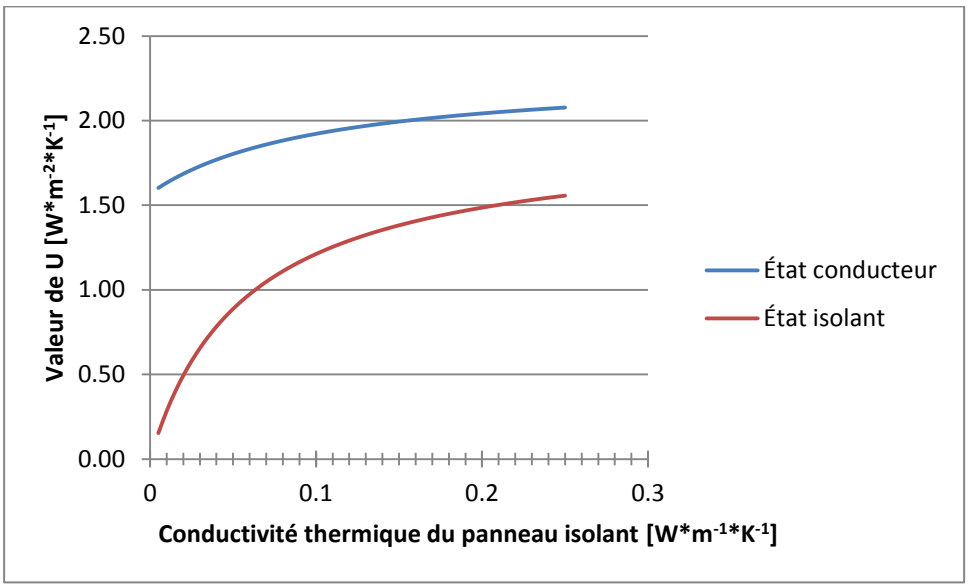

Figure 74 – Valeur de U en fonction de la conductivité thermique du panneau isolant.

Il peut par exemple être remarqué que plus la conductivité thermique du matériau est faible, plus l'écart entre valeur de U isolante et conductrice est élevé. Dans l'état conducteur, avec une résistance thermique importante, l'écart de température entre les deux colonnes d'air est donc plus élevé, et la force motrice du mouvement d'air aussi.

Ce premier élément à isolation commutable a fait l'objet d'un brevet visible dans la liste des publications.

Le deuxième élément d'isolation commutable consiste en une série de lames d'air séparées par des films plastiques métallisés. Ces films peuvent être enroulés ou non autour d'un tambour, tel un volet roulant, et sont protégés du vent par un vitrage extérieur :

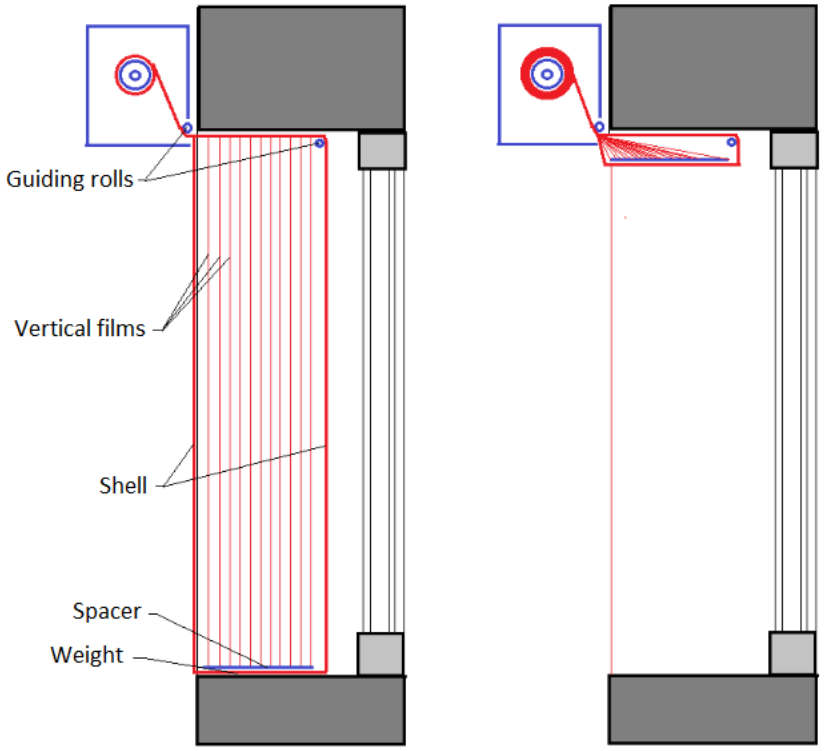

Figure 75 - Système d'isolation commutable numéro 2 devant un vitrage, dans l'état isolant (à gauche) ou conducteur (à droite).

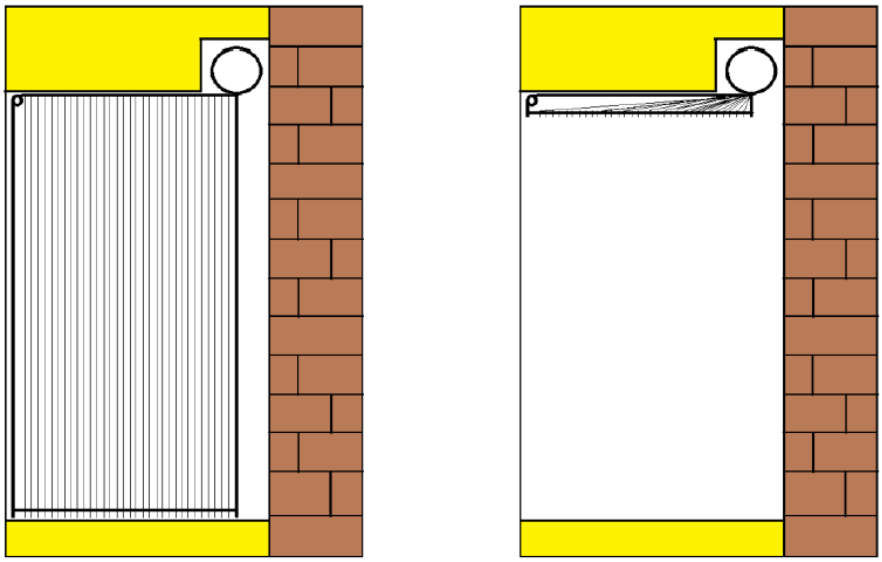

Figure 76 - Système d'isolation commutable numéro 2 devant un mur, dans l'état isolant (à gauche) ou conducteur (à droite).

Là aussi, deux états sont possibles :

- Dans l'état isolant, les films plastiques créent N fines lames d'air verticales isolantes, décuplant ainsi l'isolation thermique.
- Dans l'état conducteur, les films sont retirés et il reste une large lame d'air convective, bien moins isolante. Ceci permet de refroidir la masse du mur (ou du bâtiment) en été quand les températures extérieures sont favorables, et d'utiliser le rayonnement solaire en hiver.

Ce second système peut être appliqué devant un mur opaque ou devant une fenêtre.

Tout d'abord, ce système a fait l'objet d'une étude expérimentale, comprenant :

- La caractérisation des propriétés radiatives des films utilisés pour créer les lames d'air. Il a été montré que les films utilisés ont une couche basse émissivité sur une des deux surfaces.
- Des mesures de la valeur de coefficient thermique d'un premier prototype en état isolant :

Figure 77 – Vue extérieure du premier prototype.

En l'état isolant, la résistance thermique est comparable à une même épaisseur d'isolant traditionnel.

Ensuite, une étude théorique a été conduite à plusieurs niveaux: tout d'abord au niveau d'une seule cavité, puis de plusieurs cavités en série et l'élément de façade en entier.

Au niveau d'une cavité unique, les transferts de chaleurs convectifs et radiatifs ont été détaillés: l'impact du choix des propriétés infrarouges des parois ainsi que l'impact de

l'épaisseur des parois ont été étudiés et un modèle de convection a été sélectionné. Pour une seule cavité, dès qu'il y a une couche à faible émissivité dans la cavité, la résistance thermique totale de la cavité est dominée par le transfert de chaleur convectif. Une résistance maximale est atteinte pour une épaisseur d'environ 2 cm, et les résultats sont dépendants de la différence de température. En ajoutant une seconde couche à faible émissivité dans la cavité, la résistance thermique totale augmente seulement très faiblement en raison de l'effet dominant du transfert de chaleur convectif. L'épaisseur de la cavité doit être choisie afin de rester dans la plage purement conductive (sans convection) du transfert thermique dans l'air. A cet effet et afin de conserver un nombre limité de films plastiques, une épaisseur de 1 cm est choisie pour la cavité. Il a également été démontré que le film plastique métallisé utilisé pour le premier prototype, avec une couche à faible émissivité sur un côté et de l'autre du PET, est suffisante pour obtenir la résistance thermique quasi-maximale possible pour une cavité d'air et une épaisseur donnée.

Dans un deuxième temps, plusieurs cavités d'air en série ainsi que l'élément de façade dans son ensemble ont été analysés en utilisant le modèle présenté dans la norme ISO 15099: 2003. L'influence du nombre de cavités isolantes quand l'élément est à l'état isolant et l'influence de l'épaisseur de la cavité à l'état conducteur a été étudié pour différents types de vitrages intérieurs et extérieurs ont été étudiées.

Enfin, deux configurations différentes ont été sélectionnées pour être utilisées dans la simulation énergétique du bâtiment, avec une épaisseur totale de l'élément de 20 cm:

- Une variante avec pour paroi extérieure un verre à haute transmission solaire et comme paroi intérieure une peinture noire absorbante pour application sur un mur : avec cette configuration, une commutation des valeurs de U d'environ 0.14 à 2.76 W * m^{-2}*K^{-1} a été obtenue, ainsi qu'une commutation de 0 à 0.49 pour le facteur solaire g.
- Une variante avec pour paroi extérieure et intérieure un verre à haute transmission solaire pour application sur une fenêtre : la plage de commutation est d'environ 0.14 à 2.70 W * m^{-2}*K^{-1} pour la valeur U et de 0 à 0.84 pour la valeur g. L'influence de la différence de température entre l'air intérieur et extérieur ainsi que l'influence de la température moyenne sur la valeur de U a été étudiée. Concernant g, l'influence de l'angle d'incidence du soleil, de l'ensoleillement, de la différence de température et de la température moyenne a été étudiée.

Une comparaison entre les valeurs U mesurées et calculées montre des valeurs plus élevées que prévues, la raison probable étant l'étanchéité à l'air du raccord entre les films plastiques délimitant les cavités d'air et le cadre. Du point de vue mécanique, un point d'amélioration pour atteindre l'optimum représenté par le modèle est l'optimisation de l'étanchéité sur les côtés, en haut et en bas de l'élément tout en permettant toujours aux films d'être rétractés.

Ensuite, des simulations énergétiques dynamiques à l'échelle du bâtiment ont été

conduites. Un bâtiment bien isolé a été simulé. Deux régulations différentes ont été développées : une stratégie «simple» pour laquelle la commutation de l'élément reposait sur la différence de température entre la pièce et l'extérieur, et une régulation plus évoluée pour laquelle la commutation dépendait du flux de chaleur total vers l'intérieur du bâtiment.

Les résultats des simulations du bâtiment ont montré que pour la configuration « fenêtre », une réduction des besoins de chauffage et de refroidissement de l'ordre de 29 % pouvait être atteinte, avec la stratégie de contrôle plus évoluée: le besoin de refroidissement peut être réduit de 55 % et le besoin de chauffage peut être réduite de 11 %. Comme une surface opaque est remplacée par un élément translucide, l'éclairage artificiel est également diminué de 52 %.

Pour la configuration « mur » une réduction des besoins de chauffage et de refroidissement de l'ordre de 34 % peut être atteinte par rapport au bâtiment de référence: le besoin de refroidissement est réduit de 38 % et le besoin de chauffage de 31 % par rapport à la référence. En hiver, l'élément commuté se comporte comme un mur trombe. Il est important de remarquer que le "vrai" potentiel de cet isolation commutable est plus élevé, mais est atténué dans ce cas précis par le cadre de l'élément : les simulations ont montré l'importance d'avoir un cadre de l'élément fortement isolant afin de maintenir les avantages de la commutation de la valeur du coefficient de transmission thermique U.

L'influence de la masse thermique est très élevée sur la réduction des besoins de chauffage et de refroidissement: par exemple, dans un bâtiment avec une masse thermique plus faible, la réduction des besoins de chauffage et refroidissement n'est que de 17 %, au lieu de 34 % pour la configuration « mur » avec la stratégie de contrôle évoluée.

Le meilleur potentiel a été démontré pour une orientation sud, car les gains solaires importants entraînent des charges de refroidissement en été et de possibles gains de chaleur en hiver.

Après avoir étudié le potentiel des systèmes d'isolation commutable au niveau du bâtiment, il peut être intéressant de comparer le système étudié dans la première partie de la thèse (système 1, translucide) avec le système 2 (« store » rétractable, en configuration mur ou fenêtre). Il peut être conclu que:

- Concernant le coefficient transmission thermique U, le système 2 a la plage de commutation la plus élevée, avec des valeurs basses de U d'environ 0.14 $W*m^{-2}*K^{-1}$ et des valeurs hautes d'environ 2.70 $W*m^{-2}*K^{-1}$. Cependant, le modèle détaillé présenté dans le chapitre 4 a montré qu'en utilisant un panneau d'isolation sous vide, le système 1 pouvait atteindre une valeur de U encore plus faible à l'état isolant mais au détriment d'une valeur haute de U plus faible dans l'état conducteur. L'étude du système 1 a montré qu'avec une valeur haute de U plus élevée, le potentiel de diminution des besoins de refroidissement ainsi que d'augmentation du

confort d'été était encore plus élevé. Le système 2 a une valeur haute de U qui s'approche de ces critères.

- Le système 1 a une transmission très faible pour le spectre solaire et une valeur g très basse en raison du type d'isolation translucide utilisé. Ceci pourrait être résolu par l'utilisation d'un matériau d'isolation transparente à haute performance, comme un aérogel. Cependant, le système devrait alors être équipé d'un store extérieur pour réduire les gains solaires en été et éviter les surchauffes.
- Le système 2 a besoin de 20 cm d'épaisseur pour atteindre les propriétés thermiques visées. Le système 2 peut être un bon compromis si pour des raisons architecturales l'épaisseur est limitée.
- En ce qui concerne les coûts, le système 2 est susceptible d'être le système le moins cher des deux, car il utilise une technologie pour rétracter les films qui existe déjà pour les stores classiques ainsi qu'un matériau isolant beaucoup moins cher: l'air.

En ce qui concerne le potentiel des isolations commutables en général, les deux systèmes ont montré un potentiel important de réduction des besoins de chauffage et refroidissement pour le climat continental étudié. La masse thermique du bâtiment est un facteur déterminant pour la performance de l'isolation commutable, et la meilleure orientation est le sud. Les nombreuses simulations énergétiques des bâtiments ont montré un potentiel de réduction des besoins de chauffage et refroidissement de l'ordre de 30 % pour les bâtiments de bureau étudiés. Ce potentiel est atteint non seulement en désactivant l'isolation pendant la période de refroidissement, mais aussi en utilisant les gains solaires pendant la période de chauffage, le tout sans consommer de l'électricité pour faire fonctionner des pompes ou des ventilateurs, sans air extérieur à filtrer et de manière silencieuse.

Du point de vue scientifique, plusieurs questions demeurent concernant le potentiel des isolations commutables:
- Quel est le potentiel des isolations commutables pour d'autres climats?
- Quel est le potentiel des isolations commutables pour un bâtiment résidentiel?
- Quelle est la rentabilité économique des différentes technologies étudiées?

Après avoir démontré le potentiel des isolations commutables avec des simulations énergétiques de bâtiments et de nombreuses mesures en laboratoire, la prochaine étape serait d'équiper un bâtiment test d'une façade d'isolations commutables.

Du point de vue scientifique, concernant le modèle détaillé présenté dans le chapitre 4, la mesure du débit d'air dans l'élément et une modélisation du flux d'air avec un logiciel de CFD permettrait une validation complémentaire du modèle, ainsi qu'une meilleure compréhension des optimisations à faire afin d'augmenter le débit d'air et d'améliorer les performances globales.

Development, Characterization and Evaluation of switchable façade elements

Résumé

Un niveau important d'isolation des parois de bâtiments peut diminuer le refroidissement du bâtiment en été, quand les conditions extérieures sont favorables. Dans cette thèse, le concept d'isolations commutable, est développé : pendant les périodes de refroidissement, l'isolation commutable peut être désactivée pour refroidir la masse du bâtiment pendant la nuit. Pendant les périodes de chauffage, ce concept peut être utilisé pour utiliser les gains solaires. Dans cette thèse, le potentiel des isolations commutables est étudié pour des bureaux dans un climat continental européen. En outre, deux nouveaux concepts d'isolations commutables sont introduits et développés et caractérisés expérimentalement. Un modèle nodal détaillé a été mis en place, validé et utilisé pour conduire une étude paramétrique. Le potentiel des isolations commutables a été étudié à l'aide de simulations énergétiques dynamiques du bâtiment qui ont montré que des réductions importantes des besoins de chauffage et de refroidissement ainsi que des heures d'inconfort en été peuvent être atteintes. Plusieurs stratégies de contrôle ont été mises au point, introduites et comparées. L'influence de la masse thermique a également été étudiée, ainsi que l'influence de l'orientation ou du cadre des éléments.

Mots-clés: isolation commutable, éléments de façade, besoins de chauffage et refroidissement, étude expérimentale, modèle physique, analyse de potentiel.

Summary

Important thermal insulation levels can prevent the building to cool down during the cooling period, when the external conditions are favorable. In this thesis, the concept of switchable insulation is developed: during the cooling period, the insulation can be deactivated during the night to let the heat flow out. During the heating period, the switchable insulation can be deactivated whenever solar gains can be used. In this thesis the potential of switchable insulation for an European continental climate and for office buildings is investigated. Also, two new concepts of switchable insulation are introduced, developed and characterized experimentally. A detailed thermal model has been introduced, validated and used for a parametric analysis. The potential of switchable insulation is investigated on a building level, showing that important reductions of the heating and cooling load as well as summer discomfort hours can be achieved. Several control strategies have been developed, introduced and compared. The influence of thermal mass was also investigated, as well as the influence of the orientation or the elements' frame.

Keywords: switchable insulation, façade elements, building heating and cooling energy demand, experimental investigation, physical model, potential analysis.